Synthesis and catalytic activity of acid/basic Metal Organic frameworks

Marie Savonnet

N° d'ordre 199 - 2011 Année 2011

THESE DE L'UNIVERSITE DE LYON

Délivrée par

L'UNIVERSITE CLAUDE BERNARD LYON 1

ECOLE DOCTORALE

DIPLOME DE DOCTORAT

(arrêté du 7 août 2006)

soutenue publiquement le 6 octobre 2011

par

SAVONNET Marie

TITRE :

Synthèse de nouveaux matériaux de type MOFs à propriétés acido-basiques et évaluation en catalyse

Directeur de thèse : David FARRUSSENG

JURY :

Mme Bernadette CHARLEUX	Professeur, Université Claude Bernard Lyon 1
M Christian SERRE (Rapporteur)	DR-CNRS, Institut Lavoisier, Versailles
M Johan MARTENS (Rapporteur)	Professeur, Katholieke Universiteit Leuven
M Bruno CHAUDRET	DR-CNRS, LPCNO, Toulouse
M David FARRUSSENG	CR-CNRS, IRCELYON, Villeurbanne
M Nicolas BATS	Dr, IFP Energies Nouvelles, Solaize
Mme Catherine PINEL	DR-CNRS, IRCELYON, Villeurbanne
Mme Delphine BAZER-BACHI	Dr, IFP Energies Nouvelles, Solaize
M Vincent LECOCQ	Dr, IFP Energies Nouvelles, Solaize

UNIVERSITE CLAUDE BERNARD - LYON 1

Président de l'Université	**M. A. Bonmartin**
Vice-président du Conseil d'Administration	M. le Professeur G. Annat
Vice-président du Conseil des Etudes et de la Vie Universitaire	M. le Professeur D. Simon
Vice-président du Conseil Scientifique	M. le Professeur J-F. Mornex
Secrétaire Général	M. G. Gay

COMPOSANTES SANTE

Faculté de Médecine Lyon Est – Claude Bernard	Directeur : M. le Professeur J. Etienne
Faculté de Médecine et de Maïeutique Lyon Sud – Charles Mérieux	Directeur : M. le Professeur F-N. Gilly
UFR d'Odontologie	Directeur : M. le Professeur D. Bourgeois
Institut des Sciences Pharmaceutiques et Biologiques	Directeur : M. le Professeur F. Locher
Institut des Sciences et Techniques de la Réadaptation	Directeur : M. le Professeur Y. Matillon
Département de formation et Centre de Recherche en Biologie Humaine	Directeur : M. le Professeur P. Farge

COMPOSANTES ET DEPARTEMENTS DE SCIENCES ET TECHNOLOGIE

Faculté des Sciences et Technologies	Directeur : M. le Professeur F. Gieres
Département Biologie	Directeur : M. le Professeur F. Fleury
Département Chimie Biochimie	Directeur : Mme le Professeur H. Parrot
Département GEP	Directeur : M. N. Siauve
Département Informatique	Directeur : M. le Professeur S. Akkouche
Département Mathématiques	Directeur : M. le Professeur A. Goldman
Département Mécanique	Directeur : M. le Professeur H. Ben Hadid
Département Physique	Directeur : Mme S. Fleck
Département Sciences de la Terre	Directeur : Mme le Professeur I. Daniel
UFR Sciences et Techniques des Activités Physiques et Sportives	Directeur : M. C. Collignon
Observatoire de Lyon	Directeur : M. B. Guiderdoni
Ecole Polytechnique Universitaire de Lyon 1	Directeur : M. P. Fournier
Ecole Supérieure de Chimie Physique Electronique	Directeur : M. G. Pignault
Institut Universitaire de Technologie de Lyon 1	Directeur : M. le Professeur C. Coulet
Institut de Science Financière et d'Assurances	Directeur : M. le Professeur J-C. Augros
Institut Universitaire de Formation des Maîtres	Directeur : M. R. Bernard

Remerciements

Je tiens tout d'abord à remercier l'IFP Energies Nouvelles qui a financé ma thèse et Michel Lacroix qui m'a permis d'effectuer mes travaux de thèse au sein de l'IRCELYON.

Je souhaite également remercier mes encadrants :
Mon directeur de thèse, David Farrusseng, qui m'a très bien encadrée durant ces trois années de thèse autant sur le plan scientifique que humain. J'ai beaucoup appris à ses côtés surtout sur l'esprit de synthèse et la mise en ordre des idées de façon claire et cohérente. Enfin, j'ai beaucoup apprécié la confiance et donc la grande autonomie qu'il a su m'accorder.
Mon promoteur IFPEN, Nicolas Bats, qui m'a suivie et aidée de manière efficace tout au long de ma thèse.
Mes co-encadrants, Catherine Pinel, Delphine Bazer-Bachi et Vincent Lecocq, qui m'ont fait avancer par leurs remarques pertinentes.

Je remercie également les membres du jury qui ont accepté de juger ce travail.

Je remercie tout particulièrement Aurélie Camarata pour son aide technique pendant un an sur la « Click Chemistry », sans elle ce travail n'aurait jamais progressé aussi vite, ainsi que les services scientifiques de l'IRCELYON, en particulier Françoise pour mes nombreuses DRX, et Noëlle et Pascale pour mes isothermes et analyses élémentaires.

Merci aussi à tous mes collègues de l'IFPEN et de l'IRCELYON avec qui j'ai passé de très bons moment, en particulier Marie et Zyed de l'IFPEN qui ont organisé le voyage en Russie avec moi et tous les membres du bureau 125 de l'IRCELYON, Cyril, Olivier, Nicolas et Monsieur Bosquain. Sans oublier bien sûr la « MOF's team »…

Enfin, un grand merci à ma famille qui m'a toujours soutenue dans mes études, à tous mes amis car il n'y a pas que la thèse dans la vie et à Charles-Henri qui me supporte au quotidien…

Table of Contents

Experimental.....151

Abbreviations

ALPO	Alumino-Phosphate
APS	(3-aminopropyl)triethoxysilane
aq	aqueous
as	as-synthesized
ASTM	American Society for Testing and Materials
BET	Brunauer, Emmet, Teller
bdc	benzene-1,3-dicaboxylate
btapa	1,3,5-benzene tricarboxylic acid tris[N-(4-pyridyl)amide
btb	4,4',4''-benzene-1,3,5-triyl-tribenzoate
btc	benzene-1,3,5-tricarboxylate
btt	benzene-1,3,5-tris(1H-tetrazole)
cif	Crystallographic Information File
CMK	Carbon Metastructure at KAIST
COSY	Correlation Spectroscopy
CPO	Coordination Polymer of Oslo
CPS	(3-chloropropyl)trimethoxysilane
d	doublet
DABCO	1,4-diAzabicyclo[2.2.2]octane
DDR	decadodecasil 3R
DMAP	4-(dimethylamino)pyridine
DMF	dimethylformamide
DMOF	DABCO Metal-Organic Framework
DPG	meso-1,2-bis(4-pyridyl)-1,2-ethanediol
dppf	1,1'-bis(diphenylphosphino)ferrocene
DRIFTS	Diffuse Reflectance Infra-Red Fourier Transformation Spectroscopy
DTA	Differential Thermal analysis
EDS	Energy Dispersive Spectroscopy
FAME	fatty acid methyl ester
FAU	Faujasite
FFAs	free fatty acids

GC	Gas Chromatography
HBEA	hydrogen beta
HC	hydrocarbon
HKUST	Hong-Kong University of Science and Technology
HPA	heteropolyoxoanion
HPW	12-tungstophosphoric acid
ht	high temperature
HT	high-throughput
HY	hydrogen Y
Hz	Hertz
ICP	Inductively Coupled Plasma
IFPEN	Institut Français du Pétrole Energies Nouvelles
IM	Institut Français du Pétrole/Mulhouse
IR	Infrared
IRCE	Institut de Recherche sur la Catalyse et l'Environnement
IRMOF	IsoReticular Metal-Organic Framework
IRMOP	Isoreticular Metal–Organic Polyhedra
ITQ	Instituto de Tecnologıa Quimica
IZA	International Zeolite Association
KAIST	Korea Advanced Institute of Science and Technology
lt	low temperature
LTA	Linde Type A
m	multiplet
MAS	Magic Angle Spinning
MCM	Mobil Composition Material
MFI	Mobil-five
MIL	Matériaux de l'Institut Lavoisier
MOF	Metal-Organic Framework
MOR	Mordenite
MPc	Metal Phthalocyanine complexes
MR	Member ring
MS	Mass spectrometry

MTBE	methyl tert-butyl ether
ndc	naphthalene dicarboxylate
NMR	Nuclear Magnetic Resonance
OES	Optical Emission Spectroscopy
OMS	Ordered Mesoporous Silicas
PNB	Produit National Brut
ppm	parts per million
PSM	postsynthetic modification
PXRD	Powder X-Ray Diffraction
s	singlet
SAPO	alumino-silico-phosphate
SBA	Santa Barbara Amorphous
SBU	Secondary Building Unit
SDA	Structure Directing Agent
SEM	Scanning Electron Microscopy
t	triplet
TAZ	triazole
TCPB	1,2,4,5-tetrakis(4-carboxyphenyl)-benzene
teda	triethylenediamine
TG	thermogravimetry
TGs	triglycerides
THF	tetrahydrofuran
TIPB	1,3,5-triisopropylbenzene
TMS	trimethylsilane
UiO	University of Oslo
UMCM-1	University of Michigan Crystalline Material-1
USY	ultra stable Y
VPI	Virginia Polytechnic Institute
XRD	X-ray diffractogram
ZIF	zeolitic imidazolate framework

Introduction

Les structures poreuses qui peuvent être inorganiques, organiques ou à matrice mixte inorganique/organique représentent une classe de matériaux à forts intérêts scientifiques et technologiques. En effet, leurs cavités sont capables de stocker ou de capturer des liquides, des gaz ou des particules solides rendant ces matériaux très attractifs dans de nombreux domaines de recherche. Les solides poreux sont donc devenus au fil du temps des matériaux multifonctionnels économiquement stratégiques, en effet, actuellement ils représentent, directement ou par les activités qu'ils génèrent, 20% du PNB des pays industrialisés dans les domaines de l'énergie, la pétrochimie, la chimie fine, la médecine, la catalyse, les capteurs, la séparation et le stockage de gaz[1]… L'émergence de nouvelles applications technologiques ont requis néanmoins un grand contrôle de leurs propriétés poreuses.

Initialement limitée aux zéolithes (aluminosilicates)[2], cette famille s'est progressivement étendue aux tamis moléculaires de type aluminophosphate (ALPO) (1982)[3], aux nanotubes de carbone (1991)[4], aux silices mésoporeuses à structures ordonnées (1992)[5, 6], aux carbones mésoporeux type CMK (1999)[7] et aux solides poreux hydrides appelés MOFs (Metal-Organic Frameworks), dont le squelette tridimensionnel comporte des parties organiques et inorganiques reliées entre elles par des liaisons fortes. C'est en effet au début des années 1990 qu'un pas décisif a été franchi avec la découverte de ces nouveaux solides poreux à matrice mixte organique-inorganique. A l'inverse des solides poreux inorganiques limités à quelques cations comme constituants de la charpente, les MOFs existent pour tous les cations autres qu'alcalins. Ainsi, il est possible d'associer une infinité de combinaisons entre parties organiques et inorganiques donc une immense source de nouveaux matériaux aux possibilités d'applications restant encore inexplorées.

Bien que les MOFs présentent des stabilités thermiques et chimiques moindres que les zéolithes, ils possèdent des pores de dimensions modulables ainsi qu'une grande surface spécifique. Ainsi, ils offrent la possibilité d'ajuster, à l'échelle moléculaire, différentes fonctions, qu'elles soient catalytiques (acides, bases, redox,…) ou de séparations (tamisage moléculaire, adsorption). En associant plusieurs fonctions de façon appropriée, de nouveaux mécanismes et propriétés catalytiques sont à attendre.

D'autre part, on peut penser de façon conceptuelle que les MOFs se situent entre les zéolithes (inorganiques) et les enzymes (organiques). On peut dès lors imaginer qu'ils peuvent allier hautes activités (plus stable thermiquement que les enzymes) et hautes sélectivités (cluster polynucléaire isolé, espace confiné et reconnaissance moléculaire par la flexibilité du réseau poreux).

Il n'est donc pas étonnant qu'en vue de toutes les nombreuses potentialités dans les domaines de l'adsorption, de la séparation et de la catalyse, le nombre d'articles parus dans la littérature sur les MOFs n'a cessé d'augmenter ces dernières années (Figure 1).

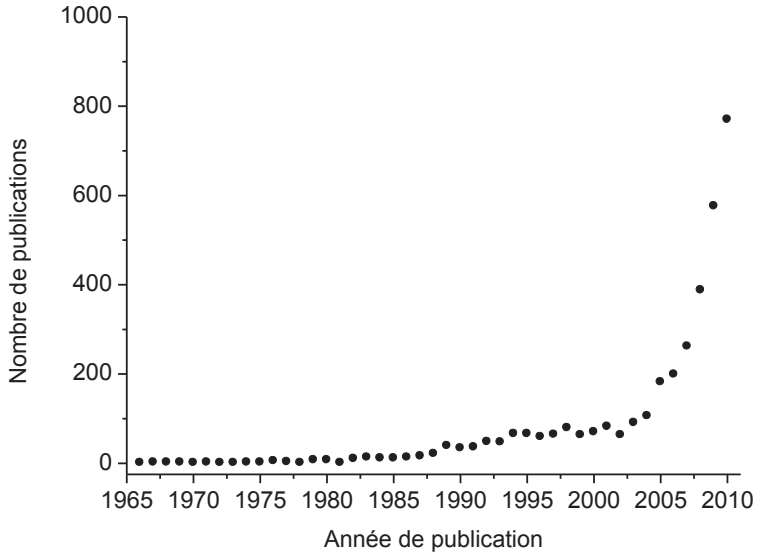

Figure 1 : Evolution du nombre annuel d'articles parus sur les MOFs depuis 1965

Ce travail de thèse s'inscrit dans le cadre d'un projet exploratoire de l'IFP Energies Nouvelles (IFPEN). Ses objectifs sont le développement de méthodes de synthèse et de caractérisation des MOFs et l'évaluation de leurs potentialités pour l'adsorption et la catalyse basique. Ainsi, l'objectif principal de cette étude est d'évaluer les potentialités de ces nouveaux matériaux jusqu'alors « curiosité de scientifiques » en tant qu'alternative aux catalyseurs et agents de séparation classiquement utilisés dans les procédés de raffinage, de pétrochimie ainsi que les procédés permettant de diversifier les sources d'énergie pour la production de carburants de synthèse.

L'IFPEN contribue de manière notable à cet élan, en développant de nouveaux catalyseurs en particulier pour la transformation de matières premières d'origine végétales en carburants ou additifs pour carburants (première génération). Le biodiesel actuellement commercialisé est issu de la réaction de transestérification des triglycérides (huile végétale, graisses animales ...) en esters méthyliques. Toutes les propriétés physiques des esters obtenus lors de la réaction de transestérification sont alors proches de celles du diesel, d'où une utilisation acceptable pour les moteurs.

La transestérification des triglycérides de l'huile végétale avec le méthanol permet d'obtenir des esters méthyliques. Le co-produit de la réaction est le glycérol. Cette réaction peut être catalysée soit par des bases (déprotonation de l'alcool), soit par des acides (activation de l'ester). Industriellement, la catalyse basique est préférée, car elle fait intervenir des catalyseurs moins corrosifs et engendre des vitesses de réactions plus importantes. Néanmoins, l'utilisation d'un catalyseur basique homogène conduit à la formation d'une émulsion entre le biodiesel et le glycérol. C'est pourquoi, des efforts importants ont été portés sur le développement de procédés mettant en jeu des catalyseurs basiques hétérogènes. En effet, aucune émulsion n'est obtenue entre l'huile et le glycérol, les produits obtenus sont d'une meilleure pureté et les produits sont plus facilement séparés.
A ce jour, un procédé industriel ESTERFIP-H mis au point par l'IFPEN produit 350 000 tonnes/an de biodiesel. Le catalyseur utilisé industriellement est un aluminate de zinc de type spinelle de formule brute $ZnAl_2O_4$.

Ainsi, dans ce contexte de catalyse basique et de valorisation des larges molécules, les MOFs possèdent deux principaux atouts : (i) un réseau poreux assez large pour permettre la diffusion et la transformation catalytique d'acides gras et (ii) des degrés de basicité et d'hydrohilicité/hydrophobicité qui peuvent être ajustés par post-fonctionnalisation afin de jouer sur les réactivités et propriétés d'adsorption.

Le principal objectif de ce travail est d'explorer des MOFs fonctionnalisés afin de les évaluer dans la réaction de transestérification.

Le **chapitre 1** de cette étude est une synthèse bibliographique basée sur quatre axes principaux : i) l'état de l'art des matériaux poreux qui confrontent les zéolithes et les silices mésoporeuses aux MOFs, ii) l'état de l'art des MOFs qui sont utilisés en catalyse acido-basique, iii) les différentes méthodes de post-modifications des MOFs qui permettent d'obtenir de nouveaux matériaux fonctionnalisés et enfin iv) les limites de cet état de l'art ainsi que les objectifs de la thèse.

Le **chapitre 2** décrit les différentes structures des MOFs pré-fonctionnalisés utilisés dans la suite de l'étude et leur caractérisation complète. Ces MOFs présentent tous une fonction amine sur leur partie organique, disponible pour le greffage de groupements fonctionnels.

Le **chapitre 3** présente les premiers travaux d'investigation portant sur une nouvelle méthode de post-fonctionnalisation de groupement basique par une réaction d'acylation et les résultats obtenus en catalyse basique pour deux MOFs fonctionnalisés.

Cette première étude nous a permis de mettre en place tous les outils nécessaires pour le développement d'une méthode plus douce et généralisable à un plus grand nombre de MOFs, portant sur leurs parois une fonction amine, par « Click Chemistry » qui sera décrite dans le **chapitre 4**, ainsi que la caractérisation de la large bibliothèque des nouveaux matériaux fonctionnels ainsi obtenus.

Le **chapitre 5** se concentrera sur les applications en catalyse de ces MOFs fonctionnels obtenus par la méthode précédemment décrite, ainsi que sur le modelage « sur mesure » de ces solides. De plus, afin d'élargir le spectre des applications de ces MOFs obtenus par « Click Chemistry », la fonctionnalisation par des groupements thiols sera abordée à la fin de ce chapitre pour des applications en adsorption et plus particulièrement pour le captage du mercure dans les eaux de production.

Enfin, une partie expérimentale rassemblera toutes les données sur les techniques et protocoles utilisés ainsi que sur les caractérisations des produits obtenus.

Cette thèse a été financée par l'IFP Energies Nouvelles et a été réalisée au sein de l'Institut de Recherche sur la Catalyse et l'Environnement (IRCELYON).

[1] G. Férey, *Actual. Chim.* **2007**, III-XV.
[2] J. Janak, M. Krejci, E. E. Dubsky, *Ann. N. Y. Acad. Sci.* **1959**, *72*, 731-738.
[3] S. T. Wilson, B. M. Lok, C. A. Messina, T. R. Cannan, E. M. Flanigen, *J. Am. Chem. Soc.* **1982**, *104*, 1146-1147.
[4] S. Iijima, *Nature* **1991**, *354*, 56-58.
[5] C. T. Kresge, M. E. Leonowicz, W. J. Roth, J. C. Vartuli, J. S. Beck, *Nature* **1992**, *359*, 710-712.
[6] J. S. Beck, J. C. Vartuli, W. J. Roth, M. E. Leonowicz, C. T. Kresge, K. D. Schmitt, C. T. W. Chu, D. H. Olson, E. W. Sheppard, S. B. McCullen, J. B. Higgins, J. L. Schlenker, *J. Am. Chem. Soc.* **1992**, *114*, 10834-10843.
[7] R. Ryoo, S. H. Joo, S. Jun, *J. Phys. Chem. B* **1999**, *103*, 7743-7746.

Chapter 1

Bibliography

I. State of art of porous materials

I.1 Zeolites

Zeolites, which form one the great family of crystalline porous materials, are broadly used in gas separation [1, 2], catalysis [3] (petrochemicals cracking) and in ion exchange beds (water purification) [4]. Zeolites are tridimensional crystalline aluminosilicates constituted by Si and Al tetrahedra linked through bridging oxygen atoms giving rise to the so-called secondary building units (SBUs) [5], constituted by rings and prisms of various sizes [6, 7].
By means of a great variety of organic molecules based on quaternary ammonium cations as Structure Directing Agents (SDAs), a large number of new zeolitic materials have been synthesized and this number is even larger since zeolites in which the structure has not been solved are reported in the open and patent literature.
Three main features determine the structural properties of zeolites: the size of their pore apertures defined by rings formed by oxygen atoms, the dimensionality of their pore systems and the Si/Al ratio.

- Pore size

Zeolites can be broadly classified as:

- Narrow-pore (3.5-4.5 Å), constituted by 8-member rings (8-MR)
- Medium-pore (4.5-6.0 Å), constituted by 10-MR
- Large-pore (6.0-9.0 Å), formed by 12-MR
- Super-large pore (>9.0 Å)

The regular nature of the pores and their apertures, whose dimensions are of the same order as molecular sizes, enable zeolites to carry out size-selective separations by molecular sieving. Depending on the type of zeolite and its pore system, the molecules can penetrate into or be excluded from the zeolite cavities. Nevertheless, the reduced pore size limited to 10 Å of zeolites is usually underlined as a key limitation to addressing the catalytic transformation of large molecules. Efforts on the postsynthethic modifications (PSM) of microporous zeolites

(aluminosilicates) and the related zeolitic materials (aluminophosphates) have been less abundant presumably due to their relatively small pores size and lack of accessible chemical functionality. Modification of as-prepared forms of zeolites is largely limited to calcinations or ion exchange of the organic-cation components of the materials. For catalysis with zeolites, the majority of the applications make use of the acidic properties of zeolites. Acid sites can be introduced by ion exchange for NH_4^+ followed by thermal decomposition.
Nevertheless, the grafting of various organic moieties onto zeolites has been reported [8]. Cauvel and co-workers functionalized zeolite Y (calcined and dealuminated) of various Si/Al ratios with (3-chloropropyl)trimethoxysilane (CPS) and (3-aminopropyl)triethoxysilane (APS) to study the influence of the Al sites and pore size on the grafting. Modification of the amine-functionalized zeolites was then performed by the addition of 4-anisoyl chloride and 2,3-butanedione. In addition, in the nineties, Corma and coworkers described Rh and Ni complexes anchored to USY-zeolite through a silane bond for hydrogenation reactions leading to higher catalytic activities compared to the case of the homogeneous catalyst [9, 10]. It was attributed to a cooperative effect of the zeolite which increases the reactants concentration inside the pores. In a similar way, the immobilization of L-Proline rhodium or nickel complexes still on USY-zeolite led to an improved enantioselectivity for the hydrogenation of dehydrophenylalanine derivatives [11, 12].

- Dimensionality of pore system

Zeolitic frameworks can be classified according to the directionality of their pore systems. For instance, LTA and FAU zeolites are based on a 3D array of super-cages, while MOR zeolites are constituted by 1D elliptical-structured pores (Figure I-1). 3D zeolites are more appropriate for adsorption and catalysis to avoid diffusional issues.

- Si/Al ratio

Each zeolite structure exhibits a phase breadth with respect to the Si/Al ratio. A distinction can be made between:

- low-silica (Si/Al<2)
- intermediate-silica (2<Si/Al <10)
- high-silica (10<Si/Al<100)

For adsorption, an increase in the silica content leads to an increasingly hydrophobic character, the transition from hydrophilic to hydrophobic behaviour occurring at a Si/Al ratio ca. 10. Among the most hydrophobic zeolites are silicalite-1 (MFI) and all-silica (DDR), having no Al in their structure (Figure I-1).

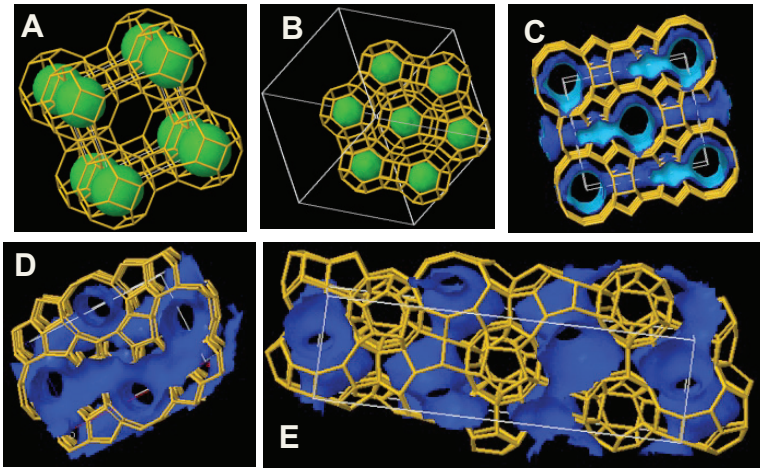

Figure I-1 : F ramework structures of zeolites: (A) LTA, (B) FAU, (C) MOR, (D) MFI and (E) DDR. Images adapted from IZA.

In the case of AlPO (alumino-phosphate) and SAPO (alumino-silico-phosphate) zeolites, in addition to Al, the structure also contains trivalent P.

I.2 Ordered mesoporous silicas (OMS)

The synthesis of mesostructured silica materials was first reported in the seminal studies of Beck *et al.*[13] and Kresge *et al.*[14] at Mobil Oil Corporation in the early 90's. This family of materials, commonly termed MCM (MCM = "Mobil Composition Material") includes a whole class of ordered mesoporous structures belonging to the M41S family, made of amorphous silica, with uniform and tunable pore size distributions (Figure I-2).

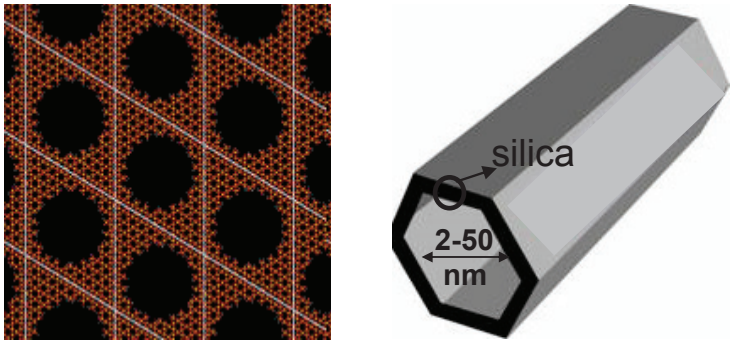

Figure I-2 : MCM-type silicas.

The synthesis of ordered mesostructured materials proceeds via a supramolecular mechanism, where a surfactant (most often cationic or non-ionic) forming lyotropic liquid crystal mesophases serves as organic template for silicate polymerization.
Unlike conventional mesoporous silicas showing intercrystalline and irregular mesoporosity, the porosity induced by the structure-directing effect of the template in mesostructured silicas is essentially internal and regular. As a result, despite the amorphous nature of pore walls, mesostructured materials show long-range crystalline arrangements translating into XRD patterns showing defined peaks at low angles (<10°).

- Pore size

The pore sizes of these MCM-based silica can be tailored on the basis of the synthesis method used and can range from about 20 to 500 Å.
In addition to MCM-based silica materials, synthesized using cationic surfactants, other ordered mesostructured silicates, aluminosilicates and metal oxide materials (e.g. SBA-15) with larger pore sizes 50-300 Å using non-ionic surfactants, most often block copolymers, have been reported as well [15, 16, 17].
In contrast to zeolites, PSM of mesoporous silicas, which possess much larger pores that are lined with reactive silanol (SiOH) groups, have been more extensively investigated [18]. Grafting of organic functionality to meoporous silica is commonly realized by reacting organosilanes, chlorosilanes or silazanes with the free silanol groups in the pore surfaces [19] (Figure I-3).

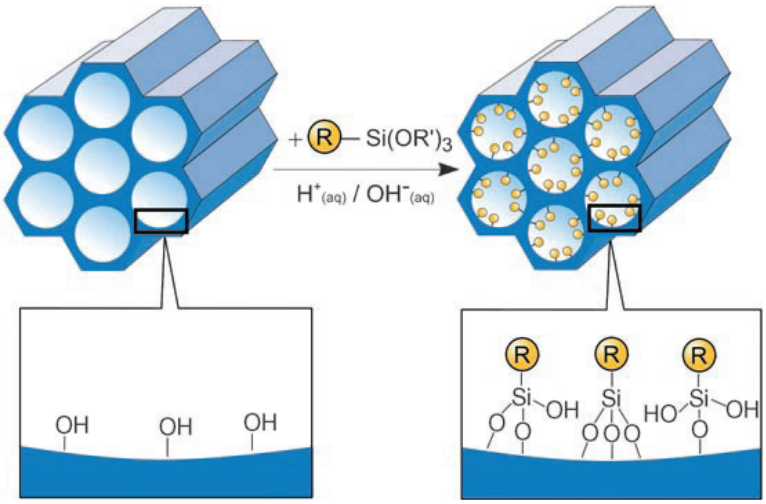

Figure I-3 : Grafting (postsynthetic functionalization) for organic modification of mesoporous pure silica phases with terminal organosilanes of the type $(R'O)_3SiR$. R=organic functional group.

Brunel and co-workers introduced amine species into MCM-41 silicas by the grafting method and used the solids as base catalysts for the Knoevenagel condensation of benzaldehyde and ethyl cyanoacetate [20, 21].

Furthermore, the post-calcination silanation of mesoporous silica such as SBA-15 led to the development of interesting mercury selective adsorbents reported by Antochshuk and coworkers, these functionalized solids being able to remove Hg contaminant from waste oils. This material was prepared via a two-step modification by attachment of anaminopropyl functionality and its subsequent conversion into a thiourea ligand [22].

Finally, Li *et al*. have systemically investigated the asymmetric epoxidation on Mn(salen) catalysts immobilized in the nanopores of mesoporous materials [23]. Some examples of chiral catalysts within the nanopores show improved catalytic performance compared to homogeneous catalysts. Thomas *et al*. reported the influence of the pore diameter on the efficacy of a silica-anchored chiral catalyst using a non convalent approach (Figure I-4). As a result, they showed that the cavity size determines the face differentiation of the substrate during the asymmetric hydrogenation of the methyl benzoylformate: in a much smaller cage, the constraints are higher and the enantioselectivity is better [24].

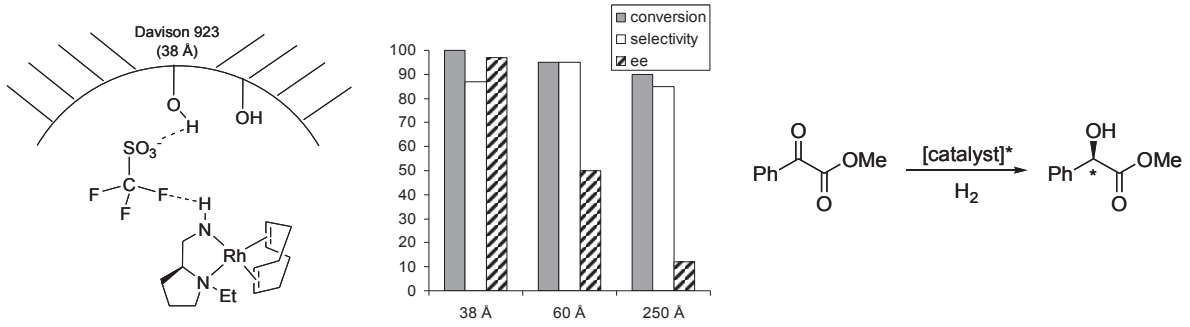

Figure I-4: Confinement of immobilized, single-site chiral catalyst enhances enantioselectivity.

- Dimensionality of pore system

Depending upon the surfactant concentration and synthesis conditions, the final silica structures exhibit hexagonal, cubic or lamellar symmetry (Figure I-5).

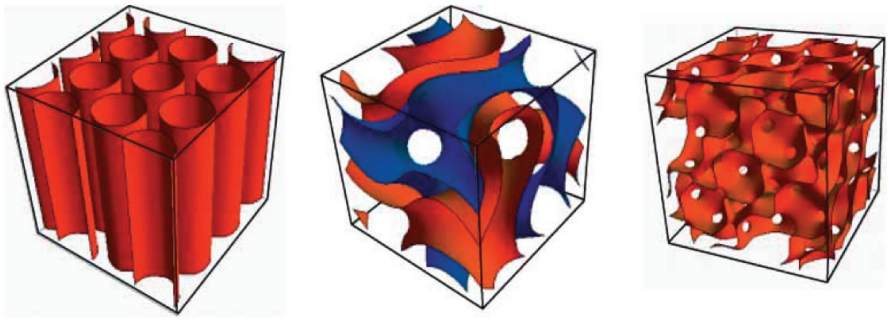

Figure I-5 : MCM-type silicas. From left to right: MCM-41, 1D hexagonal silica; MCM-48, 3D cubic silica with cylindrical pores and MCM-50, 3D cubic silica with cages.

These classical inorganic supports present some general limitations:

- **Pores of usual zeolites are too small to accommodate chiral linkers and substrates and can be hardly functionalized due to a lack of well defined anchor sites**
- **Zeolites are too rigid to exhibit "molecular recognition properties"**
- **Ordered Mesoporous Silica (such as MCMs) exhibit too large pores to impose confinement effects and leaching can easily take place, posing a problem for the retention of guest species.**
- **Amorphous structure of Ordered Mesoporous Silica can be a drawback for single-site control**

Inspired by theses pioneering examples, we will show that MOFs offer new opportunities as support for catalytic species with the additional advantages of a possible discrete variation of the pore size as well as well-defined single-sites allowing a complete characterization of the catalytic species such as for molecular catalysts.

I.3 Metal-organic frameworks (MOFs)

I.3.1 A building block construction

MOFs result from the reaction between organic and inorganic species and can be described by the organisation of secondary buildings units (SBU) or blocks, associating metallic clusters acting as nodes connected by organic linkers acting as linkers to form a net (Figure I-7) [25, 26, 27, 28, 29, 30, 31, 32, 33, 34, 35, 36]. As an analogy to zeolite frameworks, this SBU approach to MOF construction allows the design of specific nanometer-scale framework geometries with particular pore structures. In contrast to zeolites, for which a relatively limited number of structures exists (i.e., 191 to date), MOFs provide diverse combinations of coordination chemistry, polytopic linkers and terminated ligands (F-, OH- and H_2O, among others), which make it possible to design an almost infinite variety of MOF structures. Polytopic organic ligands are generally nitrogen-, and oxygen-donor rigid molecules such as bipyridine and multicarboxylic acids, respectively. The diversity in terms of ligand is infinite. For the latter, we account for more than 50 commercially available multidendate ligands. The most simple and frequently used is the terephtahlic acid (1,4-dicarboxylicbenzyl acid). Most frequent

SBUs observed are binuclear clusters called $M_2(CO_2)_4$ "paddle-wheel" such as found in MOP-1 [37], $Cu_3(btc)_2$ (HKUST-1) [38] and μ^4-oxo $M_4O(CO_2)_6$ [39, 40] such as those found in IRMOF series (Figure I-7).

The interest of this ''node and spacer'' approach is that it offers a route to functional networks with tuneable pore size [40] [31]. The strategy for increasing the pore size and volume involves the expansion of known structure types through the use of elongated but geometrically equivalent organic bridging ligands. For the IRMOF series based on MOF-5 structure, the pore size can be varied from 3.8 Å to 28.8 Å by selecting linkers of various sizes [40] (Figure I-6).

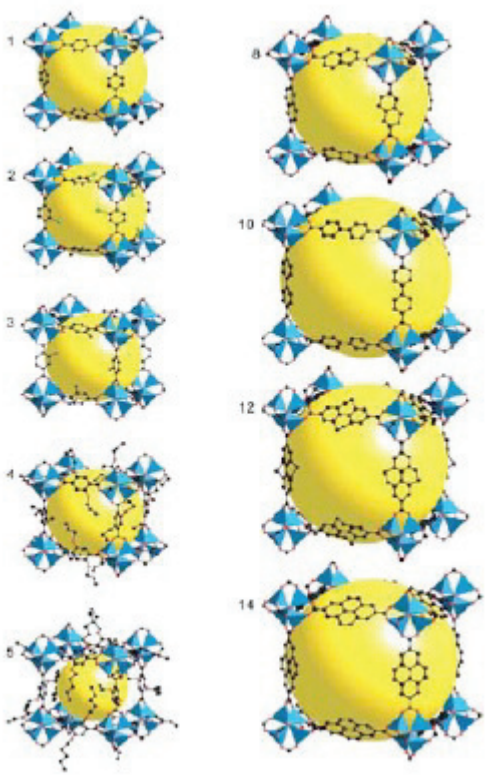

Figure I-6 : Example of 3D isoreticular compounds (IRMOFs)

Other examples are [Cu(OOC-R-COO)teda] (teda = triethylenediamine) for which the pore size can be monitor between 7 and 11 Å [41], the IRMOP series [42], the MIL-53 series [43], the MIL-88 series [44], the MOF-69 series [45] and UiO-66/68 [46].

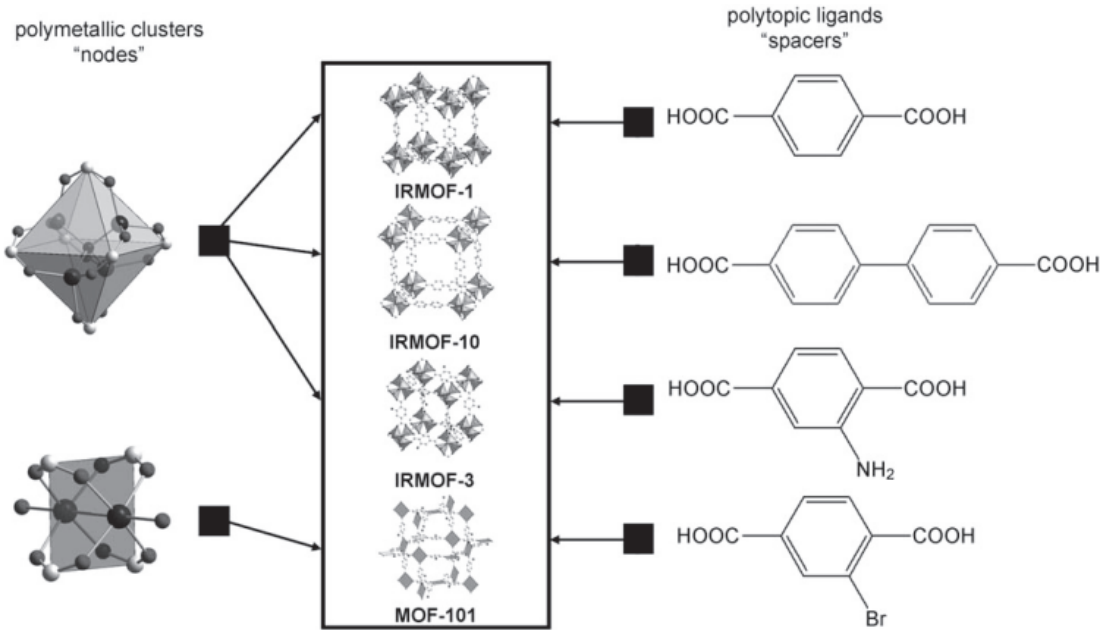

Figure I-7 : Self-assembly of polymetallic clusters [μ^4-oxo $M_4O(CO_2)_6$, $M_2(CO_2)_4$ paddlewheel] and organic linkers yielding Metal-Organic Frameworks[39, 40]

MOF materials can be classified into different families according to the dimensionality of the inorganic framework [32] (Figure I-8):

- 0D "inorganic" clusters or isolated metal ions connected by bridging organic polytopic ligands such as MOF-5 and HKUST-1.
- 1D inorganic chains such as MIL-53
- 2D inorganic layers that are separated by organic pillars such as MIL-71
- 3D structures such as MIL-73 with 3D porous channels

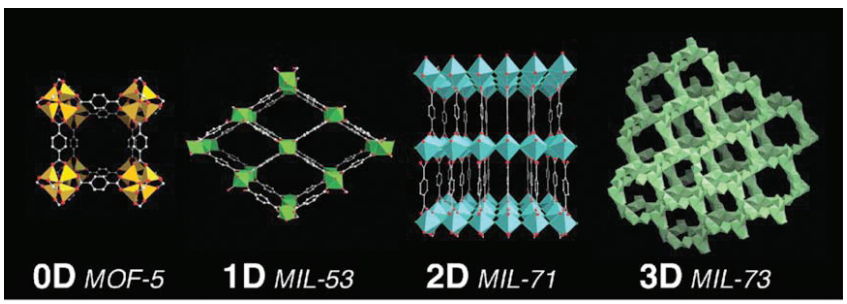

Figure I-8 : Examples of structural dimensionality

MOFs show two main pore topologies (Figure I-9):

- 3D porous channel: ZIF-8, MOF-5, HKUST-1, MIL-101…
- 1D porous channel: CPO-27, MIL-53, MIL-68... They have systems of one-dimensional channels that do not intersect, which leads to diffusion limitations.

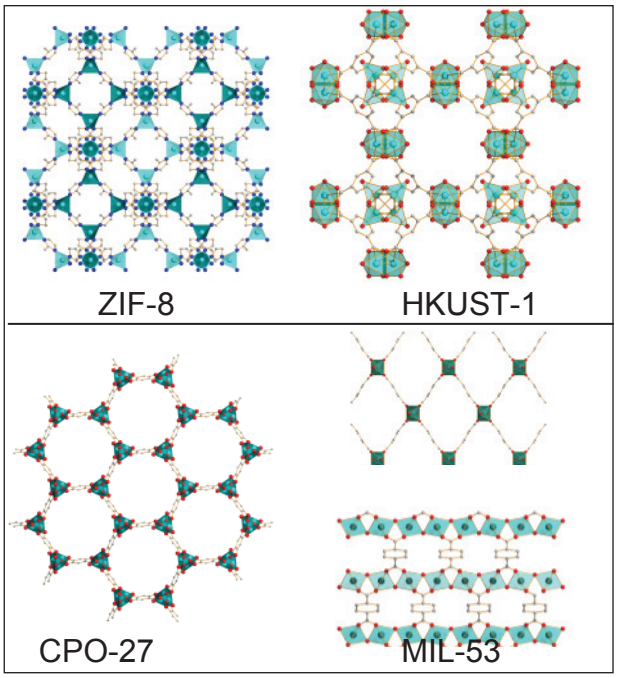

Figure I-9 : Comparison between 3D/1D porous channels

I.3.2 Bridging the pore size between zeolites and mesoporous materials

The reduced pore size of zeolites is usually underlined as a key limitation to addressing the catalytic transformation of large molecules such as polyaromatics, carbohydrates and glycerides. Intense efforts have been devoted to the discovery of aluminophosphates and zeolites with very large pores, such as VPI-5 [47], IM-12 [48], ITQ-33 [49] and ZSM-5 [50]. On the other hand, mesoporous silicate materials such as MCM-41 have pores too large to impose confinement effects for enantioselective catalysis, for example.

MOF materials actually bridge the gap between these two porous material types, since ultramicroporous to mesoporous MOFs have been reported, as shown in the arbitrary selection in Figure I-10. The size of selected potential guests is also shown in the top axis (MTBE = methyl tert-butyl ether; TIPB = 1,3,5-triisopropylbenzene). The abundant choice of

structure associated with pore size tunability is a great opportunity for designing MOFs with pore openings appropriate for generating shape selectivity. In addition, the very large cavities of isoreticular MIL-101 (34 Å) can, in principle, address triglycerides and small protein substrates [51].

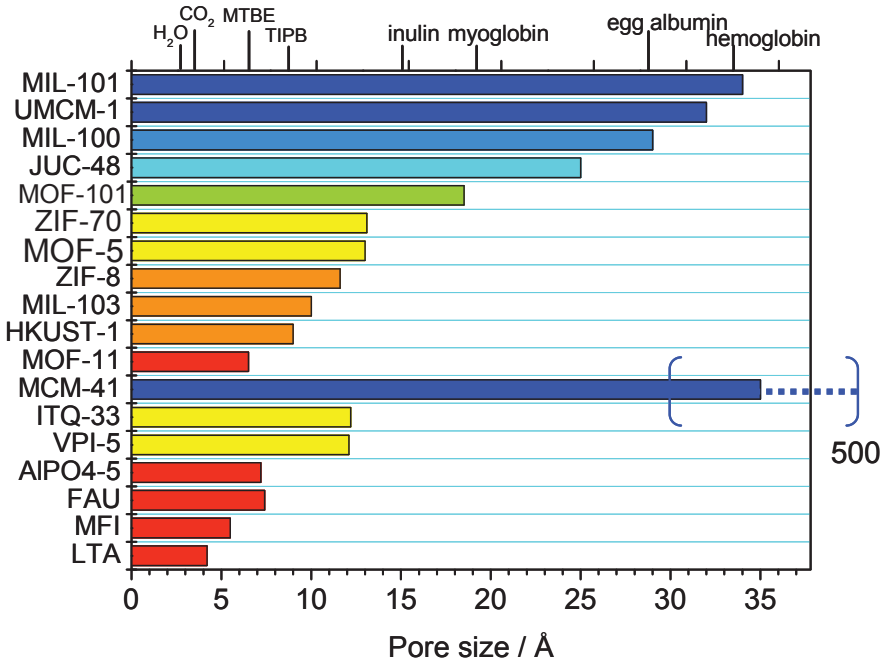

	Number of cages	Pore size (Å)	Window aperture (Å)
MIL-101	2	29-34	12-14,7*16
UMCM-1	2	14*17-27*32	14*17-27*32
MIL-100	2	25-29	5-8.6
JUC-48	1	25*28	25*28
MOF-101	1	19-21	12-14
ZIF-70	1	15.9	13.1
MOF-5	1	12	8
ZIF-8	1	11,6	3.4
MIL-103	1	10	10
HKUST-1	2	5,3-11	6.9
MOF-11	1	6*14	6
MCM-41	1	20-500	20-500

ITQ-33	1	13	13
VPI-5	1	12-13	12-13
AlPO4-5	1	7,3	7,3
FAU	1	7.4	7.4
MFI	2	5,1*5,5-5,3*5,6	5,1*5,5-5,3*5,6
LTA	1	4,1	4,1

Figure I-10: Cavity size and window aperture of porous MOFs (Å) compared with standard aluminosilicates and aluminophosphates. (Aluminosilicate = MCM-41, ITQ-33, VPI-5, FAU, MFI, LTA, aluminophospate = AlPO4-5).

I.3.3 MOFs synthesis: acid/base equilibrium

The thermodynamics and the species involved in the reaction synthesis of MOF-5 (IRMOF-1) (proof of concept) are depicted in Figure I-11. The solvated cations and anions, neutral metal-organic clusters and the formed solid coexist in the reaction medium. Without the addition of a base (solvothermal method), the kinetics is usually slow, which is a key advantage for obtaining monocrystals [52]. By adding concentrated aqueous acid solution onto IRMOF-1, the solid is completely dissolved. This method is commonly used in the context of liquid NMR to characterize organic molecules that can be entrapped or grafted into MOF networks. In contrast, the equilibrium of the reaction is, in principle, shifted to the formation of the solid when a base is added to the reaction mixture. This way by precipitation is favourable for quick generation of a large number of nuclei [53].

Nevertheless when DMF is used in solvothermal conditions, basic agents are generated in situ over the course of the reaction, which should therefore lead to higher yield and faster kinetics [54].

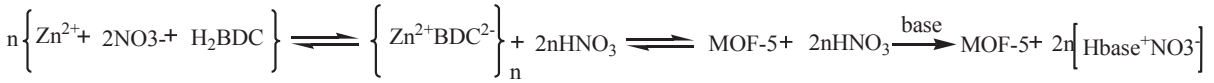

Figure I-11: Shift of the reaction equilibrium of MOF-5 by addition of a base to trap the formation of liberated acid.

It should be mentioned that among the numerous factors to consider for the synthesis of a new metal–organic framework, the most important is the maintenance of the integrity of the building blocks. It has often been observed that minor changes in concentration, solvent polarity, pH, or temperature lead to poor quality crystals, reduced yields or the formation of new phases.

Furthermore, through the use of high-throughput methods, solvothermal reactions of $FeCl_3$ and 2-aminoterephthalic acid in protic as well as aprotic reaction media were studied. It has been demonstrated that the nature of the reaction media, the concentration of the starting mixture and the temperature have impact on the structure formation of MIL-53, MIL-88 and MIL-101 [55].

The principal weakness of MOFs may lie in their lower thermal, hydrothermal and chemical stability compared to that of oxides. It is now well established that IRMOF compounds based on Zn_4O clusters are very moisture sensitive and are readily transformed to MOF-69 type [56, 57], with an accompanying drastic decrease in surface area.

Unfortunately, stability data are usually lacking in the open literature. Moreover, when reported, they are often obtained under different conditions (air or neutral atmosphere, different temperature) and by different means (TGA or thermodiffraction), which makes it barely feasible to compare these data. Usually, from TGA, the thermal stability of carboxylate- and imidazolate-based MOF is limited to 300 - 400°C in air, though this does leave the door open to most catalytic applications [58]. Low *et al.* also compared different MOFs in a "steam stability map" depicted in Figure I-12 [59].

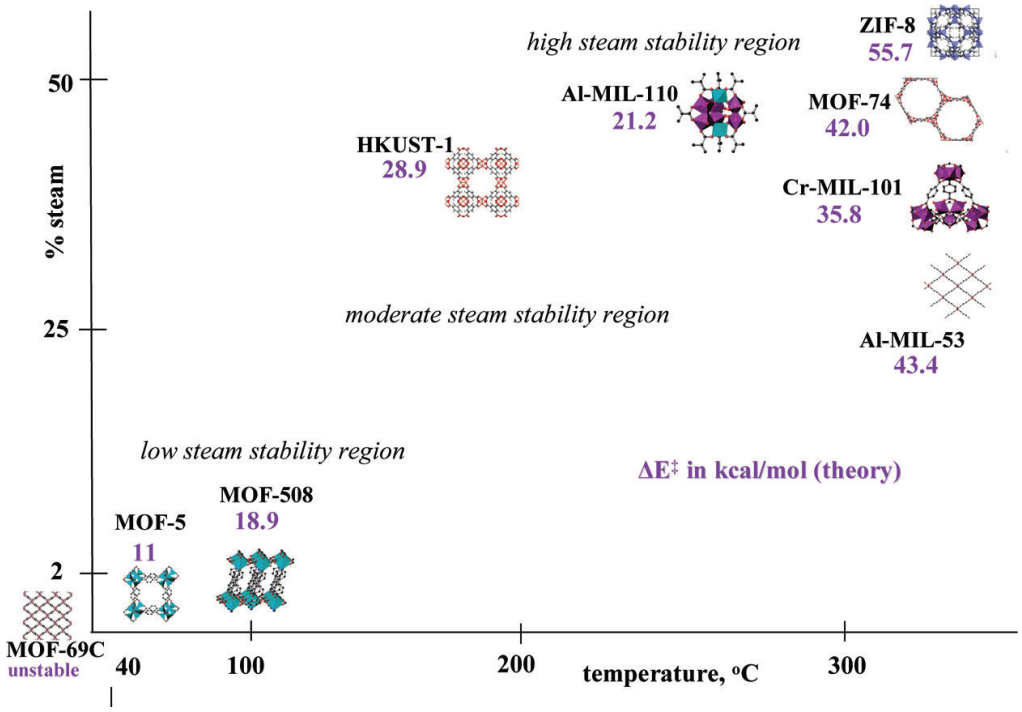

Figure I-12 : Steam stability map for different MOFs

I.3.4 Opportunities for catalysis

MOF materials can be regarded as a "new" class of catalytic materials at the frontier between zeolites and enzymes when they combine isolated polynuclear sites, guest-host dynamic responses and hydrophobic cavity environment. These points are further developed in the following.

- Isolated polynuclear sites

Cooperative catalysis involving two metal ions is a common feature in enzymatic systems. The resulting cooperative activation of both reaction partners leads to enhanced reactivity and more specific control, thus making enzymes very powerful catalysts. Some well-known examples of dinuclear and higher nuclearity metal sites in biological systems include: the diiron enzymes soluble methane monooxygenase, dicopper of cytochrome c oxidase and tricopper oxidases [60]. By analogy, polynuclear clusters are found in the 0D coordination polymers such as binuclear copper clusters called $M_2(CO_2)_4$ paddle-wheel in MOP-1 [37] and

$Cu_3(btc)_2$ (HKUST-1) [38] or trinuclear units $Fe_3O(CO_2)_6$ MIL-88 [44], IRMOP-51 [42]. Thus, clearly 0D MOFs possess accessible bio-mimetic catalytic centres.

- "Molecular recognition"

Confining substrates within the micropores of solid material can, in principle, induce or enhance (enantio)selectivities beyond those observed in homogeneous solutions. In enzymatic systems, protein units have a high affinity for specific substrates whereas molecular recognition effects are limited in zeolites due to the rigid structure [61]. Here again, MOFs materials bridge the gap between zeolites and enzymes, indeed many hybrid frameworks contain organic parts that can rotate as a result of stimuli such as light and heat [62, 63]. This is the case for frameworks such as IRMOF, MIL-53 and $[Zn_2(1,4\text{-ndc})_2(dabco)]_n$.
The MIL-53 is another good illustration of the flexibility of MOFs. The structure may shrink or expand according to the polarity of guest molecules. When water or CO_2 is adsorbed, H-bonds are formed with μ_2-OH from the framework, resulting in a shrinking of the diamond-type channel [64] (Figure I-13).

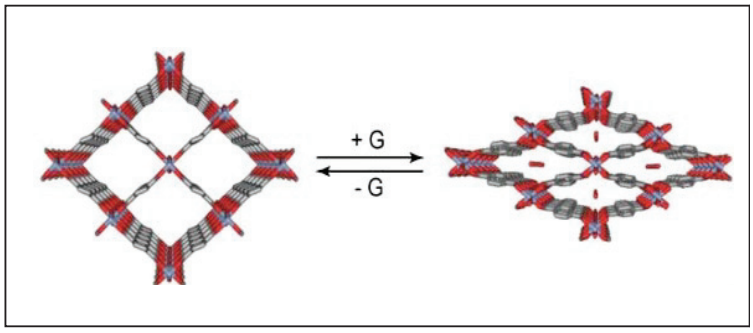

Figure I-13: Pore shape response upon guest (G) adsorption-desorption

- Hydrophobicity-hydrophilicity balance

Specific hydrophilic/hydrophobic properties might control adsorption of reagents, intermediates and products, and thus drive catalytic selectivity. The hydrophobic-hydrophilic properties of a few MOF have been investigated by water adsorption measurements [65]. HKUST-1 is highly hydrophilic, MIL-101 and MIL-100(Fe) moderately hydrophilic, whereas

ZIF-8 is highly hydrophobic. Unlike zeolites, in MOFs, different pore systems with different levels of polarity can coexist within the same structure [66].

I.4 Conclusions

The unique structural and dynamic features characteristics of MOFs described above set them apart from other traditional porous materials. Zeolites and ordered mesoporous silicia are fully inorganic and thus lack synthetic flexibility and structural diversity/tailorability.
Furthermore, pore-size tunable MOFs are regarded as bridging the gap between zeolites and mesoporous silica and are very suitable for catalysis. The low thermal stability of MOFs is certainly a limiting factor for vapor phase reactions carried out at temperatures above 300 °C.

II. State of the art of acido-basic catalytic MOFs

II.1 Context

Biphasic "liquid-solid" catalysis has been very familiar in MOF-based catalysis since the first report of cyanosilylation of aldehydes by a layered MOF with the formula Cd(4,4'-bipyridine)$_2$(NO$_3$)$_2$ [67]. A considerable amount of catalytic reactions over MOFs have been reported, mainly, acid/base reactions [68, 69], hydrogenations [70, 71], oxidations [72, 73, 74] and photocatalysis [75]…
Since this topic has been systematically reviewed by several groups [76, 77, 78, 79], we will not give details for each catalysis reaction but we focus here on the acido-basic catalysis.

II.2 Lewis Acid Catalysis

The porous-framework material HKUST-1 [Cu$_3$(btc)$_2$(H$_2$O)] [38] contains large cavities (windows diameter of 6.9Å) and has accessible copper clusters. It is an outstanding demonstration of the concept of Lewis acid MOF [80, 81]. Indeed, the coordinated water molecules are easily removed by heat treatment at 383 K, leaving open Cu(II) sites directly accessible to a reactant diffusing within the porous network (Figure II-1).

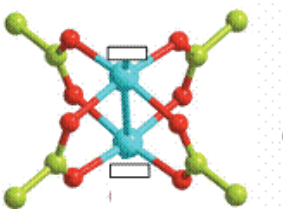

Figure II-1 : Accessible copper clusters (Cu = blue, O = red, C = green)

Various model reactions for characterizing Lewis acidity were tested: benzaldehyde cyanosilylation [81], isomerization of alpha-pinene oxide, citronellal cyclization, and rearrangement of ethylene acetal of 2-bromopropiophenone [80]. HKUST-1 was shown to be quite selective, which is typical of hard Lewis acid centers. Although the solid does not show Brønsted sites when properly activated, protic solvents may create Brønsted acidity, which can explain variations in properties when different solvents are used [82]. On the other hand, strongly coordinating solvents such as THF can bond the acidic Cu sites and thus prevent Lewis type reactions from taking place [81].

Very recently, HKUST-1 exhibited also highly improved catalytic activity as compared with the molecular sieves, H-BEA and (Al)SBA-15 in the Friedländer reaction between 2-aminobenzophenones and acetylacetone under mild reaction conditions [83].

Henschel and co-workers [84] also evaluated the behavior of MIL-101 $[Cr_3F(H_2O)_2O(bdc)_3]$ with Cr(III) sites (Figure II-2) as a cyanosilylation catalyst and the group observed that MIL-101 is more active than HKUST-1 for the cyanosilylation of aldehydes (greater Lewis acidity of Cr(III) vs Cu(II)).

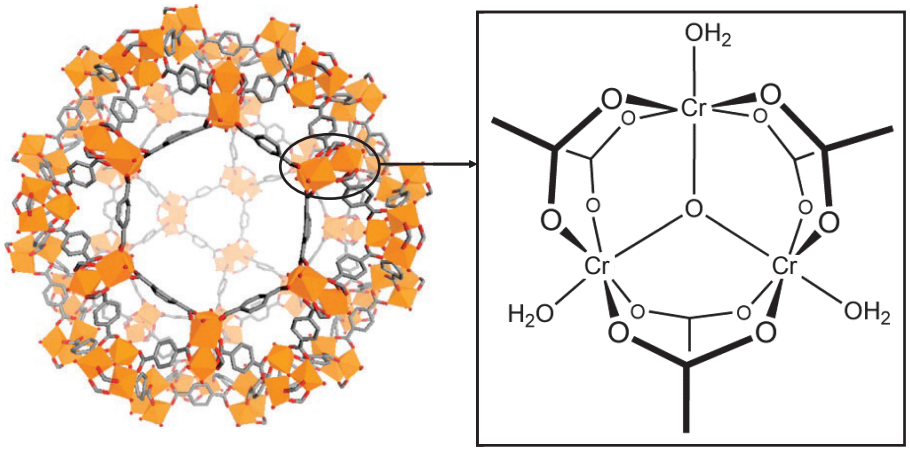

Figure II-2: A crystallographic illustration of the pore structure of MIL-101. (Cr = orange polyhedron; C = gray segment; O = red segment).

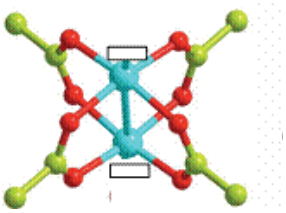

Figure II-1 : Accessible copper clusters (Cu = blue, O = red, C = green)

Various model reactions for characterizing Lewis acidity were tested: benzaldehyde cyanosilylation [81], isomerization of alpha-pinene oxide, citronellal cyclization, and rearrangement of ethylene acetal of 2-bromopropiophenone [80]. HKUST-1 was shown to be quite selective, which is typical of hard Lewis acid centers. Although the solid does not show Brønsted sites when properly activated, protic solvents may create Brønsted acidity, which can explain variations in properties when different solvents are used [82]. On the other hand, strongly coordinating solvents such as THF can bond the acidic Cu sites and thus prevent Lewis type reactions from taking place [81].

Very recently, HKUST-1 exhibited also highly improved catalytic activity as compared with the molecular sieves, H-BEA and (Al)SBA-15 in the Friedländer reaction between 2-aminobenzophenones and acetylacetone under mild reaction conditions [83].

Henschel and co-workers [84] also evaluated the behavior of MIL-101 [$Cr_3F(H_2O)_2O(bdc)_3$] with Cr(III) sites (Figure II-2) as a cyanosilylation catalyst and the group observed that MIL-101 is more active than HKUST-1 for the cyanosilylation of aldehydes (greater Lewis acidity of Cr(III) vs Cu(II)).

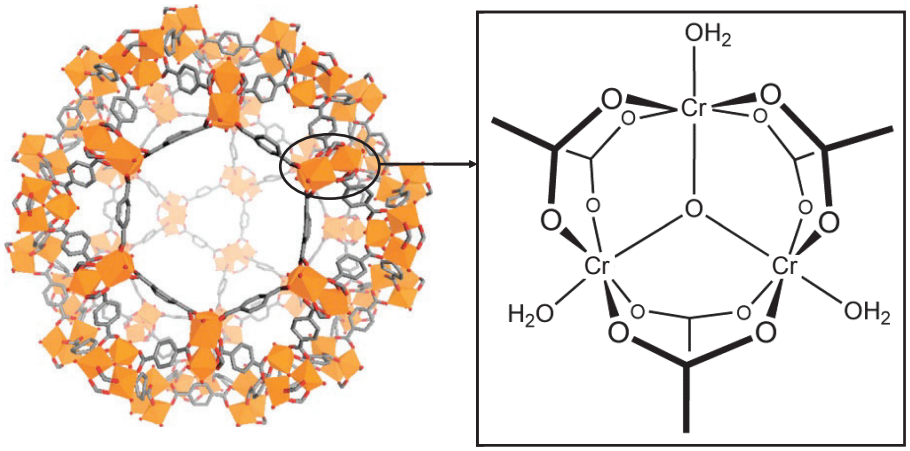

Figure II-2: A crystallographic illustration of the pore structure of MIL-101. (Cr = orange polyhedron; C = gray segment; O = red segment).

The Lewis-acid catalyzed cyanosilylation of aromatic aldehydes has also been carried out by Horike and co-workers using $Mn_3[(Mn_4Cl)_3BTT_8(CH_3OH)_{10}]_2$ with Mn(II) sites and showing high conversion yields and good substrates-size selectivity [68]. In principle, either of the two types of Mn(II) sites could function as a catalyst.

In another report, a 2D MOF containing substrate-accessible highly Lewis acidic In(III) has been used to catalyze the acetalization of benzyaldehyde with trimethyl orthoformate [85].

Lewis acid solids can also perform selective oxidations on Lewis centers as Ti-silicate (TS-1) selectively oxidizes alkenes into the corresponding epoxides. Recently, Cu^{2+} trinuclear networks showed high activity and selectivity for the peroxidative oxidation of cyclohexane to the corresponding alcohols and ketones ($MeCN/H_2O/HNO_3$ media) [86]. The structure is based on a stable $Cu_3(\mu_3\text{-OH})(\mu\text{-pyrazole})$ SBU for which the tetracoordinated metal is readily accessible as axial sites. Its activity is comparable to that of the best molecular systems, such as copper and iron complexes (32% yield and TON of 44). Although the mechanism is still unclear, these trinuclear copper networks are the most efficient catalysts reported so far for the mild peroxidation of alkanes.

II.3 Brønsted Acid Catalysis

Horcajada and co-workers have reported the catalytic activity of two different MIL-100(Fe, Cr) for Friedel–Crafts benzylation [87]. Despite their identical $[M_3OF_{0.85}(OH)_{0.15}(H_2O)_2(btc)_2]$ structures, the Fe^{3+} catalyst shows much higher catalytic activity than the Cr^{3+} catalyst and even surpasses HBEA and HY zeolites. As shown by CO chemisorption at low temperature, MIL-100(Cr^{3+}) shows Cr-OH Brønsted sites of medium acidity and several types of Lewis centers [82, 88].

Ravon *et al*. have recently tested pure Brønsted MOF materials with structurally well-identified hydroxyl centres, namely Ga(OH)(bdc) and $Zn_3(OH)_2$(bdc), also known as IM-19 and MOF-69C [89], respectively. It has been anticipated that bridging OH groups would generate a Brønsted-type acidity such as that found in the H form of zeolites [90] (Figure II-3).

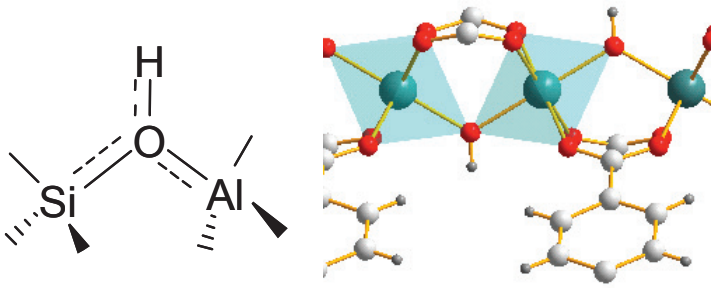

Figure II-3 : Analogy between a Brønsted acidic site on a H-form zeolite from [90] (left) and a MOF with a bridging hydroxyl between cations in MIL-53 (right)

IM-19 is the Ga form of the parent structure MIL-53, which is built from infinite chains of corner-sharing $MO_4(\mu_2\text{-}OH)_2$ ($M = Al^{3+}$, Cr^{3+}) [91], while MOF-69C consists of chains of $ZnO_2(OH)_2$ tetrahedron and $ZnO_4(OH)_2$ octahedron with μ_3-OH as the bridging species [45]. IM-19 shows full conversion for toluene terbutylation at 50°C temperature (TON = $220h^{-1}$ at 100°C) [92], while MOF-69C is 100% shape selective for the alkylation of large polycyclic aromatics such as biphenylene [93]. In contrast, MIL-53(Al) was not catalytically active in the alkylation of biphenyl [94]. Experiments combined with molecular modeling in the OH region let them conclude that the Brønsted acidity, even if very mild, follows the order: MIL-53(Al) < IM-19.

Finally, the Rosseinsky group showed that the protonation of a chiral copper-containing MOF, which is obtained by solvothermal methods from amino acid (L- or D-aspartate) and dipyridyl as struts, introduces a Brønsted acid center and facilitates the ring-opening methanolysis of a small cavity epoxide at up to 65% yield [74]. (Figure II-4)

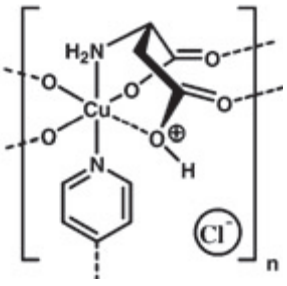

Figure II-4: Coordination environment of the protonated MOF

II.4 Base Catalysis

A few amino-functionalized MOFs have been obtained by direct self-assembly. Solvothermal synthesis using 2-aminoterephthalic acid with zinc nitrate yield IRMOF-3 [40], which shows conversion for the Knoevenagel reaction of ethylcyanoacetate and ethylacetoacetate with benzaldehyde [95].

Hasegawa and co-workers have also reported the synthesis of a catalytic MOF having the formula $[Cd(4\text{-btapa})_2(NO_3)_2]$ (btapa = 1,3,5-benzene tricarboxylic acid tris[N-(4-pyridyl)amide]) (Figure II-5) with accessible amide functionalities and the researchers showed that the amides are able of base-catalyzing the Knoevenagel condensation of benzaldehydes with malononitrile [69].

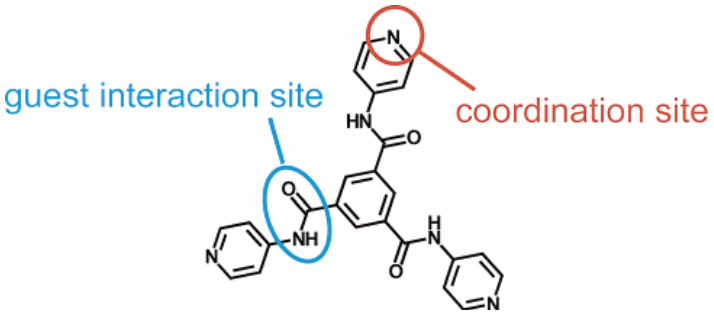

Figure II-5 : 1,3,5-Benzene Tricarboxylic Acid Tris[N-(4-pyridyl)amide] (btapa)

In an interesting alternative approach, Hwang and co-workers [96] were able to modify the interior of MIL-101 via Cr(III) coordination of one of the two available nitrogen atoms of ethylenediamine molecules (Figure II-6). The free non-coordinated ends are used as Brønsted basic catalyst, again for Knoevenagel condensation of benzaldehydes.

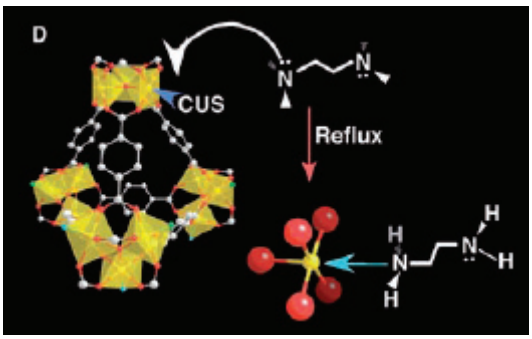

Figure II-6 : Surface functionalization of the dehydrated MIL-101 through selective grafting of amine molecules (i.e. ethylenediamine) onto coordinatively unsaturated sites

Using a pyridine-functionalized derivative of tartaric acid and a Zn(II) source, Seo and co-workers were able to synthesize a 2D MOF called POST-1 (Figure II-7). The trinuclear SBU [$Zn_3(\mu_3$-O)(tartrate)] interconnected through coordinating Zn ions and some pyridyl groups, generates a hexagonal porous system. Other pyridyl groups point toward the center of large 1D chiral channels (13Å) which are found to catalyze transesterification reactions [97].

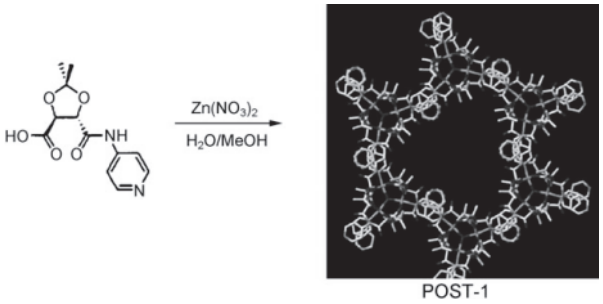

Figure II-7 : Formation of POST-1

Very recently, the zeolite imidazolate framework ZIF-8 is shown for the first time to be able to catalyze transesterification reaction oil with significant activity likely due to the presence of Zn_{II} species as Lewis acid sites, as well as Brønsted acid sites (NH groups), together with basic sites (OH groups and N- moeties mainly), located at the external surface [98]. This work reveals the interest of MOFs for this reaction.

With the exception of POST-1, there are few examples of MOF materials containing free Lewis bases that are accessible for catalytic applications. This might be due to experimental issues in the synthesis of free nitrogen-donating MOF materials. Indeed, when nitrogen-containing aromatic moieties in carboxylic-based ligands (such as pyridine/imidazole dicarboxylates [99]) are used, the N electronic doublet usually strongly coordinates to the metal ion and is therefore not available for substrate activation.

Thus, the development of others functionalization methods are required to avoid the coordination chemistry of N-donating ligand with the assembly of the SBU.

When self-assembly fails for the synthesis of MOFs with functional linkers, the post-functionalization of a parent MOF appears to be a very valuable alternative. This consists in modifying the organic part of the MOF by a chemical reaction which takes place within the porous framework (Figure II-8).

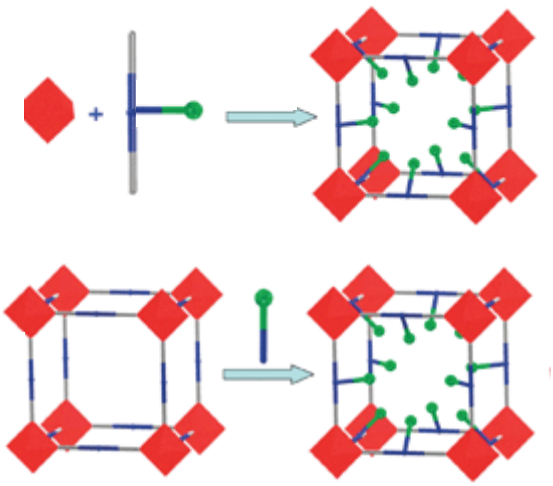

Figure II-8 : Concept of self-assembly and postsynthetic modification by covalent bond

In this case, the parent MOF must possess accessible reactive functions.

III. Design of Functional MOFs by Postsynthetic Modification

Different routes have been developed to access post-functionalized MOFs based on different chemical interactions while keeping the same the native structure. These transformations may involve non covalent interactions, coordination or covalent bonds.

III.1 Postsynthetic modifications of MOFs by encapsulation

Non-covalent modification of metal-organic frameworks commonly implies guest exchange or removal from their cavity. The unique host–guest chemistry of MOFs can be used to modify or generate new properties by loading the cavities with functional molecules or metal nanoparticles without compromising the structure integrity.

Such an approach has recently been undertaken to encapsulate inorganic clusters such as metallic nanoparticles, polyoxometalates and molecular catalysts.

Nanosized metallic particles dispersed in sharply microporous metal-organic frameworks are of a great interest in the field of catalysis. Chemical vapor infiltration of organometallic precursors was shown to be an appropriate method for very high loading of nanoparticles based on Pt, Au, Pd [100, 101] and Ru [102] into the porosity of MOF-5. The Pd-based catalyst

was found to be active for the CO oxidation and olefin hydrogenation. More recently, chemical-based methods have been developed using wetness impregnation. Sabo *et al.* reported composite of Pd-supported MOF-5 prepared by impregnation showing a catalytic activity superior to that found for Pd/C for the hydrogenation of various alkenes and esters in three-phase reactions [57].

The possibility of encapsulating Keggin-type heteropolyoxoanions (HPAs), and particularly 12-tungstophosphoric acid (HPW) in HKUST-1 [103, 104, 105] and MIL-101 [106, 107] appears as an attractive pathway to exploit the acid catalytic activity of isolated HPA species. Recently, Wee and co-workers show that HPW/$Cu_3(BTC)_2$ nanomaterial outperformed ultrastable zeolite Y in the esterification reaction of acetic acid with 1-propanol [108].

Finally, Kokrick and co-workers encapsulate large Metal phthalocyanine complexes (MPc) in cavities of MIL-101 for the selective oxidation of tetralin into 1-tetralone [109].

Nevertheless, concerning the irreversible in-situ encapsulation, the size of the guest is crucial as far as it has to perfectly fit with cavity of the MOF, whereas the post-impregnation treatments (reversible) can lead to the leaching of the guest specie.

III.2 Post-functionalization of MOFs based on coordination chemistry

There are two general approaches for coordinate covalent modifications.

In the first scenario, coordinating ligands such as alkylamines or pyridines can be introduced into the framework to bind the metal nodes of the SBUs where unsaturated metal sites are present [96, 110, 111] (Figure II-6).

In the second common scenario, the organic linker of the MOF may have metal binding groups (e.g., –OH) that do not play a role in the framework structure, and hence can be metallated in a PSM manner. For example, Wu and coworkers [112] prepared a MOF from Cd^{2+} and (R)-6,6′-dichloro-2,2′-dihydroxy-1,1′-binaphthyl-4,4′-bipyridine and obtained a structure with free, uncoordinated hydroxyl groups that could be metallated with $Ti(O^iPr)_4$ (Figure III-1).

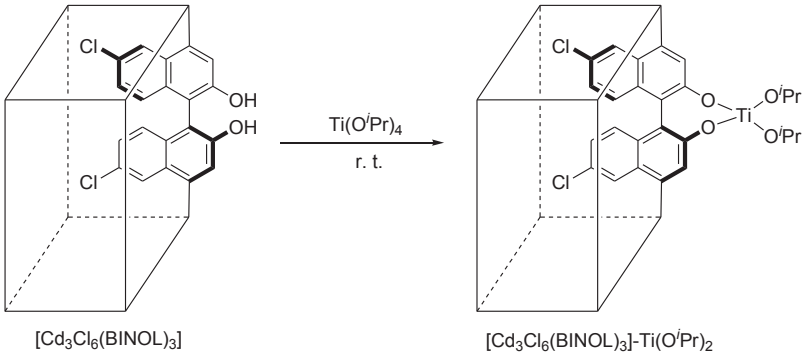

Figure III-1 : MOF-supported chiral titanium complex

Unfortunately, this coordination chemistry method is restricted to robust MOFs presenting free coordination sites on the ligands or on the metal nodes not frequently found.

III.3 Post-functionalization of MOFs by covalent bond

The first example of post-functionalization of MOF by covalent bond appeared in 2000 with Seo *et al.* [97] where they treated a MOF called POST-1 in DMF with excess of CH_3I to convert the free pyridil group within the MOF to N-methylpyridium ions (Figure III-2).

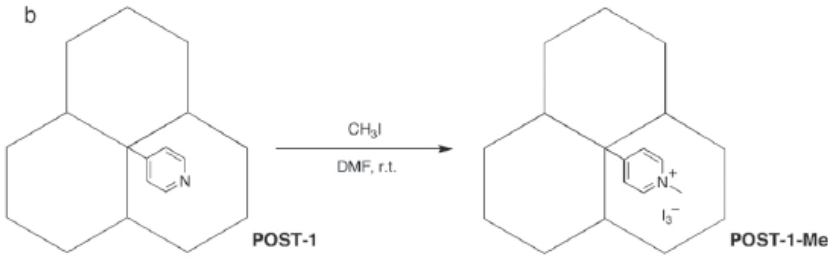

Figure III-2 : Earliest report of covalent postsynthetic modification of MOF

Although being challenging, the application of classical organic chemistry to MOFs, having on their walls reactive groups such as amino in the cases of IRMOF-3 [40], DMOF-1-NH_2 [113], UMCM-1-NH_2 [113, 114, 115], MOF-LIC-1 [116], MIL-53-NH_2 [55], MIL-88-NH_2 [44] and MIL-101-NH_2 [55] or formyl in ZIF-90 [117] or hydroxyl in Zn_2(TCPB)(DPG) [118] (TCPB = 1,2,4,5-tetrakis(4-carboxyphenyl)-benzene; DPG=meso-1,2-bis(4-pyridyl)-1,2-ethanediol), has been envisaged by many research teams. They succeeded in creating covalent bonds into MOFs

following different approaches based on the reactivity of amino- or formyl-or hydroxyl - containing MOFs to form amides or imines or carboxylic acid, some examples even reported sophisticated "click chemistry" applied to MOFs when other, rather than the modification of the organic linkers, dealt with the reactivity of bridging hydroxyl groups.

III.3.1 Chemical modification by amide coupling

Among simple organic reactions involving an amino substituent, the formation of an amide by reaction with a carboxylic acid or an anhydride or an isocyanate were the first envisaged.
IRMOF-3 was quantitatively transformed into IRMOF-3-AM1 with acetic anhydride in a single-crystal-to-single-crystal fashion [119]. Powder X-ray diffraction (PXRD) revealed that cristallinity is well-retained and liquid ^{1}H NMR and ESI-MS analysis after digestion validates a functionalization rate of 85%. Covalent transformation of IRMOF-3 was subsequently expanded to reactions with larger acid anhydrides ($O[CO(CH_2)_nCH_3]_2$,n = 1-18), where the degree of modification strictly follows an inverse correlation to the size of the anhydride (less than 10% for n=18) [120]. Most recently, the Cohen group has demonstrated the generality of their approach by working on additional MOF designated DMOF-NH_2 , UMCM-NH_2 [113] and UiO-66-NH_2 [121, 122] with various anhydrides [123] (Figure III-3). Wang *et al.* reported also “tandem” modification strategies. In the first strategy, IRMOF-3 was consecutively modified with two different anhydrides, namely, crotonic anhydride and acetic anhydride. In the second strategy, IRMOF-3 was treated with crotonic anhydride and bromination reaction was targeted [124].

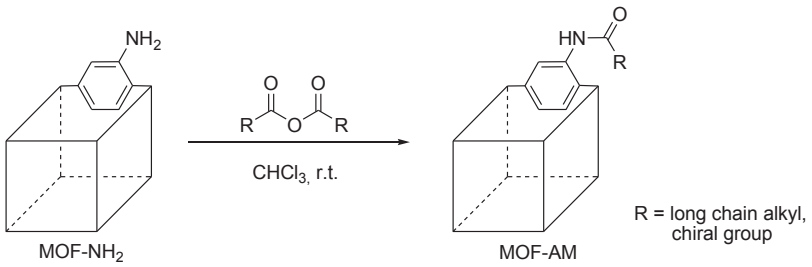

Figure III-3 : Scheme of representative PSM reactions of NH_2-bdc based MOF with various anhydrides

Finally, post-modification of IRMOF-3 was further investigated using isocyanates where different isocyanates were grafted with percent conversions varying from no reaction (*tert*-butyl isocyanate) to 99% (trimethylsilyliosocyanate) [125]. Volkringer *et al.* transformed recently the free amino groups of MIL-53-Al-NH_2 into reactive iso(thio)cyantes using diphosgene or thiophosgene (Figure III-4). Attempt to modify IRMOF-3 and UMCM-1-NH_2 with phosgene reagents resulted in the destruction of these MOFs due to the formation of HCl as a byproduct. Therefore, MIL-53-Al-NH_2 was used for these reactions because of its greater chemical stability (particularly with respect to acid) when compared with zinc-carboxylate MOFs [126]. Hence, MIL-53-Al-NH_2 can be successfully modified with formic acid [127].

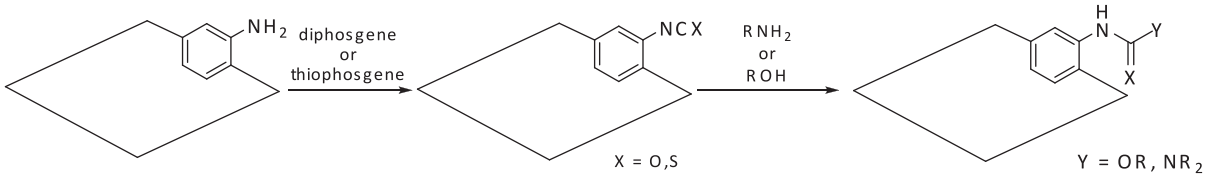

Figure III-4 : Transformation of MIL-53(Al)–NH_2 into MIL-53(Al)–NCX (X=O or S) using phosgene reagents, followed by sequential reactions with amines and alcohols to produce (thio)urea and (thio)carbamate-bearing MILs.

Moreover, a study of Gamez and co-workers showed that MOF-LIC-1 prepared from Gd(III) and NH_2-bdc has been modified with two different functionalities (ethylisocyanate and acetic acid). It has to be mentioned that MOF-LIC-1 is more degraded in the presence of acetic acid than in ethylisocyanate [116].

These methods developed so far are nevertheless not very generically applicable, since they can either be applied only to the most robust MOFs that can withstand relatively harsh conditions or required the synthesis of asymmetric anhydrides.

III.3.2 Chemical modification by imine condensation

Another approach of the amines reactivity is their condensation with an aldehyde to form the corresponding imine. Rosseinsky *et al.* choose this strategy and reported the modification of IRMOF-3 by reaction with salicylaldehyde (formally named 2-hydroxybenzaldehyde) [128]. Several spectroscopic analyses showed a partial modification of the MOF with around 13 %

conversion. The reaction produced a functionalized MOF having both free imine and hydroxyl moieties in its cavity, making it a good candidate as ligand for metal complexation. Doonan and coworkers followed a similar strategy to modify the UMCM-1-NH_2, built from both NH_2-bdc and btb (4,4',4''-benzene-1,3,5-triyl-tribenzoate) ligands, using the 2-pyridinecarboxaldehyde to achieve the formation of a MOF containing both imine and pyridine in its cavity in 87 % yield, the crystallinity and the porosity remaining after modification [115] (Figure III-5). More surprisingly, Doonan *et al.* reported exactly the same surface area for the both starting and modified MOFs (3200 m²/g).

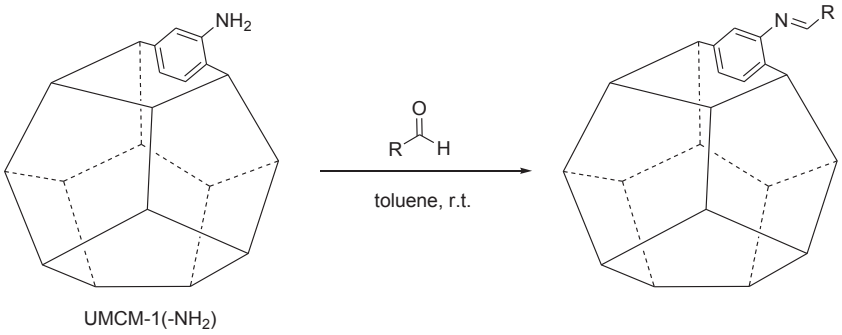

Figure III-5 : Condensation of an aldehyde to the amino moiety of the UMCM-1-NH_2.

In a reverse way, imine condensation can also occur between a formyl group on the MOF and an amine added as reagent. Morris *et al.* used also that approach to modify his ZIF-90 containing imidazolate-2-carboxaldehyde as linker [117]. The presence of the free aldehyde functionality inside the framework allows the covalent modification of ZIF-90 with ethanolamine to form the corresponding imine (Figure III-6).

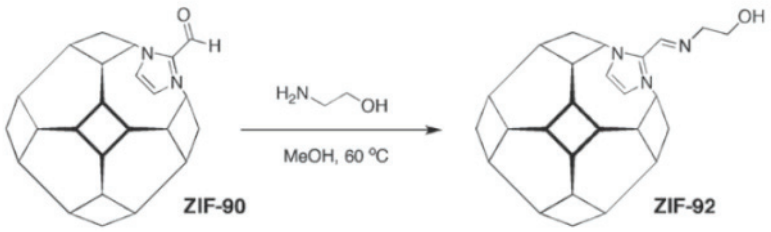

Figure III-6 : Condensation of an amine to the formyl moiety of the ZIF-90.

However, the generation of water molecules during imine condensation requires moisture resistant frameworks.

III.3.3 Chemical modification by ring opening reactions

Britt and coworkers [129] carried out interesting ring opening reactions with IRMOF-3 to generate acid (sulfonate) and basic (alkylamine) groups. These groups were introduced by treating IRMOF-3 with either 1,3-propanesultone or 2-methylaziridine in $CHCl_3$ at 45°C (Figure III-7). For the reaction with 1,3-propanesultone, 57% of the amine sites in IRMOF-3 were converted to the sulfonate group, as gauged by elemental analysis. **Nevertheless, in this work, all attempts to reproduce these results have failed.**

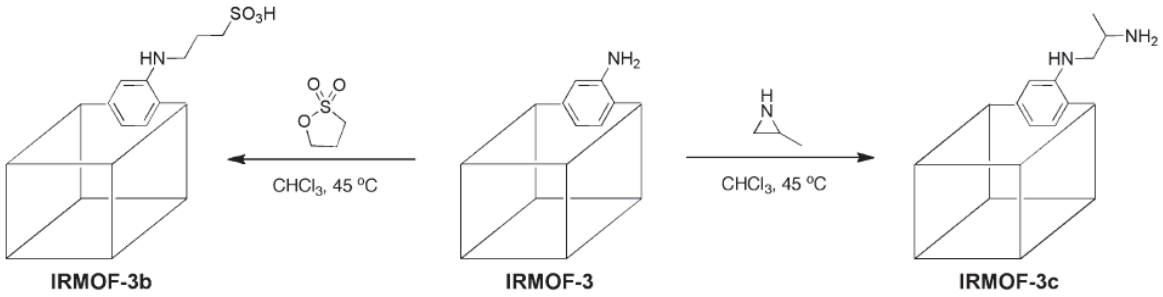

Figure III-7 : Modification of IRMOF-3 via ring opening reactions

Gadzikwa *et al.* [118] obtained a Zn^{2+} paddlewheel MOF with TCPB and DPG containing free diol groups, which they termed DO-MOF. The diols were found to readily undergo modification with succinic anhydride resulting in a ring opened product with free carboxylic groups (Figure III-8).

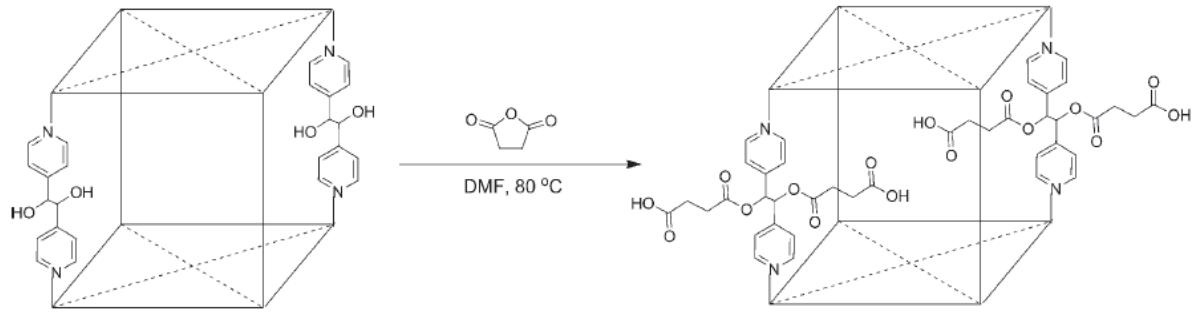

Figure III-8 : Covalent modification of the diol groups of DO-MOF (left) with succinic anhydride

III.3.4 Reactivity of hydroxyl groups

Among the few MOFs possessing bridging OH groups, the most famous is the 2-dimensional MIL-53 formulated as $M^{III}(OH)(bdc)$ where M^{III} can be Al, Cr [130], Ga [131] or Fe [132] . The postsynthetic modification of this inorganic linker, in contrast with the functionalization of organic ligands, is much less studied but must be highlighted as an alternative method, related to the OH reactivity in mesoporous silicates.

Starting from the MIL-53(Al), Meilikhov and coworkers used the highly reactive 1,1'-ferrocenediyl-dimethylsilane to perform the sylilation of the OH group, bridging AlO_6 octahedra, under solvent-free gas-phase conditions in order to form the oxydimethyl(ferrocenyl)silane analogue [133] (Figure III-9). According to ^2H MAS NMR experiments, 25% of the hydroxyl groups were modified following the protocol. Intensity variations were found in the PXRD data which were attributed to the pore filling but TG analysis showed no weight loss up to decomposition temperature of the network itself, indicating a strong binding of the ferrocenyl silane to the framework.

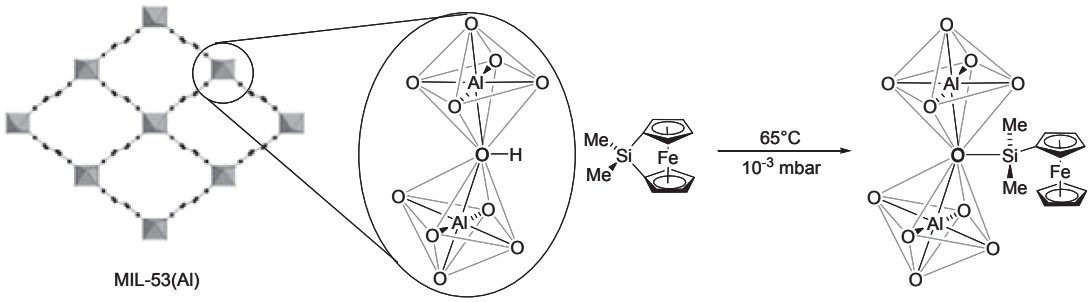

Figure III-9 : Silylation of OH bridging groups in the MIL-53(Al).

III.3.5 Chemical modification by "Click Chemistry"

The "Click Chemistry" was introduced by Sharpless and coworkers in 2001 and consists on the azide alkyne Huisgen cycloaddition, i.e. the reaction of an alkyne with azido-functionalized compound catalyzed by copper(I) species to form a triazole heterocycle [134] . It proceeds efficiently even at micromolar concentrations of reactants with high yields and high specificity in the presence of various functional groups. The first important application of this reaction in polymer chemistry is undeniably the synthesis of functionalized polymers (either end-functionalized or side-functionalized). Numerous examples of macromolecular

architectures were recently obtained by click modification (macrocycles, amphiphillic block copolymer, multiarms stars polymers…) [135].

Such key features prompt its application for the modification of well-defined MOFs. Two recent studies by Goto *et al.* and by Gadzikwa *et al.* deal with the use of click chemistry for the post-functionalization of MOFs.

Goto *et al.* prepared the N_3-MOF-16 [136] derived from its parent IRMOF-16, using a bis(azidomethyl) functionnalized *p*-terphenyl-4,4″-dicarboxylate derivative as ligand combined with zinc nitrate in DEF. The N_3-MOF-16 was allowed to react with terminal alkynes under copper catalysis to form the corresponding MOF decorated with triazole moieties (Figure III-10).

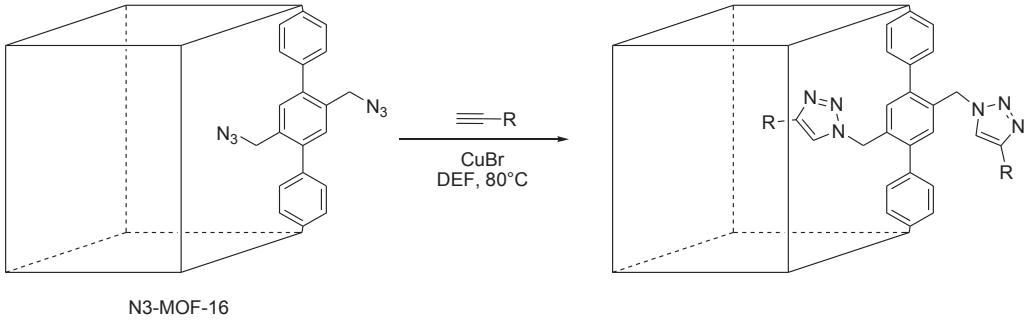

Figure III-10 : "clickable" azido-functionalized N_3-MOF-16

The parent MOF material was however built from an azide linker that is not commercially available; this required a five-step synthesis. Moreover, the chemical instability of azide significantly limits the synthesis of the desired MOF by a solvothermal method, which may require high temperatures.

Gadzikwa *et al.* reported the synthesis of a Zn-cornered, mixed-ligand MOF bearing TMS-protected acetylenes composed by dimeric Zn(II) secondary building units, 2,6-naphthalenedicarboxylate, and bipyridyl ligand, namely the 3-[(trimethylsilyl) ethynyl]-4-[2-(4-pyridinyl)ethenyl]pyridine, called TO-MOF. The bipyridyl ligand presents an acetylene moiety protected by a terminal trimethylsilane (TMS) which provides a suitable platform for postsynthetic modification [137] (Figure III-11).

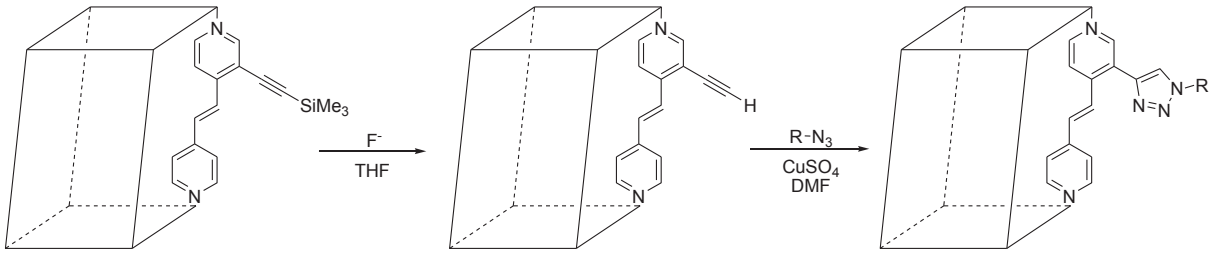

Figure III-11 : From TMS-protected alkyne containing MOF to triazole-anchored structure via Huisgen cycloaddition.

This deprotection may be viewed as an activation step for the subsequent click reaction, and can be performed selectively to provide additional control over the manipulation of MOF properties. There are able to "activate" the exterior of MOF crystals exclusively by taking advantage of the prohibitively large size of the deprotecting agent (tetrabutylammonium fluoride) [137]. Recently, they developed a clever strategy to selectively modify both the surface and the interior of the MOFs. Deprotecting agent was added in a medium that is immiscible with the pore solvent, thus limiting the desilylation to the external surfaces of the MOF crystals. After the subsequent click reaction, the interior surfaces could be deprotected completely and "decorated" with a different azide [138].

Nevertheless, the use of various fluoride sources can cause slight dissolution of the crystals in the case of long-term deprotection.

III.4 Application to catalysis of organometallics at MOFs surfaces

Covalent and coordinate modifications have also been subsequently used in two steps. Not all MOFs have unsaturated metal sites at the SBUs or metal binding groups built into the organic linkers. However, by combining covalent and afterward coordinate covalent modification, the organic linker can be appended with a ligand and subsequently mettaled. Rosseinsky and co-workers executed the first dual covalent coordinate modifications using IRMOF-3 by converting the free amine groups into Schiff base ligands with salicyaldehyde, as earlier mentioned. The resulting chelator was metalled with $VO(acac)_2$ and the material, characterized by liquid state NMR and PXRD analysis, was examined as a heterogeneous

oxidation catalyst [128] (Figure III-12). This latter study inspired several subsequent investigations on organometallics on MOF surfaces that are not all detailed below [74, 139, 140]. Starting from the same approach, Zhang *et al.* reported later a dichloro gold (III) complex supported in IRMOF-3 through coordination to the salycilidene group (Figure III-12) [141]. The state of the gold species as well as its stability was confirmed by UV-Vis analysis, PXRD and TEM, excluding the formation of metallic gold particles. The Au@IRMOF-3 material catalyzed domino coupling and cyclization reactions in liquid phase with higher activities than the homogeneous and gold supported catalysts reported earlier. Moreover, the Au(III) species remain after reaction and the catalyst is fully recyclable.

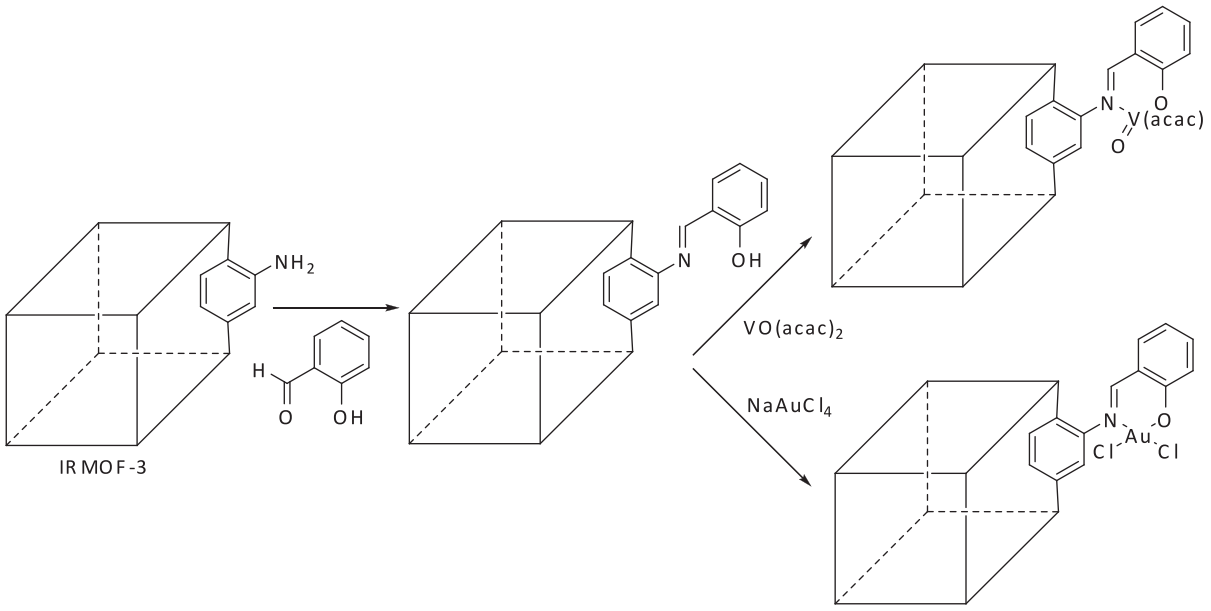

Figure III-12 : IRMOF-3 containing V(IV)/Au(III) Schiff base complex by tandem post-functionalization.

Tanabe *et al.* applied the postsynthetic modification principle to the synthesis of MOF-supported Cu/Fe catalysts [142]. By reacting the amino functionalized UMCM-1-NH_2 with different cyclic anhydrides under mild conditions, the corresponding amides were obtained with moderate yields (35 to 50%) while the structural integrity of the framework is maintained. Then, addition of iron (III) or copper (II) salt led to the formation of the supported complexes, UMCM-1-AMFesal and UMCM-1-AMCupz respectively. The latter were tested in the Mukaiyama-aldol reaction which is an extensively studied C-C bond formation involving Lewis-type catalyst. The UMCM-1-AMFesal was found to catalyze the

reaction at room temperature with moderate activity but being robust, retaining full activity over 3 catalytic cycles and remaining crystalline.

In the mean time, Doonan and coworkers [115] described the preparation of a supported palladium-diimino species using the post-modification method starting from the same MOF. By reacting the 2-pyridinecarboxaldehyde with the UMCM-1-NH_2, they obtained the corresponding N-N ligand able to chelate palladium dichloride. The coordination of the palladium atom was supported by EXAFS analysis indicating the presence of two Pd-Cl and two Pd-N bonds. However, having this promising heterogeneized palladium catalyst in hand, its catalytic application has never been reported so far.

In the specific case of organometallics, a lack of unambiguous characterization remains, since numerous converging multi-technique approaches are required to identify the coordination and the oxidation state of the supported metal.

IV. Conclusions and objectives

Amino-MOFs have been shown to be excellent platforms for the grafting of various groups such as anhydride acids, isocyanates, cyclic compounds, aldehydes, acids and phosgenes (Figure IV-1).

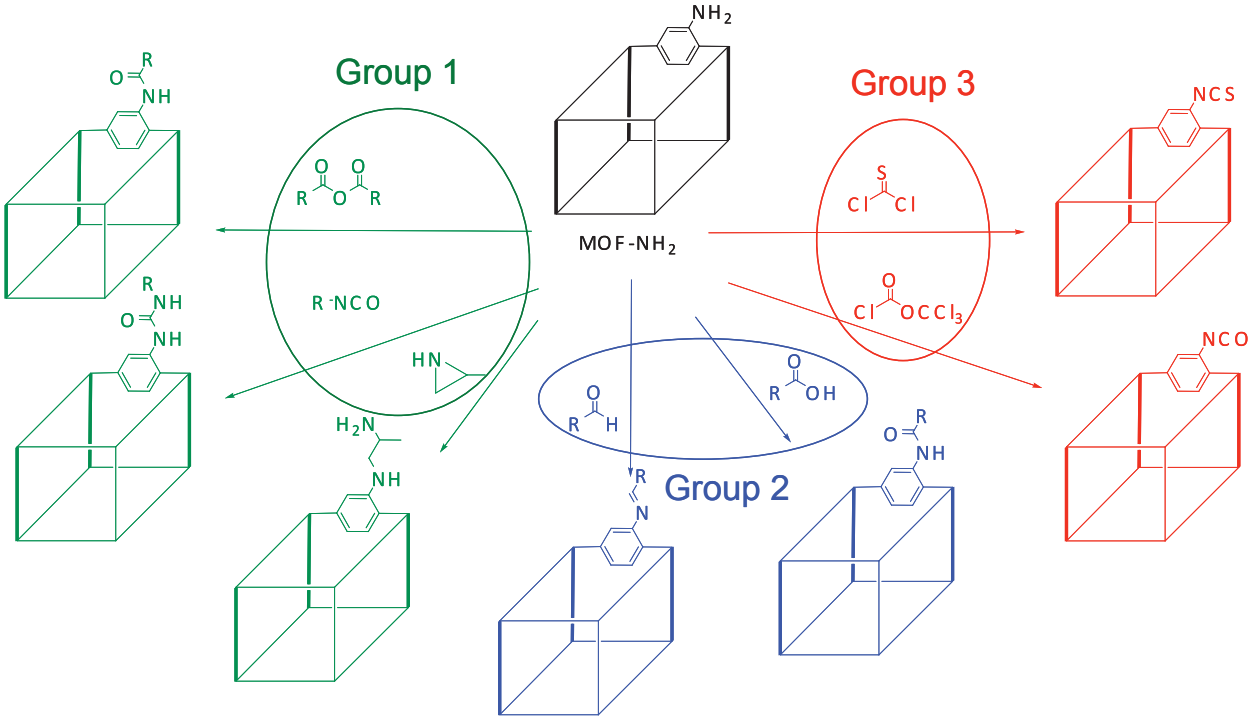

Figure IV-1 : Postsynthetic modification (PSM) using covalent-type grafting methods

These methods developed so far are nevertheless not very generically applicable, since only few functional commercial derivates of group 1 are available. Furthermore, the generation of water molecules during the grafting of group 2 requires moisture resistant frameworks and group 3 can be applied only to the most robust MOFs that can withstand relatively harsh conditions.

Another critical point in the post-functionalization methodologies is the lack of control of the modification yield. Indeed, the "too" high rate of functionalization of a framework with a quite big molecule could led to the distortion of the structure, a possible loss of crystallinity and a slow destruction of the framework. Furthermore, for catalytic applications, a high functionalization rate leads to a high number of active sites but also to their low accessibility, a slow molecular diffusion and finally to a loss of efficiency. The correlation between the post-functionalization yield and the application of the modified MOF is thus decisive.

The objectives of this work were: (i) to develop novel methods of PSM that can be applied to all kinds of amino-MOFs over a very wide range of pore size (micro to meso), chemical stability (low to high) and structural flexibility, using a great variety of grafted chemical functions (acidic, chelating, basic, aromatic, aliphatic and hydrophilic) (ii) to finely tune reactivities and adsorption properties by adjusting the degree of basicity, the hydrophilicity/hydrophobicity balance and the numbers of sites (iii) to explore these functionalized MOF materials in acid-base catalysis.

V. References

[1] M. W. Ackley, S. U. Rege, H. Saxena, *Microporous Mesoporous Mater.* **2003**, *61*, 25-42.
[2] J. Janak, M. Krejci, E. E. Dubsky, *Ann. N. Y. Acad. Sci.* **1959**, *72*, 731-738.
[3] A. Corma, *Chem. Rev.* **1997**, *97*, 2373-2419.
[4] M. Pansini, C. Colella, M. Degennaro, *Desalination* **1991**, *83*, 145-157.
[5] W. M. Meier, *Molecular Sieves, Society of Chemical Industry Ed.* **1968**.
[6] D. W. Breck, *Zeolite Molecular Sieves: Structure, Chemistry and Use, Wiley, New York* **1974**.
[7] R. M. Barrer, *Zeolites and clay materials as sorbents and molecular sieves, Academic Press, London,* **1978**.
[8] A. Cauvel, D. Brunel, F. DiRenzo, P. Moreau, F. Fajula, in *Catalysis by Microporous Materials, Vol. 94* (Eds.: H. K. Beyer, H. G. Karge, I. Kiricsi, J. B. Nagy), Elsevier Science Publ B V, Amsterdam, **1995**, pp. 286-293.
[9] A. Corma, M. I. de Dios, M. Iglesias, F. Sanchez, in *Heterogeneous Catalysis and Fine Chemicals Iv, Vol. 108* (Eds.: H. U. Blaser, A. Baiker, R. Prins), Elsevier Science Publ B V, Amsterdam, **1997**, pp. 501-507.
[10] A. Corma, M. Iglesias, F. Sanchez, *Catal. Lett.* **1995**, *32*, 313-318.
[11] A. Carmona, A. Corma, M. Iglesias, A. Sanjose, F. Sanchez, *J. Organomet. Chem.* **1995**, *492*, 11-21.
[12] A. Corma, M. Iglesias, C. Delpino, F. Sanchez, *J. Organomet. Chem.* **1992**, *431*, 233-246.
[13] J. S. Beck, J. C. Vartuli, W. J. Roth, M. E. Leonowicz, C. T. Kresge, K. D. Schmitt, C. T. W. Chu, D. H. Olson, E. W. Sheppard, S. B. McCullen, J. B. Higgins, J. L. Schlenker, *J. Am. Chem. Soc.* **1992**, *114*, 10834-10843.
[14] C. T. Kresge, M. E. Leonowicz, W. J. Roth, J. C. Vartuli, J. S. Beck, *Nature* **1992**, *359*, 710-712.
[15] D. Y. Zhao, Q. S. Huo, J. L. Feng, B. F. Chmelka, G. D. Stucky, *J. Am. Chem. Soc.* **1998**, *120*, 6024-6036.
[16] P. Behrens, *Angew. Chem., Int. Ed.* **1996**, *35*, 515-518.
[17] D. M. Antonelli, J. Y. Ying, *Current Opinion in Colloid & Interface Science* **1996**, *1*, 523-529.
[18] A. P. Wright, M. E. Davis, *Chem. Rev.* **2002**, *102*, 3589-3614.
[19] F. Hoffmann, M. Cornelius, J. Morell, M. Fröba, *Angew. Chem., Int. Ed.* **2006**, *45*, 3216-3251.
[20] D. Brunel, *Microporous Mesoporous Mater.* **1999**, *27*, 329-344.
[21] D. Brunel, A. C. Blanc, A. Galarneau, F. Fajula, *Catal. Today* **2002**, *73* 139-152.
[22] V. Antochshuk, O. Olkhovyk, M. Jaroniec, I. S. Park, R. Ryoo, *Langmuir* **2003**, *19*, 3031-3034.
[23] C. Li, H. Zhang, D. Jiang, Q. Yang, *Chem. Commun.* **2007**, 547-558.
[24] J. M. Thomas, R. Raja, *Acc. Chem. Res.* **2008**, *41*, 708-720.
[25] O. M. Yaghi, H. L. Li, C. Davis, D. Richardson, T. L. Groy, *Acc. Chem. Res.* **1998**, *31*, 474-484.
[26] M. Eddaoudi, D. B. Moler, H. L. Li, B. L. Chen, T. M. Reineke, M. O'Keeffe, O. M. Yaghi, *Acc. Chem. Res.* **2001**, *34*, 319-330.
[27] J. Kim, B. L. Chen, T. M. Reineke, H. L. Li, M. Eddaoudi, D. B. Moler, M. O'Keeffe, O. M. Yaghi, *J. Am. Chem. Soc.* **2001**, *123*, 8239-8247.

[28] M. O'Keeffe, M. Eddaoudi, H. Li, T. Reineke, O. M. Yaghi, *J. Solid State Chem.* **2000**, *152*, 3-20.
[29] G. Férey, *J. Solid State Chem.* **2000**, *152*, 37-48.
[30] M. W. Hosseini, *Acc. Chem. Res.* **2005**, *38*, 313-323.
[31] N. L. Rosi, M. Eddaoudi, J. Kim, M. O'Keeffe, O. M. Yaghi, *Crystengcomm.* **2002**, 401-404.
[32] G. Férey, *Chem. Mater.* **2001**, *13*, 3084-3098.
[33] M. J. Rosseinsky, *Microporous Mesoporous Mater.* **2004**, *73*, 15-30.
[34] S. Kaskel, *Porous Metal-Organic Frameworks*, Wiley-VCH Verlag GmbH, **2008**.
[35] J. P. Zhang, X. M. Chen, *J. Am. Chem. Soc.* **2008**, *130*, 6010-6017.
[36] B. Wang, A. P. Cote, H. Furukawa, M. O'Keeffe, O. M. Yaghi, *Nature* **2008**, *453*, 207-211.
[37] M. Eddaoudi, J. Kim, J. B. Wachter, H. K. Chae, M. O'Keeffe, O. M. Yaghi, *J. Am. Chem. Soc.* **2001**, *123*, 4368-4369.
[38] S. S. Y. Chui, S. M. F. Lo, J. P. H. Charmant, A. G. Orpen, I. D. Williams, *Science* **1999**, *283*, 1148-1150.
[39] M. Eddaoudi, J. Kim, M. O'Keeffe, O. M. Yaghi, *J. Am. Chem. Soc.* **2002**, *124*, 376-377.
[40] M. Eddaoudi, J. Kim, N. Rosi, D. Vodak, J. Wachter, M. O'Keeffe, O. M. Yaghi, *Science* **2002**, *295*, 469-472.
[41] K. Seki, W. Mori, *J. Phys. Chem. B* **2002**, *106*, 1380-1385.
[42] A. C. Sudik, A. R. Millward, N. W. Ockwig, A. P. Cote, J. Kim, O. M. Yaghi, *J. Am. Chem. Soc.* **2005**, *127*, 7110-7118.
[43] T. Loiseau, C. Mellot-Draznieks, H. Muguerra, G. Férey, M. Haouas, F. Taulelle, *Comptes Rendus Chimie* **2005**, *8*, 765-772.
[44] S. Surble, C. Serre, C. Mellot-Draznieks, F. Millange, G. Férey, *Chem. Commun.* **2006**, 284-286.
[45] N. L. Rosi, J. Kim, M. Eddaoudi, B. Chen, M. O'Keeffe, O. M. Yaghi, *J. Am. Chem. Soc.* **2005**, *127*, 1504-1518.
[46] J. H. Cavka, S. r. Jakobsen, U. Olsbye, N. Guillou, C. Lamberti, S. Bordiga, K. P. Lillerud, *J. Am. Chem. Soc.* **2008**, *130*, 13850-13851.
[47] M. E. Davis, C. Saldarriaga, C. Montes, J. Garces, C. Crowder, *Zeolites* **1988**, *8*, 362-366.
[48] J.-L. Paillaud, B. Harbuzaru, J. l. Patarin, N. Bats, *Science* **2004**, *304*, 990-992.
[49] A. Corma, M. J. Diaz-Cabanas, J. L. Jorda, C. Martinez, M. Moliner, *Nature* **2006**, *443*, 842-845.
[50] K. Na, C. Jo, J. Kim, K. Cho, J. Jung, Y. Seo, R. J. Messinger, B. F. Chmelka, R. Ryoo, *Science* **2011**, *333*, 328-332.
[51] A. Sonnauer, F. Hoffmann, M. Froba, L. Kienle, V. Duppel, M. Thommes, C. Serre, G. Férey, N. Stock, *Angew. Chem., Int. Ed.* **2009**, *48*, 3791-3794.
[52] J. L. C. Rowsell, O. M. Yaghi, *Microporous Mesoporous Mater.* **2004**, *73*, 3-14.
[53] L. M. Huang, H. T. Wang, J. X. Chen, Z. B. Wang, J. Y. Sun, D. Y. Zhao, Y. S. Yan, *Microporous Mesoporous Mater.* **2003**, *58*, 105-114.
[54] S. Hausdorf, J. Wagler, R. Mossig, F. Mertens, *J. Phys. Chem. A* **2008**, *112*, 7567-7576.
[55] S. Bauer, C. Serre, T. Devic, P. Horcajada, J. Marrot, G. Férey, N. Stock, *Inorg. Chem.* **2008**, *47*, 7568-7576.
[56] S. Hausdorf, F. Baitalow, J. Seidel, F. Mertens, *J. Phys. Chem. A* **2007**, *111*, 4259-4266.

[57] M. Sabo, A. Henschel, H. Froede, E. Klemm, S. Kaskel, *J. Mater. Chem.* **2007**, *17*, 3827-3832.
[58] K. S. Park, Z. Ni, A. P. Cote, J. Y. Choi, R. D. Huang, F. J. Uribe-Romo, H. K. Chae, M. O'Keeffe, O. M. Yaghi, *Proc. Natl. Acad. Sci.* **2006**, *103*, 10186-10191.
[59] J. J. Low, A. I. Benin, P. Jakubczak, J. F. Abrahamian, S. A. Faheem, R. R. Willis, *J. Am. Chem. Soc.* **2009**, *131*, 15834-15842.
[60] E. I. Solomon, A. J. Augustine, J. Yoon, *Dalton Trans.* **2008**, 3921-3932.
[61] T. F. Degnan, *J. Catal.* **2003**, *216*, 32-46.
[62] A. Kuc, A. Enyashin, G. Seifert, *J. Phys. Chem. B* **2007**, *111*, 8179-8186.
[63] E. Y. Lee, S. Y. Jang, M. P. Suh, *J. Am. Chem. Soc.* **2005**, *127*, 6374-6381.
[64] F. o.-X. Coudert, M. Jeffroy, A. H. Fuchs, A. Boutin, C. Mellot-Draznieks, *J. Am. Chem. Soc.* **2008**, *130*, 14294-14302.
[65] P. Küsgens, M. Rose, I. Senkovska, H. Fröde, A. Henschel, S. Siegle, S. Kaskel, *Microporous Mesoporous Mater.* **2009**, *120*, 325-330.
[66] M. Kawano, T. Kawamichi, T. Haneda, T. Kojima, M. Fujita, *J. Am. Chem. Soc.* **2007**, *129*, 15418-15419.
[67] M. Fujita, Y. J. Kwon, S. Washizu, K. Ogura, *J. Am. Chem. Soc.* **1994**, *116*, 1151-1152.
[68] S. Horike, M. Dinca, K. Tamaki, J. R. Long, *J. Am. Chem. Soc.* **2008**, *130*, 5854-5855.
[69] S. Hasegawa, S. Horike, R. Matsuda, S. Furukawa, K. Mochizuki, Y. Kinoshita, S. Kitagawa, *J. Am. Chem. Soc.* **2007**, *129*, 2607-2614.
[70] B. Gomez-Lor, E. Gutierrez-Puebla, M. Iglesias, M. A. Monge, C. Ruiz-Valero, N. Snejko, *Inorg. Chem.* **2002**, *41*, 2429-2432.
[71] X. Zhang, F. Xamena, A. Corma, *J. Catal.* **2009**, *265*, 155-160.
[72] S.-H. Cho, B. Ma, S. T. Nguyen, J. T. Hupp, T. E. Albrecht-Schmitt, *Chem. Commun.* **2006**, 2563-2565.
[73] M. H. Alkordi, Y. L. Liu, R. W. Larsen, J. F. Eubank, M. Eddaoudi, *J. Am. Chem. Soc.* **2008**, *130*, 12639-12641.
[74] M. J. Ingleson, J. P. Barrio, J. B. Guilbaud, Y. Z. Khimyak, M. J. Rosseinsky, *Chem. Commun.* **2008**, 2680-2682.
[75] M. Alvaro, E. Carbonell, B. Ferrer, F. Xamena, H. Garcia, *Chem.-Eur. J.* **2007**, *13*, 5106-5112.
[76] D. Farrusseng, S. Aguado, C. Pinel, *Angew. Chem., Int. Ed.* **2009**, *48*, 7502-7513.
[77] L. Q. Ma, C. Abney, W. B. Lin, *Chem. Soc. Rev.* **2009**, *38*, 1248-1256.
[78] J. Lee, O. K. Farha, J. Roberts, K. A. Scheidt, S. T. Nguyen, J. T. Hupp, *Chem. Soc. Rev.* **2009**, *38*, 1450-1459.
[79] A. Corma, H. Garcia, F. X. L. Xamena, *Chem. Rev.* **2010**, *110*, 4606-4655.
[80] L. Alaerts, E. Seguin, H. Poelman, F. Thibault-Starzyk, P. A. Jacobs, D. E. De Vos, *Chem.-Eur. J.* **2006**, *12*, 7353-7363.
[81] K. Schlichte, T. Kratzke, S. Kaskel, *Microporous Mesoporous Mater.* **2004**, *73*, 81.
[82] A. Vimont, J. M. Goupil, J. C. Lavalley, M. Daturi, S. Surble, C. Serre, F. Millange, G. Férey, N. Audebrand, *J. Am. Chem. Soc.* **2006**, *128*, 3218-3227.
[83] E. Perez-Mayoral, J. Cejka, *Chemcatchem.* **2011**, *3*, 157-159.
[84] A. Henschel, K. Gedrich, R. Kraehnert, S. Kaskel, *Chem. Commun.* **2008**, 4192-4194.
[85] F. Gandara, B. Gornez-Lor, E. Gutierrez-Puebla, M. Iglesias, M. A. Monge, D. M. Proserpio, N. Snejko, *Chem. Mater.* **2008**, *20*, 72-76.
[86] C. Di Nicola, Y. Y. Karabach, A. M. Kirillov, M. Monari, L. Pandolfo, C. Pettinari, A. J. L. Pombeiro, *Inorg. Chem.* **2007**, *46*, 221-230.

[87] P. Horcajada, S. Surble, C. Serre, D. Y. Hong, Y. K. Seo, J. S. Chang, J. M. Greneche, I. Margiolaki, G. Férey, *Chem. Commun.* **2007**, 2820-2822.
[88] T. Krahl, A. Vimont, G. Eltanany, M. Daturi, E. Kemnitz, *J. Phys. Chem. C* **2007**, *111*, 18317-18325.
[89] N. L. Rosi, M. Eddaoudi, J. Kim, M. O'Keeffe, O. M. Yaghi, *Angew. Chem., Int. Ed.* **2002**, *114*, 294-297.
[90] A. Corma, *J. Catal.*, *216*, 298-312.
[91] F. Millange, C. Serre, G. Férey, *Chem. Commun.* **2002**, 822-823.
[92] U. Ravon, M. Savonnet, D. Farrusseng, A. Simon-Masseron, G. Chaplais, D. Bazer-Bachi, N. Bats, V. Lecocq, **2008**, FR 0805536.
[93] U. Ravon, M. Savonnet, S. Aguado, M. E. Domine, E. Janneau, D. Farrusseng, *Microporous Mesoporous Mater.* **2010**, *129*, 319-329.
[94] U. Ravon, G. Chaplais, C. Chizallet, B. Seyyedi, F. Bonino, S. Bordiga, N. Bats, D. Farrusseng, *Chemcatchem.* **2010**, *2*, 1235-1238.
[95] J. Gascon, U. Aktay, M. D. Hernandez-Alonso, G. P. M. van Klink, F. Kapteijn, *J. Catal.* **2009**, *261*, 75-87.
[96] Y. K. Hwang, D. Y. Hong, J. S. Chang, S. H. Jhung, Y. K. Seo, J. Kim, A. Vimont, M. Daturi, C. Serre, G. Férey, *Angew. Chem., Int. Ed.* **2008**, *47*, 4144-4148.
[97] J. S. Seo, D. Whang, H. Lee, S. I. Jun, J. Oh, Y. J. Jeon, K. Kim, *Nature* **2000**, *404*, 982-986.
[98] C. Chizallet, S. Lazare, D. Bazer-Bachi, F. Bonnier, V. Lecocq, E. Soyer, A. A. Quoineaud, N. Bats, *J. Am. Chem. Soc.* **2010**, *132*, 12365-12377.
[99] H. Hayashi, A. P. Cote, H. Furukawa, M. O/'Keeffe, O. M. Yaghi, *Nat. Mater.* **2007**, *6*, 501-506.
[100] S. Hermes, F. Schroder, S. Amirjalayer, R. Schmid, R. A. Fischer, *J. Mater. Chem.* **2006**, *16*, 2464-2472.
[101] S. Hermes, M. K. Schroter, R. Schmid, L. Khodeir, M. Muhler, A. Tissler, R. W. Fischer, R. A. Fischer, *Angew. Chem., Int. Ed.* **2005**, *44*, 6237-6241.
[102] F. Schroeder, D. Esken, M. Cokoja, M. W. E. van den Berg, O. I. Lebedev, G. van Tendeloo, B. Walaszek, G. Buntkowsky, H. H. Limbach, B. Chaudret, R. A. Fischer, *J. Am. Chem. Soc.* **2008**, *130*, 6119-6130.
[103] C.-Y. Sun, S.-X. Liu, D.-D. Liang, K.-Z. Shao, Y.-H. Ren, Z.-M. Su, *J. Am. Chem. Soc.* **2009**, *131*, 1883-1888.
[104] G. Hundal, Y. K. Hwang, J.-S. Chang, *Polyhedron* **2009**, *28*, 2450-2458.
[105] L. Yang, H. Naruke, T. Yamase, *Inorg. Chem. Commun.* **2003**, *6*, 1020-1024.
[106] J. Juan-Alcañiz, E. V. Ramos-Fernandez, U. Lafont, J. Gascon, F. Kapteijn, *J. Catal.* **2010**, *269*, 229-241.
[107] G. Férey, C. Mellot-Draznieks, C. Serre, F. Millange, J. Dutour, S. Surblé, I. Margiolaki, *Science* **2005**, *309*, 2040-2042.
[108] L. H. Wee, S. R. Bajpe, N. Janssens, I. Hermans, K. Houthoofd, C. E. A. Kirschhock, J. A. Martens, *Chem. Commun.* **2010**, *46*, 8186-8188.
[109] E. Kockrick, T. Lescouet, E. V. Kudrik, A. B. Sorokin, D. Farrusseng, *Chem. Commun.* **2011**, *47*, 1562-1564.
[110] O. K. Farha, K. L. Mulfort, J. T. Hupp, *Inorg. Chem.* **2008**, *47*, 10223-10225.
[111] A. Demessence, D. M. D'Alessandro, M. L. Foo, J. R. Long, *J. Am. Chem. Soc.* **2009**, *131*, 8784-8786.
[112] C. D. Wu, A. Hu, L. Zhang, W. B. Lin, *J. Am. Chem. Soc.* **2005**, *127*, 8940-8941.
[113] Z. Q. Wang, K. K. Tanabe, S. M. Cohen, *Inorg. Chem.* **2009**, *48*, 296-306.
[114] K. Koh, A. G. Wong-Foy, A. J. Matzger, *Angew. Chem., Int. Ed.* **2008**, *47*, 677-680.

[115] C. J. Doonan, W. Morris, H. Furukawa, O. M. Yaghi, *J. Am. Chem. Soc.* **2009**, *131*, 9492-9493.
[116] P. Gamez, J. S. Costa, C. A. Black, O. Roubeau, S. J. Teat, J. Reedijk, *Eur. J. Inorg. Chem.* **2008**, 1551-1554.
[117] W. Morris, C. J. Doonan, H. Furukawa, R. Banerjee, O. M. Yaghi, *J. Am. Chem. Soc.* **2008**, *130*, 12626-12627.
[118] T. Gadzikwa, O. K. Farha, K. L. Mulfort, J. T. Hupp, S. T. Nguyen, *Chem. Commun.* **2009**, *25*, 3720-3722.
[119] Z. Q. Wang, S. M. Cohen, *J. Am. Chem. Soc.* **2007**, *129*, 12368-12369.
[120] K. K. Tanabe, Z. Q. Wang, S. M. Cohen, *J. Am. Chem. Soc.* **2008**, *130*, 8508-8517.
[121] S. J. Garibay, S. M. Cohen, *Chem. Commun.* **2010**, *46*, 7700-7702.
[122] M. Kandiah, S. Usseglio, S. Svelle, U. Olsbye, K. P. Lillerud, M. Tilset, *J. Mater. Chem.* **2010**, *20*, 9848-9851.
[123] S. J. Garibay, Z. Q. Wang, K. K. Tanabe, S. M. Cohen, *Inorg. Chem.* **2009**, *48*, 7341-7349.
[124] Z. Q. Wang, S. M. Cohen, *Angew. Chem., Int. Ed.* **2008**, *47*, 4699-4702.
[125] E. Dugan, Z. Q. Wang, M. Okamura, A. Medina, S. M. Cohen, *Chem. Commun.* **2008**, 3366-3368.
[126] C. Volkringer, S. M. Cohen, *Angew. Chem., Int. Ed.* **2010**, *49*, 4644-4648.
[127] T. Ahnfeldt, D. Gunzelmann, T. Loiseau, D. Hirsemann, J. Senker, G. Férey, N. Stock, *Inorg. Chem.* **2009**, *48*, 3057-3064.
[128] M. J. Rosseinsky, M. J. Ingleson, J. P. Barrio, J. B. Guilbaud, Y. Z. Khimyak, *Chem. Commun.* **2008**, 2680-2682.
[129] D. Britt, C. Lee, F. J. Uribe-Romo, H. Furukawa, O. M. Yaghi, *Inorg. Chem.* **2010**, *49*, 6387-6389.
[130] G. Férey, M. Latroche, C. Serre, F. Millange, T. Loiseau, A. Percheron-Guegan, *Chem. Commun.* **2003**, 2976.
[131] C. Volkringer, T. Loiseau, N. Guillou, G. Férey, E. Elkaim, A. Vimont, *Dalton Trans.* **2009**, 2241-2249.
[132] T. R. Whitfield, X. Q. Wang, L. M. Liu, A. J. Jacobson, *Solid State Sci.* **2005**, *7*, 1096-1103.
[133] M. Meilikhov, K. Yusenko, R. A. Fischer, *J. Am. Chem. Soc.* **2009**, *131*, 9644-9645.
[134] H. C. Kolb, M. G. Finn, K. B. Sharpless, *Angew. Chem., Int. Ed.* **2001**, *40*, 2004-2021.
[135] J.-F. Lutz, *Angew. Chem., Int. Ed.* **2007**, *46*, 1018-1025.
[136] Y. Goto, H. Sato, S. Shinkai, K. Sada, *J. Am. Chem. Soc.* **2008**, *130*, 14354-14355.
[137] T. Gadzikwa, G. Lu, C. L. Stern, S. R. Wilson, J. T. Hupp, S. T. Nguyen, *Chem. Commun.* **2008**, 5493-5495.
[138] T. Gadzikwa, O. K. Farha, C. D. Malliakas, M. G. Kanatzidis, J. T. Hupp, S. T. Nguyen, *J. Am. Chem. Soc.* **2009**, *131*, 13613-13615.
[139] X. P. Zhou, Z. T. Xu, M. Zeller, A. D. Hunter, *Chem. Commun.* **2009**, 5439-5441.
[140] K. Oisaki, Q. W. Li, H. Furukawa, A. U. Czaja, O. M. Yaghi, *J. Am. Chem. Soc.* **2010**, *132*, 9262-9264.
[141] X. Zhang, F. X. Llabrés i Xamena, A. Corma, *J. Catal.* **2009**, *265*, 155-160.
[142] K. K. Tanabe, S. M. Cohen, *Angew. Chem., Int. Ed.* **2009**, *48*, 7424-7427.

Chapter 2

Synthesis and Characterization of Amino-MOFs

I. Introduction

As previously reported in the bibliographic part, amino-MOFs have been shown to be excellent platforms for the grafting of various groups. This chapter reports the synthesis, the structure and the characterization (PXRD analyses, BET measurements, liquid state NMR of digested solids, TGA and SEM) of seven different amino-MOFs used in the following study as "starting materials": DMOF-NH_2 ((**1**), MIL-68(In)-NH_2 **(2)**, CAU-1 **(3)**, MIL(53)-Al-NH_2 **(4)**, MIL-101(Fe)-NH_2 **(5)**, IRMOF-3 **(6)** and $ZnF(NH_2)_2TAZ$ **(7)**.
1, **3**, **4**, **5**, **6** and **7** were reproduced from literature whereas **2** was discovered and patented at the laboratories. The detailed synthetic protocols can be found in the experimental part.

II. DMOF-NH_2 (1)

II.1 Synthesis

DMOF-NH_2 [$Zn_2(C_8H_5O_4N)_2(C_6H_{12}N_2)$] was prepared according to a procedure published by Wang and coworkers [1] and detailed in the experimental part. The addition of 1,4-diazabicyclo(2.2.2)octane (DABCO) in a solution of zinc nitrate and NH_2-bdc in DMF immediately generated a large amount of white DMOF-NH_2 precipitate.

II.2 Structure description

It is a zero-dimensional-type MOF (isolated clusters) with a layered structure made of Zn carboxylate sheets supported by DABCO pillars that weakly coordinate to the Zn paddlewheel (Figure II-1). This confers a certain degree of flexibility to DMOF-NH_2 [2]. The channel diameter is about 5.6 Å.

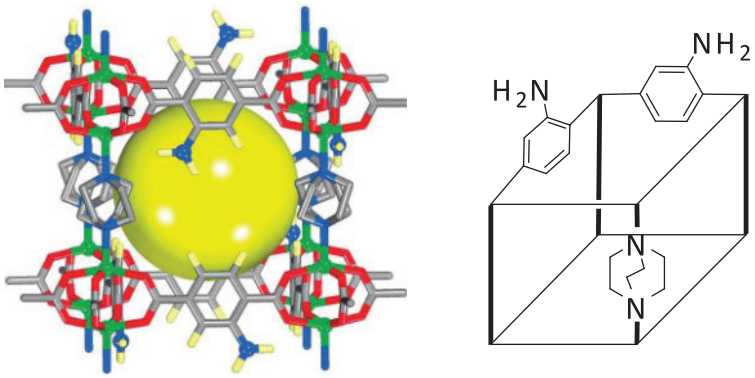

Figure II-1 : Diagram of DMOF-NH_2 (Zn = green, C =grey; N = blue, O = red; the yellow ball indicates the size of the pore openings) (left) and its simplified scheme (right)

II.3 Characterization

II.3.1 Powder X-Ray Diffraction (PXRD)

Experimental PXRD patterns match with the simulated pattern obtained from Crystallographic Information File (cif) (Figure II-2). Nevertheless, as described in literature, the crystallinity of the parent DMOF-NH_2 is strongly affected by post treatments such as solvent removal and/or solvent exchange [2, 3] (Figure II-3).

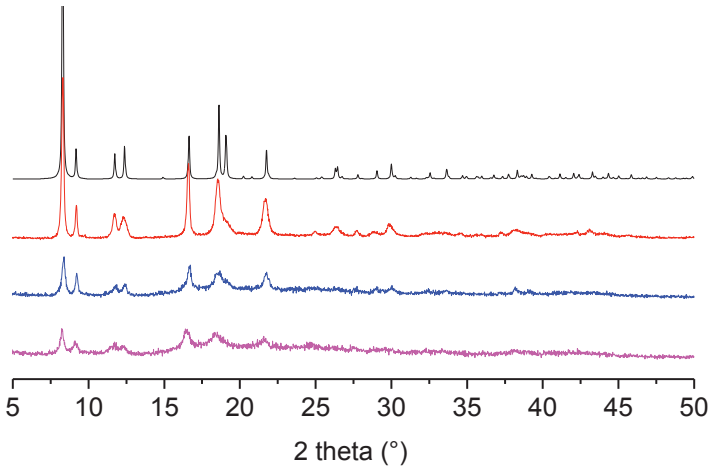

Figure II-2 : PXRD pattern of simulated DMOF-NH_2 (black), DMOF-NH_2 (red), DMOF-NH_2 soaked in THF (blue) and DMOF-NH_2 soaked in THF /CH_2Cl_2 (pink).

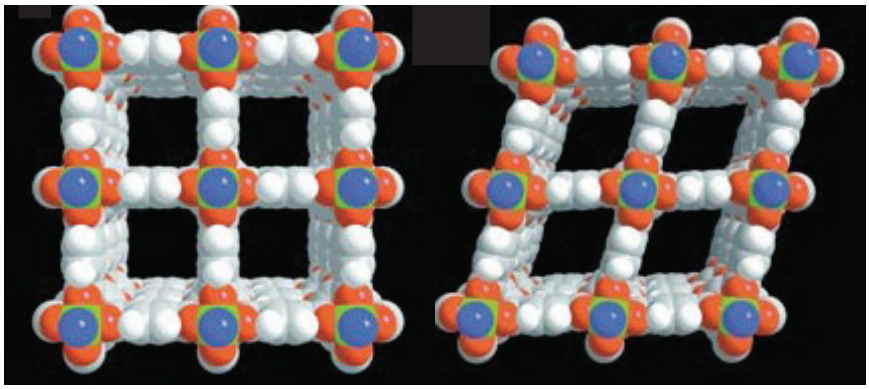

Figure II-3 : Space-filling representations of evacuated DMOF (left) and of the benzene-inclusion DMOF (right). (Zn = green; N = blue; O = red; C = grey; H = white. The guest molecules and DABCO hydrogens are not shown.)

II.3.2 Nitrogen physisorption at 77K

Typical isotherm of type I is observed (Figure II-4). The measured BET surface area and the microporous volume are 1320 m^2/g and 0.54 cm^3/g respectively, which are comparable, but expectedly lower than, that of DMOF (the reported surface area of DMOF is 1450 m^2/g [2])

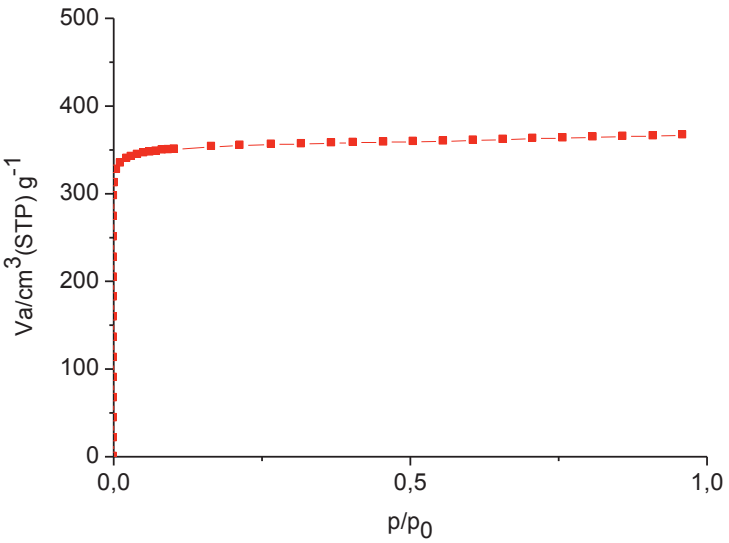

Figure II-4 : N_2 adsorption isotherm of DMOF-NH_2

II.3.3 Thermogravimetric Analysis (TGA)

TGA data indicate that as-synthesized DMOF-NH_2 loses H_2O and DMF (23.8%) in the temperature range of 100–200°C, and the resulting porous framework (57.7%) starts to decompose after 300°C, which is in good agreement with the data reported by Wang and co-workers [1] (Figure II-5).

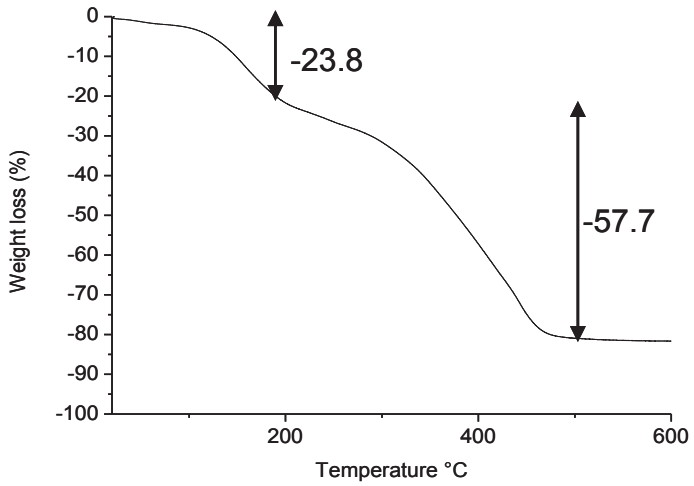

Figure II-5 : TGA of as-synthesized DMOF-NH_2

II.3.4 ^{1}H liquid NMR

All NMR spectra are recorded with the same automated procedure for routine analysis. Amino-MOF samples are commonly digested and dissolved in DCl/D_2O/DMSO-d_6. ^{1}H NMR spectra from the digested DMOF-NH_2 show the presence of the NH_2-bdc and DABCO in the expected relative concentration for DMOF-NH_2 (1:0.56 as calculated from ^{1}H NMR integration, expected value: 1:0.5) (Figure II-6). The spectrum of as-synthesized DMOF-NH_2 confirms the presence of DMF detected by TGA. Although ^{1}H liquid NMR doesn't provide any structural data (spatial arrangement, function distribution, interactions...), this method can give useful chemical information (detection of some impurities or remaining solvents). Thus, all ^{1}H NMR spectra of the MOFs based on 2-amino-terepththalate present almost the same resonance signals corresponding to the aromatic protons of free 2-aminoterephathalic acid in NMR tube solution. Only a small shift can appear arising from the different DCl concentrations in each NMR tube. Unfortunately, ^{1}H NMR analysis cannot be performed on

$ZnF(NH_2)_2TAZ$ due to the absence of ^1H on the linker and MIL(53)-Al-NH_2 samples are digested by using DCl/D_2O/DMSO-d_6 followed by dilute $NaOD/D_2O$ due to their high chemical stability.

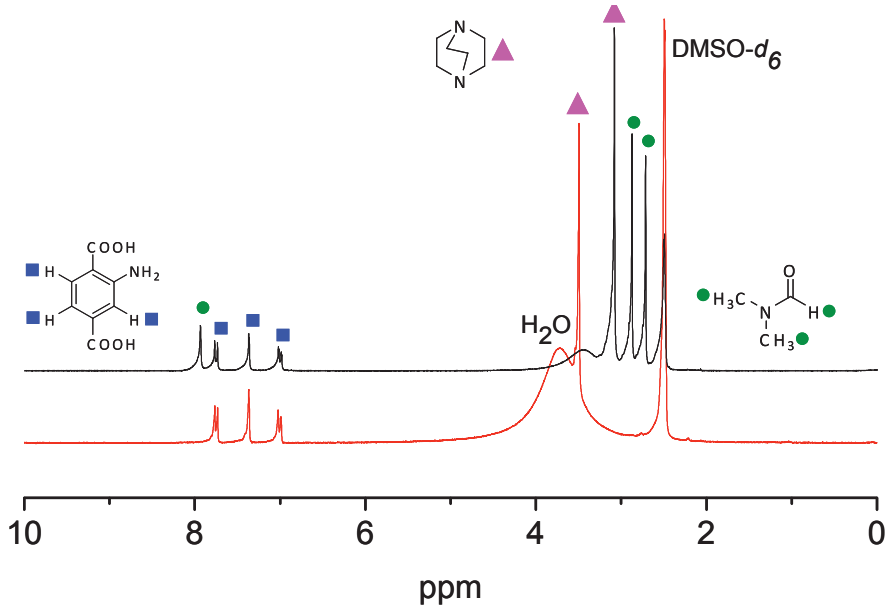

Figure II-6 : ^1H NMR spectra of as-synthesized DMOF-NH2 (top) and DMOF-NH_2 (bottom) samples digested in DCl/D_2O (Blue squares, green circles and pink triangle represent signals of aromatic protons of NH_2-bdc, protons of DMF and equivalent protons of DABCO, respectively)

II.3.5 Scanning Electron Microscopy (SEM)

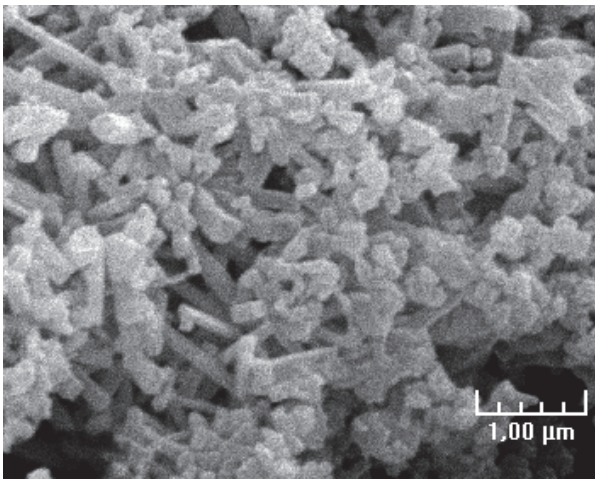

Figure II-7 : SEM photograph of DMOF-NH_2

The SEM photograph of DMOF-NH_2 shows rectangular-shaped crystallites of about 1 µm.

III. MIL-68(In)-NH_2 (2)

III.1 Synthesis

MIL-68(In)-NH_2 [(In(OH)($C_8H_5O_4N$)] has been prepared following the protocol presented in a recent patent [4] and detailed in the experimental part. In contrast with MIL-68-In [5], it was obtained by precipitation reaction from a mixture of indium nitrate and NH_2-bdc in DMF in which DABCO solution was added.

III.2 Structure description

MIL-68(In)-NH_2 framework is built up from infinite straight chains of metal-centered $InO_4(OH)_2$ octahedra connected to each other through the NH_2-bdc ligands, generating 1D channels. The octahedral units are linked together via two hydroxyl groups located in trans positions, two adjacent octahedra also being connected via the carboxylate functions. These corner-sharing octahedral species MO_6 form a network of three- and six-membered windows, generating two types of channels. The diameter openings of MIL-68 parent structure are 6 Å and 17 Å, respectively, for the triangular and hexagonal rings (Figure III-1).

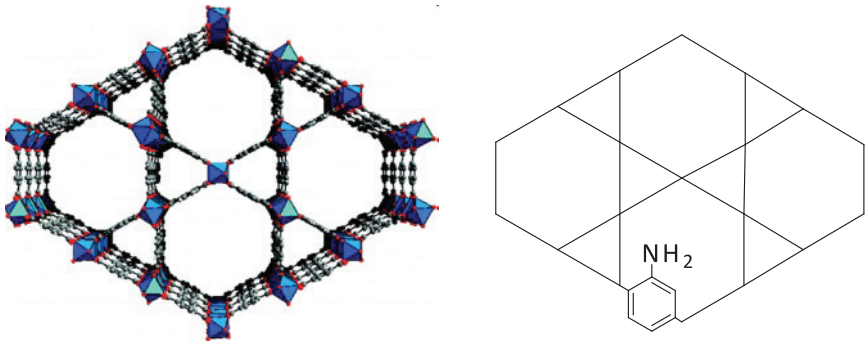

Figure III-1 : Parent structure of MIL-68(In) (In = green, C =grey, O = red)(left) and the simplified scheme of MIL-68(In)-NH_2 (right)

III.3 Characterization

III.3.1 PXRD

Experimental PXRD patterns match with the simulated pattern obtained from Crystallographic Information File (cif) (Figure III-2).

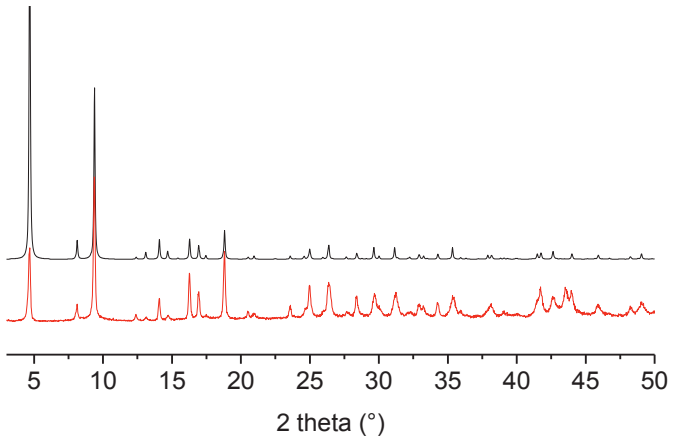

Figure III-2 : Powder X-ray diffraction patterns of simulated MIL-68(In) (top) and of experimental MIL-68(In)-NH_2 (bottom).

III.3.2 Nitrogen physisorption at 77K

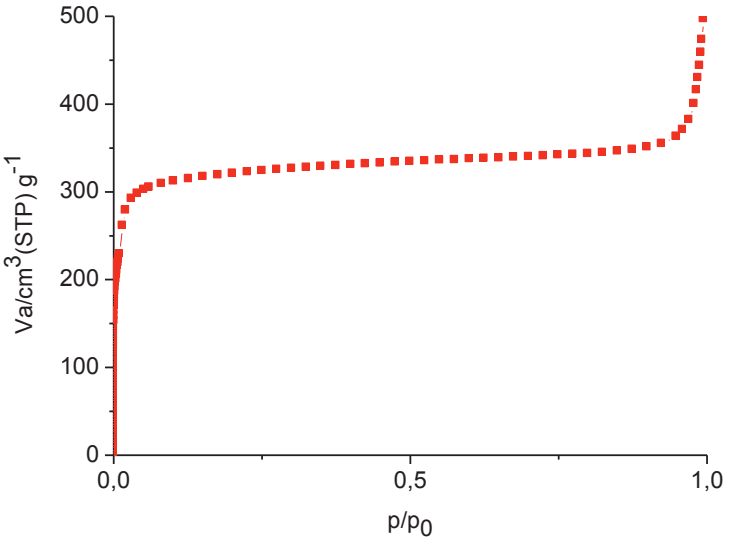

Figure III-3 : N_2 adsorption isotherm of MIL-68(In)-NH_2

In the case of MIL-68(In)-NH_2, higher surface area and micropore volume values (1120 m^2/g and 0.49 cm^3/g, respectively) were obtained than those obtained by Volkringer *et al.* for MIL-68(In) (0.42 cm^3/g) [5] (Figure III-3). We have found that longer equilibrium time was required for adsorption measurements.

III.3.3 TGA

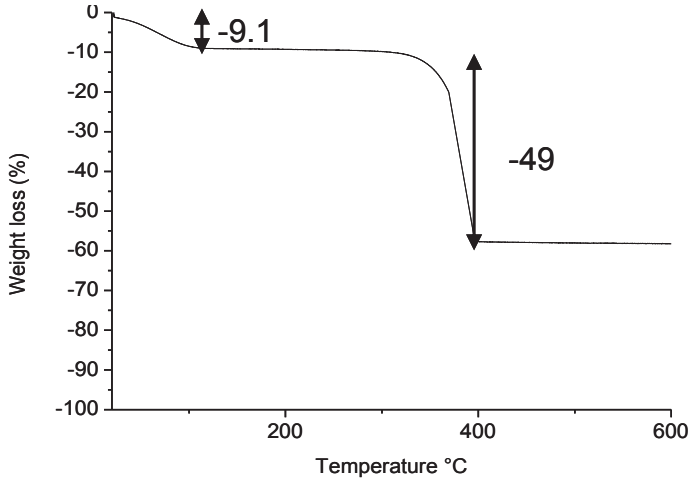

Figure III-4 : TGA of as-synthesized MIL-68(In)-NH_2

The first loss of 9.1% in the temperature range of 15–120°C is due to the guest molecules of CH_2Cl_2 and at higher temperatures (after 350°C), the decomposition of the frameworks begins (-49%), which matches with the TGA data of MIL-68 [5] (Figure III-4).

III.3.4 SEM

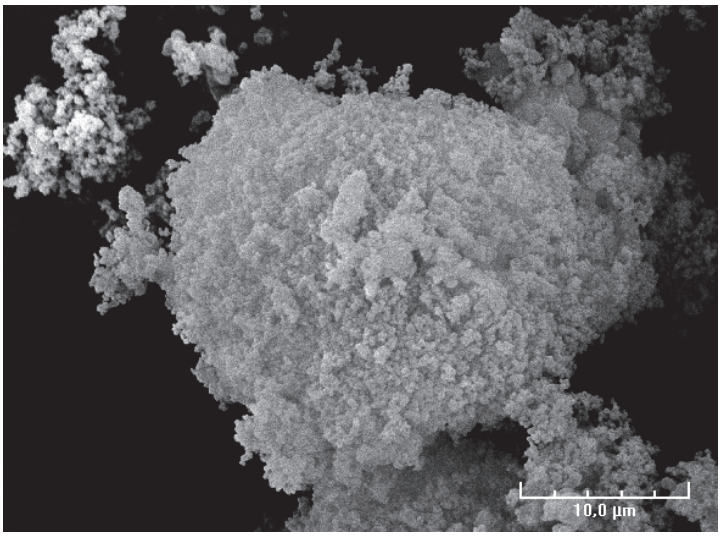

Figure III-5 : SEM picture of MIL-68(In)-NH_2

SEM picture of MIL-68(In)-NH_2 (Figure III-5) shows fine microcrystalline grains (<0.1 µm grain diameter).

IV. CAU-1 (3)

IV.1 Synthesis

CAU-1 $[Al_4(OH)_2(OCH_3)_4(C_8H_5O_4N)_3]$ was synthesized solvothermally from a mixture of aluminium chloride and NH_2-bdc in MeOH using procedure described in [6] and detailed in the experimental part.

IV.2 Structure description

The CAU-1 framework is built up from a pseudo-body-centered-cubic arrangement of 8-ring build-ing blocks $[Al_8(OH)_4(OCH_3)_8]^{12+}$ linked by 12 aminoterephthalate ions. The wheel-shaped 8-rings are built from corner- and edge-sharing AlO_6 octahedra through hydroxide and methoxide groups. The Al(III) is coordinated to three carboxylate oxygen atoms, one hydroxide and two methoxide ions. Each wheel is connected to 12 others units by

aminoterephthalate linkers with four linkers in the plane of the 8-rings as well as four above and below the ring. Hence, a 3D microporous framework is formed with two types of cages, distorded octahedra and distorded tetrahedra, with diameter of 10 Å and 4.5 Å, respectively (Figure IV-1).

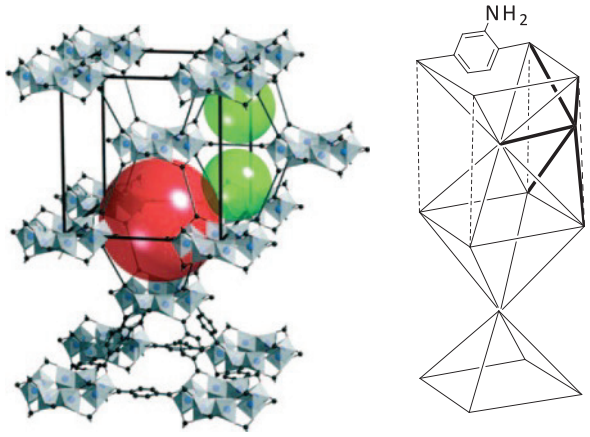

Figure IV-1: Diagram of CAU-1 (Al = grey, C =black; O = blue; the red and green balls indicate the different size of the pore openings; for clarity some of the phenyl rings are replaced by straight lines, and the disordered NH_2 groups are omitted) (left) and its simplified scheme (right)

IV.3 Characterization

IV.3.1 PXRD

Experimental PXRD patterns match with the simulated pattern obtained from Crystallographic Information File (cif) (Figure IV-2).

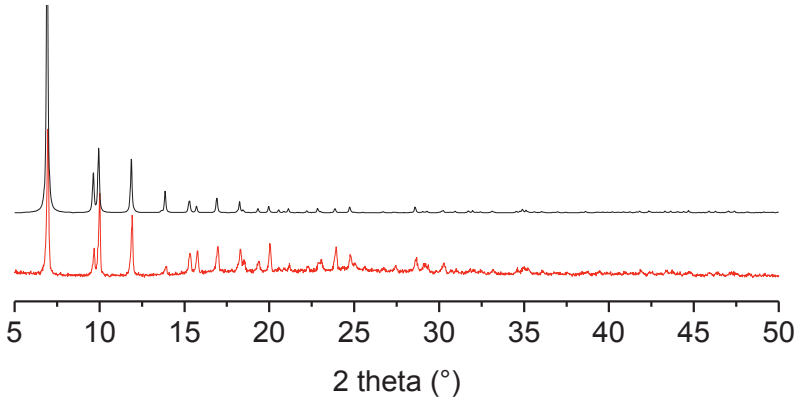

Figure IV-2 : Powder X-ray diffraction patterns of simulated CAU-1 (top) and of experimental CAU-1 (bottom).

IV.3.2 Nitrogen physisorption at 77K

The porous structure has been studied by N_2 sorption measurement. The sorption isotherm of CAU-1 exhibits type I behavior (Figure IV-3). The BET surface area is approximately 1434 m^2/g and a microporous volume of 0.52 cm^3/g is determined (Expected value: 0.52 cm^3/g [6]).

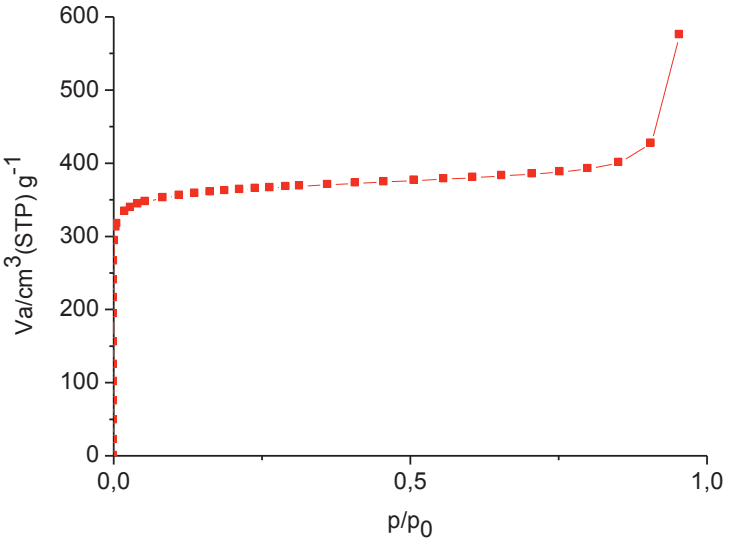

Figure IV-3 : N_2 adsorption isotherm of CAU-1

IV.3.3 SEM

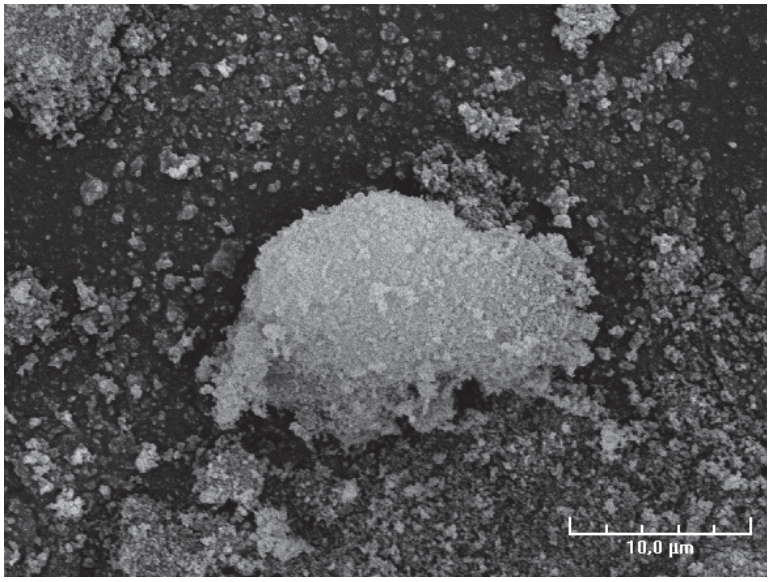

Figure IV-4 : SEM picture of CAU-1

SEM picture of CAU-1 (Figure IV-4) shows fine microcrystalline grains (<0.1 µm grain diameter).

V. MIL-53(Al)-NH_2 (4)

V.1 Synthesis

The synthesis of MIL-53(Al)-NH_2 [$Al(OH)(C_8H_5O_4N)$] was adapted from the procedure described in [7] and detailed in the experimental part. MIL-53(Al)-NH_2 was synthesized solvothermally from a mixture of aluminium chloride and NH_2-bdc in MeOH.

V.2 Structure description

The MIL-53(Al)-NH_2 framework is built up from chains of corner-sharing Al(III) octahedra connected by μ_2-OH and carboxylate groups. These chains are connected by aminoterephthalate ions to form a 1D rhombohedral-shape channel system (Figure V-1). The

combination of these chains allows the formation of three different 3D frameworks. In parent MIL-53 (as) structure, the tunnels (7.3 Å x 7.7 Å) are occupied by disordered bdc template molecules. The total removal of the template upon heating at 275°C generates the MIL-53(ht) form showing empty pores of 8.5 Å x 8.5 Å. The reversible adsorption of water at room temperature gives rise to MIL-53(lt) with channel dimensions of 2.6 Å x 13.6 Å. Here, the MIL-53(Al)-NH_2 (lt) framework was prepared.

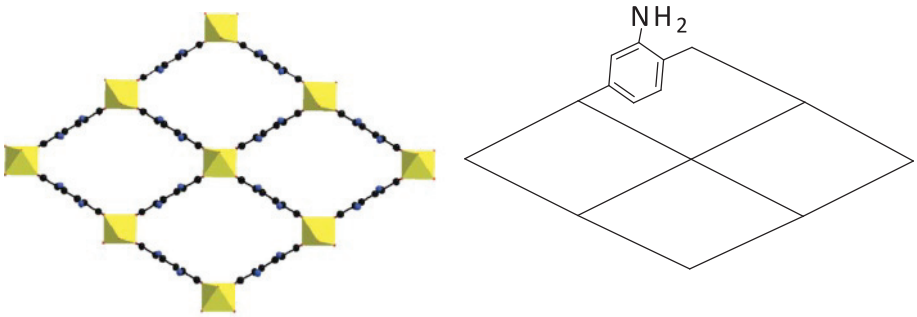

Figure V-1: Structure of MIL-53(Al)-NH_2 (Al = yellow, C =black; O = red, N= blue) (left) and its simplified scheme (right)

V.3 Characterization

V.3.1 PXRD

Experimental PXRD patterns match with the simulated pattern obtained from Crystallographic Information File (cif) (Figure V-2).

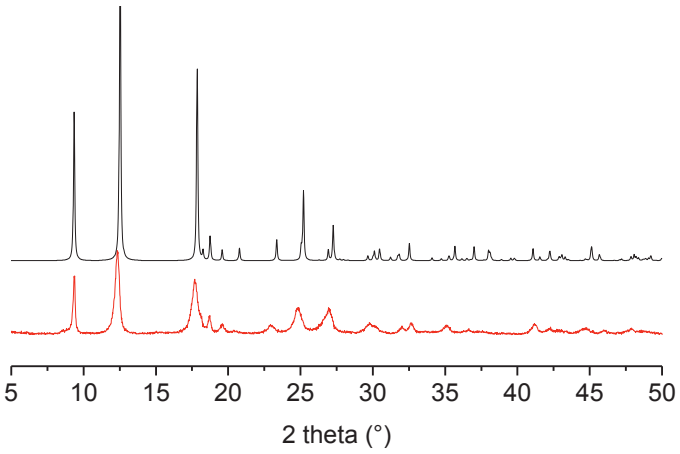

Figure V-2 : Powder X-ray diffraction patterns of simulated MIL-53(lt) (top) and experimental MIL-53(Al)-NH_2 (bottom).

V.3.2 Nitrogen physisorption at 77K

In contrast to the others amino-MOFs the sorption curve of MIL-53(Al)-NH_2 shows hysteresis behavior reflecting the flexibility of the framework (Figure V-3). The same isotherm shape is obtained in a previous works of Ahnfeldt *et al.* [8]. The measured BET surface area and the microporous volume are 940 m²/g and 0.37 cm^3/g, respectively, which are comparable, but expectedly lower than that of the parent structure MIL-53(Ga) without amino (the reported microporous volume of MIL-53(Ga) is 0.47 cm^3/g) [9]). These values are calculated from the desorption branch.

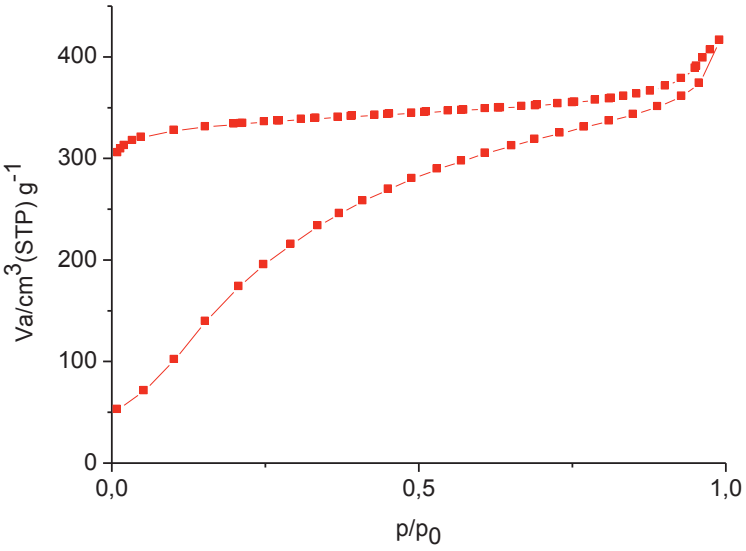

Figure V-3 : N_2 adsorption isotherm of MIL-53(Al)-NH_2

V.3.3 SEM

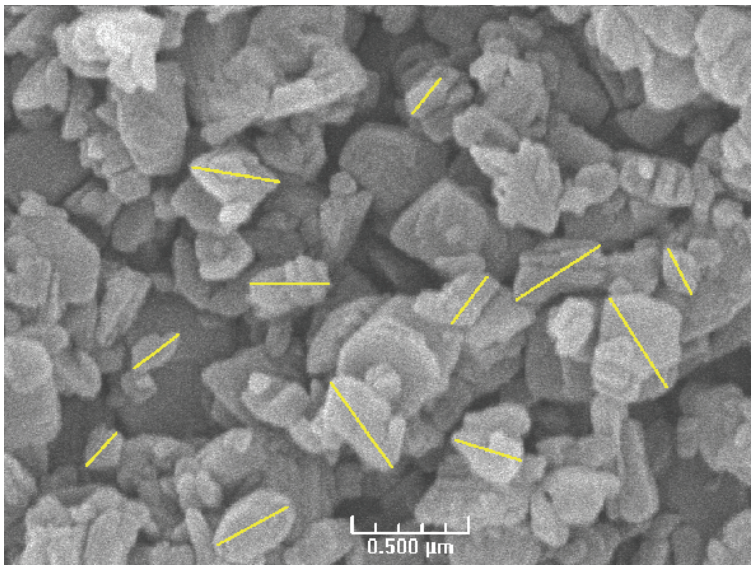

Figure V-4 : SEM photograph of MIL-53(Al)-NH_2

The SEM image (Figure V-4) show small hexagonally shaped crystals with 0.2-0.5 µm diameter.

VI. MIL-101(Fe)-NH_2 (5)

VI.1 Synthesis

MIL-101(Fe)-NH_2 [$Fe_3O(solv)_3Cl(C_8H_5O_4N)_3$ (solv = H_2O, DMF] was synthesized solvothermally from a mixture of $FeCl_3$•$6H_2O$ and NH_2-bdc in DMF [7]. The synthesis was detailed in the experimental part.

VI.2 Structure description

This solid is built up from trimers of Fe octahedra with terminal (Cl and OH) ligands. Their linkage to the rigid carboxylate ligands (NH_2-bdc) generates microporous supertetrahedral units (Figure VI-1). The resulting cubic cell volumes are huge with two types of mesoporous

cages limited by pentagonal faces for the smaller and by pentagonal and hexagonal faces for the larger. After the removal of the guest molecules, the free internal diameters of parent structure MIL-101(Fe) are close to 29 and 34 Å.

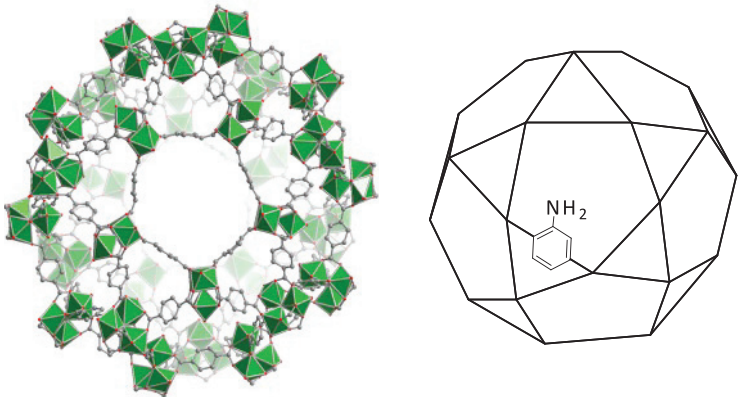

Figure VI-1 : Parent structure of MIL-101(Fe) (Al = green, C =grey; O = red) (left) and the simplified scheme of MIL-101(Fe)-NH_2 (right)

VI.3 Characterization

VI.3.1 PXRD

Experimental PXRD patterns match with the simulated pattern obtained from Crystallographic Information File (cif) (Figure VI-2).

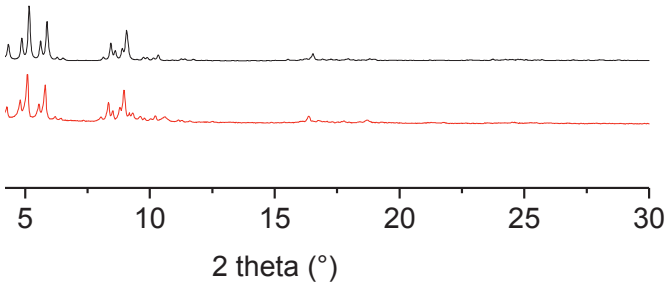

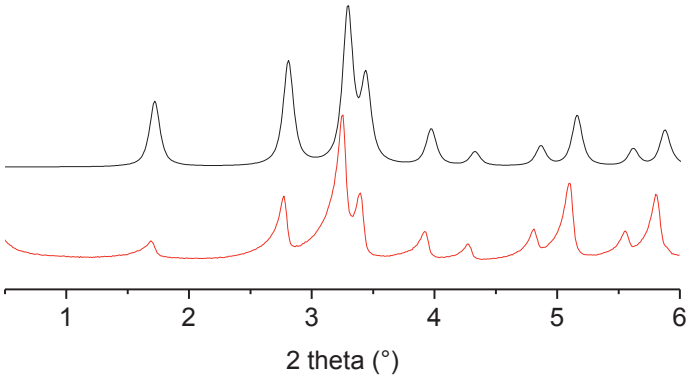

Figure VI-2 : Powder X-ray diffraction patterns of simulated MIL-101(Fe) (black) and experimental MIL-101(Fe)-NH_2 (red).

VI.3.2 Nitrogen physisorption at 77K

As clearly shown by the Figure VI-3, MIL-101(Fe)-NH_2 exhibits the highest pore volume (1.12 cm^3/g) and surface area (2436 m^2/g). In literature, it is found that MIL-101(Cr)-NH_2 exhibits a pore volume of 1.22 cm^3/g [10].

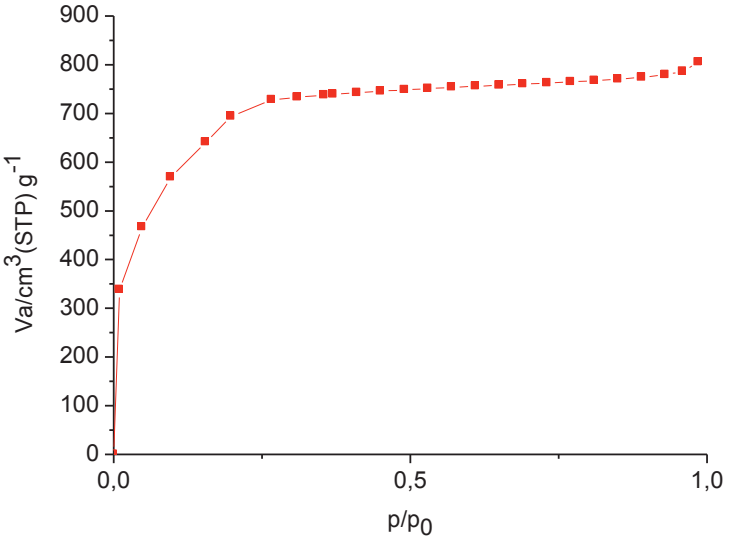

Figure VI-3 : N_2 adsorption isotherm of MIL-101(Fe)-NH_2

VI.3.3 ^{1}H liquid NMR

In contrast to others amino-MOFs, very broad peaks and low resolution were obtained in MIL-101(Fe)-NH_2 spectrum due to the presence of paramagnetic iron species (Figure VI-4).

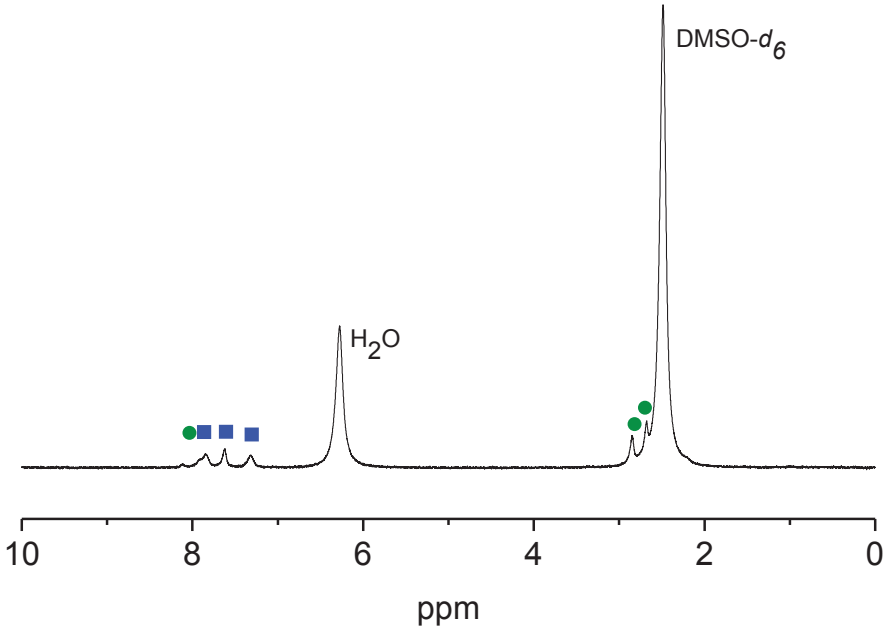

Figure VI-4 : ^{1}H NMR spectra of as-synthesized MIL-101(Fe)-NH_2 (Blue squares and green circles represent signals of aromatic protons of NH_2-bdc and protons of DMF, respectively)

VI.3.4 SEM

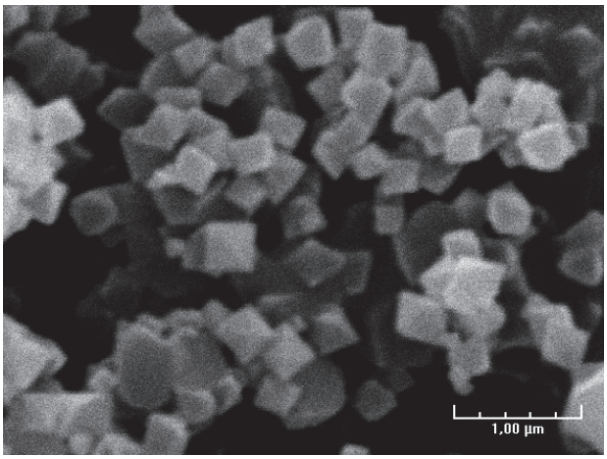

Figure VI-5 : SEM photograph of MIL-101(Fe)-NH_2

As shown in scanning electron microscopy (SEM) image (Figure VI-5), the dimensions of the MIL-101 crystals range from 0.2 up to 0.3 µm.

Some impurities of MIL-88 (hexagonal shaped crystals of about 1µm in size) were found in MIL-101 sample (Figure VI-6).

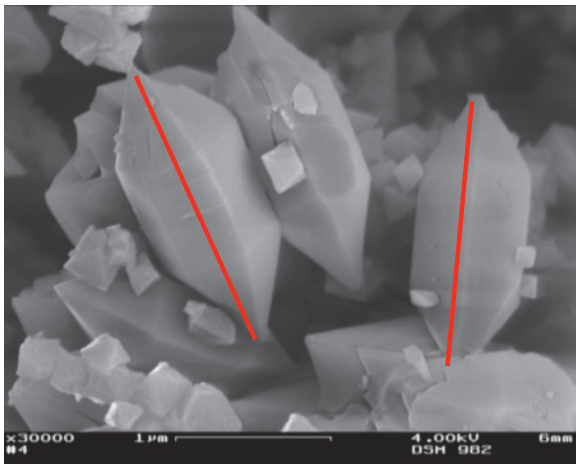

Figure VI-6 : SEM photograph of MIL-88

VII. IRMOF-3 (6)

VII.1 Synthesis

IRMOF-3 [$Zn_4O(C_8H_5O_4N)_3$] was prepared by precipitation according to the procedure reported by Huang *et al.* [11] and detailed in the experimental part. This material was synthesized from a solution of Zn^{2+} and 2-aminoterephthalic acid in which the addition of triethylamine generates a tetrazinc cluster in situ.

VII.2 Structure description

The IRMOF-3 framework consists of Zn_4O tetrahedral subunits linked in octahedral arrays by NH_2-bdc groups to form a porous material with channel windows of 7.4 Å. The Zn edges of the tetrahedra are bridged by six carboxylate groups forming octahedral nodes, linked one another with the aromatic rings of the NH_2-bdc linker resulting in a 3D cubic network (Figure VII-1).

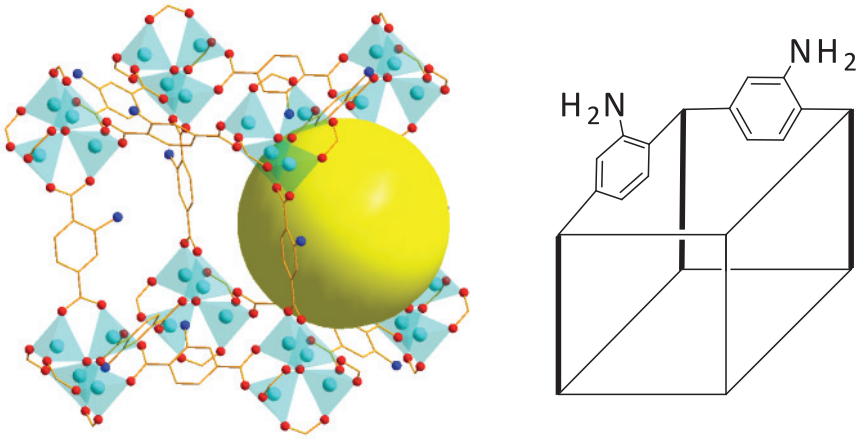

Figure VII-1 : Diagram of IRMOF-3 (Zn = turquoise, C =orange; N = blue, O = red; the yellow ball indicates the size of the pore openings) (left) and its simplified scheme (right)

VII.3 Characterization

VII.3.1 PXRD

The PXRD peak positions of experimental and simulated pattern are essentially the same, except for the peak intensities at 6.8° and 9.7° (Figure VII-2). However, Chen *et al.* rationalized this phenomenon based on their single-crystal structures and concluded that pore filling effects from the zinc species (and partly the solvent molecules) are responsible for the pronounced variations in PXRD peak intensities [12].

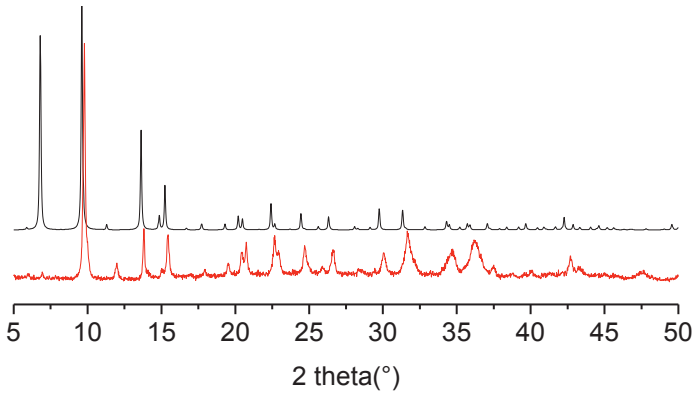

Figure VII-2 : Simulated PXRD pattern from IRMOF-3.cif file (top) and experimental pattern of IRMOF-3 (bottom).

VII.3.2 Nitrogen physisorption at 77K

Lower surface area and micropore volume values (623 m^2/g and 0.32 cm^3/g, respectively) were obtained than those obtained in literature (Figure III-3). Recently, Hausdorf *et al*. highlighted the transformation of IRMOF materials into MOF-69C under moist conditions. According to these results, it is possible that the IRMOF materials also contain minor amounts of Zn-(μ_3OH)-Zn or of MOF-69C microcrystallites that can explain the decrease in porous volume [13, 14].

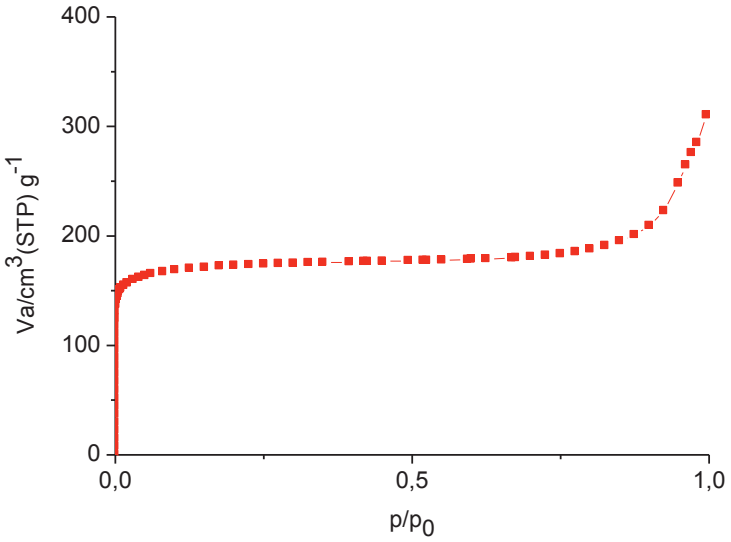

Figure VII-3 : N_2 adsorption isotherm of IRMOF-3

VII.3.3 Scanning Electron Microscopy (SEM)

The SEM photograph of IRMOF-3 shows cubic-shaped crystallites of about 1 µm (Figure VII-4).

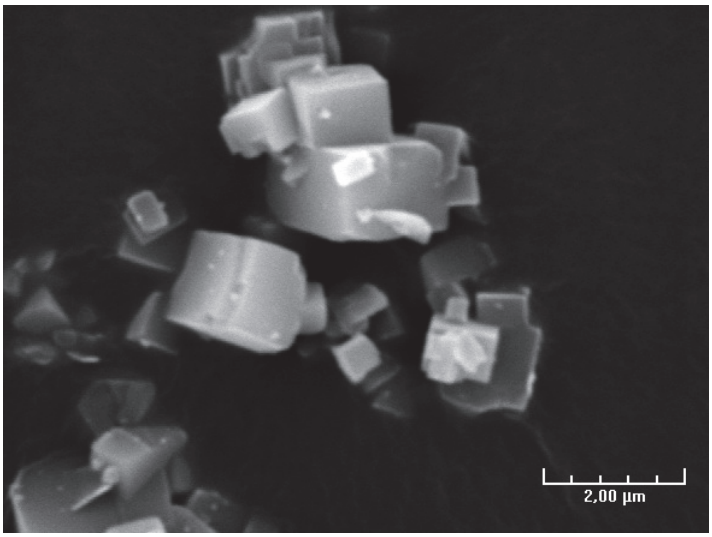

Figure VII-4 : SEM photograph of IRMOF-3

VIII. $ZnF(NH_2)_2TAZ$ (7)

VIII.1 Synthesis

$ZnF(NH_2)_2TAZ$ [$ZnF(C_2H_5N_5)$] was prepared by precipitation according to a procedure published by Goforth and co-workers [15] and detailed in the experimental part. This material was synthesized solvothermally from a mixture of 3,5-diamino-1,2,4-triazole $(NH_2)_2TAZ$ and $ZnF_2 \cdot 4H_2O$ in water.

VIII.2 Structure decription

The three-dimensional structure of the compound displays open-ended, tubular channels, which are constituted of covalently bonded hexanuclear metallamacrocycles ($Zn_6F_6((NH_2)_2TAZ)_6$). The tubular channels are subsequently covalently joined into a honeycomb-like hexagonal array to generate the three-dimensional porous framework with NH_2 groups pointing into the channels (channel diameter ~ 4.7 Å) (Figure VIII-1).

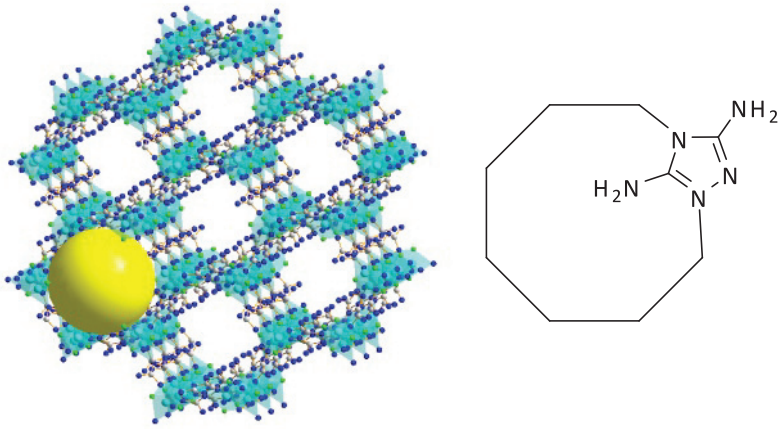

Figure VIII-1: Diagram of $ZnF(NH_2)_2TAZ$ (Zn = turquoise, C =grey; N = blue, F = green; the yellow ball indicates the size of the pore openings) (left) and its simplified scheme (right)

VIII.3 Characterization

VIII.3.1 PXRD

Experimental PXRD patterns match with the simulated pattern obtained from Crystallographic Information File (cif) (Figure VIII-2).

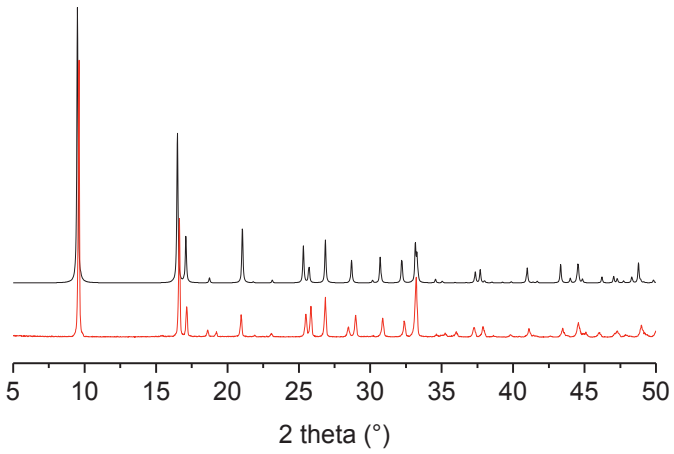

Figure VIII-2 : Simulated PXRD pattern from $ZnF(NH_2)_2TAZ$ (top) and experimental pattern of $ZnF(NH_2)_2TAZ$ (bottom).

VIII.3.2 Nitrogen physisorption at 77K

Nitrogen adsorption isotherm of $ZnF(NH_2)_2TAZ$ was not performed because of its extremely slow uptake. Nevertheless, physisorption of CO_2 performed on $ZnF(NH_2)_2TAZ$ at 303K, 1 atm revealed an uptake of 8.5 $cm^3.g^{-1}$.

VIII.3.3 SEM

The SEM photograph of $ZnF(NH_2)_2TAZ$ shows rectangular-shaped crystallites of about 5 µm.

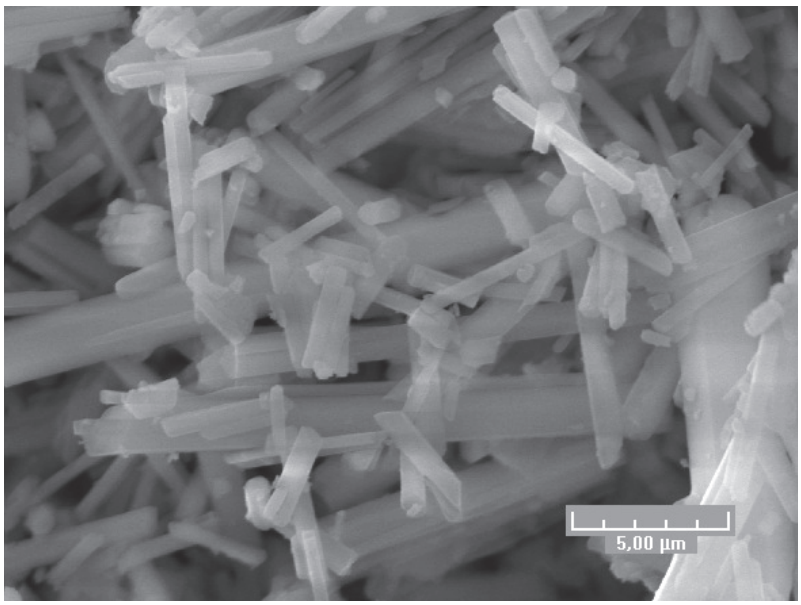

Figure VIII-3 : SEM photograph of $ZnF(NH_2)_2TAZ$

IX. Summary

Table IX-1 : Main characteristics of the amino-MOFs prepared in this study.

MOF	Metal	Linker	Synthesis	Pores channels	Pores size (Å)	Surface area[a] ($m^2.g^{-1}$)	Microporous volume[b] ($cm^3.g^{-1}$)	Crystallytes size (µm)
DMOF-NH_2 **1**	Zn	NH_2-bdc + DABCO	Precipitation	3D	5.6	1320	0.54	0.8-1
MIL-68(In)-NH_2 **2**	In	NH_2-bdc	Precipitation	1D	6 - 17	1120	0.49	<0.1
CAU-1 **3**	Al	NH_2-bdc	Sovolthermal	3D	4.5 - 10	1434	0.52	<0.1
MIL-53(Al)-NH_2 **4**	In	NH_2-bdc	Sovolthermal	1D	8.5	1155	0.42	0.2-0.5
MIL-101(Fe)-NH_2 **5**	Fe	NH_2-bdc	Sovolthermal	3D	29 - 34	2436	1.12	0.2-0.3
IRMOF-3 **6**	Zn	NH_2-bdc	Precipitation	3D	7.4	623	0.32	1
$ZnF(NH_2)_2TAZ$ **7**	Zn	$(NH_2)_2$ -TAZ	Sovolthermal	1D	4.7	-	-	5

[a] From BET analysis [b] From t-plot analysis

Table IX-1 summarizes the main characteristics of these materials. IRMOF-3, DMOF-NH_2 and MIL-68(In)-NH_2 were synthesized by precipitation, whereas the others by solvothermal synthesis. $ZnF(NH_2)_2TAZ$, DMOF-NH_2 and CAU-1 exhibit the smallest pore size (4.7, 6 Å and 4 -10 Å, respectively) and MIL-101 the largest (29-34 Å). In terms of pore network, $ZnF(NH_2)_2TAZ$, MIL-53 and MIL-68 have monodirectional channels (1D), whereas the other materials have 3D pore structure. The MIL-53 structure allows large breathing phenomena upon external stimuli. Some of the MOFs selected present chemical features that may interfere with grafting processes, namely CAU-1, which exhibits hydroxy and methoxy bridging groups, as well as MIL-68(In)-NH_2 and MIL-53(Al)-NH_2, which are built from inorganic nodes with hydroxyl bridging groups. In addition, the trinuclear nodes of MIL-101(Fe)-NH_2 show uncoordinated centers as well as terminating Cl and OH. The weakly coordinated DABCO to the Zn paddlewheel lowers the chemical stability of DMOF-NH_2 (it is easily soluble in acidic or basic media). By contrast, MIL-53(Al)-NH_2 is barely soluble in aqueous acidic solution. Finally, for DMOF-NH_2, MIL-53(Al)-NH_2, MIL-101(Fe)-NH_2, IRMOF-3 and $ZnF(NH_2)_2TAZ$, crystallite sizes are of about 0,2-5 µm whereas crystallite are significantly smaller for MIL-68(In)-NH_2 and CAU-1 as observed by SEM.

X. References

[1] Z. Q. Wang, K. K. Tanabe, S. M. Cohen, *Inorg. Chem.* **2009**, *48*, 296-306.
[2] D. N. Dybtsev, H. Chun, K. Kim, *Angew. Chem., Int. Ed.* **2004**, *43*, 5033-5036.
[3] J. J. Low, A. I. Benin, P. Jakubczak, J. F. Abrahamian, S. A. Faheem, R. R. Willis, *J. Am. Chem. Soc.* **2009**, *131*, 15834-15842.
[4] M. Savonnet, D. Bazer-Bachi, C. Pinel, V. Lecocq, N. Bats, D. Farrusseng, *FR 09/05.101* **2009**.
[5] C. Volkringer, M. Meddouri, T. Loiseau, N. Guillou, J. Marrot, G. Ferey, M. Haouas, F. Taulelle, N. Audebrand, M. Latroche, *Inorg. Chem.* **2008**, *47*, 11892-11901.
[6] T. Ahnfeldt, N. Guillou, D. Gunzelmann, I. Margiolaki, T. Loiseau, G. Ferey, J. Senker, N. Stock, *Angew. Chem., Int. Ed.* **2009**, *48*, 5163-5166.
[7] S. Bauer, C. Serre, T. Devic, P. Horcajada, J. Marrot, G. Ferey, N. Stock, *Inorg. Chem.* **2008**, *47*, 7568-7576.
[8] T. Ahnfeldt, D. Gunzelmann, T. Loiseau, D. Hirsemann, J. Senker, G. Ferey, N. Stock, *Inorg. Chem.* **2009**, *48*, 3057-3064.
[9] G. Chaplais, A. Simon-Masseron, F. Porcher, C. Lecomte, D. Bazer-Bachi, N. Bats, J. Patarina, *Phys. Chem. Chem. Phys.* **2009**, *11*, 5241-5245.
[10] K. M. L. Taylor-Pashow, J. Della Rocca, Z. G. Xie, S. Tran, W. B. Lin, *J. Am. Chem. Soc.* **2009**, *131*, 14261-14263.
[11] L. M. Huang, H. T. Wang, J. X. Chen, Z. B. Wang, J. Y. Sun, D. Y. Zhao, Y. S. Yan, *Microporous Mesoporous Mater.* **2003**, *58*, 105-114.
[12] B. Chen, X. Wang, Q. Zhang, X. Xi, J. Cai, H. Qi, S. Shi, J. Wang, D. Yuan, M. Fang, *J. Mater. Chem.* **2010**, *20*, 3758-3767.
[13] S. Hausdorf, F. Baitalow, J. Seidel, F. Mertens, *J. Phys. Chem. A* **2007**, *111*, 4259-4266.
[14] S. Hausdorf, J. Wagler, R. Mossig, F. Mertens, *J. Phys. Chem. A* **2008**, *112*, 7567-7576.
[15] A. M. Goforth, C.-Y. Su, R. Hipp, R. B. Macquart, M. D. Smith, H.-C. zur Loye, *J. Solid State Chem.* **2005**, *178*, 2511-2518.

Chapter 3

Postsynthetic modification by acylation reaction

I. Introduction

This work was carried out at the beginning of the project in 2008. At this time, only a few amino-MOFs (IRMOF-3 [1], $ZnF(NH_2)_2TAZ$ [2]) were already known in literature and post-functionalization methods were restricted to grafting reactions involving amines with anhydrides [3, 4] or isocyanates [5, 6] . Nevertheless, only a few functional and commercial anhydride acids or isocyanates derivates were available. Furthermore, the stability of MOFs in water was not well known, consequently the risk was anticipated by using a reaction of acylation without release of water.

For this purpose, both IRMOF-3 **6** and $ZnF(NH_2)_2TAZ$ **7** were post-functionalized with pyridine groups in order to increase the hydrophobicity while maintaining a similar level of basicity (pKa ~5 for aniline and pyridine). The grafting on solids was also performed by acylation because of the large library of commercial acyl chlorides including nicotinoyl chloride.

II. Grafting reaction

II.1 Homogeneous conditions

Firstly, the grafting was performed in homogeneous conditions with dimethyl-2-aminoterephthalate and nicotinoyl chloride in dichloromethane at room temperature (Scheme II-1). A large excess of triethylamine was used to trap the liberation of HCl. A yield of 60% was obtained.

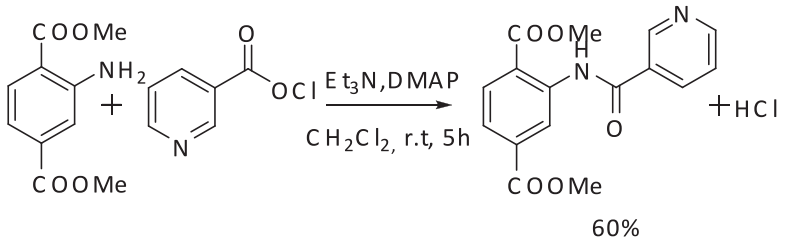

Scheme II-1 : Reaction of dimethyl-2-aminoterephthalate with nicotinoyl chloride

As reference grafted compound, the aromatic shifts were assigned by (Correlation Spectroscopy) COSY NMR experiments.

II.2 Functionalized IRMOF-3 **(6b)**

In the same conditions into IRMOF-3 **6**, no reaction was observed. DMF was used instead of dichloromethane and at 110°C instead of 30°C to increase the solubility and diffusion of nicotinoyl chloride into the pores allowing the reaction.

In a typical postsynthetic modification procedure, a suspension of **6** in DMF is treated with nicotinoyl chloride for 5 days at 110°C, then filtered and washed three times with DMF to provide functionalized IRMOF-3 **6b**.

II.2.1 Proofs of grafting

Infrared analyses of **6** and **6b** reveal a significant decrease in the two signals centred at 3500 and 3390 cm^{-1} corresponding to the stretching vibrational modes of $–NH_2$ species. The integration of these bands allows an estimation of ~50% functionalization for IRMOF-3. The peak at 3070 cm^{-1}, assigned to νArC-H, reveals the presence of the nicotinoyl group, while the absence of a signal at 3600 cm^{-1} indicates that there are no Zn-OH bonds [7].

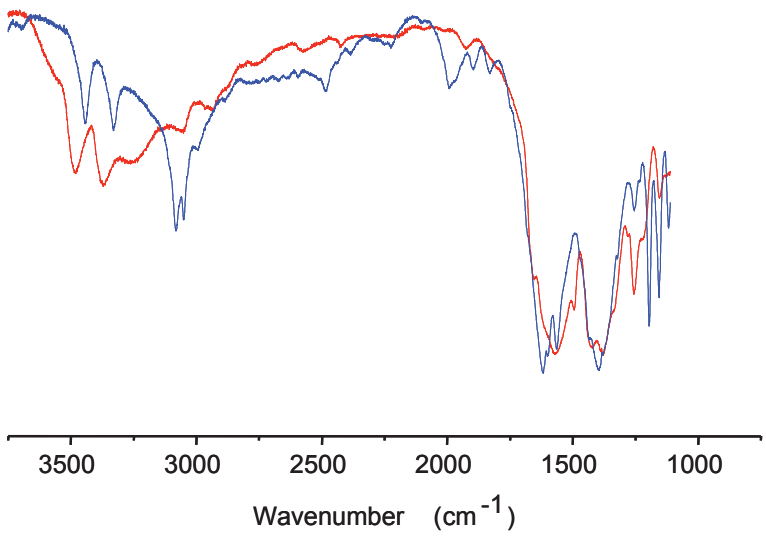

Figure II-1 : FT-IR spectra of 6 (red) and 6b (blue).

Further proof of grafting is revealed by ^{1}H NMR analysis of digested **6b** in $DCl/D_2O/DMSO\text{-}d_6$. New aromatic shifts of **6b** correspond to the aromatic shift of reference grafted compound. The ^{1}H integration between peaks of **6** and **6b** indicates a grafting rate of ~40%, which is close to that obtained via infrared measurements. Although the washing routine with DMF removes unreacted nicotinoyl chloride, 0.3 molecules per unit cage still remain in the porous network of **6b**. The peak at 7.9 ppm is characteristic of the formyl proton of residual DMF (Figure II-2).

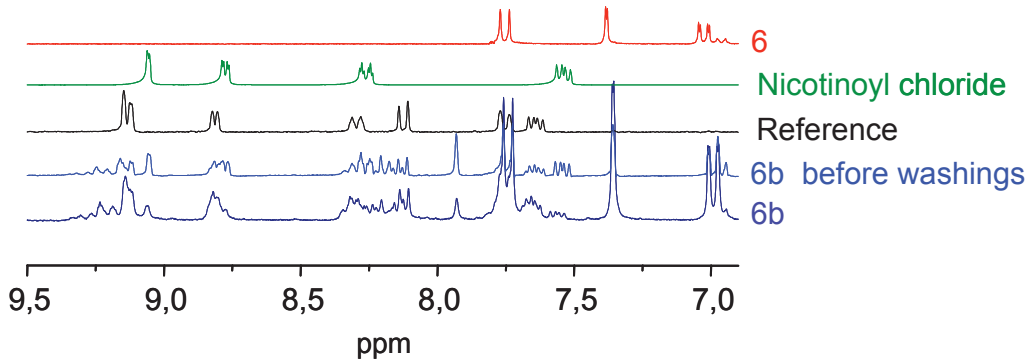

Figure II-2 : ^{1}H NMR enlargement of digested 6, nicotinoyl chloride, reference, digested 6b before washings and digested 6b

The negative mode MS clearly shows a base peak at m/z 285.1 ($M\text{-}H^-$) corresponding to the grafted linker.

In addition, the decrease of the microporous surface from 650 $m^2\ g^{-1}$ for **6** to 180 $m^2\ g^{-1}$ for **6b** confirms a reduction in free available space provoked by the introduction of basic groups and the presence of residual acid in the pore, which might be the cause of the loss of crystallinity.

II.3 Functionalized $ZnF(NH_2)_2TAZ$ **(7b)**

In contrast, the crystallinity of the functionalized zinc triazolate **7b** is fully preserved (Figure II-3). Unfortunately, the NMR quantification of the grafting rate cannot be performed on **7b** due to the absence of ^{1}H on the linker. A grafting rate of approximatively 60% was measured by elementary analysis based on the N and C contents. In addition, mass spectrometry

analysis performed after digestion shows a signal at *m/z*=309 corresponding to the doubly functionalized linker.

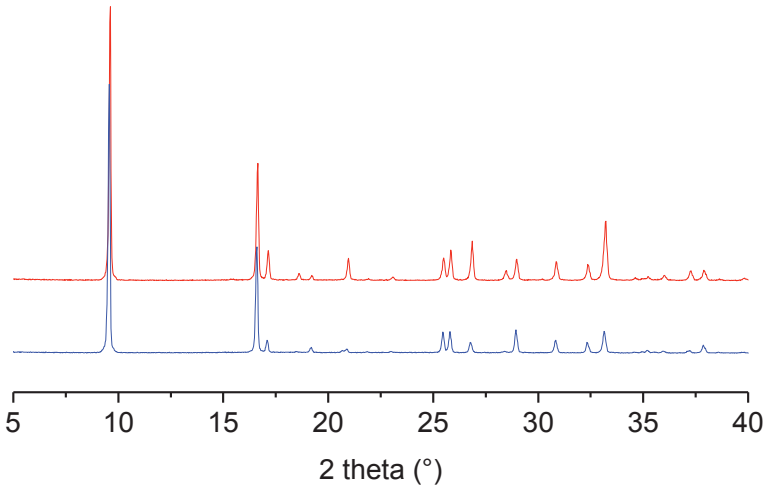

Figure II-3 : XRD pattern of 7 (top) and 7b (bottom)

III. Catalytic reactions

Catalytic materials were evaluated using aza-Michael reaction and simple transesterification as model reactions. Knoevenagel condensations are usually chosen as model reactions for evaluating base catalysts. However, the condensation liberates water which in our case could modify the structure of IRMOF-3 [8, 9, 10]. In contrast, aza-Michael condensations do not liberate water and is appropriate to probe weak demanding base reactions [11, 12]. In addition, the aza-Michael reaction has found practical applications. The conjugate addition of amines to α,β-unsaturated compounds to form β-amino carbonyl compounds constitutes a key reaction in the synthesis of various complex natural products, antibiotics, β-amino alcohols and chiral auxiliaries [13] (Figure III-1).

In an aim of probing the catalytic centres and getting read off possible mass transfer limitations, ethyldecanoate was used as model compound for transesterification instead of bulkier triglycerides (See appendix A).

For comparison purposes, alkylamino-functionalized mesoporous ordered silica MCM-41 (Mobil Composition of Matter No.41) **8** and corresponding post-functionalized compounds with 1.5% mol based on amino groups **8b** were prepared following the same procedure and

then tested. Moreover, test reactions were carried out in homogeneous conditions with molecular analogues, namely aniline and pyridine which are the corresponding active centres for **6**, **7**, **8** and **6b**, **7b**, **8b,** respectively.

III.1 Aza-Michael reaction

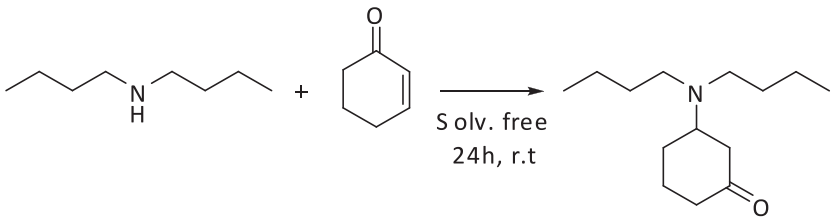

Figure III-1 : Diagram of one example of the aza-Michael reaction. Reaction of dibutylamine with cyclohexen-1-one

Cyclic and acyclic aliphatic amines underwent 1,4-addition with different α,β-unsaturated compounds to afford the corresponding Aza-Michael product without formation of byproduct (Table III-1). The molecular catalysts i.e. aniline and pyridine show similar yields which is consistent with their very close pKa, 4.6, and 5.2, respectively. Clearly, the functionalized MOF materials exhibit superior yields with regards to their molecular analogues and also with regards to MCM functionalized materials. Finally, highest yields are always found for post-functionalized materials **6b**, **7b** and **8b**, with respect to their parent forms **6**, **7** and **8**. These self-consistent results point out the superiority of MOF catalysts over molecular and inorganic analogues. It has to be pointed out that the difference in yields according to the substrates results from the electrophilic character of the acceptor and the relative nucleophilicity of the donor. Highest yields are achieved for the most activated acceptor and/or the most nucleophilic donor.

Table III-1 : Catalytic results of aza-Michael reactions at room temperature based on 1.5 mol% on basic (aniline or pyridine type) groups and with a stoechiometry donor:acceptor of 1.0:1.1.

	Yield (%)							
Substrates	**Aniline**	**Pyridine**	**6**	**6b**	**7**	**7b**	**8**	**8b**
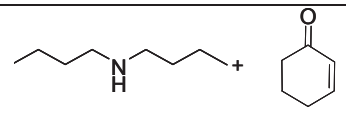	17±2	19±2	44±2	**47±2**	23±2	28±2	21±2	34±2
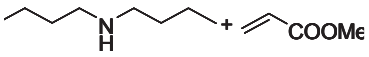	66±2	70±2	76±2	77±2	59±2	**79±2**	63±2	65±2
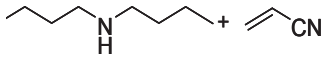	59±2	57±2	66±2	72±2	42±2	**85±2**	72±2	80±2
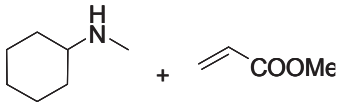	82±2	83±2	90±2	**94±2**	88±2	90±2	84±2	86±2
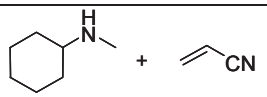	79±2	81±2	76±2	**94±2**	75±2	87±2	76±2	85±2
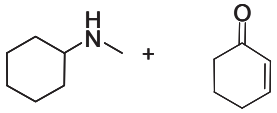	19±2	22±2	24±2	29±2	20±2	**33±2**	18±2	24±2

III.2 Transesterification reaction

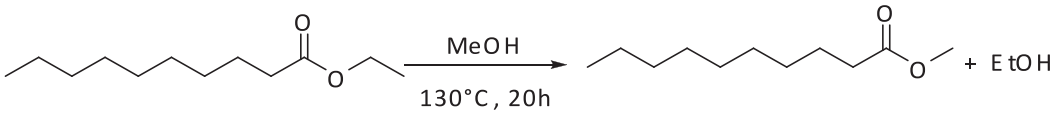

Figure III-2 : Diagram of transesterification of ethyldecanoate with methanol

For ethyldecanoate transesterification with MeOH (1:28) (Figure III-2), all MOF compounds reach 95% conversion after 24 h stirring at 180°C (1.5 mol% catalyst), which corresponds to equilibrium. Catalytic runs were carried out at lower temperature (130 °C) in order to discriminate activities between the various MOFs (Figure III-3). Here again, **6** and **6b** show the highest catalytic activities, with a significant enhancement of the yield after post-functionalization with pyridine. The small pore size of **7** can explain the limitations to addressing the catalytic transformation of bulkier ethyldecanoate. On the other hand, for the MCM catalysts, a decrease in activity was observed after functionalization. **8** have pores too large to show the confinement effects imposed by pyridine groups.

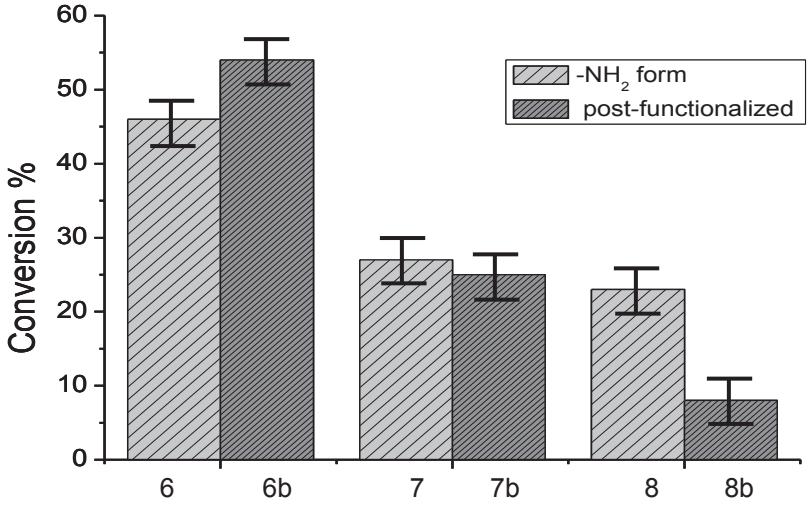

Figure III-3 : Catalytic results of the transesterification of ethyldecanoate with MeOH (1:28) at 130 °C for 24 h.

Aza-Michael reaction does not require strong basic sites since it can proceed on pyridine polymers [11]. In contrast, stronger immobilized nitrogen bases such as guanidines are required for low temperature transesterification (e.g. 80°C). However, weaker sites such as described

herein are sufficient to perform the reaction in current process conditions (T=190°C, P~30 bars).

III.3 Conclusions

We anticipate that the superiority of functionalized MOFs (**6b** and **7b**) against MCM analogue catalysts arises from the activation of the substrates via strong adsorption in the organic micropore framework whereas such confinement is not found in inorganic mesoporous MCM materials.

IV. Conclusions

Regarding this first strategy, limitations appear concerning the reaction conditions as well as the supports themselves.

The main issues were the known weak stability of IRMOF-3 and the window size of $ZnF(NH_2)_2TAZ$.
The generation of HCl molecules not entirely trapped by triethylamine during acylation reaction, might be the cause of the loss of crystallinity of functionalized IRMOF-3. Furthermore, the size of $ZnF(NH_2)_2TAZ$ is critical for the accessibility of bulky reactant (ethyldecanoate) inside the cavities. Finally, traces of nicotinoyl chloride which could remains blocked inside the pores (even after repeated DMF washings) could interfere during catalysis processes involving the functionalized MOF.

Although the concept of post-functionalized Metal-Organic Frameworks to base catalysis was validated, valuable alternatives lie in the development of all kinds of generic post-functionalization methods that are soft, do not liberate byproducts that may react or remain blocked in the pores, and enable grafting of a wide variety of chemical functions with high efficiency and selectivity (Chapter 4).
In the years 2007-2009, many new amino-MOFs were published and the stability issue of IRMOF materials revealed [9, 10, 14].

V. References

[1] L. M. Huang, H. T. Wang, J. X. Chen, Z. B. Wang, J. Y. Sun, D. Y. Zhao, Y. S. Yan, *Microporous Mesoporous Mater.* **2003**, *58*, 105-114.

[2] A. M. Goforth, C.-Y. Su, R. Hipp, R. B. Macquart, M. D. Smith, H.-C. zur Loye, *J. Solid State Chem.* **2005**, *178*, 2511-2518.

[3] Z. Q. Wang, S. M. Cohen, *J. Am. Chem. Soc.* **2007**, *129*, 12368-12369.

[4] K. K. Tanabe, Z. Q. Wang, S. M. Cohen, *J. Am. Chem. Soc.* **2008**, *130*, 8508-8517.

[5] E. Dugan, Z. Q. Wang, M. Okamura, A. Medina, S. M. Cohen, *Chem. Commun.* **2008**, 3366-3368.

[6] P. Gamez, J. S. Costa, C. A. Black, O. Roubeau, S. J. Teat, J. Reedijk, *Eur. J. Inorg. Chem.* **2008**, 1551-1554.

[7] U. Ravon, M. E. Domine, C. Gaudillere, A. Desmartin-Chomel, D. Farrusseng, *New J. Chem.* **2008**, *32*, 937-940.

[8] S. S. Kaye, A. Dailly, O. M. Yaghi, J. R. Long, *J. Am. Chem. Soc.* **2007**, *129*, 14176-14177.

[9] S. Hausdorf, F. Baitalow, J. Seidel, F. Mertens, *J. Phys. Chem. A* **2007**, *111*, 4259-4266.

[10] S. Hausdorf, J. Wagler, R. Mossig, F. Mertens, *J. Phys. Chem. A* **2008**, *112*, 7567-7576.

[11] V. P. R. Raje, R. P. Bhat, S. D. Samant, *Synlett* **2006**, *16*, 2676-2678.

[12] I. P. Beletskaya, E. A. Tarasenko, A. R. Khokhlov, V. S. Tyurin, *Russ. J. Organ. Chem.* **2010**, *46*, 461-467.

[13] M. E. T. Jung, Barry M.; Fleming, Ian, *Comp. Org. Synth.* **1991**, *4*, 30.

[14] M. Sabo, A. Henschel, H. Froede, E. Klemm, S. Kaskel, *J. Mater. Chem.* **2007**, *17*, 3827-3832.

Chapter 4

Combinatorial Synthesis of Metal-Organic Frameworks libraries by Click-Chemistry

I. Introduction

One of the most popular reactions within the Click Chemistry concept is the Cu^{I}-catalyzed Huisgen cycloaddition of azides with alkynes. The catalytic cycle of "Click Chemistry" is reported in Figure I-1 : the sequence begins with the coordination of the alkyne to the Cu(I) species (step **A**), displacing one of the acetonitrile ligands, then the azide replaces one of the ligands and binds to the copper atom via the nitrogen proximal to carbon, forming intermediate **3**. In the next step, the nitrogen of the azide in **3** attacks the C-2 carbon of the acetylide, forming the unusual six-membered copper (III) metallacycle **4**. After ring contraction, which forms the triazolyl-copper derivative **5**, proteolysis of **5** releases the triazole product, thereby completing the catalytic cycle [1].

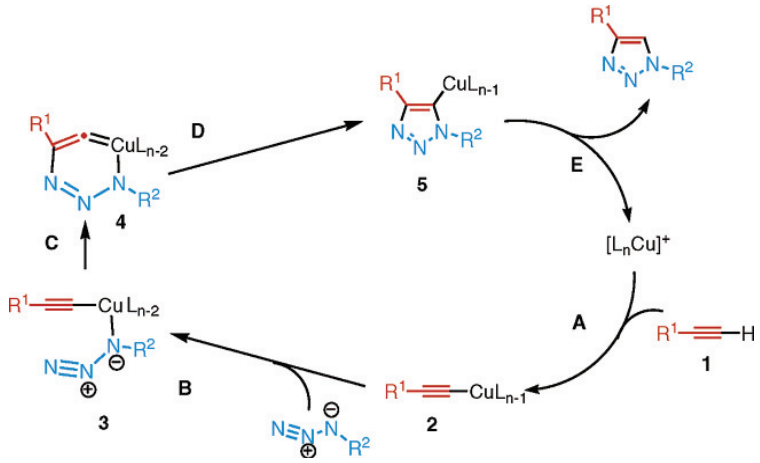

Figure I-1: Cu^{I}-catalyzed Huisgen cycloaddition of azides with alkynes mechanism

"Click" reactions possess numerous advantages. Not only it proceeds efficiently in mild conditions with high yields and high specificity but it allows also the grafting of various functional groups, which yield no by-product. Such key features prompted us to use it for the modification of well-defined MOFs.

Two recent studies by Goto *et al.* and by Gadzikwa *et al.* deal with the use of Click Chemistry for the post-functionalization of MOFs. Goto *et al.* reported that the parent MOF material was built from an azide linker, while in a reverse way, Gadzikwa *et al.* [2, 3] prepared MOF bearing TMS-protected acetylenes (Figure I-2).

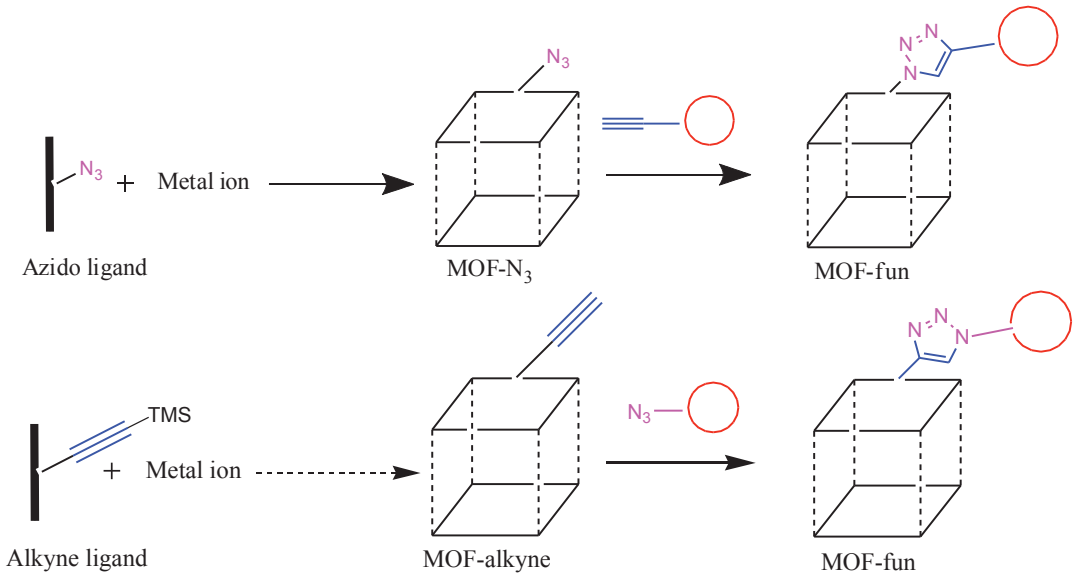

Figure I-2 : Goto *et al* (top) and Gadzikwa *et al.* (bottom) strategies

Although these strategies are very promising, they both have some limitations. They synthesized their MOF-bearing azide or alkyne groups, as suitable platforms for "Click Chemistry", by self-assembly. The starting azido or alkyne ligands are not commercially available [4] and require multi-step syntheses. Moreover, the chemical instability of azide significantly limits the synthesis of the desired MOF by a solvothermal method, which may require high temperatures. According to the second way, the silyl-protected groups have to be deprotected in the presence of various fluoride sources that cause slight dissolution of the crystals in the case of long-term deprotection.

In this chapter, we present an alternative method of PSM using Click Chemistry reaction that can be applied to all kinds of amino-MOFs over a very wide range of pore size (micro to meso), chemical stability (low to high) and structural flexibility, using a great variety of grafted chemical functions (acidic, coordinative, basic, aromatic, aliphatic and hydrophilic). The first step involves an original method to convert a MOF in its amino form to the corresponding azide compound (MOF-N_3). Next, the desired functionalized material (MOF-

fun) is obtained by "clicking" a synthon onto the azide without isolation of the intermediate (Figure I-3).

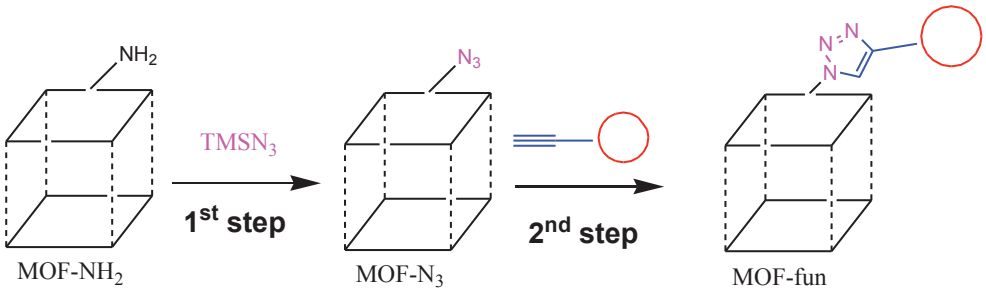

Figure I-3 : MOF-NH_2 and its functionalized forms MOF-N_3 and MOF-fun

This strategy will be applied to amino-MOFs (**1**, **2**, **3**, **4** and **5**) previously described in Chapter 2. Firstly, the optimization of this method will be presented, then its generic application to amino-MOFs. Finally, the control effect of the grafting rate on the porous volume of the host MOF will be also studied. Some characterizations can be find in Appendix.

II. Investigation of experimental conditions in solution

The reaction conditions for a sequential one-pot procedure were optimized in homogeneous conditions by using dimethyl-2-aminoterephthalate with phenylacetylene (chosen as proof of concept).

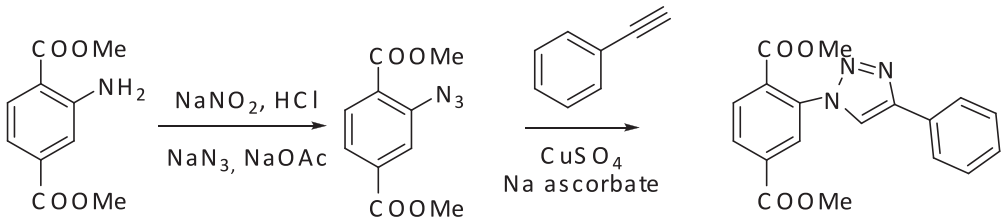

Figure II-1 : Typical reaction conditions for azide formation following by azide-alkyne cycloaddition

The common way to generate azide compounds from the corresponding amines is via the displacement of the appropriate diazonium salt by using potential explosive sodium azide NaN_3.

Concerning the step of Click Chemistry, the key is the generation of Cu^{I} required for the azide-alkyne cycloaddition, which is commonly achieved by adding Cu^{II} and a reducing agent [5] such as sodium ascorbate (Figure II-1).

It must be noted that the usual technique for preparing azide compounds from the corresponding amines via their diazonium salts [6] cannot generally be applied to MOFs. Indeed, as described in experimental part, all amino-MOFs (**1**, **2**, **3**, **5**, **6** and **7**) except MIL-53-Al-NH_2 **4** dissolve rapidly under acidic conditions (DCl/D_2O/DMSO) for liquid ^1H NMR analyses.

We have instead investigated another pathway that uses soft conditions and involves stable (*t*-BuONO) and non-explosive compounds ($TMSN_3$) [7]. Furthermore, concerning the second step, the direct use of Cu^{I} salts ($Cu^{I}(CH_3CN)_4PF_6$) was preferred in order to limit the number of reactants that could remain blocked inside the pores (Figure II-2).

Thus, in a typical synthesis (Figure II-2), dimethyl-2-aminoterephthalate was dissolved in THF and cooled to 0°C in an ice bath. To this stirred mixture was added *t*-BuONO, followed by a dropwise addition of $TMSN_3$. The resulting solution was stirred at room temperature for one night. Phenylacetylene and $Cu^{I}(CH_3CN)_4PF_6$ were then added, and this mixture was stirred overnight at room temperature. The mixture was concentrated under vacuum and the organics were extracted by CH_2Cl_2 and washed with water, saturated $NaHCO_3$ (aq) and brine. After drying over Na_2SO_4, the solvent was taken off under reduced pressure. The yield obtained was 80%.

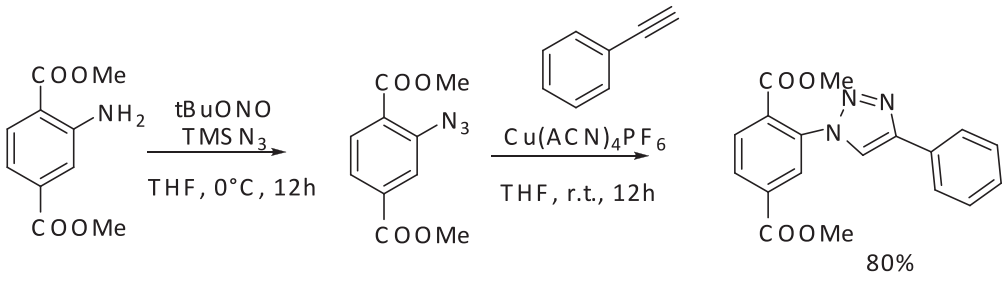

Figure II-2 : One-pot, two-Step functionalization of reference compound

III. Generation of functionalized MOFs

The five parent MOFs are DMOF-NH_2 **1**, MIL-68(In)-NH_2 **2**, CAU-1 **3**, MIL-53(Al)-NH_2 **4** and MIL-101(Fe)-NH_2 **5**, described in Chapter 2. The post-modification of the MOFs proceeds as previously described and has been applied to all cases described herein (Figure III-1). In a typical synthesis, the freshly-dried amino-MOF is treated with tBuONO and $TMSN_3$ in THF for one night at room temperature to produce the corresponding azide intermediate MOF **(1a, 2a, 3a, 4a, 5a)**. In the same vessel, functionalized MOF is obtained by adding an appropriate amount of alkyne in the presence of $Cu^I(CH_3CN)_4PF_6$, followed by continuous stirring for 12 h. The alkynes used in this study are phenylacetylene **b**, diethylpropargylamine **c**, hexyne **d**, propargyl alcohol **e**, propiolic acid **f** and propargylamine **g**. Extensive washings were carried out to remove copper catalyst from the solids.

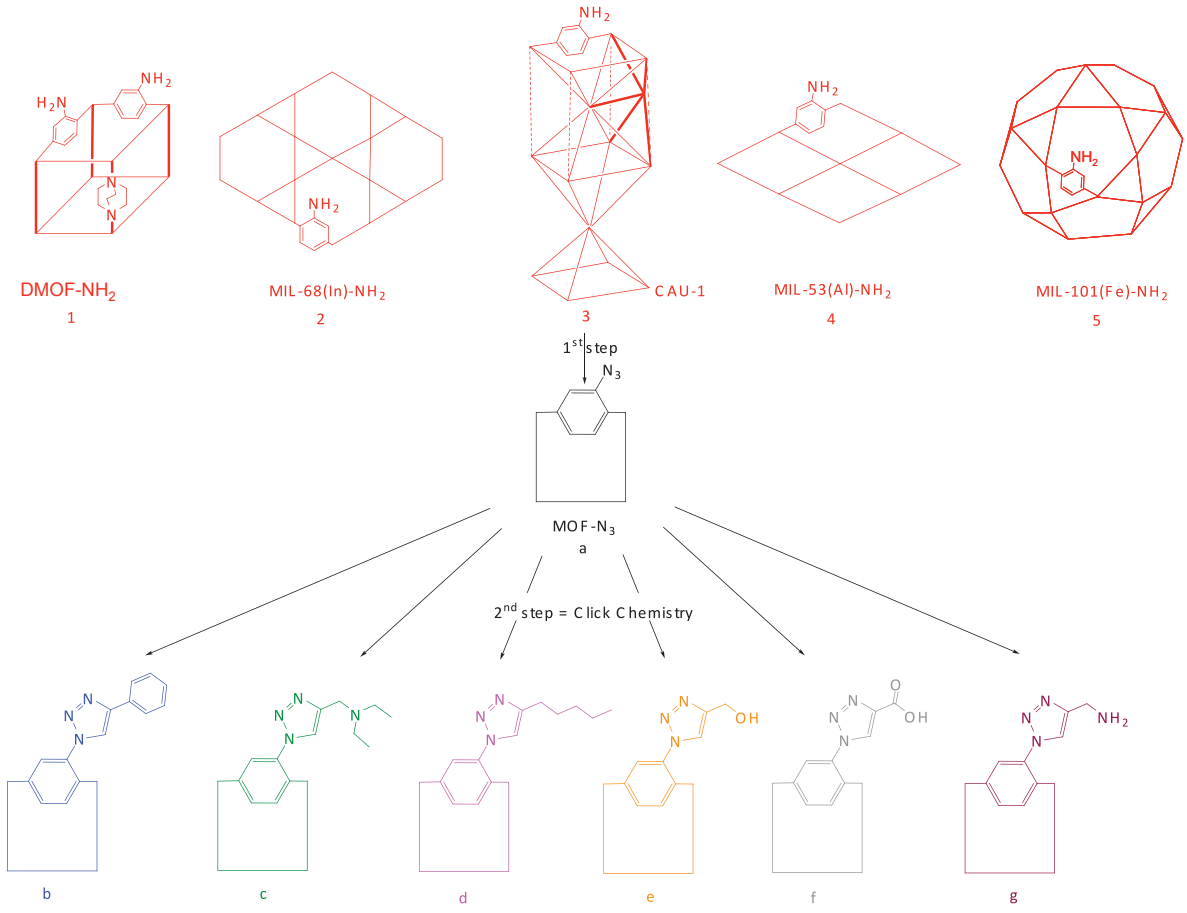

Figure III-1 : Strategy for the generation of functionalized MOFs

III.1 Determination of the grafting rate calculated from liquid ^{1}H NMR integration

Liquid ^{1}H NMR analysis was carried out in order to obtain unambiguous quantifications of the degree of post-modification for the first and the second steps. The samples derived from parent MOFs **1**, **2**, **3** and **5** were digested and dissolved in dilute DCl/D_2O/DMSO-d_6 solution, whereas the compounds derived from **4** required dissolution in DCl/D_2O/DMSO-d_6 followed by NaOD/D_2O because of their high chemical stability as reported in Chapter 2.

III.1.1 First step: azide formation

This first step of functionalization is already highly relevant to obtain MOFs-bearing nitrene groups through photoactivation [8]. Liquid ^{1}H NMR allows to prove that the complete conversion of the amino to the azide can be achieved for all types of MOFs on a quantitative manner. The spectrum of digested DMOF-N_3 **1a** reveals the formation of the azide corresponding compound through the appearance of new aromatic signals (7.73-7.83ppm, m, ArH). This coincides with the complete disappearance of the aromatic signals of DMOF-NH_2 **1** (7.15 ppm, d, 1H, J = 8.3Hz; 7.44 ppm, s, 1H; 7.8 ppm, d, 1H, J = 8.3Hz) (Figure III-2), thus indicating full conversion to the azide form. The ^{1}H NMR spectra of **2a**, **3a**, **4a** and **5a** can be found in Appendix A.

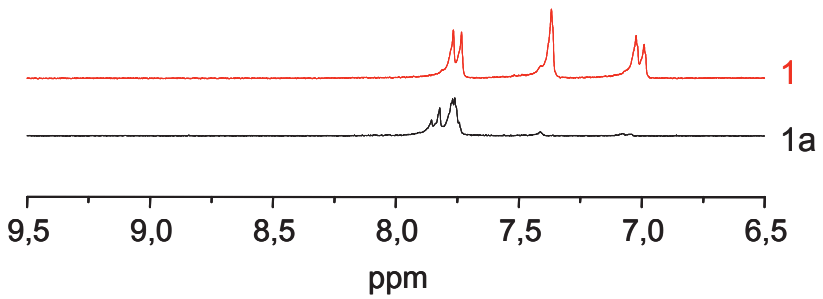

Figure III-2 : ^{1}H NMR enlargement in the aromatic region of digested 1 and 1a

A detailed kinetic analysis of the first step reactions for each amino-MOF was performed in order to determine when can take place the alkyne addition.

The kinetics of the conversion of **1**, **2**, **3**, **4** and **5** was followed by ^{1}H NMR analysis (Figure III-3). We have observed that for an equal excess of $TMSN_3$, the kinetics are much slower for MIL-68(In)-NH_2 **2** and MIL-53(Al)-NH_2 **4** than for the other parent MOFs. This likely arises from their 1D porous structure, which limits the diffusion rate of $TMSN_3$ to the center of the crystallites. Nevertheless, a contraction of the channels cannot be ruled out for the MIL-53 structure. For MIL-68(In)-NH_2 **2** and MIL-53(Al)-NH_2 **4**, a larger excess of $TMSN_3$ shall therefore be used in order to allow complete conversion in a few hours.

Conversely, the apparent kinetics is faster for 3D porous structures with high porous volume, such as MIL-101(Fe)-NH_2 **5**. While DMOF-NH_2 **1** was completely converted to **1a** after 12h, for equal ratio **5a** was formed within only 30 mn.

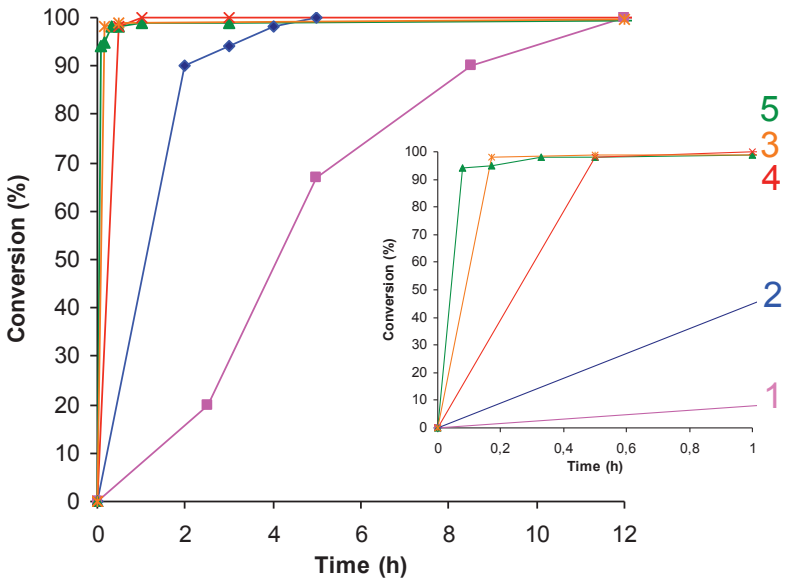

Figure III-3 : Kinetics of conversion of 1, 2, 3, 4 and 5. The $TMSN_3$: MOF ratio is 6, 38, 17, 78 and 6 respectively.

In a scientific way, the experiments do not facilitate a "fair" comparison of the kinetics since conditions are not exactly the same. Our objective was different and pragmatic oriented. In a context of combinatorial approach, we wanted to keep the same reaction time (12h) for all the MOF PSM. Consequently, a larger excess of reactants shall therefore be used depending on the MOF structure to complete the reaction in 12h.

III.1.2 Second step: "click reaction"

After the cycloaddition step, new aromatic shifts on ^{1}H NMR spectra of the post-modified digested compounds **1b**, **1c**, **1d** and **1e** confirm that the corresponding triazole derivative is formed as the sole product (Figure III-4). Moreover the proton of the triazole moiety has a chemical shift in the range 8.5-9.5 ppm depending on the nature of the alkynyl group. This enables straightforward quantification while providing a visible indicator that the reactions have proceeded, in contrast to condensation reactions, for which the degree of conversion is usually more difficult to identify. The ^{1}H NMR spectra of **2**, **3**, **4** and **5** derivates can be found in Appendix A.

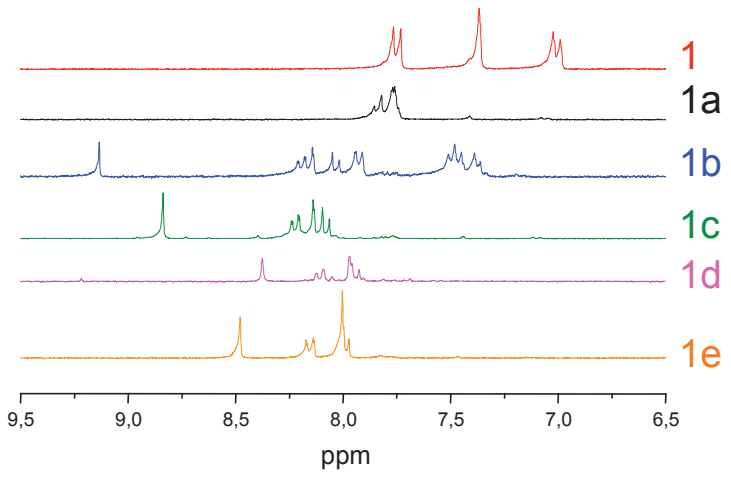

Figure III-4 : ^{1}H NMR enlargement in the aromatic region of digested 1, 1a, 1b, 1c, 1d and 1e

Table III-1 reports the degree of modification for the five parent MOFs, i.e., the conversion of $-NH_2$ to $-N_3$ and that of $-N_3$ to the corresponding functional triazolate when large excess of alkynes are used. Due to the very broad peaks and the low resolution obtained in ^{1}H NMR for MIL-101(Fe) systems (Chapter 2) containing paramagnetic iron species, only one grafting reaction was conducted as proof of concept. For this system, the calculations of grafting rates by peaks integration were not possible.

Table III-1 : Degrees of postmodification (%) of amino-MOFs with different alkynes measured by liquid ^{1}H NMR analysis and reactant/MOF ratios.

	a $TMSN_3$	**b** 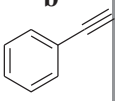	**c** 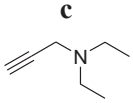	**d** 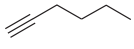	**e** 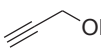	**f** 	**g** 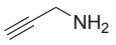
1 DMOF-NH_2	**>99** 6 eq	**>99** 32 eq	**>99** 8.5 eq	**>99** 8.5 eq	**>99** 8.5 eq	dissolution [b]	[a]
2 MIL-68(In)-NH_2	**>99** 38 eq	**80±2** 68 eq	**45±2** 136 eq	**>99** 68 eq	**>99** 68 eq	**68±2** 51 eq	**>99** 68 eq
3 CAU-1	**>99** 17 eq	**>99** 28 eq	**>99** 28 eq	**>99** 17 eq	**>99** 17 eq	**>99** 28 eq	[a]
4 MIL-53(Al)-NH_2	**>99** 78 eq	**82±3** 68 eq	**55±3** 68 eq	**60±2** 68 eq	**>99** 57 eq	**55±2** 22 eq	[a]
5 MIL-101(Fe)-NH_2	**>99** 6 eq	**>99** 56 eq	[a]	[a]	[a]	[a]	[a]

[a] not performed. [b] the solid dissolves in the media

One can also see that the Huygens [3+2] addition reaction generally proceeds very well; for most of the systems, full conversion is achieved for the second step. That said, complete functionalization for DMOF-NH_2 **1** and CAU-1 **3** is achieved even with bulky groups, while a lower degree of modification is obtained for the 1D rod-shaped structured materials, MIL-68(In)-NH_2 **2** and MIL-53(Al)-NH_2 **4**. Here again, a larger excess of alkynes has been used for **2** and **4** to favor the reaction. To obtain fully-functionalized **1d**, the alkyne:MOF ratio is 8.5:1 versus 68:1 for **2d**. It has to be pointed out that DMOF-NH_2 **1** cannot be functionalized with propiolic acid derivative **f**, since the starting solid dissolves when the acid is added.

III.2 Solid state characterizations

III.2.1 Qualitative infrared spectroscopy monitoring of the PSM

Qualitative proof of azide formation and the subsequent (3 + 2) cycloaddition can be also obtained by IR spectroscopy (Figure III-5). The appearance of the IR absorption band at 2123 cm^{-1} is characteristic of the N_3 asymmetric stretching vibration of DMOF-N_3 **1a**. Its complete disappearance after the cycloaddition step is proof of total conversion to the final compound **1b**, **1c, 1d** or **1e**. In the case of **2b, 2c, 2f** and **4b, 4c, 4d, 4f** (See Appendix B)**,** the less intense -N_3 signal is well in line with the partial conversion as quantified by ^{1}H NMR (Table III-1).

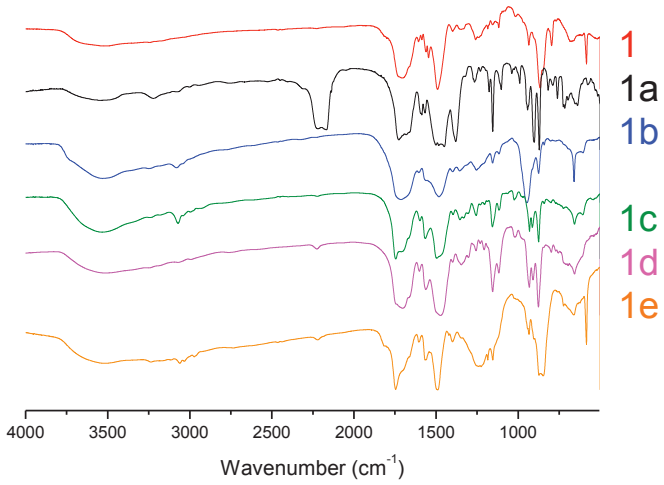

Figure III-5 : FTIR spectra of 1, 1a, 1b, 1c, 1d and 1e

III.2.2 PXRD analyses

Except when propiolic acid (which can interact with the inorganic node) was used, powder X-ray diffraction (PXRD) confirmed that the long-range order was preserved for all post-modified MOFs as presented in Table III-1 (Appendix C), even for post-modified DMOF compounds (Figure III-6), which are based on the most fragile of the structures considered, as previously reported. This preservation of long-range order arises from the softness of this method, which allows its application to all kinds of amino-MOFs. Indeed, both reaction steps proceed at room temperature and do not liberate byproducts such as water, acids or bases that could damage the structure [9, 10].

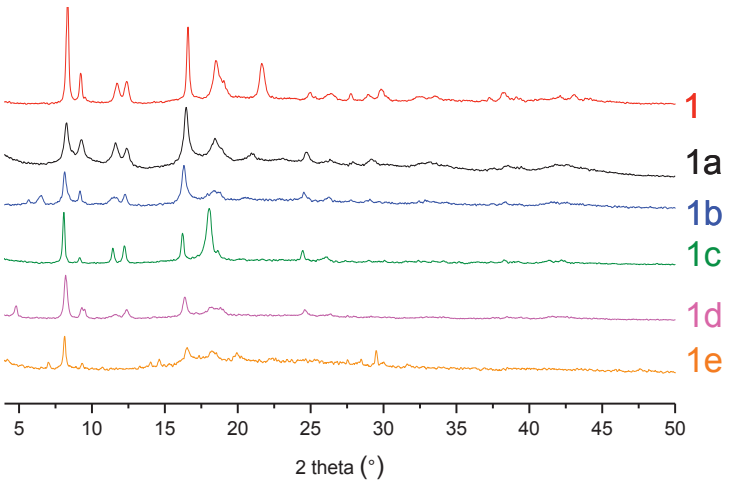

Figure III-6 : PXRD patterns of 1, 1a, 1b, 1c, 1d and 1e

Furthermore, the automatic indexing program DICVOL was used for the lattice parameters determination of **1a**, **2a**, **3a** and **4a** and the values of the lattice parameters were refined by Le Bail technique (full-pattern matching). As can be seen below, there is a good correlation between the data reported in the literature and the experiments (Table III-2).

Table III-2 : Comparison of the Lattice Parameters of Parent MOF and Modified Azide-MOF

	Parent MOF	MOF-N_3
DMOF-1	[11]quadratic system, *P4/m*, a= b = 10.929 Å, c=9.608 Å	quadratic system, *P4/m* a =b = 10.837 Å, c = 9.614 Å
MIL-68(In)	[9]orthorhombic system, *Cmcm* a = 21.7739 Å; b = 37.677 Å; c = 7.233 Å	orthorhombic system, *Cmcm* a = 21.804 Å; b = 37.517 Å; c = 7.207 Å
CAU-1	[12]quadratic system, *I4/mmm,* a = b = 18,3517 Å; c = 17,7772Å	quadratic system, *I4/mmm* , a = b = 18,384 Å; c = 17,803 Å
MIL-53(Al)	[9]Monoclinic system, *Cc*, a = 19.722 Å ; b = 7.692 Å; c = 6.578 Å	Monoclinic system, *Cc*, a = 19.892 Å ; b = 8.066 Å; c = 6.639 Å

IV. Effect of the grafting rate on the porous volume

IV.1 Size selectivity study by molecular modeling

The sterical demand of the biggest functional group (phenylacetylene **b**) was studied by molecular modelling to confirm the feasibility of a complete functionalization.

The structure of **1b** has been obtained starting from the crystallographic data of DMOF-NH_2 **1**. The NH_2 groups of **1** were replaced with (4-phenyl-1,2,3-triazol-1-yl) groups. In order to relax the obtained structure, a geometric optimization followed by a NPT Molecular Dynamics simulation has been performed. The Universal Force Field (UFF) [13] combined with the self consistent charge equilibration method (Qeq) [14] as implemented in the Accelrys MS Forcite package was used to mimic the energetic interactions of the system.

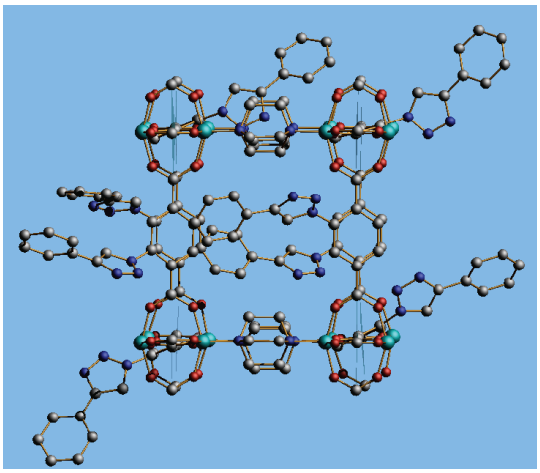

Figure IV-1 : Modelling of 1b

In order to estimate the sterical demand caused by the introduction of the 4-phenyl-1,2,3-triazol-1-yl groups, the different energetic contributions where compared to those obtained for **1** at the end of a geometrical optimization employing the same methodology as in the case of **1b** (Table IV-1).

Table IV-1 : Energetic contributions for 1 and 1b after geometric optimization allowing cell deformation

	1	**1b**	ΔE
Intramolecular Energy (kcal/mol)	2555	3446	891 (+35 %) *
Van der Waals (kcal/mol)	221	133	-88 (-40 %)
Electrostatic Energy (kcal/mol)	-3033	-2666	367 (+12 %)

* Without subtracting the intramolecular interactions corresponding to the 1,2,3-triazol-1-yl groups.

The cell parameters obtained for both materials at the end of the respective geometric optimizations are as well compared in Table IV-2:

Table IV-2 : Cell parameters for 1 and 1b after geometric optimization allowing cell deformation.

	Lx (Å)	Ly (Å)	Lz (Å)
1	20.889	20.785	19.109
1b	20.813	20.810	19.001

As it can be expected the functionalization causes an increment of the intramolecular energy (35%) at the same time that it generates a slightly higher electrostatic repulsion (10%). In the first case, it should be stressed that the totality of these increments cannot be attributed to sterical effects since an important part comes already from the addition of the new intramolecular interactions of the new groups. In order to account for this effect the intramolecular energy of the 1,2,3-triazol-1-yl groups has been computed separately following the previously described methodology. Once this correction has been done the increment obtained is only 126 kcal/mol (5%). These values seem quite reasonable taking into account the size of the 4-phenyl-1,2,3-triazol-1-yl groups. **In addition, no significant changes are observed for the cell parameters confirming the feasibility of a complete functionalization.**

IV.2 Control of the grafting rate

The post-modification yield, also called PSM degree, can be controlled by the amount of alkynes added (default or excess). The impact of the grafting rate with **b** on the porous volume was studied for **1**, **2** and **3** porous structures. All samples underwent desorption at only 100°C prior to N_2 physisorption at 77 K. This soft degassing procedure is required in order to prevent the azide from decomposing.

Samples with lower degree of modification were prepared and quantified by ^{1}H NMR (Figure IV-2). They are obtained by adjusting the amount of penylacetylene to **1a, 2a** and **3a**. There are denoted hereafter **2b-10**, **1b-15**, **2b-20**, **3b-20**, **1b-40**, **2b-50**, and **1b-80** for degrees of modification with **b** of 10%, 15%, 20%, 40%, 50% and 80%, respectively.

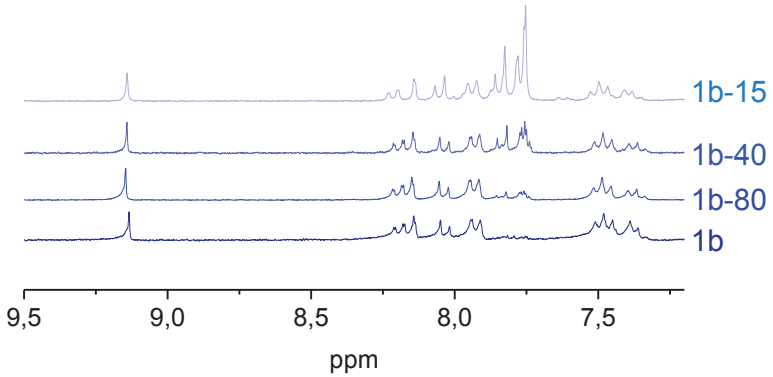

Figure IV-2 : ^{1}H NMR of 1b-15, 1b-40, 1b-80 and 1b

As shown by the N_2 adsorption isotherms of **1** (Figure IV-3), **2** (Figure IV-4) and **3** (Figure IV-5) derivates, an increased degree of modification leads to lower the microporous volume. It can nevertheless be seen that the isotherms maintain their type I shape, which indicates that microporosity is maintained whatever the degree of PSM.

In chapter 1, we have shown that the crystallinity of the parent DMOF-NH_2 **1** is strongly affected by post treatments such as solvent removal and/or solvent exchange. That is in line with the higher drop of surface areas and microporous volumes for functionalized derivates of **1** than for **2** and **3** (Table IV-3).

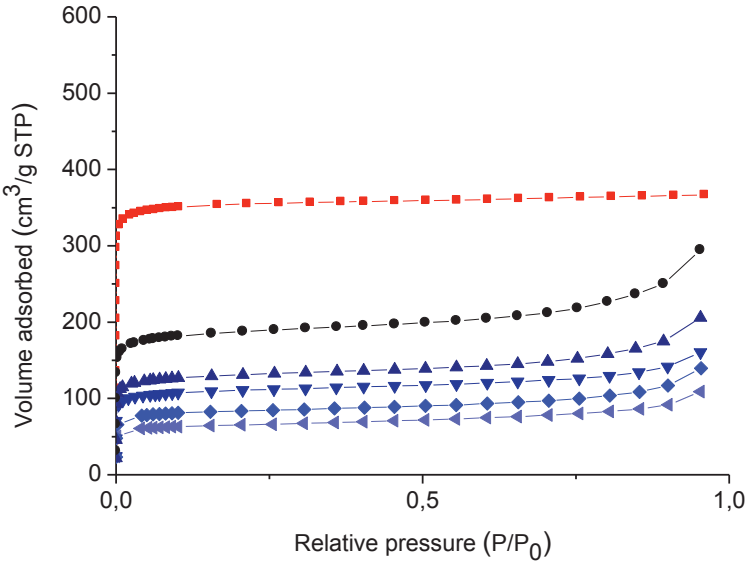

Figure IV-3 : N_2 isotherms at 77K of 1 (■), 1a (●), 1b-15 (▲), 1b-40 (▼), 1b-80 (♦) and 1b (◄)

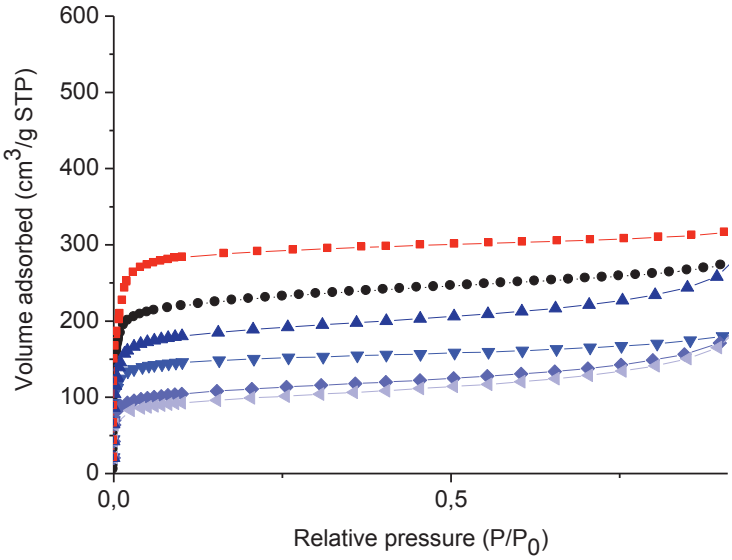

Figure IV-4 : N_2 isotherms at 77K of 2 (■), 2a (●), 2b-10 (▲), 2b-20 (▼), 2b-50 (♦) and 2b-80 (◄)

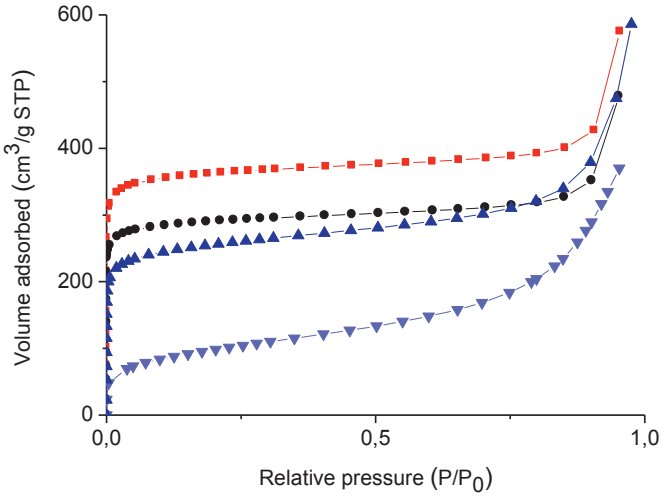

Figure IV-5 : N_2 isotherms at 77K of 3 (■), 3a (●), 3b-20 (▲) and 3b (▼)

Table IV-3 : Effect of the degree of modification with phenylacetylene b on apparent BET surface areas and microporous volume of 1, 2 and 3

MOF	Degree of modification (%)	BET surface area ($cm^2.g^{-1}$)	Microporous volume ($cm^3.g^{-1}$)
1	-	1320± 102	0.54± 0.02
1a	0± 1	695 ± 30	0.23± 0.01
1b-15	15± 3	485 ± 25	0.18± 0.01
1b-40	40± 5	400± 20	0.15± 0.01
1b-80	80± 5	310± 15	0.10± 0.01
1b	100± 1	244± 9	0.08± 0.01
2	-	1120± 108	0.49± 0.02
2a	0± 1	800± 42	0.30± 0.02
2b-10	10± 3.4	717± 40	0.23± 0.02
2b-20	20± 5	571± 26	0.20± 0.01
2b-50	50± 5	399± 18	0.13± 0.01
2b-80	80± 2	360± 21	0.10±0.01
3	-	1434± 132	0.52± 0.02
3a	0± 1	1147± 112	0.42± 0.03
3b-20	20± 2.5	954± 46	0.28±0.02
3b	100± 1	347± 24	0.10± 0.01

Figure IV-6 illustrates the impact of the degree of modification with **b** on the apparent BET surface area measurements of MIL-68(In)-N_3 **2a** and CAU-1-N_3 **3a**. The progressive introduction of the 4-phenyl-1,2,3-triazolate moiety into the porous network reduces the surface area and microporous volume in the same manner for both MOFs. For both porous structures, the apparent surface area decreases linearly as a function of the degree of modification. Once full conversion is achieved, the surface areas have decreased by a factor of about 2.5 to 3 with respect to the parent azide-MOF (from 800 to 360 m .g^{-1} for MIL-68 and from 1150 to 350 $m^2.g^{-1}$ for CAU-1) (Table IV-3). Similar results are obtained when the evolution of the microporous volume are considered (Figure IV-7).

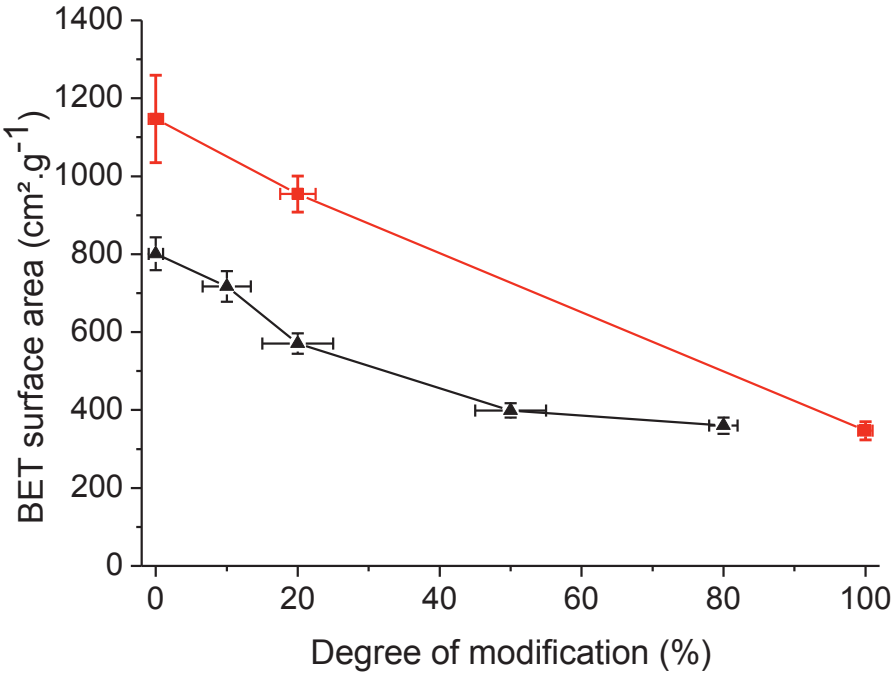

Figure IV-6 : Effect of the degree of modification with phenylacetylene b on apparent BET surface areas of MIL-68(In)-N_3 2a (▲) and CAU-1-N_3 3a (■)

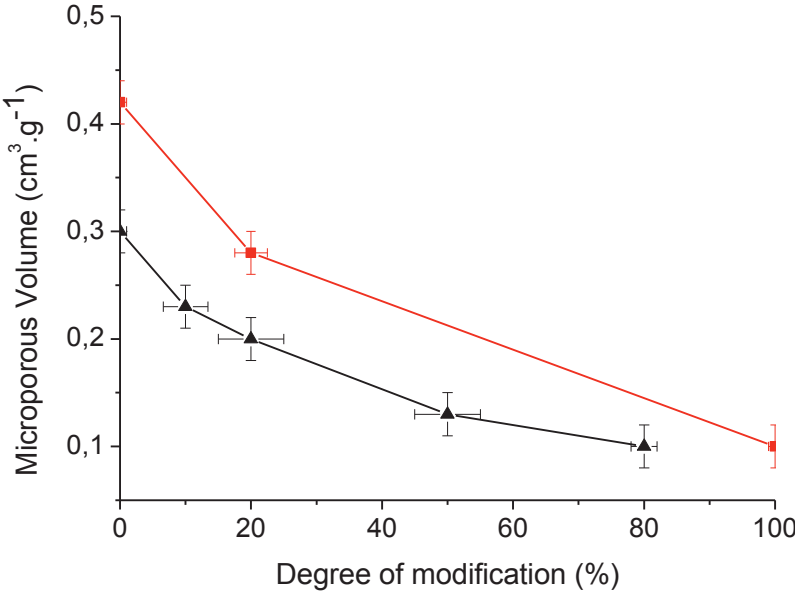

Figure IV-7 : Effect of the degree of modification with phenylacetylene (b) on microporous volumes of MIL-68(In)-N_3 (2a) (▲) and CAU-1-N_3 (3a) (■)

V. Conclusions

This generic PSM method makes it possible to generate multi-dimensional libraries of original MOFs that could not be obtained by traditional solvothermal synthesis. The classic, most common method of creating new functional MOFs is to focus on the synthesis by self-assembly from pre-functionalized linkers, ultimately using high-throughput (HT) methods [15, 16, 17]. Although this approach regularly provides outstanding new materials, it is not very appropriate when, for instance, one seeks to engineer a functional MOF for a given catalytic application. It is, in fact, usually difficult to predict whether a functional MOF will be obtained by self-assembly, and numerous synthesis trials are usually required to provide an adequate number of new well-defined MOFs. For practical applications, it is more efficient to start from already-available amino-MOF platforms and to then insert functionalities by PSM. This study demonstrates that a very high success rate (>90%) can be achieved in producing porous coordination polymers of diverse properties, including adsorption and catalysis. In addition, this generic method presents the advantage of being easily implemented for the parallel synthesis of a large library of MOFs using conventional automated workstations.

Of equal importance is the robustness of this technique: not every member of the MOF library would require complete solid characterization, since PSM is successfully achieved in all

cases. The PSM degree can be easily measured if desired by using liquid NMR after sample digestion. This method is therefore of high practical value and will allow the acceleration of MOFs testing by HT methods for the development of catalysts or adsorbents.

In addition to its practical advantages, this novel PSM procedure presents several benefits for the engineering of MOF catalysts: 1) the softness of the method places almost no restriction on the choice of amino-MOFs, 2) the grafted moieties can possess reactive functional groups such as acid or base, and 3) the grafting rate can be precisely controlled by adjusting the MOF:alkyne ratio. It is therefore possible to engineer MOF catalysts in a rational manner, considering multiple independent factors, with an initial MOF structure that is appropriate in terms of its pore size or other intrinsic functions, and with various new functions to be inserted in optimized percentages. Thanks to the strict control of synthetic conditions, the precise optimization of these parameters can be achieved.

In conclusion, this original PSM technique provides a high level of control for the engineering of tailor-made catalysts. It should also enable the preparation of diverse libraries of functional porous solids with a high degree of reliability for HT testing in catalysis and adsorption applications, while opening new doors for the design of catalysts that combine different antagonistic functions in a confined area, providing a synthetic tool to one of the key challenges in catalysis.

VI. References

[1] F. Himo, T. Lovell, R. Hilgraf, V. V. Rostovtsev, L. Noodleman, K. B. Sharpless, V. V. Fokin, *J. Am. Chem. Soc.* **2004**, *127*, 210-216.

[2] T. Gadzikwa, G. Lu, C. L. Stern, S. R. Wilson, J. T. Hupp, S. T. Nguyen, *Chem. Commun.* **2008**, 5493-5495.

[3] T. Gadzikwa, O. K. Farha, C. D. Malliakas, M. G. Kanatzidis, J. T. Hupp, S. T. Nguyen, *J. Am. Chem. Soc.* **2009**, *131*, 13613-13615.

[4] Y. Goto, H. Sato, S. Shinkai, K. Sada, *J. Am. Chem. Soc.* **2008**, *130*, 14354-14355.

[5] V. V. Rostovtsev, L. G. Green, V. V. Fokin, K. B. Sharpless, *Angew. Chem., Int. Ed.* **2002**, *41*, 2596-2599.

[6] M. E. C. Biffin, J. Miller, D. B. Paul, *In The Chemistry of the Azido group* **1971**, *(Ed.: S. Patai), Wiley, New York*, 147-176.

[7] K. Barral, A. D. Moorhouse, J. E. Moses, *Org. Lett.* **2007**, *9*, 1809-1811.

[8] H. Sato, R. Matsuda, K. Sugimoto, M. Takata, S. Kitagawa, *Nat. Mater.* **2010**, *9*, 661-666.

[9] C. Volkringer, S. M. Cohen, *Angew. Chem., Int. Ed.* **2010**, *49*, 4644-4648.

[10] M. Savonnet, S. Aguado, U. Ravon, D. Bazer-Bachi, V. Lecocq, N. Bats, C. Pinel, D. Farrusseng, *Green Chem.* **2009**, *11*, 1729-1732.

[11] D. N. Dybtsev, H. Chun, K. Kim, *Angew. Chem., Int. Ed.* **2004**, *43*, 5033-5036.

[12] T. Ahnfeldt, N. Guillou, D. Gunzelmann, I. Margiolaki, T. Loiseau, G. Férey, J. Senker, N. Stock, *Angew. Chem., Int. Ed.* **2009**, *48*, 5163-5166.

[13] A. K. Rappe, C. J. Casewit, K. S. Colwell, W. A. Goddard, W. M. Skiff, *J. Am. Chem. Soc.* **1992**, *114*, 10024-10035.

[14] A. K. Rappe, W. A. Goddard, *J. Phys. Chem.* **1991**, *95*, 3358-3363.

[15] M. Banerjee, S. Das, M. Yoon, H. J. Choi, M. H. Hyun, S. M. Park, G. Seo, K. Kim, *J. Am. Chem. Soc.* **2009**, *131*, 7524-7525.

[16] S. Bauer, C. Serre, T. Devic, P. Horcajada, J. Marrot, G. Férey, N. Stock, *Inorg. Chem.* **2008**, *47*, 7568-7576.

[17] P. M. Forster, N. Stock, A. K. Cheetham, *Angew. Chem., Int. Ed.* **2005**, *44*, 7608-7611.

Chapter 5

Tailoring Metal-Organic Framework catalysts and adsorbents by Click Chemistry

I. Introduction

MOFs of the most recent generation present molecular recognition properties [1, 2, 3] originating from their considerable dynamic flexibility [4, 5, 6] which is usually under the control of host-guest interactions. It is acknowledged that MOFs could ultimately mimic enzymes using a "locking" concept favoring high chemo-, regio- and enantioselectivity [7, 8, 9, 10, 11, 12]. MOFs could indeed be viewed as potential "artificial enzymes" combining several properties in a concerted fashion at the nanometer scale. Fairly few MOFs bear more than one reactive function, however. The catalytic properties of these materials have, to date, essentially relied on the features of the inorganic nodes [13]. For example, inorganic clusters with unsaturated coordination (such as HKUST-1) or bridging hydroxyl groups (such as MIL-53) have been shown to perform Lewis [14, 15, 16] and Brønsted [17] type catalysis, respectively.

One solution for synthesizing advanced MOFs suitable for more specialized and sophisticated applications is the controlled addition of more complex functionalities into the porous network. If the physical environment of the pores and the cavities within MOFs can be modified, the interactions with guest species can in turn be adapted, thereby fine-tuning the chemical reactivity. In previous chapter, we have reported an original PSM method starting from amino derived MOFs. The first step consists in converting the amino group into azido (N_3). Without isolation nor purification, the desired functionalized MOF material is obtained by grafting the corresponding alkyne using "Clik Chemistry". On different MOFs, we showed that this novel PSM method presents key benefits for the engineering of MOFs : i) the softness of the method places no restriction on the choice of amino-MOFs and ii) the grafting yield can be precisely controlled by adjusting the MOF:alkyne ratio.

In this chapter, we demonstrate that PSM by Click Chemistry enables the engineering of MOFs for application in base catalysis. The controlled post-modification of MOFs by both basic and hydrophobic groups allows a rational design of catalytic MOFs for the transesterification [18, 19] reaction. We show that outstanding synergistic catalytic effects can be obtained by an optimal formulation.

Continuing our efforts in synthesizing of functionalized MOFs and in investigating their applications, we prepared in the end of this chapter thiol-functionalized MOF materials by "Click Chemistry" in order to investigate their complexation affinities for heavy metal ions.

II. Application to base catalysis

II.1 Transesterification reaction

The model reaction considered here is the transesterification of ethyldecanoate in methanol (Figure II-1).

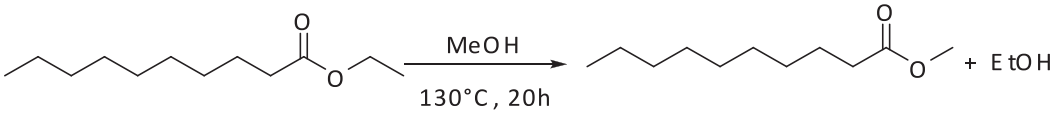

Figure II-1 : Diagram of transesterification of ethyldecanoate in methanol

For this reaction to proceed efficiently, both substrates must be co-adsorbed into the MOF, and MeOH should be activated by a base in order to favour the nucleophilic attack on the carbonyl group.

II.2 Catalysts

The DMOF parent structure was selected as the starting platform since it contains neither Lewis nor Brønsted acid groups that could have a catalytic effect. Two different functional groups were selected for post-modification: a 1,2,3-triazolyl substituted with phenyl, corresponding to **b** compounds, or tertiary amine at the 4-position, corresponding to **c** compounds (Figure II-2). They are obtained by reacting the DMOF-N_3 **1a** with phenylacetylene to give **1b** and with propargylamine to give **1c**. The former **1b** presents moderate basicity originating from the triazolyle group (pKa ≈ 1,2) as well as strong hydrophobicity, whereas the latter **1c** is a much stronger base (pKa ≈ 11 for alkylamines). A bifunctionalized MOF modified with **b** groups (phenyl) and then subsequently modified with **c** groups (tertiary amine) on the remaining azido sites was obtained and hereafter denoted **1h**. The degree of modification of the MOF catalysts is given in Table II-1.

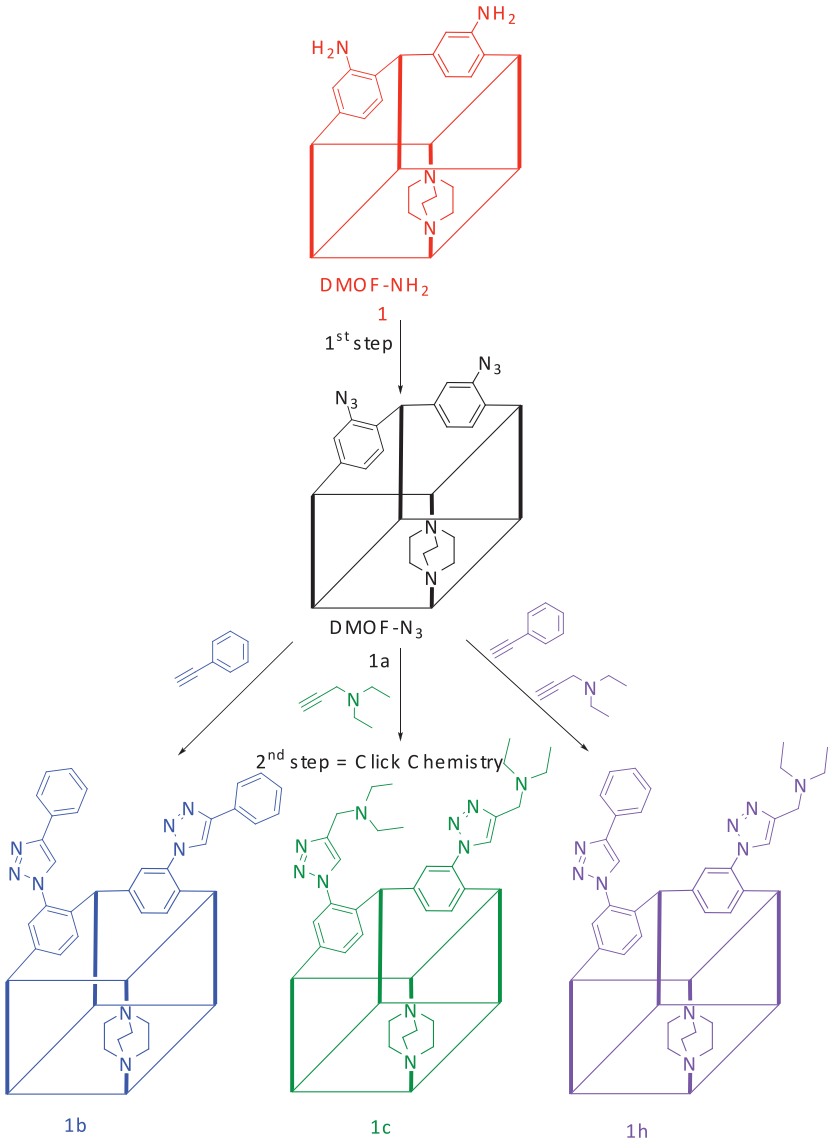

Figure II-2 : Synthesis of MOF catalysts by « Click Chemistry »

II.2.1 Characterization

Clear proof of the azide formation and of the subsequent full (3+2) cycloaddition can be characterized by liquid ^{1}H NMR on a quantitative manner. The spectrum of digested DMOF-N_3 **1a** reveals the formation of the azido corresponding compound through the appearance of new aromatic signals (7.73-7.83 ppm). This coincides with the complete disappearance of the aromatic signals of DMOF-NH_2 **1** (7.15 ppm, 7.44 ppm, 7.8 ppm,) (Figure II-3), thus indicating almost full conversion to the azide form. After the cycloaddition step, new aromatic shifts of the post-modified compounds **1b** and **1c** confirm that the corresponding triazole

derivative is formed as the sole product. The post-digestion ^{1}H NMR spectrum of **1h** shows contributions of both **b** and **c** and also of the remaining azide in a 30:30:40 ratio.

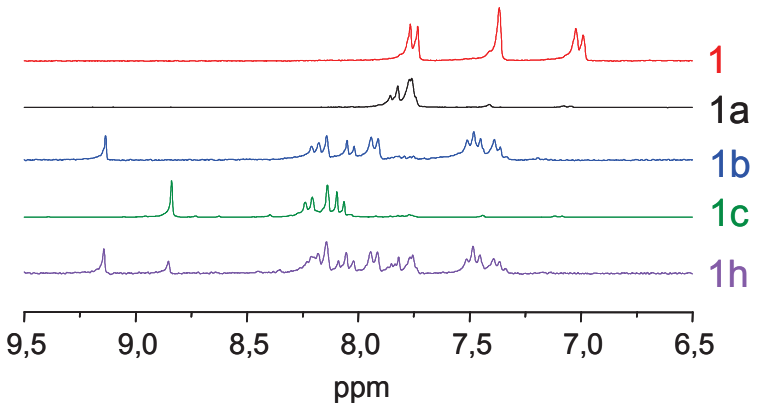

Figure II-3 : ^{1}H NMR enlargement in the aromatic region of digested 1, 1a, 1b, 1c and 1h

IR spectroscopy studies confirm these results (Figure II-4). The appearance of the IR absorption band at 2123 cm^{-1} is characteristic of the N_3 asymmetric stretching vibration of DMOF-N_3 **1a**. In the cases of **1b** and **1c**, its disappearance after the cycloaddition step is proof of almost total conversion to the final compound. In the case of **1h**, the less intense –N_3 signal is well in line with the partial conversion as quantified by ^{1}H NMR. Despite solvent effects on DMOF crystallinity [20, 21], powder X-ray diffraction patterns (PXRD) indicates that long-range order is preserved for all samples (Figure II-5).

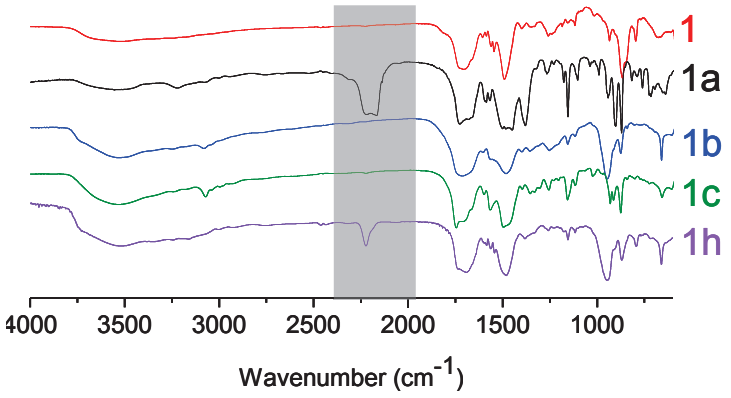

Figure II-4 : FT-IR of 1, 1a, 1b, 1c and 1h

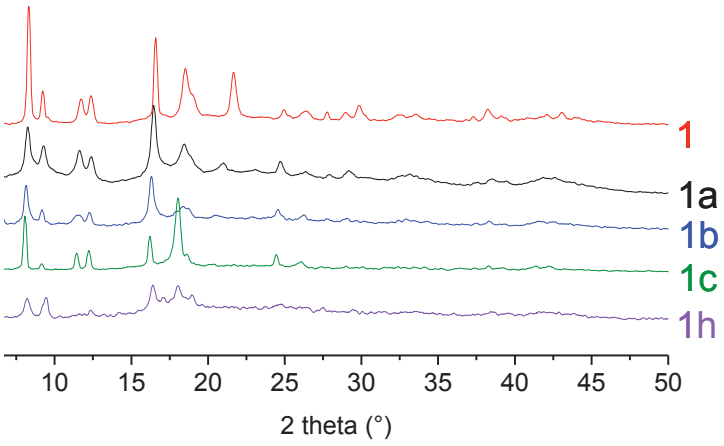

Figure II-5 : Powder XRD patterns of 1, 1a, 1b, 1c and 1h

Following similar methodology, samples with variable degree of modification were prepared. They are obtained by adjusting the amount of alkyne reactants, phenylacetylene or diethylpropargylamine, with respect to **1a**. There are denoted hereafter **1b-15**, **1b-40** and **1b-80** for degrees of modification with **b** groups (phenyl) of 15%, 40% and 80% respectively, and **1c-40**, **1c-85** for degrees of modification with **c** groups (tertiary amine) of 40% and 85% respectively. Synthesis details and characterization can be found in the experimental part.

1b-40, **1c-40** and **1h** possess microporous structures characterized by isotherm shapes (N_2 at 77K) of type I (Figure II-6).

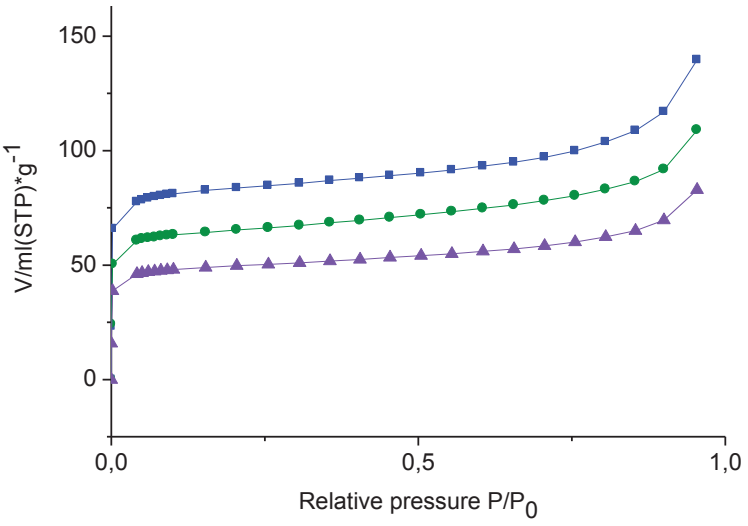

Figure II-6 : N_2 adsorption isotherms of 1b-40 (■), 1c- 40 (●) and 1h (▲)

II.3 Catalytic results

These DMOF catalysts were involved in the transesterification of ethyldecanoate with methanol and all the catalytic results are summarized in the Table II-1. It is worthy to note that the transesterification conversion obtained using the unmodified DMOF-NH_2 **1** as catalyst is not higher than that obtained without catalyst (c.a. 10%, entries 1 and 2).

Table II-1 : Transesterification conversion of functionalized MOFs and reference catalysts[a]

Entry	Catalyst	b (%)	c (%)	conversion (%)
1	none	-	-	10
2	**1**	-	-	10
3	**1b-40**	40	-	48
4	**1b-40** [b]	40	-	0
5	**1b-80**	80	-	82
6	**1c-40**	-	40	21
7	**1c-85**	-	85	28
8	**1h**	**30**	**30**	**84**
9	$Cu(ACN)_4PF_6$ [c]	-	-	32
10	$Cu(OAc)_2$ [c]	-	-	40
11	**linker b** [c]	100	-	30
12	**linker c** [c]	-	100	21

[a] Conditions: ethyldecanoate (2.5 mL) is allowed to react in methanol (10 mL) using 20 mg of DMOF catalyst (~0.03 mmol MOF, c.a 0.06 mmol –NH_2) at 130°C for 20h [b] 2-ethyl-1-butanol is used instead of methanol [c] Homologue catalysts used under homogenous conditions (Figure II-7); 0.3 mmol of catalyst are used.

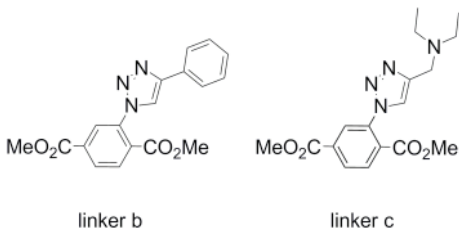

Figure II-7 : Molecular homologues of the catalysts 1b and 1c.

Figure II-8 illustrates also how the degree of modification affects ethyldecanoate conversion in the case of the monofunctionalized materials. It appears that the activity of these DMOF materials increases linearly with the degree of modification. The syntheses and tests were

performed twice for **1b-80** in order to verify experimental reproducibility; both times the ethyldecanoate conversion was approximately 80% (Table II-1, entry 5).

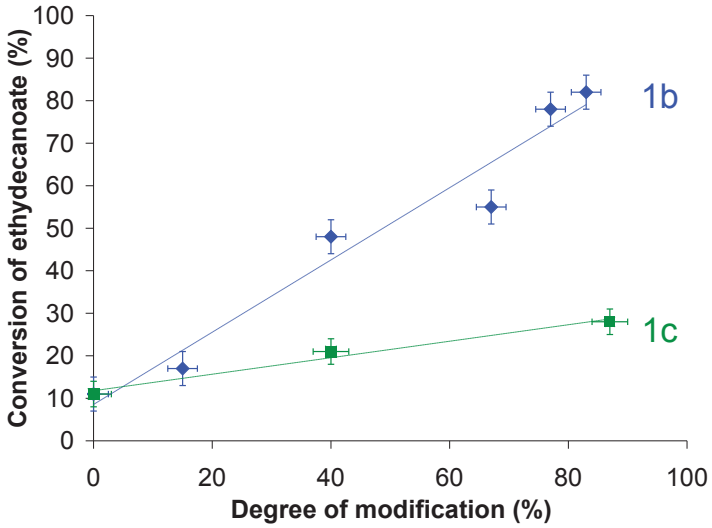

Figure II-8*:* Effect of the degree of modification for (b) (♦) and (c) (■) on ethyldecanoate conversion at 130°C after 20 h

Figure II-9 shows the kinetic studies of ethyldecanoate conversion for **1** and **1b-80**.

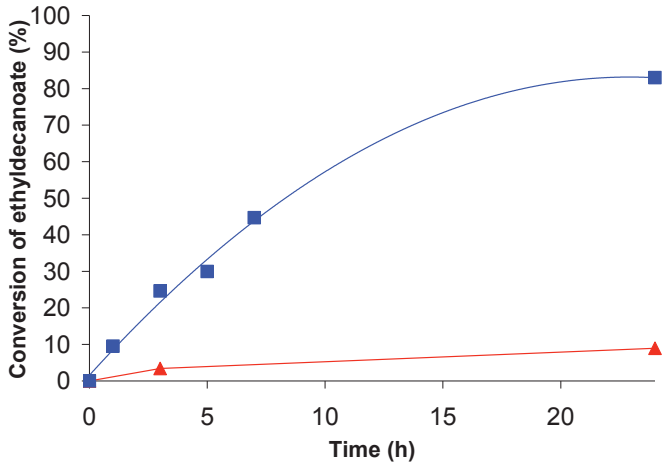

Figure II-9 : Kinetic studies of ethyldecanoate conversion for 1 (▲) and 1b-80 (■)

The DMOF grafted with **c** groups could have been expected to show better activity based on the higher basic strength of the trialkylamine compared to that of the phenyl substituent. Surprisingly, the introduction of hydrophobic functions via **b** exhibits a more beneficial effect on catalytic activity. Furthermore, the corresponding organic functionalized linker found in **1b** and **1c,** respectively **linker b** (dimethyl-2-(4-phenyl-1H-1,2,3-triazol-1-yl)-terephthalate) and **linker c** (dimethyl-2-(4-diethylaminomethyl-1H-1,2,3-triazol-1-yl)-terephthalate), were synthesized (Figure II-7). The **linker b** and the **linker c** were tested in the transesterification reaction under homogeneous conditions and show moderate activity compared to the corresponding grafted MOFs with conversions of 30% and 21% respectively (Table II-1, entries 11 and 12) against 82% for **1b-80** (entry 5) and 28% for **1c-85** (entry 7). These results confirm the moderate activity of the triazolyl group itself.

In contrast, the tandem post-modified **1h** shows outstanding performances compared to the monofunctionalized DMOF samples. Although **1h** contains only 30% of **b** and 30% of **c**, 84% conversion was achieved (entry 8). Under similar reaction conditions, using **1b-40** and **1c-40** with similar degree of modification, the conversion only reached 48% and 21%, respectively (entries 3 and 6). This superior activity can be attributed to a synergistic effect resulting from the combination of both basic and hydrophobic groups at molecular level.
In order to assess our hypothesis of a synergistic basic-hydrophobic effect, liquid adsorption isotherms with an ethyldecanoate/isooctane mixture were investigated for **1** and for **1b-40**, containing 40% of 4-phenyl-1,2,3-triazolyl functions (Figure II-10).

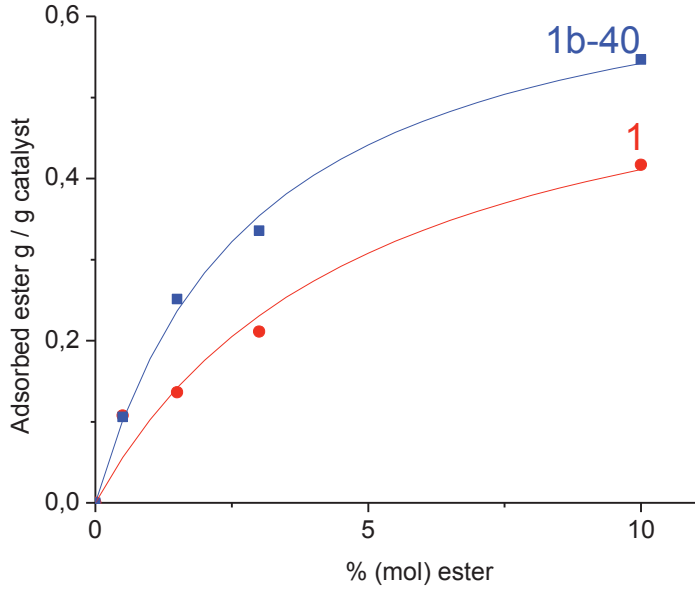

Figure II-10 : Liquid adsorption isotherms of ethyldecanoate in the ethyldecanoate/isooctane mixture for 1(●) and 1b-40 (■)

These adsorption measurements confirm the stronger hydrophobicity of the latter material. Consequently, we suggest that the higher apparent activity of **1b** compared to **1c** should be due to a more appropriate co-adsorption ratio of both substrates inside the pores on the more hydrophobic MOF. Hence, **1h** with a tandem functionalization reaches an optimal basic/hydrophobic balance to perform the reaction.

Moreover, the use of a bulky primary alcohol in the transesterification reaction has been also used to confirm that the reaction takes place into the porous system and not only at the surface [19]. The transesterification with 2-ethyl-1-butanol, which is a much bulkier substrate than methanol, was carried out using the MOF **1b-40**. As shown in the Table II-1, no conversion was obtained in 2-ethyl-1-butanol against 48% in MeOH (entry 4). This clearly indicates that the reaction proceeds into the pores framework when MeOH is used, whereas the reaction does not take place in the case of a bulky alcohol due to the molecular sieving property of the MOF.

Powder XRD shows that DMOF materials remain mostly crystalline after catalysis although peak broadening is observed (Figure II-11). As discussed previously, it may arise from the intrinsic flexibility of the DMOF structure [22].

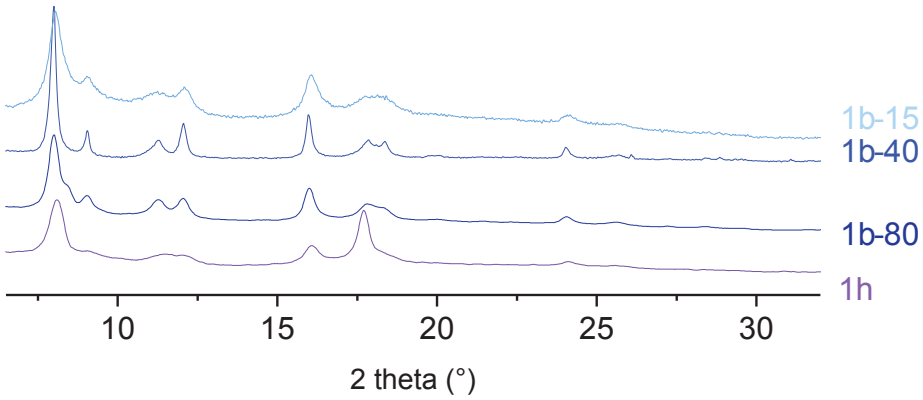

Figure II-11 : PXRD patterns of post-catalysis 1b-15, 1b-40, 1b-80 and 1h

Most important, under catalytic conditions the robustness of the solid towards leaching was investigated. When the catalyst is filtered off, the reaction does not proceed any longer (Figure II-12). The unstable azide groups started to decompose up to 100°C. After catalysis, we observed therefore the disappearance of aromatic DMOF-N_3 signals (Figure II-13).

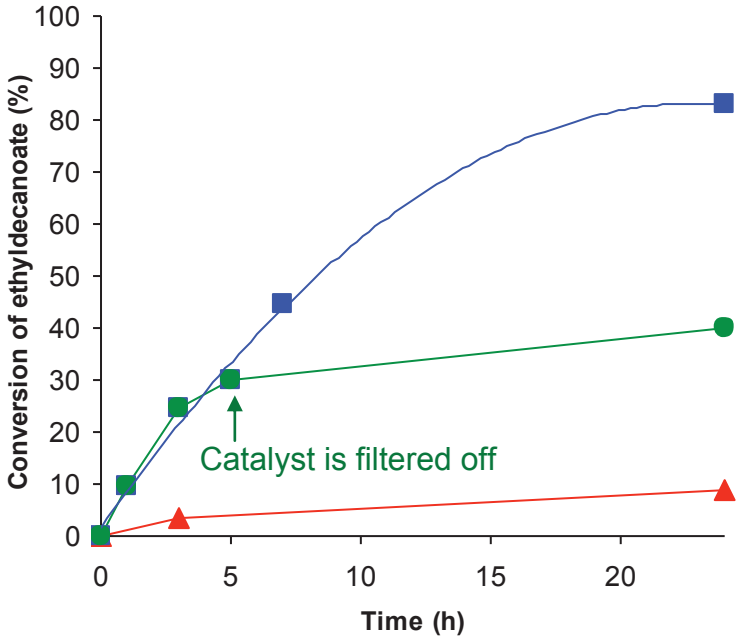

Figure II-12 : Kinetic studies of ethyldecanoate conversion for 1 (▲), 1b-80 (■) and for leaching test (●)

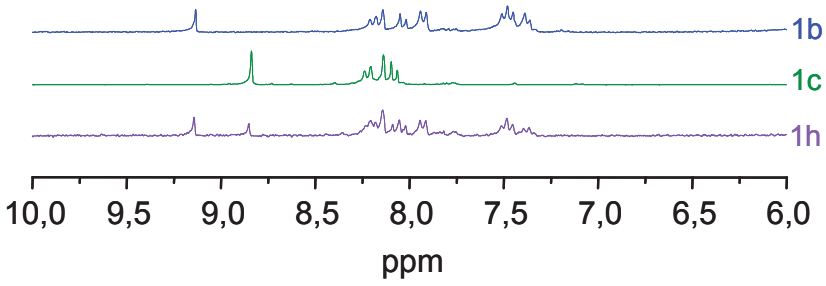

Figure II-13 : ^{1}HNMR of post-catalysis 1b, 1c and 1h

As far as the elemental analyses performed on our samples show the presence of 1 to 2 wt% of Cu in the solids, we investigated the effect of copper on our catalytic system. According to the molecular formula of the functionalized MOFs and to the catalyst quantity used in the reaction, the amount of copper present in our tests corresponds to 0.002-0.004 mmol. Although the exact nature and oxidation state of the copper is not known, it might be possible that some of the copper remain as $Cu^{I}(ACN)_4PF_6$ in the pore after the Click Chemistry and may act as a catalyst [23]. Control experiments carried out with 0,3 mmol of $Cu(ACN)_4PF_6$ or $Cu(OAc)_2$, corresponding to 100 times more Cu than really contained in our MOFs, show a catalytic activity lower than that obtained using our functionalized DMOF (Table II-1).

II.4 Others catalytic results

Some of the MOFs selected previously present chemical features that may interfere in catalytic processes, namely CAU-1 **3**, which exhibits hydroxy and methoxy bridging groups, as well as MIL-68(In)-NH_2 **2** and MIL-53(Al)-NH_2 **4**, which are built from inorganic nodes with hydroxyl bridging groups. The DMOF parent structure was previously selected as the starting platform since it contains neither Lewis nor Brønsted acid groups that could have a catalytic effect. In fact, the transesterification conversion obtained using the unmodified **2**, **3** and **4** as catalyst is not higher than that obtained without catalyst (10%) (Table II-2). **2**, **3** and **4** modified with the two previous functional groups (phenyl **b** and tertiary amine **c)** and carboxylic acid function **f** were selected and also tested in the same reaction (Table II-2).

Table II-2 : Catalytic performances and composition of PSM MOF catalysts

Catalyst	**b** (%)	**c** (%)	**f** (%)	Conversion (%)
1b-40	40	-	-	48
1b-80	80	-	-	82
1c-40	-	40	-	21
1c-85	-	85	-	28
2	-	-	-	10
2b-20	20	-	-	34
2c-20	-	20	-	12
2c-80	-	80	-	15
2f-70	-		70	14
3	-	-	-	10
3b	100	-	-	17
3c	-	100	-	24
3f	-	-	100	14
4	-	-		10
4f-60			60	18

Thus, the Brønsted acid sites (hydroxy centers) contained into MIL-68(In) **2** and MIL-53(Al) **3** or the acetylene carboxylic acid **f** seem to be not strong enough to show real catalytic improvements in the transesterification reaction. As a consequence, a grafting of more acidic groups like sulfonic acid derived compounds will be envisaged in chapter 6.

Furthermore, lower conversions were obtained for **2**, **3** and **4** derivates. Here again, conversion seems to depend on the co-adsorption of both substrates inside the pores, indeed **2** and **4** possess monodirectional channels, while access to distorted octahedral and distorted tetrahedral cages (with effective accessible diameters of approximately 10 and 4.5 Å) of **3**, is only possible through its small triangular windows (free aperture of 3-4 Å), restricting the adsorption in liquid phase.

III. Application to adsorption

Mercury, a toxin known to cause neurological impairment in humans, is of great environmental concern. One promising technique for achieving the removal of low levels of mercuric ions from produced water is to trap them using complexing ligands (e.g., thiols) that are covalently linked to a high surface area support [24]. Accordingly, various forms of thiol-functionalized mesostructured silica have been examined as candidates for mercury remediation [25, 26, 27, 28, 29]. These trapping agents offer very high surface areas, well-defined pore sizes, and high thiol group loadings with up to 50% of the framework silicon centers being functionalized[30, 31].

To synthesize improved adsorbents for the removal of toxic heavy metal ions from produced water is a continuing research objective of environmental pollution control processes. Continuing our efforts in synthesizing of functionalized MOFs and in investigating their applications, we prepared thiol-functionalized MOF materials by "Click Chemistry" in order to investigate their complexation affinities for heavy metal ions (Figure III-1). Indeed, in terms of adsorption properties, MOF materials exhibit two major differences with respect to classical adsorbents: 1) Very high adsorption capacities per mass unit due to very large microporous volumes 2) high number of binding sites.

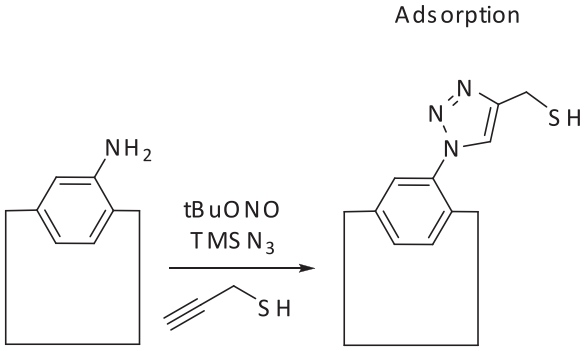

Figure III-1 : Strategy for organosulfur-functionalized MOFs

III.1 Synthesis of functionalized MOFs with organosulfur groups

III.1.1 Synthesis of thioalkynes

A non-protected and a protected thioalkynes (propargylthiol and propargyl-xanthate, respectively) were synthesized for the cycloaddition on MOF-N_3.

III.1.2 Synthesis of propargyl-thiol

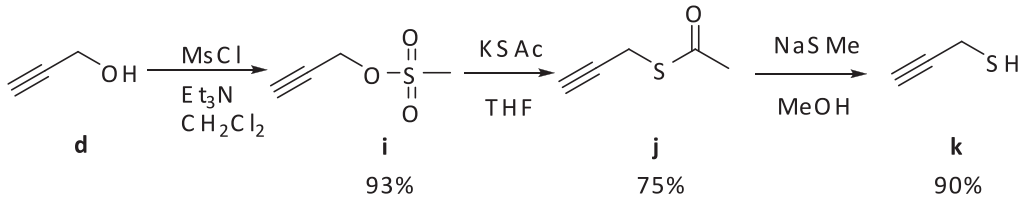

The synthesis of propargyl-thiol was achieved in three steps from the commercially available propargyl-alcohol **d**. The alcohol was first converted to the corresponding mesylate **i** in 93% yield following a literature method[32]. Then, the propargyl-thioacetate **j** was prepared with a 75% yield by reacting **i** with potassium acetate [33]. Finally, propargyl-thiol **k** was obtained in a 90% yield by the reduction of propargyl-thioacetate **j**, followed by acidification [33]. Although **k** can be obtained after fractional distillation at reduced pressure, both the relatively high volatility (bp_{170} 39°C) and instability of this compound (it has been reported to polymerize explosively upon attempted distillation at ordinary pressure [34]) make the procedure unattractive in the laboratory. Thus, after extraction with dichlromethane, propargyl-thiol was kept in solution and ^{1}H NMR analysis of the solution indicates an approximate propargyl-thiol concentration of 0.12 mol.L^{-1}which corresponds to a 90% yield. Although the high volatility, the reported instability and the characteristic repulsive smell of **k** make advisable its immediate use, the solutions prepared can be stored in the freezer for several weeks without noticeable losses if kept under argon in a well-stoppered flask.

III.1.3 Synthesis of *o*-ethyl S-propargyl-xanthate

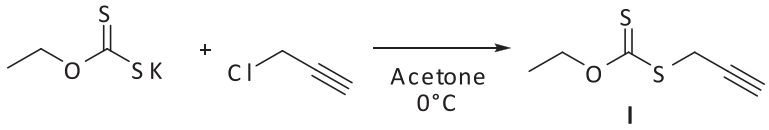

l

88%

The synthesis of propargyl-xanthate **l** in a 88% yield was adapted from the procedure described in [35]. The deprotection step of propargyl-xanthate **l** to propargyl-thiol **k** would take place onto the MOF.

III.2 Cycloaddition of thioalkynes

The main difficulty in the cycloaddition of thioalkynes is the competition for Cu binding. Catalytic effect of copper(I) can be inhibitory due to the blocking of coordination sites on the metal by the -SH or -SR functions. Indeed, some copper proteins utilize a sulfur atom in their active sites, including enzymes. For example, copper-thioneins utilize the SH group of cysteine ligands to efficiently deliver and/or store copper ions. In synthetic bioinorganic coordination chemistry, a variety of sulfur containing ligands and copper complexes have been studied in recent years [36].

Consequently, even if an excess of copper was used in the case of the cycloaddition of propargyl-thioacetate **j** and propargyl-thiol **k** on DMOF-N_3 **1a** and MIL-68-N_3 **2a**, no "Click Chemistry" reaction took place. In contrast, the delocalized bond existing in the propargyl-xanthate **l** allows to have a weaker-donor environment that minimizes the tendency to form inhibitory copper chelates. Partial conversions of 22% and 5%, quantified by ^{1}H NMR (Figure III-2), were obtained for **1a** and **2a**, denoted **1l-22** and **2l-5** respectively (Table III-1). Here again, a lower degree of modification is obtained for the 1D rod-shaped structured material (MIL-68) which limits the diffusion to the center of the crystallites. The study was stopped at this step for **2l-5** due its very low degree of modification. Powder X-ray diffraction (PXRD) of **2l-22** confirmed that the long-range order was preserved (Figure III-3).

Table III-1 : Degree of modification of thiol-functionalized-MOFs with different alkynes

Alkynes	MOF-N_3	Degree of modification (%)
k	**2a**	0
j	**1a**	0
	2a	0
l	**1a**	22
	2a	5

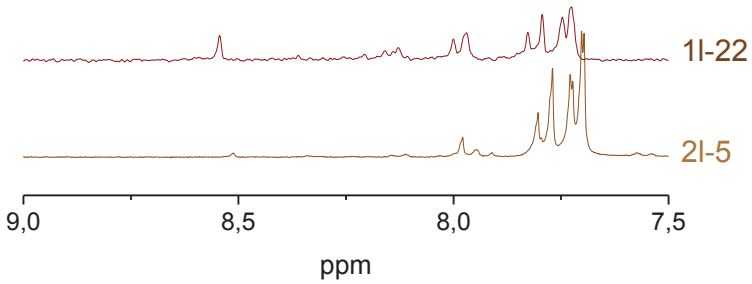

Figure III-2 : ^{1}H NMR enlargement in the aromatic region of digested 1l-22 and 2l-5

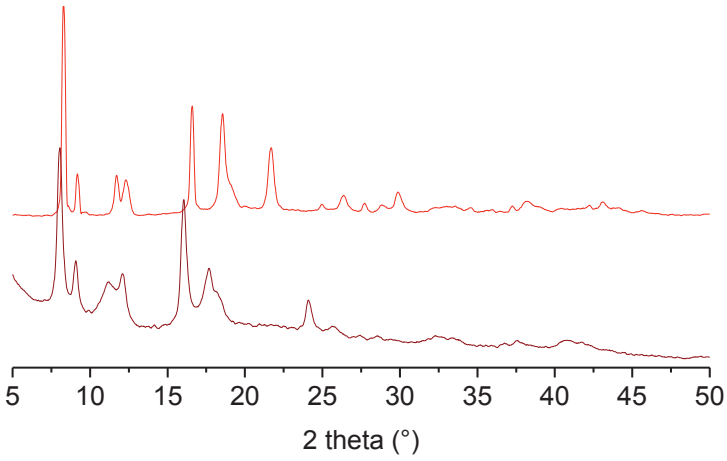

Figure III-3 : PXRD patterns of 1 and 1l-22

Unfortunately, the structure of **1l-22** was destroyed during the reduction step of xanthate by addition of propylamine in THF. Indeed, the weakly coordinated DABCO to the Zn paddlewheel of **1l-22** lowers its chemical stability in basic media (competition between DABCO and propylamine).

III.3 Sulfonic acid-functionalized MOFs

Conversion to sulfonic acid-functionalized MOF should have been carried out by two routes in a solution of hydrogen peroxide and formic acid, either by using directly the thioactetate-functionalized MOF [37] or by using directly the thiol-functionalized MOF [38].
Nevertheless, in an unrelated single step reaction, Britt and coworkers [39] carried out ring opening reactions with the amine-bearing IRMOF-3 to generate sulfonate groups (Figure III-4).

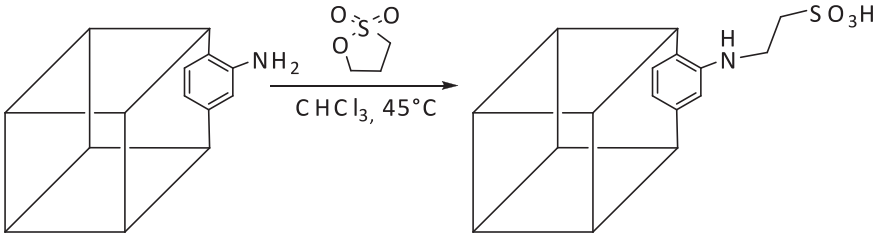

Figure III-4 : Modification of IRMOF-3 with 1,3-propanesultone via ring opening reaction

Thus, this reaction has been tested on IRMOF-3, DMOF-NH_2, MIL-68-In-NH_2 without and with different solvents ($CHCl_3$, anhydrous CH_2Cl_2, isopropanol), at different temperatures (25°C, 45 °C and reflux in $CHCl_3$) and in homogeneous conditions from dimethylaminoterephthelate and benzylamine, but no reaction took place.

IV. Conclusions

In conclusion, we were able in a single framework to successively introduce new basic catalytic centers (amino groups) and hydrophobic groups (phenyl groups) in order to enhance the catalytic activity of our solid. Thanks to the strict control of the synthetic conditions, the precise optimization of these parameters can be achieved. In the case of the transesterification of ethyldecanoate with methanol, the best activity is obtained using tandem post-modification involving at each step a low degree of modification. The resulting bifunctionalized MOF provides an optimized balance between catalytic activity, through the basicity, and substrates co-adsorption, through the hydrophobicity. More generally, this post-functionalization methodology based on an original "one-pot" Click Chemistry enables the engineering of MOF catalysts in a rational manner, considering multiple independent factors and starting from an initial MOF structure that is appropriate in terms of pore size or intrinsic functionalities [40]. This opens new perspective for the rational design of multifunctional solid catalysts.

The preliminary adsorption study was based on the investigations of functionalized MOFs for high added value products as fine chemical or specialized industrial niches as mercury trapping, for which the cost was not an issue.

Although the cycloaddition of thioalkynes remains a difficult task, the way of using protected thioalkyne as propargyl-xanthate is very promising. Nevertheless, at the moment, the existing starting MOF structures do not allow to pursue this study. In fact, a novel amino-MOF structure is needed to achieve this work: 1) with 3D porous channels, 2) appropriate pore sizes and 3) a high chemical stability to support the reduction step.

V. References

[1] R. Matsuda, R. Kitaura, S. Kitagawa, Y. Kubota, R. V. Belosludov, T. C. Kobayashi, H. Sakamoto, T. Chiba, M. Takata, Y. Kawazoe, Y. Mita, *Nature* **2005**, *436*, 238-241.

[2] S. Horike, R. Matsuda, D. Tanaka, S. Matsubara, M. Mizuno, K. Endo, S. Kitagawa, *Angew. Chem., Int. Ed.* **2006**, *45*, 7226-7230.

[3] S. Bureekaew, S. Shimomura, S. Kitagawa, *Sci. Tech. Adv. Mater.* **2008**, *9*, 1-12.

[4] S. Horike, S. Shimomura, S. Kitagawa, *Nature Chem.* **2009**, *1*, 695-704.

[5] S. Kitagawa, M. Kondo, *Bull. Chem. Soc. Jpn.* **1998**, *71*, 1739-1753.

[6] J. A. R. Navarro, E. Barea, A. Rodriguez-Dieguez, J. M. Salas, C. O. Ania, J. B. Parra, N. Masciocchi, S. Galli, A. Sironi, *J. Am. Chem. Soc.* **2008**, *130*, 3978-3984.

[7] D. Farrusseng, S. Aguado, C. Pinel, *Angew. Chem., Int. Ed.* **2009**, *48*, 7502-7513.

[8] J. Lee, O. K. Farha, J. Roberts, K. A. Scheidt, S. T. Nguyen, J. T. Hupp, *Chem. Soc. Rev.* **2009**, *38*, 1450-1459.

[9] K. P. Lillerud, U. Olsbye, M. Tilset, *Top. Catal.* **2010**, *53*, 859-868.

[10] D. Bradshaw, J. B. Claridge, E. J. Cussen, T. J. Prior, M. J. Rosseinsky, *Acc. Chem. Res.* **2005**, *38*, 273-282.

[11] D. Bradshaw, T. J. Prior, E. J. Cussen, J. B. Claridge, M. J. Rosseinsky, *J. Am. Chem. Soc.* **2004**, *126*, 6106-6114.

[12] C. J. Kepert, T. J. Prior, M. J. Rosseinsky, *J. Am. Chem. Soc.* **2000**, *122*, 5158-5168.

[13] A. Corma, H. Garcia, F. X. L. Xamena, *Chem. Rev.* **2010**, *110*, 4606-4655.

[14] L. Alaerts, E. Seguin, H. Poelman, F. Thibault-Starzyk, P. A. Jacobs, D. E. De Vos, *Chem.-Eur. J.* **2006**, *12*, 7353-7363.

[15] K. Schlichte, T. Kratzke, S. Kaskel, *Microporous Mesoporous Mater.* **2004**, *73*, 81.

[16] A. Dhakshinamoorthy, M. Alvaro, H. Garcia, *Chem.-Eur. J.* **2010**, *16*, 8530-8536.

[17] U. Ravon, M. E. Domine, C. Gaudillere, A. Desmartin-Chomel, D. Farrusseng, *New J. Chem.* **2008**, *32*, 937-940.

[18] C. Chizallet, S. Lazare, D. Bazer-Bachi, F. Bonnier, V. Lecocq, E. Soyer, A. A. Quoineaud, N. Bats, *J. Am. Chem. Soc.* **2010**, *132*, 12365-12377.

[19] J. S. Seo, D. Whang, H. Lee, S. I. Jun, J. Oh, Y. J. Jeon, K. Kim, *Nature* **2000**, *404*, 982-986.

[20] M. Savonnet, D. Bazer-Bachi, N. Bats, J. Perez-Pellitero, E. Jeanneau, V. Lecocq, C. Pinel, D. Farrusseng, *J. Am. Chem. Soc.* **2010**, *132*, 4518-4519.

[21] J. J. Low, A. I. Benin, P. Jakubczak, J. F. Abrahamian, S. A. Faheem, R. R. Willis, *J. Am. Chem. Soc.* **2009**, *131*, 15834-15842.

[22] D. N. Dybtsev, H. Chun, K. Kim, *Angew. Chem., Int. Ed.* **2004**, *43*, 5033-5036.

[23] M. B. Smith, J. March, *Addition to Carbon–Hetero Multiple Bonds*, John Wiley & Sons, Inc., **2006**.

[24] U. S. EPA., *Capsule Report: Aqueous Mercury Treatment; Office of Research and Development* **1997**.

[25] S. J. L. Billinge, E. J. McKimmy, M. Shatnawi, H. J. Kim, V. Petkov, D. Wermeille, T. J. Pinnavaia, *J. Am. Chem. Soc.* **2005**, *127*, 8492-8498.

[26] L. Mercier, T. J. Pinnavaia, *Adv. Mater.* **1997**, *9*, 500-503.

[27] X. Feng, G. E. Fryxell, L. Q. Wang, A. Y. Kim, J. Liu, K. M. Kemner, *Science* **1997**, *276*, 923-926.

[28] A. M. Liu, K. Hidajat, S. Kawi, D. Y. Zhao, *Chem. Commun.* **2000**, 1145-1146.

[29] M. H. Lim, C. F. Blanford, A. Stein, *Chem. Mater.* **1998**, *10*, 467-470.

[30] Y. Mori, T. J. Pinnavaia, *Chem. Mater.* **2001**, *13*, 2173-2178.

[31] J. Shah, S.-S. Kim, T. J. Pinnavaia, *Chem. Commun.* **2004**, 572-573.
[32] G. L. Bundy, C. H. Lin, J. C. Sih, *Tetrahedron* **1981**, *37*, 4419-4429.
[33] L. Benati, G. Calestani, R. Leardini, M. Minozzi, D. Nanni, P. Spagnolo, S. Strazzari, *Org. Lett.* **2003**, *5*, 1313-1316.
[34] K. Sato, O. Miyamoto, *Nippon Kagaku Zasshi* **1956**, *77*, 1409-1411.
[35] J. Mazzolini, I. Mokthari, R. Briquet, O. Boyron, F. Delolme, V. Monteil, D. Bertin, D. Gigmes, F. D'Agosto, C. Boisson, *Macromolecules* **2010**, *43*, 7495-7503.
[36] Y. Lee, D.-H. Lee, A. A. N. Sarjeant, K. D. Karlin, *J. Inorg. Biochem.* **2007**, *101*, 1845-1858.
[37] K. Higashiura, K. Ienaga, *J. Org. Chem.* **1992**, *57*, 764-766.
[38] F. P. Ballistreri, G. A. Tomaselli, R. M. Toscano, *Tetrahedron Lett.* **2008**, *49*, 3291-3293.
[39] D. Britt, C. Lee, F. J. Uribe-Romo, H. Furukawa, O. M. Yaghi, *Inorg. Chem.* **2010**, *49*, 6387-6389.
[40] O. M. Yaghi, M. O'Keeffe, N. W. Ockwig, H. K. Chae, M. Eddaoudi, J. Kim, *Nature* **2003**, *423*, 705.

Experimental

I. Characterization techniques

I.1 X-Ray Diffraction (XRD)

Powder X-ray diffraction patterns were recorded using a Bruker D5005 diffractometer (Bragg–Brentano geometry, graphite monochromator, Cu Kα radiation) and a Bruker D8 ADVANCE diffractometer (Bragg–Brentano geometry, Cu Kα radiation, 50 kV, 35 mA, λ= 0.154184 nm).

PXRD analyses are essential (in the absence of suitable single crystal) to determine if the material possess the expected crystal structure. Experimental results have to match with the data reported in the literature or with the simulated pattern obtained from Crystallographic Information File (cif). Nevertheless, this technique suffers from the inability to detect amorphous by-products, if any, and by the sometimes weak response to the presence of crystalline impurities and/or structural distortions [1].

I.2 ^{1}H Nuclear Magnetic Resonance (^{1}H NMR)

All NMR spectra were recorded with the same automated procedure for routine analysis on a Bruker Avance 250 spectrometer operating at 250 MHz for ^{1}H. The following abbreviations were used: s, singlet; d, doublet; t, triplet; and m, multiplet. Chemical shifts were given in ppm and coupling constants were reported in Hz. Spectra were calibrated using the deuterium signals of DMSO. Approximately 5mg of MOF derivate samples were commonly digested and dissolved in 0.45 mL of DMSO-d_6 and 0.05 mL of dilute DCl (35% DCl in D_2O). Due to their high chemical stability, approximately 5mg of MIL-53 derivate samples were dissolved by using DCl/D_2O/DMSO-d_6 followed by 0.05 mL of dilute NaOD (in D_2O). MIL-53 derivate samples were also digested in HF/ DMSO-d_6 and the same results were obtained. For safety reasons, however, the use of HF solution was restricted in our laboratory and not allowed to be used routinely. As an alternative solution, the use of DCl/D_2O/DMSO-d_6 followed by NaOD/D_2O/DMSO-d_6 allowed complete digestion. Also lower resolution and signal noise ratio were observed for ^{1}H NMR sample, this protocol allowed the quantification of grafting rate (with a lower accuracy however).

^{1}H liquid NMR is a powerful tool to characterize the organic part of digested MOFs. Hence, it is mainly used after PSM to determine the post-functionalization yield. Although ^{1}H liquid NMR doesn't provide any structural data (spatial arrangement, function distribution, interactions...), this method can give useful chemical information, on the basis that the new function was stable under "digestion" conditions. Furthermore, in routine solid-state NMR, resolution problems may occur especially with paramagnetic metallic nuclei or, to a lesser extent, with materials slightly functionalized for which the peaks observed could thus be difficult to attribute.

I.3 N_2 physisorption

The apparent BET surface areas and the microporous volumes were obtained by N_2 adsorption at 77K. N_2 isotherms were carried out using a BELSORP max porosimeter (BEL Japan). In the low-pressure region (p/po <10^{-2}), the adsorption measurements were carried out by doses of 3-6 cm^3(STP)/g with equilibrium times in the range 1620-3600 s. Care was taken of the absence of diffusional limitation in the adsorption measurements, especially at low pressure. Helium was used as backfill gas to measure the freespace volume of the cell before the N_2 adsorption measurements. BET specific surfaces were determined from recorded adsorption data at $0.05 < p/po < 0.25$, while the pore volume was determined from the N_2 adsorbed volume at $p/po = 0.99$.

Permanent and robust microporous structures were characterized by isotherm shapes (N_2 at 77K) of type I with little or no hysteresis as in the general case of zeolites.

The BET (Brunauer–Emmett–Teller) analysis is the standard method for determining surface areas from nitrogen adsorption isotherms and was originally derived for multilayer gas adsorption onto flat surfaces [2]. In MOFs, adsorption occurs through a pore-filling mechanism rather than by layer formation. Nevertheless, even if BET assumptions are not valid to measure surface area of microporous materials, this method provides meaningful and accurate measurements in the case of MOF materials [3, 4]. The measurement of the BET area gives also evidences that species, linked or not, arre trapped inside the pores, reducing the accessible volume.

Prior to the gas adsorption/desorption tests, **2**, **3**, **4**, **6, 6b**, **7** and **7b** were degassed for one night at 180°C under secondary vacuum to remove adsorbed moisture and vapours, while **2** and **5** were degassed for one night at 120°C.
All derivatives of **1**, **2**, **3 4** and **5** were degassed for one night at 100°C under secondary vacuum.

I.4 Infrared (IR) Spectroscopy

IR spectra were recorded on a Fourier Transform Vector 22 Bruker spectrometer in KBr pellets in the 400-4000 cm^{-1} region.

I.5 Thermogravimetry (TG) and Differential Thermal analysis (DTA)

TG-DTA have been carried out on a SETARAM type Setsys Evolution 12 apparatus (heating rate of 2 °C min-1) coupled with a mass spectrometer PFEIFFER, type Omnistar.

I.6 Scanning Electron Microscopy (SEM)

Scanning Electron Microscopy was carried out on a JEOL 5800 LV microscope equipped with an Oxford Isis 300 analytical system (Energy Dispersive Spectroscopy (EDS) detector).

I.7 Elementary analysis (ICP-OES)

Elemental analysis was measured by Inductively Coupled Plasma Optical Emission Spectroscopy (ICP-OES). The samples were dissolved in a boiling sulphuric and nitric acid mixture under reflux conditions and metal contents were analyzed using ICP-OES Activa spectrometer (Jobin-Yvon).
Determination of C, H, and N content was determined by chemical micro-analyses using coulometric and catharometric detections and infra-red cells.

I.8 Mass spectroscopy (MS)

ESI mass spectra were obtained on a Thermo-Finnigan LCQ Advantage mass spectrometer.

I.9 Gas Chromatography (GC)

Analyses were performed by on a HP 6890N (Agilent) equipped with a 30 m HP5 column (95% dimethylpolysyloxane, 5% diphénylpolysiloxane) and with helium as gas vector.

II. Chemicals

All chemicals were used as received without any further purification.

Solvents: *N,N'*-dimethylformamide, DMF, C_3H_7NO (Aldrich, 99.8%); dichloromethane, CH_2Cl_2 (Acros Organics, 99.99%); tetrahydrofuran, THF, C_4H_8O (Aldrich, 99%); methanol, MeOH, CH_4O (Sigma-Aldrich, 99 %); acetonitrile, C_2H_4N (Sigma-Aldrich, 99.9%); acetone, C_3H_6O (Sigma-Aldrich, 99%), hydrochloric acid, HCl (Acros Organics, 37%)

Deuterated Solvents for NMR: deuterium chloride, DCl (Aldrich, 99% D); deuterated dimethyl sulfoxide, DMSO-d_6, C_2D_6OS (Eurisotop, 99.8% D); sodium deuteroxide, NaOD (Aldrich, 99% D); and hydrogen fluoride, HF (Merck, 40%), deuterated chloroform, $CDCl_3$ (Eurisotop, 99.8% D)

Metallic precursors: zinc fluoride, $ZnF_2 \cdot 4H_2O$ (Alfa Aesar, 98%), indium nitrate, $In(NO_3).4H_2O$ (Alfa Aesar, 99.99%); zinc nitrate, $Zn(NO_3)_2 \cdot 4H_2O$ (Merck, 98.5%); aluminium chloride, $AlCl_3.6H_2O$ (Sigma-Aldrich, 98%); iron chloride, $FeCl_3.6H_2O$ (Fluka, 97%); tetrakis(acetonitrile)copper(I) hexafluorophosphate, $Cu^I(CH_3CN)_4PF_6$ (Aldrich, n.c)

Organics: 2-aminoterephthalic acid, NH_2-bdc, $C_8H_7NO_4$ (Alfa Aesar, 99%); terephthalic acid, bdc, $C_8H_6O_4$ (Aldrich, 98%); 3,5-diamino-1,2,4-triazole, $(NH_2)_2$TAZ, $C_2H_5N_5$ (Alfa Aesar, 98+%); 1,4-diazabicyclo[2.2.2] octane, DABCO, $C_6H_{12}N_2$ (Aldrich, 98%); nicotinoyl chloride hydrochloride, $C_6H_5Cl_2NO$ (Aldrich, 97%) ; *tert*-butyl nitrite, tBuONO, $C_4H_9NO_2$ (Aldrich, 90%); trimethylsilyl azide, $TMSN_3$, $C_3H_9N_3Si$ (Aldrich, 99.5%); phenylacetylene, C_8H_6 (Aldrich, 98%); diethylpropargylamine, $C_7H_{13}N$ (Fluka, 90%); 1-hexyne, C_6H_{10} (Aldrich, 97%); propargyl alcohol, C_3H_4O (Aldrich, 99%); propargylamine, C_3H_5N (Aldrich, 98%); propiolic acid, $C_3H_2O_2$ (Aldrich, 95%); propargyl chloride, C_3H_3Cl (Aldrich, 98%); triethylamine, Et_3N, $C_6H_{15}N$ (Riedel-de Haën, 99%); 4-(dimethylamino)pyridine, DMAP, $C_7H_{10}N_2$ (Aldrich, 99%); potassium ethyl xanthogenate, $C_2H_5OCS_2K$ (Fluka, 98%); sodium thiomethoxide, CH_3SNa, (Sigma, 95%); methanesulfonyl chloride, CH_3SO_2Cl (Aldrich, 99.7%); mesitylene, C_9H_{12} (Fluka, 99.8%)

Catalytic reactions: ethyldecanoate, $C_{12}H_{24}O_2$ (Fluka, 99%); dibutylamine, $C_8H_{19}N$ (Fluka, 99%); N-Methylcyclohexylamine, $C_7H_{15}N$ (Aldrich, 99%); methyl acrylate, $C_4H_6O_2$ (aldrich, 99%); acrylonitril, C_3H_3N (Aldrich, 99%); cyclohexen-1-one, C_6H_8O (Fluka, 98%); methanol, MeOH, CH_4O (Aldrich, 99%); toluene, C_7H_8 (Chimie-Plus, 99%); decane, $C_{10}H_{22}$ (Alfa Aesar, 99%).

III. CHAPTER 2: Synthesis and Characterization of Amino-MOFs

III.1 DMOF-NH_2 **(1)**

DMOF-NH_2 was prepared according to a procedure published by Wang and co-workers [5]. $Zn(NO_3)_2 \cdot 4H_2O$ (0.781 g, 3.00 mmol) and 2-amino-1,4-benzenedicarboxylic acid (0.554 g, 3.03 mmol) were dissolved in 75 mL of DMF. DABCO (0.542 g, 4.815 mmol) was then added to the solution, which immediately generated a large amount of white precipitate. The mixture was filtered using a Pyrex® glass funnel of fine porosity. The powder was washed with 3 × 8 mL of DMF followed by 3 × 8 mL of CH_2Cl_2. The powder was then soaked in 10 mL of CH_2Cl_2 for three days with fresh CH_2Cl_2 added every 24 h. After three days of soaking, the powder was dried under vacuum at room temperature for one night. Yield: 40%. 0.30 g. ^{1}H NMR, 250 MHz, (DCl/D_2O/DMSO-d_6, 25°C) δ: 3.52 (s, 6.68H, DABCO), 7.13 (d, J = 8.3H, 1H, z), 7.47 (s, 1H), 7.79 (d, J = 8.3Hz, 1H,). Relative concentration of NH_2-bdc and DABCO in DMOF-NH_2: ~1:0.56. (Expected value: 1:0.5). BET surface area: 1320 $m^2.g^{-1}$.

III.2 MIL-68-In-NH_2 **(2)**

MIL-68(In)-NH_2 was prepared following the protocol presented in a recent patent [6]. It was obtained by precipitation in a 100 mL Pyrex® beaker using a mixture of 4.82 mL (4.14 mmol) of 0.86 M indium nitrate in DMF and 10.06 mL (3.32 mmol) of 0.33 M 2-aminoterephthalic acid in DMF. The reaction mixture was stirred for 5 min, then 4.83 mL (6.67 mmol) of 1.38 M DABCO in DMF were added. The reaction mixture was stirred for 2 h at room temperature. The precipitate obtained was washed with DMF at 160°C, then soaked in CH_2Cl_2 for 24 h. Yield: 85%. 0.88 g. ^{1}H NMR, 250 MHz, (DCl/D_2O/DMSO-d_6, 25°C) δ: 7.15 (d, J = 8.3Hz, 1H), 7.44 (s, 1H), 7.80 (d, J = 8.3Hz, 1H). BET surface area: 1120 $m^2.g^{-1}$.

III.3 CAU-1 **(3)**

CAU-1 was provided by T. Ahnfeldt and Prof. Dr. N. Stock of the Christian-Albrechts-University in Kiel, Germany. ^{1}H NMR, 250 MHz, (DCl/D_2O/DMSO-d_6, 25°C) δ: 6,88 (d, J = 8 Hz, 1H); 7,03 (s, 1H); 7,6 (d, J = 8 Hz, 1H). BET surface area: 1434 $m^2.g^{-1}$.

III.4 MIL-53(Al)-NH_2 **(4)**

The synthesis of MIL-53(Al)-NH_2 was adapted from the procedures described in [7]. 2-aminoterephthalic acid (NH_2-bdc, 0.120 g, 0.66 mmol) was suspended in water (28 mL, 1.55 mmol) in a 40 mL Teflon®-lined stainless steel digestion bomb. 1.10 mL (0,44 mmol) of a 0.4 M $AlCl_3.6H_2O$ solution and 0.56 mL (0.22 mmol) of a 0.4 M NaOH solution were added. The reaction mixture was heated for 24 h without stirring at 110°C. The resulting precipitate was washed with water and DMF at 160°C, then soaked in CH_2Cl_2 for 24 h and dried at 80°C in air. Yield: 95%. 0.1g. ^{1}H NMR, 250 MHz, (DCl/NaOD/D_2O/DMSO-d_6, 25°C) δ: 7.15 (d, J = 8.3Hz 1H), 7.44 (s, 1H), 7.80 (d, J = 8.3Hz, 1H). BET surface area: 940 $m^2.g^{-1}$.

III.5 MIL-101(Fe)-NH_2 **(5)**

MIL-101(Fe)-NH_2 was synthesized from aminoterephthalic acid using a procedure described in [7]. A mixture of $FeCl_3 \cdot 6H_2O$ (1.0812 g, 4.00 mmol) and NH_2-bdc (0.3623 g, 1.65 mmol) was suspended in DMF (24 mL) and heated at 110°C for 24 h. After filtration, a brown microcrystalline product was obtained. The crystals were washed three times with DMF and three times with dichloromethane, then dried at room temperature under vacuum. Yield: 66%. 0.72 g. ^{1}H NMR 250 MHz, (DCl/D_2O/DMSO-d_6) δ: 7.32 (s, 1H); 7,63 (s, 1H); 7,86 (s, 1H). BET surface area: 2436 $m^2.g^{-1}$ Porous volume: 1.12 $cm^3.g^{-1}$.

III.6 IRMOF-3 **(6)**

IRMOF-3 was prepared according to the procedure reported by Huang *et al.* [8]: 4.4 mL (31.6 mmol) of triethylamine was directly added to a DMF solution (80 mL) containing 2.4g (8 mmol) of $Zn(NO_3)_2 \cdot 4H_2O$ and 0.66g (4 mmol) of 2-aminoterephthalic acid under stirring at room temperature for 90 min. The powder was collected by repeated centrifugation and thorough DMF washing for three times. Then, they were dried at 130 °C under static air. Yield: 49%.1.18 g. ^{1}H NMR, 250 MHz, (DCl/D_2O/DMSO-d_6, 25°C) δ: 6.99 (dd, J = 1.7 Hz, J = 8.3Hz, 1H); 7.36 (s, 1H); 7.74 (dd, J = 1.7 Hz, J = 8.3Hz, 1H). BET surface area: 623 ± 21 $m^2.g^{-1}$.

III.7 $ZnF(NH_2)_2TAZ$ **(7)**

$ZnF(NH_2)_2TAZ$ was prepared by placing a mixture of 0.2 g (2 mmol) of 3,5-diamino-1,2,4-triazole, 0.35 g (2 mmol) of $ZnF_2 \cdot 4H_2O$ and 10 mL of water into a 40 mL Teflon® lined autoclave. The resulting mixture was stirred for 5 min prior to sealing the autoclave. The autoclave was then placed in an oven and heated to 160 °C for 3.5 days [9].
Yield: 80%. 0.28 g.

IV. CHAPTER 3: Postsynthetic modification by acylation reaction

IV.1 Homogeneous conditions

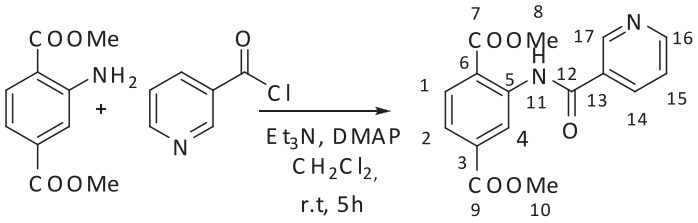

One equivalent of dimethylaminoterephthelate (1,5g, 7 mmol) was diluted in 20 mL of CH_2Cl_2 and treated with three equivalents of nicotinoyl chloride (3g, 21 mmol) in the presence of an excess of Et_3N (9 mL, 42 mmol) and DMAP (0.3 g, 2.1 mmol) at room temperature for five hours. The organic phase was washed three times with 20 mL of water, dried over $MgSO_4$ and concentrated in vacuum. The product was recrystallized from dichloromethane. Yield: 60%. 0.90 g. COSY NMR (^1H–^1H), 250 MHz (DMSO-d_6, 25°C) δ (ppm) 3.89 (s, $3H_{10}$), 3.91 (s, $3H_{11}$), 7.64 (dd, J = 4.8 Hz, 8.2 Hz, $1H_2$), 7.82 (dd, J = 1.7 Hz, 8.2 Hz, $1H_4$), 8.06 (d, J = 8.2 Hz, $1H_{15}$), 8.30 (td, J = 1.7Hz, 8.2Hz, $1H_1$), 8.82 (dd, J = 1.7 Hz, J = 4.8 Hz, $1H_{14}$) 8.89(d, J = 1.7 Hz, $1H_{16}$), 9.13 (d, J = 1.7 Hz, $1H_{17}$), 11.42 (s, $1H_{11}$). ^{13}C RMN, 63 Hz, (CDCl3, 25°C)) : δ (ppm) 52.61 (s,$1C_8$), 52.94 (s,$1C_{10}$), 118.410 (s, $1C_2$), 121.39 (s,$1C_4$), 123.64 (s, $1C_{15}$), 123.80 (s, $1C_1$), 131.02 (s,$1C_{14}$), 134,35 (s, $1C_6$) 135.09 (s,$1C_3$), 135.60 (s,$1C_5$), 141.33 (s,$1C_{13}$), 148.76 (s,$1C_{16}$), 152.67 (s,$1C_{17}$), 163.74 (s,$1C_{12}$), 165.95 (s,$1C_7$), 168.49 (s,$1C_9$). MS (ESI) *m/z* = 313 [M]-

IV.2 Functionalized IRMOF-3 **(6b)**

A sample of IRMOF-3 **6** (0.85 g, 3.15 mmol equiv of -NH_2) activated at 250 °C for 12 h was suspended in dry DMF and treated with nicotinoyl chloride (0.35 g, 2.45 mmol) in the presence of an excess of Et_3N (0.7 mL, 3.3 mmol) and DMAP (0.1 g, 0.7 mmol) at 100 °C for five days. The resulting powder was collected by filtration, then thoroughly washed three times with DMF and dried under vacuum at 170 °C for 12 h. Although the washing routine with DMF removes unreacted nicotinoyl chloride, 0.3 molecules per unit cage still remain in the porous network. Degree of modification: 40%. ^1H NMR, 250 MHz, (DCl/D_2O/DMSO-d_6,

25°C) δ: 7.64 (dd, J = 4.8 Hz, J = 8.2 Hz, 1H,), 7.82 (dd, J = 1.7 Hz, J = 8.2 Hz, 1H), 8.06 (d, J = 8.2 Hz, 1H), 8.30 (td, J = 1.7Hz, J = 8.2Hz, 1H,), 8.82 (dd, J = 1.7 Hz, J = 4.8 Hz, 1H) 8.89 (d, J = 1.7 Hz, 1H), 9.13 (d, J = 1.7 Hz, 1H), 11.42 (s, 1H). MS (ESI) *m/z* = 285 [M]-. BET surface area: 179 ± 5 $m^2.g^{-1}$

IV.3 Functionalized $ZnF(NH_2)_2TAZ$ **(7b)**

A sample of $ZnF(NH_2)_2TAZ$ **7** (0.28 g, 3.11 mmol equiv of $-NH_2$) was suspended in dry DMF and treated with nicotinoyl chloride (1.4 g, 9.8 mmol) in the presence of an excess of Et_3N (1.4 mL, 6.6 mmol) and DMAP (0.2 g, 1.4 mmol) at 100 °C for five days. The resulting powder was collected by filtration, then thoroughly washed three times with DMF and dried under vacuum at 170 °C for 12 h. MS (ESI) *m/z* = 308 [M]-.
$[ZnF(C_{14}H_{11}N_7O_2)_{0,6}(C_2H_5N_5)_{0,4}]$ Zn Calculated: Zn 21.13, C 35.69, H 2.80, N 28.05, F 6.14
Found: Zn 20.29, C 36.46, H 2.82, N 32.58, F 5.95

IV.4 Functionalized MCM-41 **(8b)**

MCM-41-NH_2 **8** was prepared by addition of the 3-aminopropyltrialkoxysilane (3 g) to a suspension of freshly activated MCM-41 (3 g) in refluxing toluene (50 mL) and then stirred for 1.5 h. After distillation of a toluene fraction containing ethanol, the heating and distillation sequences were repeated two times. The modified solid was filtered, washed in Soxhlet apparatus with diethyl ether and dichloromethane, and then dried at 120°C. A sample of MCM-41-NH_2 **8** (0.85 g, 3 mmol equiv of $-NH_2$) activated at 160 °C for 12 h was suspended in dry DMF and treated with nicotinoyl chloride (0.35 g, 2.45 mmol) in the presence of an excess of Et_3N (0.7 mL, 3.3 mmol) and DMAP (0.1 g, 0.7 mmol) at 100 °C for five days. The resulting powder was collected by filtration, then thoroughly washed three times with DMF, soaked in dichloromethane and dried under vacuum.

IV.5 Catalytic reactions

IV.5.1 Aza-Michael reaction

The reaction of the donor group (5 mmol) with the acceptor group (5.5mmol) in the presence of 1.5 mol% of catalyst based on amino group was carried out at room temperature for 24 h. After reaction was completed and catalyst filtered off, a sample of the filtrate was diluted in *n*-decane with 5% toluene as external standard and analyzed by GC.
T (injector): 250°C
T (detector): 300°C
T (oven): 50°C (10 min) - 35°C/min-250°C (5 min).
Injected volume: 1.0 μL

IV.5.2 Transesterification reaction

Ethyldecanoate (2.5 mL, 0.01 mol) and methanol (10 mL, 0.25 mol) along with 1.5 mol% catalyst based on basic (amino or aniline) groups were made to react in a Teflon® lined stainless steel digestion bomb (TopIndustrie) for 24 h at 180 °C or 130°C. After reaction, the catalyst was recovered by filtration and a sample of the filtrate was diluted in CH_2Cl_2 and analyzed by GC using mesitylene as external standard.
T (injector): 250°C
T (detector): 300°C
T (oven): 35°C (5 min)- 4°C/min - 125°C- 35°C/min- 300°C (10 min)
Injected volume: 1.0 μL

V. CHAPTER 4: Combinatorial Synthesis of Metal-Organic Frameworks libraries by Click-Chemistry

V.1 Homogeneous conditions

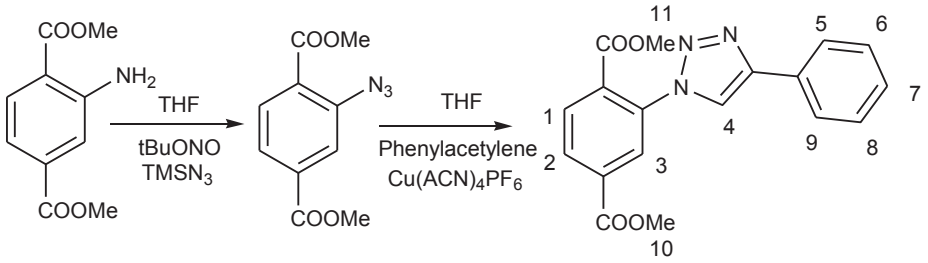

Dimethyl-2-aminoterephthalate (0.190 g, 0.91 mmol) was dissolved in THF (4 mL) in a 25 mL round-bottomed flask and cooled to 0°C in an ice bath. To this stirred mixture was added tBuONO (141 mg, 0.16 mL, 1.37 mmol), followed by a dropwise addition of $TMSN_3$ (126 mg, 0.14 mL, 1.10 mmol). The resulting solution was stirred at room temperature for one night. Phenylacetylene (140 mg, 0.150 mL, 1.37 mmol) and $Cu^{I}(CH_3CN)_4PF_6$ (48 mg, 0.26 mmol) were then added, and this mixture was stirred overnight at room temperature. The mixture was concentrated under vacuum and the organics were extracted by CH_2Cl_2 and washed with water, saturated $NaHCO_3$ (aq) and brine. After drying over Na_2SO_4, the solvent was taken off under reduced pressure. Yield: 80%. 0.152 g. ^{1}H NMR, 250 MHz, (DMSO-d_6, 25°C) δ: 3.69 (s, $3H_{10}$), 3.93 (s, $3H_{11}$), 7.45 (m, $3H_{6\text{-}7\text{-}8}$), 7.95 (d, J= 8 Hz, $2H_{5\text{-}9}$), 8.07 (d, J= 8.5Hz, $1H_1$), 8.24 (d, J= 7Hz, $2H_{3\text{-}2}$), 9.22 (s, $1H_4$).

V.2 Experimental Details for the post-functionalization of DMOF-NH_2

V.2.1 DMOF-N_3 **(1a)**

In a typical synthesis, the freshly dried DMOF-NH_2 (80 mg, 0.27 mmol equiv of -NH_2) was placed into a vial (10 mL capacity) with 3.0 mL of THF, 0.22 mL (1.84 mmol, 7 eq) of tBuONO and 0.2 mL (1.51 mmol, 6 eq) of $TMSN_3$. The sample was left to react for one night at room temperature to produce the azide intermediate corresponding compound .The reaction was quenched by decanting the solvent. Excess reactants were removed by washing three times in THF followed by three times in CH_2Cl_2. Drying at room temperature yielded 65 mg

of DMOF-N_3 **1a**. Degree of modification: 100% ^{1}H NMR, 250 MHz, (DCl/D_2O/DMSO-d_6, 25°C) δ: 3.56 (s, 6.5H, DABCO), 7.73-7.83 (m, 3H, ArH), BET surface area: 695m².g^{-1}

V.2.2 One pot post-functionalization of DMOF-NH_2 with phenylacetylene **(1b)**

In a typical synthesis, the freshly dried DMOF-NH_2 **1** (80 mg, 0.27 mmol equiv of -NH_2) was placed into a vial (10 mL capacity) with 3.0 mL of THF, 0.22 mL (1.84 mmol, 7 eq) of tBuONO and 0.2 mL (1.51 mmol, 6 eq) of $TMSN_3$. The sample was left to react for one night at room temperature to produce the azide intermediate corresponding compound. Phenylacetylene (0.96 mL, 8.8 mmol, 36 eq) and an amount of $Cu^I(CH_3CN)_4PF_6$) (48 mg, 0.26 mmol, 1 eq) in 1 mL of THF were added and the mixture was stirred continuously for 24 h. After decantation, the supernate was removed. The solid was washed three times by THF (x 8 ml) and three times by CH_2Cl_2 (x 8 ml) in order to remove unreactive substrates. The solid was then dried under vacuum at room temperature to yield 60 mg of **1b**. Degree of modification: 100%. ^{1}H NMR, 250 MHz, (DCl/D_2O/DMSO-d_6, 25°C) δ: 3.52 (s, 6H, DABCO), 7.45 (m, 3H), 7.92 (d, J= 7Hz, 2H), 8.03 (d, J= 8Hz, 1H), 8.18 (m, 2H), 9.14 (s, 1H). ^{13}C NMR, 62.8 MHz, (DCl/D_2O/DMSO-d_6, 25°C) δ: 122.8, 125.2, 125.6, 126.4, 128.2, 128.9, 129, 130.1, 130.4, 130.9, 132.1, 134.1, 135.1, 146.6, 165.4, 166. MS (ESI) m/z = 310 [M] + , BET surface area: 244m².g^{-1}

V.3 Generalization of postsynthetic modification by click chemistry

In a typical synthesis, the freshly-dried amino-MOF (80 mg), (**1, 2**, **3**, **4** or **5**) was treated with tBuONO and $TMSN_3$ in THF for one night at room temperature to produce the corresponding intermediate azide compound, azide-MOF **a**. In the same vessel, functionalized MOF was obtained by adding an excess of alkynes in the presence of $Cu^I(CH_3CN)_4PF_6$ in THF, with the mixture continuously stirred for 24 h. The alkynes used in this study are phenylacetylene **b**, diethylpropargylamine **c**, hexyne **d**, propargyl alcohol **e**, propiolic acid **f** and propargylamine **g**. After decantation, the supernate was removed. The solid was washed three times by THF (x 8 mL) and three times by CH_2Cl_2 (x 8 mL) in order to remove unreactive substrates. The solid was then dried under vacuum at room temperature to yield the final compound.

	equiv of –NH_2	tBuONO $TMSN_3$	Cu^I b	Cu^I c	Cu^I d	Cu^I e	Cu^I f	Cu^I g
1	0.27 mmol	0.22 mL (1.84 mmol, 7 eq) 0.2 mL (1.51 mmol, 6 eq)	48 mg (0.13 mmol, 0.5 eq) 0.96 mL (8.8 mmol, 32 eq)	24 mg (0.06 mmol, 0.25 eq) 0.33 mL (2.3 mmol, 8.5 eq)	24 mg (0.06 mmol, 0.25 eq) 0.26 mL (2.3 mmol, 8.5 eq)	24 mg (0.06 mmol, 0.25 eq) 0.134 mL (2.3 mmol, 8.5 eq)	[b]	[a]
2	0.26 mmol	1.5 mL (12.5 mmol, 48 eq) 1.3 mL (9.88 mmol, 38 eq)	96 mg (0.26 mmol, 1 eq) 1.9 mL (17.6 mmol, 68 eq)	192 mg (0.52 mmol, 2 eq) 4.88mL (35.6 mmol, 136 eq)	144 mg (039 mmol, 1.5 eq) 2.02mL (17.6 mmol, 68 eq)	96 mg (0.26 mmol, 1eq) 1.54mL (26.6 mmol, 68 eq)	96 mg (0.26 mmol,1eq) 1.08mL (17.6 mmol, 51 eq)	96 mg (0.26 mmol, 1eq) 1.13mL (17.6 mmol, 68 eq)
3	0.3 mmol	0.74 mL (6.3 mmol, 21 eq) 0.65 mL (5 mmol, 17 eq)	55 mg (0.15 mmol, 0.5eq) 0.92 mL (8.4 mmol, 28 eq)	58 mg (0.15 mmol, 0.5eq) 1.18 ml (8.5 mmol, 28 eq)	55 mg (0.15 mmol, 0.5eq) 0.59 ml (5.1 mmol, 17 eq)	55 mg (0.15 mmol, 0.5eq) 0.3 ml (5.1 mmol, 17 eq)	55 mg (0.15 mmol, 0.5eq) 0.52 ml (8.4 mmol, 28 eq)	[a]
4	0.36 mmol	[c] 3.8 mL (32 mmol, 89 eq) 3.6 mL (28 mmol, 78 eq)	192 mg (0.52 mmol, 1.5eq) 2.7 mL (24.6 mmol, 68eq)	264 mg (0.71 mmol, 2eq) 3.3 mL (23 mmol, 68eq)	192 mg (0.52 mmol, 1.5eq) 2.8 mL (24.4 mmol, 68eq)	132 mg (0.36 mmol, 1eq) 1.2 mL (20.6 mmol, 57eq)	66mg (0.18 mmol, 0.5eq) 0.5 mL (8.1 mmol, 22eq)	[a]
5	0.3 mmol	0.3 mL (2.1 mmol, 7 eq) 0.27mL (1.8 mmol, 6 eq)	110 mg (0.3 mmol, 1 eq) 1.8 mL (16.8 mmol, 56 eq)	[a]	[a]	[a]	[a]	[a]

[a]: not performed; [b]: dissolution; [c]: performed in ethanol

V.4 Effect of the grafting rate on the porous volume

MOF	Degree of modification (%)	Amount of $Cu(ACN)_4PF_6$	Amount of **b**
1b-15	15± 3	6 mg (0.016 mmol, 0,06 eq)	0.12 mL (1.1 mmol, 4 eq)
1b-40	40± 5	12 mg (0.032 mmol, 0.125 eq)	0.24 mL (2.2 mmol, 8 eq)
1b-65	65 ± 5	24 mg (0.065 mmol, 0.25 eq)	0.48 mL (4.4 mmol, 16 eq)
1b-80	80± 5	36mg (0.1 mmol, 0,375 eq)	0.72 mL (6.6 mmol, 24 eq)
2b-10	10± 3.4	24 mg (0.06 mmol, 0.3 eq)	0.48 mL (4.4 mmol, 21 eq)
2b-20	20± 5	36 mg (0.1 mmol, 0.45 eq)	0.72 mL (6.6 mmol, 31.5 eq)
2b-50	50± 5	48 mg (0.13 mmol, 0.6 eq)	0.96 mL (8.8 mmol, 42 eq)
2b-80	80± 2	96 mg (0.26 mmol, 1.2eq)	1.9 mL (17.6 mmol, 84 eq)
3b-20	20± 2.5	27 mg (0.074mmol, 0.27eq)	0.46 mL (4.2 mmol, 15.5 eq

1b- 40

$[Zn_2(C_{16}H_9N_3O_4)_{0,8}(C_8H_3N_3O_4)_{1,2}(C_6H_{12}N_2)](CH_2Cl_2)_{1,4}]$

Calculated: Zn 15.25

Found: Zn 15.27, Cu 1.47

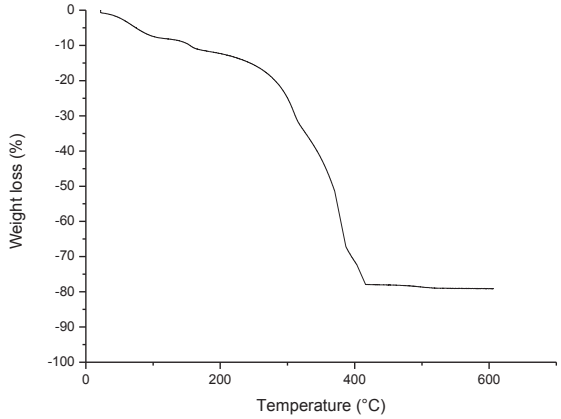

The TGA data indicate that **1b-40** loses its guest molecules CH_2Cl_2 (8.1%) in the temperature range of 15–120°C, then the unstable azide groups are decomposed between 120-220°C (4%). The resulting porous framework (63%) starts to decompose after 220°C.

1b- 80

$[Zn_2(C_{16}H_9O_4N_3)_{1,6}(C_8H_3O_4N_3)_{0,4}(C_6H_{12}N_2)]\ (CH_2Cl_2)_{0,8}$

Calculated: Zn 14.79, C 48.34, H 3.33, N 12.67.

Found: Zn 14.29, C 46.46, H 3.24, N 12.58, Cu 0.64.

2b-20

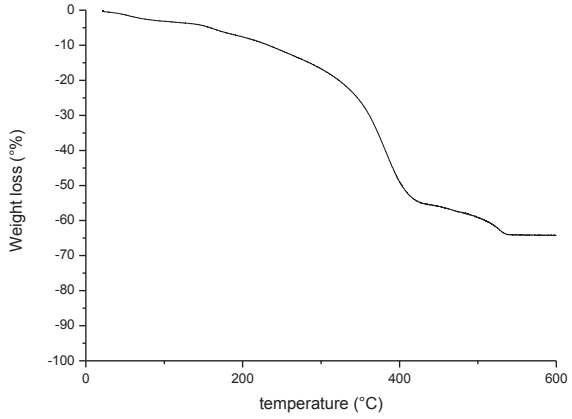

The TGA data indicate that **2b-20** loses its guest molecules H_2O (3.5%) in the temperature range of 15–120°C, then the unstable azide groups are decomposed between 120-220°C (8%). The resulting porous framework (52%) starts to decompose after 270°C.

3b-10

$[Al_4(OH)_2(OCH_3)_4(C_8H_3O_4N_3)_{2,7}(C_{16}H_9O_4N_3)_{0,3}]$

Calculated: Al 11.83, C 40.03, H 2.74

Found: Al 10.04, C 37, H 2.75.

VI. CHAPTER 5: Tailoring Metal-Organic Framework catalysts and adsorbents by Click Chemistry

VI.1 Application to base catalysis

VI.1.1 Catalysts

MOF	Degree of modification (%)	Amount of $Cu(ACN)_4PF_6$ used	Amount of **b** used
1b-15	15± 3	6 mg (0.016 mmol, 0,06 eq)	0.12 mL (1.1 mmol, 4 eq)
1b-40	40± 5	12 mg (0.032 mmol, 0.125 eq)	0.24 mL (2.2 mmol, 8 eq)
1b-65	65 ± 5	24 mg (0.065 mmol, 0.25 eq)	0.48 mL (4.4 mmol, 16 eq)
1b-80	80± 5	36mg (0.1 mmol, 0,375 eq)	0.72 mL (6.6 mmol, 24 eq)

MOF	Degree of modification (%)	Amount of $Cu(ACN)_4PF_6$ used	Amount of **c** used
1c-40	40± 5	6 mg (0.014 mmol, 0.05 eq)	0.08 mL (0.54 mmol, 2 eq)
1c-85	85± 5	17 mg (0.04 mmol, 0.15 eq)	0.25 mL (1.7 mmol, 6.3 eq)

1b- 40

$[Zn_2(C_{16}H_9N_3O_4)_{0,8}(C_8H_3N_3O_4)_{1,2}(C_6H_{12}N_2)](CH_2Cl_2)_{1,4}$

Calculated: Zn 15.25

Found: Zn 15.27, Cu 1.47

1b- 80

$[Zn_2(C_{16}H_9O_4N_3)_{1,6}(C_8H_3O_4N_3)_{0,4}(C_6H_{12}N_2)]\ (CH_2Cl_2)_{0,8}$

Calculated: Zn 14.79, C 48.34, H 3.33, N 12.67.

Found: Zn 14.29, C 46.46, H 3.24, N 12.58, Cu 0.64.

1c-85

$[Zn_2(C_{15}H_{16}N_4O_4)_{1,7}(C_8H_3N_3O_4)_{0,3}(C_6H_{12}N_2)](CH_2Cl_2)_{0,6}$

Calculated: Zn 14.65

Found: Zn 14.68, Cu 1.05

DMOF-N_3 (80 mg, 0.25 mmol eq of -N_3) **1a** was placed into a vial (10 mL capacity) with 3.0 mL of THF, 18 mg (0.045 mmol, 0.2 eq) of $Cu^I(CH_3CN)_4PF_6$ and 0.36 mL (2.5 mmol, 10 eq) of phenylacetylene **b**. The sample was left to react for one night at room temperature. Next, 80 mg (0.2 mmol, 0.8 eq) of $Cu^I(CH_3CN)_4PF_6$ and 2 mL (14 mmol, 56 eq) of diethylpropargylamine **c** in THF were added and the mixture was stirred continuously for 24 h. After decantation, the supernate was removed. The solid was washed three times by THF (x 8 mL) and three times by CH_2Cl_2 (x 8 mL) in order to remove unreactive substrates. The solid was then dried under vacuum at room temperature to yield **1h.**

1h

$Zn_2(C_{16}H_9N_3O_4)_{0,6}(C_8H_3N_3O_4)_{0,8}(C_{15}H_{16}N_4O_4)_{0,6}(C_6H_{12}N_2)(CH_2Cl_2)_3(H_2O)_2$

Calculated: Zn 12.2, C 38.09, H 3.7, N 11.2

Found: Zn 13.01, C 36.9, H 2.91, N 8.04

Linker b

See V.1

Linker c

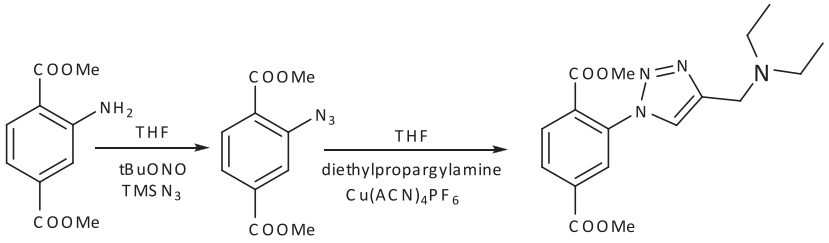

Dimethyl-2-aminoterephthalate (0.190 g, 0.91 mmol) was dissolved in THF (4 mL) in a 25 mL round-bottomed flask and cooled to 0°C in an ice bath. To this stirred mixture was added tBuONO (141 mg, 0.16 mL, 1.37 mmol), followed by a dropwise addition of $TMSN_3$ (126 mg, 0.14 mL, 1.10 mmol). The resulting solution was stirred at room temperature for one

night. Diethylpropargylamine (0.190 mL, 1.37 mmol) and $Cu^{I}(CH_3CN)_4PF_6$ (48 mg, 0.26 mmol) were then added, and this mixture was stirred overnight at room temperature. The mixture was concentrated under vacuum and the organics were extracted by CH_2Cl_2 and washed with water, saturated $NaHCO_3$ (aq) and brine. After drying over Na_2SO_4, the solvent was taken off under reduced pressure. The yield obtained was 70%. ^{1}H NMR 250 MHz, (DMSO-d_6) δ: 1.02 (t, J= 7Hz, 6H), 2.44 (q, J= 7Hz, 4H), 3.48 (s, 2H), 3.64 (s, 3H), 3.92 (s, 3H), 8.04 (d, J= 8Hz,1H), 8.19 (t, J= 8Hz, 2H), 8.62 (s, 1H).

VI.1.2 Catalytic results

All catalytic measurements for the transesterification reaction were carried out in a Teflon®-lined stainless steel digestion bomb (TopIndustrie) under stirring. Ethyldecanoate (2.5 mL) and methanol (10 mL) were made to react in the presence of 20 mg catalyst for 24 h at 130°C. After the reaction, the catalyst was recovered by filtration, and a sample of the filtrate was diluted in CH_2Cl_2 and analyzed by gas chromatography using mesitylene as external standard. Carbon mass balances always exceeded 97%. (Injected volume: 1.0 μL)

T (injector): 250°C

T (detector): 300°C

T (oven): 35°C (5 min)- 4°C/min - 125°C- 35°C/min- 300°C (10 min)

VI.2 Application to adsorption

VI.2.1 Synthesis of thioalkynes

Synthesis of propargylthiol

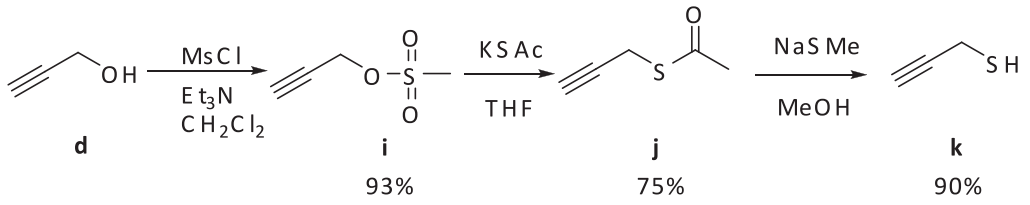

A solution of 4.28g (0.0742 mol) of propargyl alcohol **d** in 200 mL of CH_2Cl_2 was cooled to -20°C and treated with 30 mL (0.215 mol) of triethylamine (added in one portion) followed by 12 mL (0.158 mol) of methanesulfonyl chloride, added dropwise via addition funnel with good stirring over 15 min. After an additional 20 min at -20°C, 20 mL of ice/water was added and stirring was continued 5 min longer. Standard acidic workup afforded 9.25 g (0.069 mol) of pure propargyl methanesulfonate **i**. Yield: 93%.^{1}H NMR, 250 MHz, ($CDCl_3$, 25°C) δ: 2.16 (s, 1H), 3.12 (s, 3H), 4.85 (d, J= 2.5Hz, 2H).

Propargyl methanesulfonate **i** (9.25 g, 0.069 mol) was dissolved in 400 mL of THF with potassium thioacetate (7.88 g, 0.069 mol) and the mixture was left stirring at room temperature for one night. The mixture was concentrated under vacuum and the organics were extracted by CH_2Cl_2 and washed with water, saturated $NaHCO_3$ (aq) and brine. After drying over Na_2SO_4, the solvent was taken off under reduced pressure to afford 5.89 g (0.0517 mol) of propargyl thioacetate **j**. Yield: 75%.^{1}H NMR, 250 MHz, ($CDCl_3$, 25°C) δ: 2.16 (s, 1H), 3.12 (s, 3H), 4.85 (d, J= 2.5Hz, 2H).

Propargyl thioacetate **j** (1.14 g, 0.010 mol) and sodium thiomethoxide (0.7 g, 0.010 mol) were suspended in MeOH and the reaction mixture was stirred at room temperature for 1 hour. The solution was then added to aqueous HCl (200 mL/0.1N). The aqueous solution was extracted with CH_2Cl_2 and the combined organic layers were washed with brine, dried over Na_2SO_4, filtered and concentrated. At this point, ^{1}H NMR analysis of the solution (final volume 75 mL) indicates an approximative propargylthiol **k** concentration of 0.12 mol.L^{-1} which corresponds to a 90% yield. Yield: 90%. ^{1}H NMR, 250 MHz, ($CDCl_3$, 25°C) δ: 2.02 (t, J= 7.5Hz, 1H), 2.26 (t, J= 2.7Hz, 1H), 3.26 (dd, J= 2.7Hz, J= 4.8Hz, 2H).

Synthesis of *o*-ethyl S-propargyl-xanthate **l**

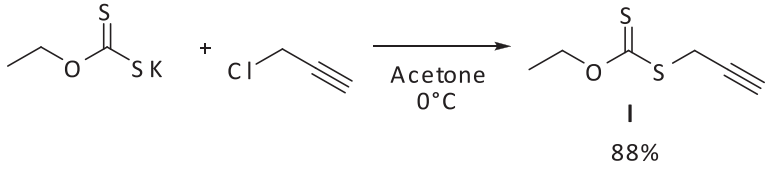

l

88%

A solution of propargyl chloride (7.8 mL, 0.105 mol) in 120 mL of acetone was cooled to 0°C. Potassium ethyl xanthogenate (16 g, 0.099 mol) was added slowly and stirring was

continued 30 min longer at 0°C. The solution was left under stirring overnight at room temperature. The mixture was concentrated under vacuum to give pure o-ethyl-S-propargyl-xanthate **l** (14 g, 0.087). Yield: 88%. ^{1}H NMR, 250 MHz, ($CDCl_3$, 25°C) δ: 1.43 (t, J= 2.6Hz, 3H), 2.23 (t, J= 2.6Hz, 1H), 3.86 (d, J=2.6 Hz, 2H), 4.66 (q, J= 7.1Hz, 2H).

VI.2.2 Cycloadddtion of thioalkynes

With propargylthiol **(k)**

MIL-68-In-N_3 **2a** (20 mg, 0.060 mmol equiv of $-N_3$) was suspended in a solution of propargylthiol in CH_2Cl_2 (2mL, 0.5 mol.L^{-1}) and $Cu^I(CH_3CN)_4PF_6$ (40 mg, 0.1 mmol) was added. The reaction mixture was stirred one night at room temperature. After decantation, the supernate was removed. The solid was washed three times by CH_2Cl_2 (x 8 mL) in order to remove unreactive substrates. The solid was then dried under vacuum at room temperature to yield the final compound. ^{1}H NMR analysis of the product indicated that no reaction took place.

With propargyl-thioacetate **(j)**

DMOF-N_3 **1a** (20 mg, 0.06 mmol equiv of $-N_3$) was placed into a vial (10 mL capacity) with 3.0 mL of ACN. A solution of propargyl thioacetate **j** (0.4g, 3.5 mmol) and $Cu^I(CH_3CN)_4PF_6$ (40 mg, 0.1 mmol) in 3 mL of ACN was added. The reaction mixture was stirred one night at room temperature. After decantation, the supernate was removed. The solid was washed three times by ACN and three times by CH_2Cl_2 (x 8 mL) in order to remove unreactive substrates. The solid was then dried under vacuum at room temperature to yield the final compound. ^{1}H NMR analysis of the product revealed that no reaction took place.

The same procedure was applied to MIL-68-In-N_3 **2a** (40 mg, 0.12 mmol equiv of $-N_3$) and ^{1}H NMR analysis of the product revealed that no reaction took place.

With xanthate **(l)**

DMOF-N_3 **1a** (20 mg, 0.06 mmol equiv of $–N_3$) was placed into a vial (10 mL capacity) with 3.0 mL of ACN. A solution of *o*-ethyl S-propargyl-xanthate **l** (0.6g, 3.75 mmol) and $Cu^{I}(CH_3CN)_4PF_6$ (40 mg, 0.1 mmol) in 3 mL of ACN was added. The reaction mixture was stirred one night at room temperature. After decantation, the supernate was removed. The solid was washed three times by ACN and three times by CH_2Cl_2 (x 8 mL) in order to remove unreactive substrates. The solid was then dried under vacuum at room temperature to yield 15 mg of DMOF-xanthate **1l-22**. Degree of modification: 22 %. ^{1}H NMR, 250 MHz, (DCl/D_2O/DMSO-d_6, 25°C) δ: 1.31 (t, J= 7Hz, 3H), 4.48 (s, 2H), 4.61 (q, J= 7Hz, J= 7.3Hz, 2H), 7.96-7.99 (m, 2H), 8.10-8.17 (m, 1H), 8.54 (s, 1H).
The same procedure was applied to MIL-68-In-N_3 **2a**. Degree of modification: 5%

DMOF-xanthate **1l-22** (15 mg, 0.01 mmol equiv of –xanthate) was placed into a vial (10 mL capacity) with 3.0 mL of THF. Propylamine was added (0.04 mL, 0.4 mmol) and the reaction mixture was stirred one night at room temperature. ^{1}H NMR analysis of the product revealed that the MOF structure was destroyed.

VI.2.3 Sulfonic acid-functionalized MOFs

Amino-MOF	**Solvent**	**Temperature**	**Amount of propanesultone used**
IRMOF-3	$CHCl_3$ CH_2Cl_2 CH_2Cl_2 (anhydrous) Isopropanol -	45°c	3 eq
MIL-68(IN)-NH_2	$CHCl_3$	25°C 45°C reflux	3 eq
Homogeneous conditions	**Solvent**	**Temperature**	**Amount of propanesultone used**
Dimethylamino terephthelate	$CHCl_3$	45°C	3eq
benzylamine	$CHCl_3$	45°C	3eq

VIII. References

[1] J. Hafizovic, M. Bjorgen, U. Olsbye, P. D. C. Dietzel, S. Bordiga, C. Prestipino, C. Lamberti, K. P. Lillerud, *J. Am. Chem. Soc.* **2007**, *129*, 3612-3620.

[2] S. Brunauer, P. H. Emmett, E. Teller, *J. Am. Chem. Soc.* **1938**, *60*, 309-319.

[3] K. S. Walton, R. Q. Snurr, *J. Am. Chem. Soc.* **2007**, *129*, 8552-8556.

[4] T. Duren, F. Millange, G. Ferey, K. S. Walton, R. Q. Snurr, *J. Phys. Chem. C* **2007**, *111*, 15350-15356.

[5] Z. Q. Wang, K. K. Tanabe, S. M. Cohen, *Inorg. Chem.* **2009**, *48*, 296-306.

[6] C. Volkringer, M. Meddouri, T. Loiseau, N. Guillou, J. Marrot, G. Ferey, M. Haouas, F. Taulelle, N. Audebrand, M. Latroche, *Inorg. Chem.* **2008**, *47*, 11892-11901.

[7] S. Bauer, C. Serre, T. Devic, P. Horcajada, J. Marrot, G. Ferey, N. Stock, *Inorg. Chem.* **2008**, *47*, 7568-7576.

[8] L. M. Huang, H. T. Wang, J. X. Chen, Z. B. Wang, J. Y. Sun, D. Y. Zhao, Y. S. Yan, *Microporous Mesoporous Mater.* **2003**, *58*, 105-114.

[9] A. M. Goforth, C.-Y. Su, R. Hipp, R. B. Macquart, M. D. Smith, H.-C. zur Loye, *J. Solid State Chem.* **2005**, *178*, 2511-2518.

Conclusions

Cette dernière partie s'articule autour de trois axes :

- un résumé de l'avancée des travaux de cette thèse en se plaçant dans le contexte historique, notamment en soulignant les avancées conjointes de l'état de l'art
- une discussion générale sur les avantages et inconvénients de la méthode de post-fonctionnalisation développée
- les perspectives de l'application des MOFs pour la séparation et la catalyse

Cette étude a réellement été initiée en février 2008 lors de mon stage de Master en collaboration avec l'IFP Energies Nouvelles et l'IRCELYON, qui précédait ma thèse. A cette date, le domaine « de l'application des MOFs à la catalyse » était encore peu exploré. La littérature relative à ces nouveaux matériaux était surtout orientée vers la synthèse de MOFs à volumes poreux très élevés pour le stockage de l'hydrogène, du méthane et du dioxyde de carbone. Ainsi, c'est véritablement en parallèle de mes trois années de thèse, que le nombre d'études portant sur la génération de MOFs fonctionnalisés (par voie directe ou par post-modification) en vue d'applications catalytiques, a connu son envol.

Au début de ce projet, les seules voies de post-fonctionnalisations proposées impliquaient des réactions de condensations d'anhydrides et d'isocyanates non fonctionnels pour un seul MOF portant des fonctions amine sur ses parois (IRMOF-3). Aucune application catalytique de ces matériaux fonctionnalisés n'était décrite dans la littérature et le greffage de certains isocyanates était limité à de faibles conversions (27%), ce qui empêchait de ce fait un contrôle du taux de greffage. Par ailleurs, peu de dérivés d'isocyanates et d'anhydrides sont facilement disponibles commercialement, restreignant ainsi une approche généralisable de post-fonctionnalisation.

Les objectifs que nous nous étions alors fixés étaient :

- la synthèse de nouveaux amino-MOFs stables : matériaux de base pour la post-fonctionnalisation
- le développement d'une méthode de post-fonctionnalisation généralisable à de nombreux MOFs portant des fonctions amines et à un grand nombre de groupements fonctionnels
- un contrôle quantitatif du taux de greffage en développant une méthode efficace de caractérisation

- l'utilisation de ces MOFs fonctionnalisés dans une réaction catalytique d'intérêt industriel

Du fait de la grande disponibilité des dérivés des chlorures d'acyles, notre première investigation a donc porté sur une nouvelle réaction de greffage par acylation, appliquée aux deux MOFs portant des fonctions amines, connus au moment de l'étude, l'IRMOF-3 et le $ZnF(NH_2)_2TAZ$. Lors de ce travail, les outils de caractérisations ont pu être développés et maîtrisés. En particulier, la RMN liquide du proton après digestion du MOF par traitement acide qui permet de calculer le taux de greffage exact par simple intégration de pics. Ces matériaux fonctionnalisés par un groupement pyridine ont été évalués dans deux réactions modèles et comparés à leurs analogues homogènes et mésoporeux. Malgré des activités supérieures, cette première voie a été abandonnée, car elle présentait une contrainte trop importante : la libération d'acide chlorhydrique durant le greffage qui, malgré un fort excès de base, restreignait son utilisation à des MOFs robustes.

En effet, entre-temps, de nouvelles structures d'amino-MOFs ont été décrites dans la littérature et parmi elles, celles qui seront utilisées dans la suite du projet, le DMOF-NH_2 (2009), le CAU-1(2009), le MIL-53(Al)-NH_2 (2008) et le MIL-101(Fe)-NH_2 (2008). Le MIL-68(In)-NH_2, présentant une structure analogue au MIL-68(In) mais un mode synthèse différent, a d'ailleurs été découvert aux laboratoires, en marge de cette thèse. Ces matériaux décrits dans le chapitre 2 présentent des propriétés structurales et physico-chimiques différentes.

Ainsi, nous nous sommes orientés vers une réaction de greffage plus douce, plus généralisable et qui ne libère pas de sous-produit susceptible de rester bloqué dans les pores ou de dégrader nos matériaux. Une des réactions de « Click Chemistry » les plus populaires, la cycloaddition 1,3-dipolaire de Huisgen entre un azoture et un alcyne pour former un triazolate, remplissait tous ces critères. Dans la littérature, deux études reportaient alors l'utilisation de cette réaction pour la post-fonctionnalisation des MOFs. Cependant, elles décrivaient toutes deux, l'obtention du MOF intermédiaire portant la fonction azoture ou alcyne par auto-assemblage. Hors, la synthèse du ligand azoture ou du ligand alcyne pouvait s'avérer délicate et nécessitait de longues étapes. C'est pourquoi, l'objectif de cette deuxième étude était d'appliquer cette méthode de « Click Chemistry » directement aux amino-MOFs déjà connus dans la littérature. La première étape consiste à convertir la fonction amine en fonction azoture. Puis, sans

isolation ni purification, le MOF fonctionnalisé est obtenu par « Click Chemistry » en ajoutant l'alcyne correspondant.
La transformation d'amino-MOF en MOF-azoture par un protocole « doux » constitue la découverte centrale de cette thèse.
Cette nouvelle voie a permis d'obtenir un nombre très important de nouveaux matériaux susceptibles d'être intéressants en catalyse et séparation.

L'étude catalytique a essentiellement été menée sur le DMOF-NH_2 choisi comme matériau d'étude, car il ne contient ni site d'acide de Lewis, ni site d'acide de Brønsted dans sa structure initiale. Les résultats obtenus ont montré que l'introduction de sites basiques (fonctions amines) et/ou de groupements hydrophobes (fonctions phényles) par « Click Chemistry » améliorait de façon non significative l'activité catalytique du solide dans une réaction de transestérification. De plus, grâce à un contrôle précis des conditions de greffage (taux de greffage, choix des alcynes), la meilleure activité a été obtenue pour un MOF bifonctionnel présentant un ratio optimisé entre sites basiques pour l'activité catalytique et sites hydrophobes pour une co-adsorption optimale des substrats à l'intérieur des pores. Ceci ouvre donc la voie à la conception sur mesure de catalyseurs multifonctionnels.

Ainsi, cette seconde étude a permis d'atteindre nos objectifs évoqués au début de ce mémoire.

Nous avons su reproduire six amino-MOFs décrits dans la littérature, dont les propriétés physico-chimiques ont été parfaitement caractérisées et contrôlées. Ces matériaux ont été utilisés comme structures de base pour notre étude. Un nouveau amino-MOF (le MIL-68(In)-NH_2) a même été synthétisé et caractérisé.
Nous avons également démontré qu'une nouvelle voie de post-fonctionnalisation pouvait être appliquée dans des conditions très douces à tous les types d'amino-MOFs ainsi qu'à quasi toutes les fonctions chimiques souhaitées. Cette large bibliothèque de nouveaux matériaux obtenue par synthèse combinatoire a pu être caractérisée. Cette voie permet une plus grande généralisation que la condensation des anhydrides ou des isocyanates qui ne dispose pas d'un grand nombre de dérivés fonctionnels. De plus, elle ne libère pas de sous-produit (eau, acide…) pouvant altérer ces matériaux. Enfin, le taux de greffage peut être contrôlé (de 10 à 100%) permettant ainsi de modeler sur mesure des catalyseurs, où un ratio optimisé entre

fonctions basiques et hydrophobes permet d'obtenir un effet synergétique important dans la réaction de transestérification.

Discussion générale sur la méthode de post-fonctionnalisation par « Click Chemistry » :

D'un point de vue industriel, même si cette voie par « Click Chemistry » favorise l'obtention de matériaux fonctionnels par rapport à la voie anhydride, elle comporte néanmoins deux étapes qui nécessitent donc des quantités de réactifs et de solvants plus importantes. Ainsi, une industrialisation de la voie « Click Chemistry » serait sûrement plus coûteuse que la voie anhydride, même si cette dernière oblige la synthèse d'anhydrides asymétriques pour des applications en catalyse.
De plus, les intermédiaires azotures, même si, dans notre cas ils sont stables du fait de leur aromaticité et des conditions très douces de températures, nécessitent tout de même des précautions particulières en matière de sécurité.
Cependant, cette étude a été réalisée dans un contexte d'approche combinatoire, où un fort excès en réactifs a été utilisé afin d'obtenir des taux de greffage élevés dans un temps imparti (12h). Ainsi, en vue d'une industrialisation, se limiter à des taux de greffage plus faibles en allongeant les temps de réactions, et donc aller vers une utilisation quantitative des réactifs, permettraient de réduire considérablement les coûts.

Perspectives :

80% des procédés catalytiques utilisent aujourd'hui des solides acides, les coûts des zéolithes et silices-alumines étant de l'ordre de 1-5 $/kg. Les stabilités chimiques et thermiques inférieures des MOFs et leurs coûts plus élevés (précurseurs, solvants) sont donc un très sérieux frein pour les applications de raffinage ou pour la synthèse de grands intermédiaires chimiques. D'autre part, très peu de MOFs préparés par synthèse directe (« self-assembly ») possèdent des sites catalytiques acides ou basiques de forces moyennes ou fortes. Ainsi, une étape de synthèse supplémentaire est indispensable pour les fonctionnaliser et les rendre éventuellement intéressants pour la catalyse, et donc les coûts sont considérablement augmentés.

C'est pourquoi, au niveau industriel, l'avenir de ces matériaux réside sûrement dans des applications de chimie plus fine ou de niches industrielles, dans lesquelles le coût du catalyseur et de son recyclage sont moins limitants [1]. La fonctionnalisation par les fonctions thiols par exemple pour le captage du mercure dans les eaux de production a été investiguée dans le chapitre 5. Même si l'étude n'a pas encore abouti, il s'avère que la voie de protection par les xanthates puis de déprotection, est assez prometteuse. Ce concept pourrait être appliqué à d'autres greffages sensibles comme celui des acides aminés ou d'autres fonctions très réactives.

Cependant, l'attractivité des MOFs pour des études fondamentales en catalyse reste élevée. En effet, contrairement aux silices mésoporeuses amorphes, où la distribution des groupements silanols est quasi-aléatoire et statistique, les MOFs sont des matériaux cristallins. Ainsi, les positions atomiques peuvent être connues. La modélisation moléculaire permet de connaître exactement les distances entre les sites (par exemple, entre une fonction –OH et –NH_2 ou entre deux fonctions –NH_2). D'autre part, on peut concevoir la construction de sites catalytiques isolés à l'échelle moléculaire en utilisant lors de la synthèse des MOFs, un mélange de ligands pré-fonctionnalisés/non fonctionnalisés (par exemple, acide téréphtalique/acide 2-aminotéréphthalique), diluant ainsi les fonctions amines de façon statistique et donc les futurs groupements fonctionnels greffés.

De plus, le taux de greffage, la nature des fonctions greffées et la taille des pores peuvent être ajustés de façon indépendante. La variation d'un seul paramètre ne modifiant pas le reste du matériau. Ainsi, un contrôle moléculaire précis des MOFs permettrait de les utiliser comme solides de références dans des réactions catalytiques, reliant directement leur structure (parfaitement connue) à l'activité, en s'affranchissant ainsi des approches empiriques « essai-erreur».

Par contre, dans le cas de taux de greffages inférieurs à 100%, la question de la distribution et de la localisation des fonctions greffées est encore non résolue. Les méthodes microscopiques actuelles ne nous permettent pas encore d'accéder à une cartographie précise des matériaux. Pour cela, des techniques de microscopies ou spectroscopies à hautes résolutions spatiales (ordre<100nm) restent à développer.

[1] G. Akiyama, R. Matsuda, H. Sato, M. Takata, S. Kitagawa, *Adv. Mater.* **2011**, *23*, 3294-3297.

Appendixes

I. APPENDIX A: Transesterification reactions of triglycerides with methanol

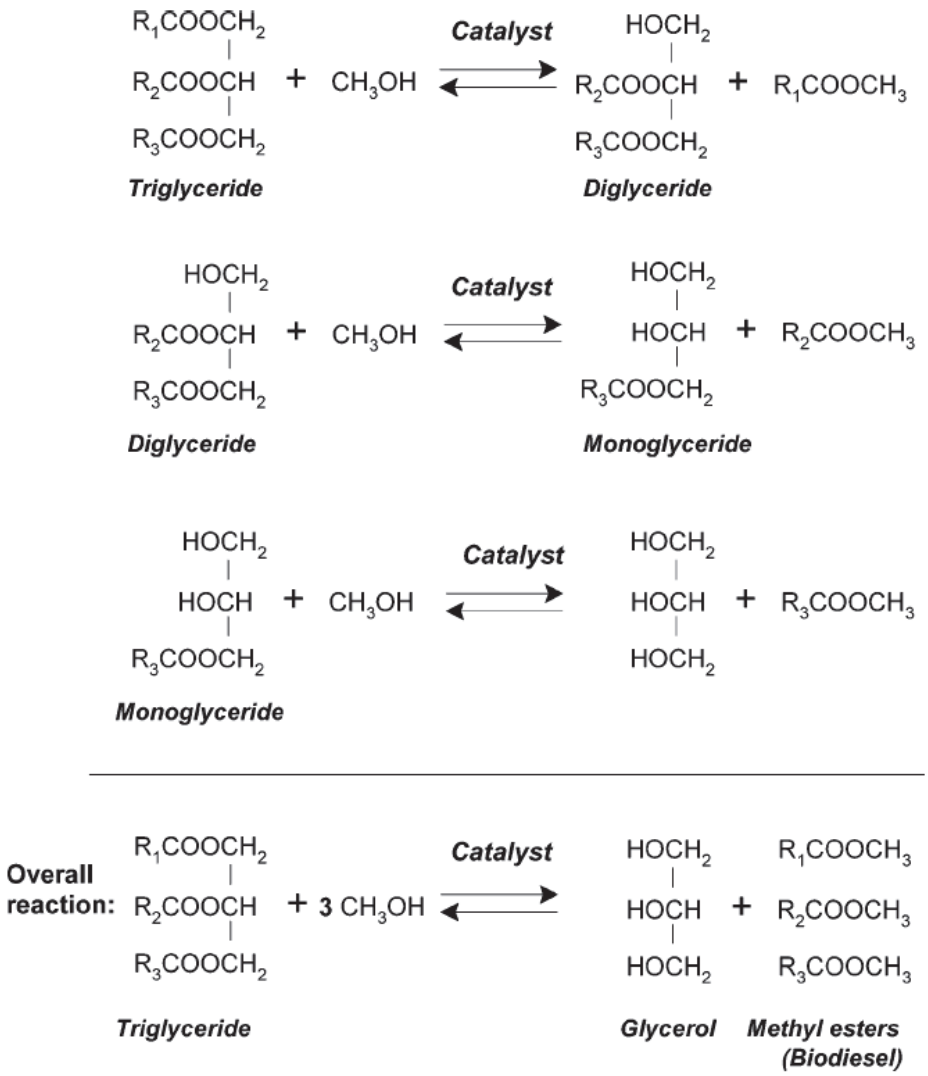

II. APPENDIX B: ^{1}H NMR enlargement in the aromatic region of digested 2, 3, 4 and 5 derivates

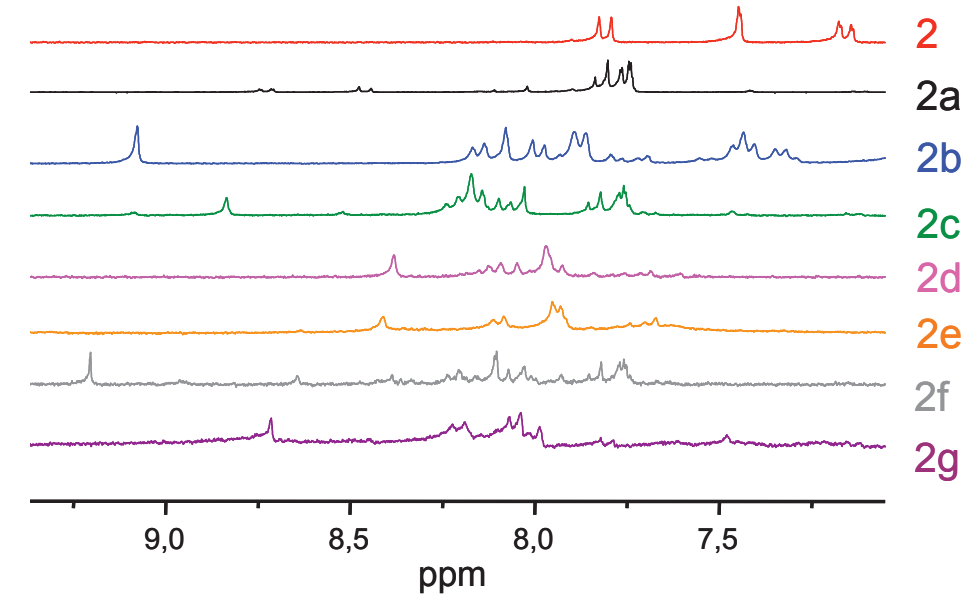

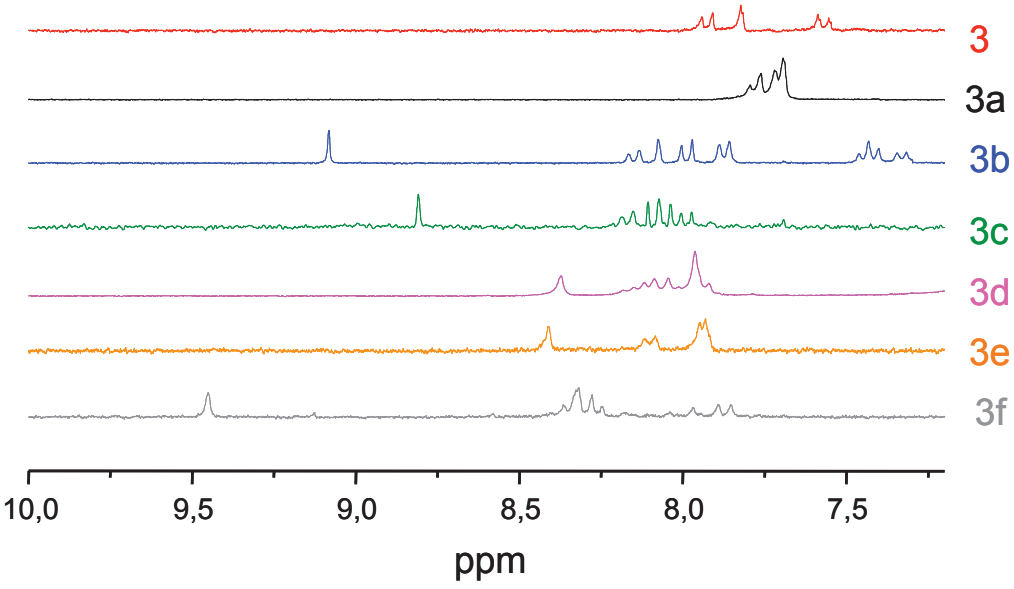

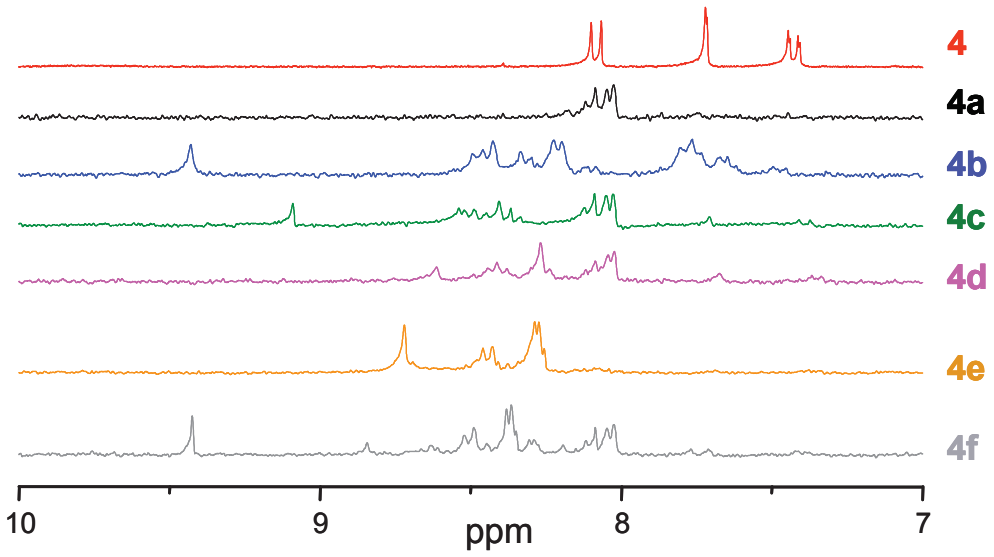
4
4a
4b
4c
4d
4e
4f
10
9
ppm
8
7

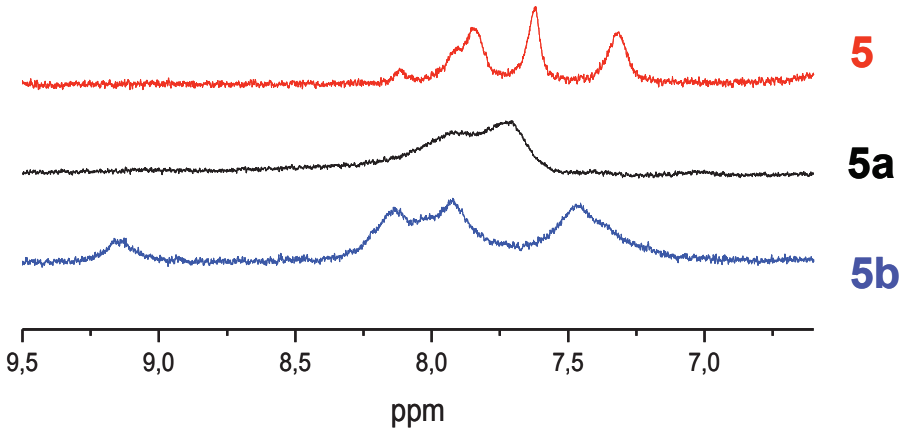
5
5a
5b
9,5
9,0
8,5
8,0
7,5
7,0
ppm

III. APPENDIX C: FTIR spectra of 2, 3, 4 and 5 derivates

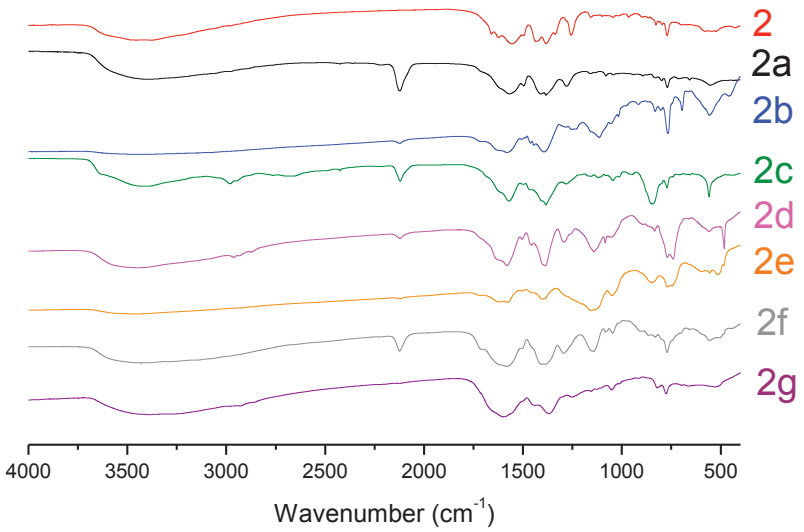

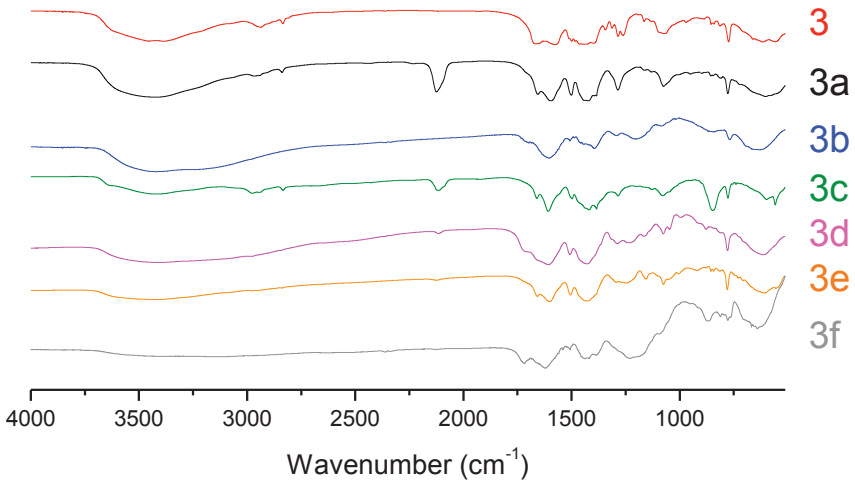

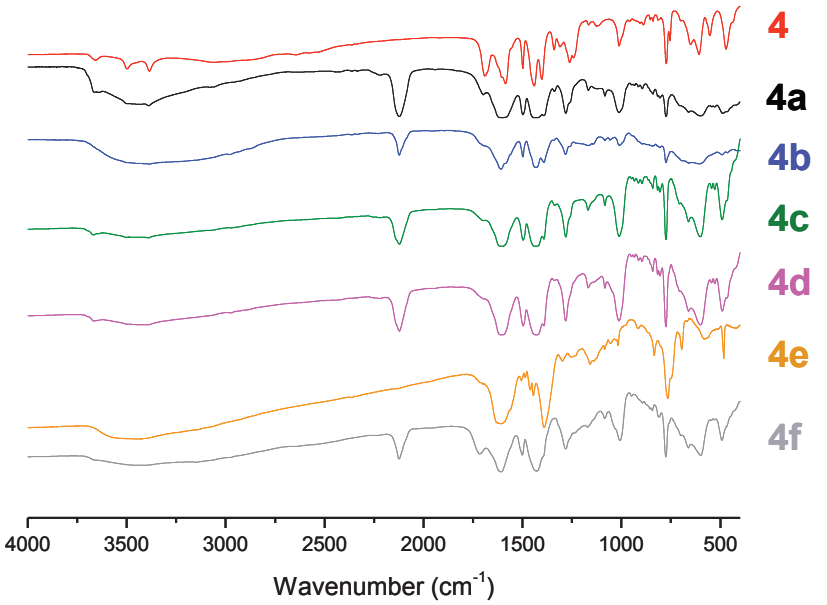
4
4a
4b
4c
4d
4e
4f
4000
3500
3000
2500
2000
1500
1000
500
Wavenumber (cm-1)

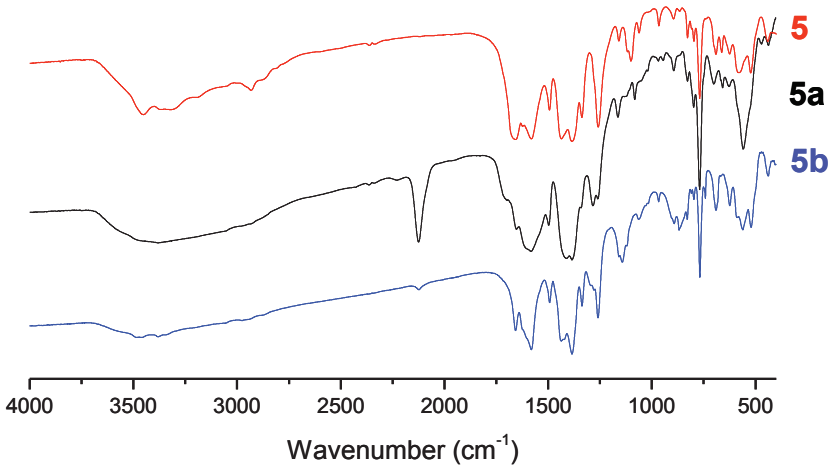
5
5a
5b
4000
3500
3000
2500
2000
1500
1000
500
Wavenumber (cm-1)

IV. APPENDIX D: PXRD patterns of 2, 3, 4 and 5 derivates

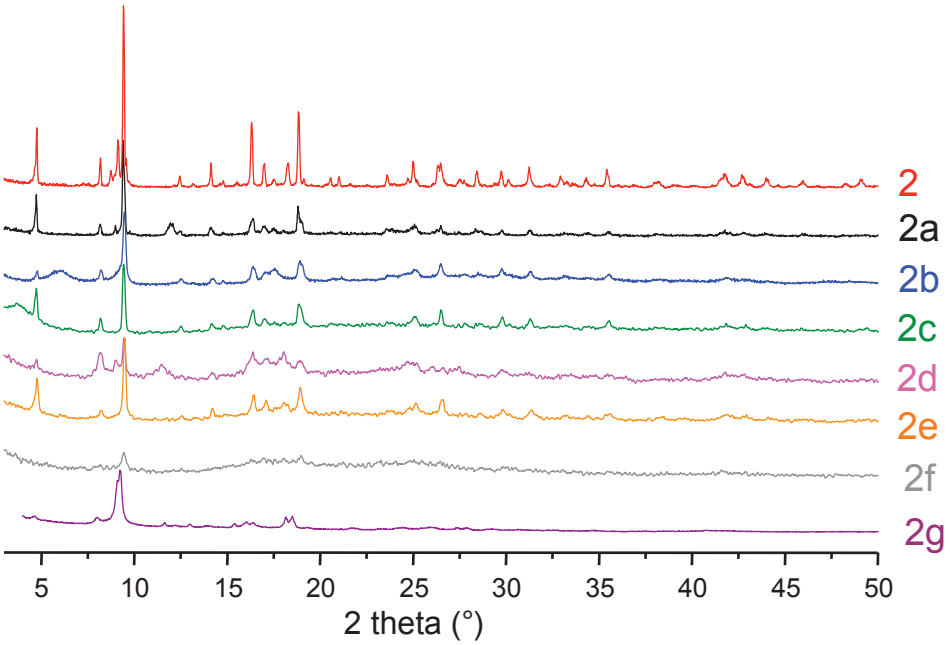

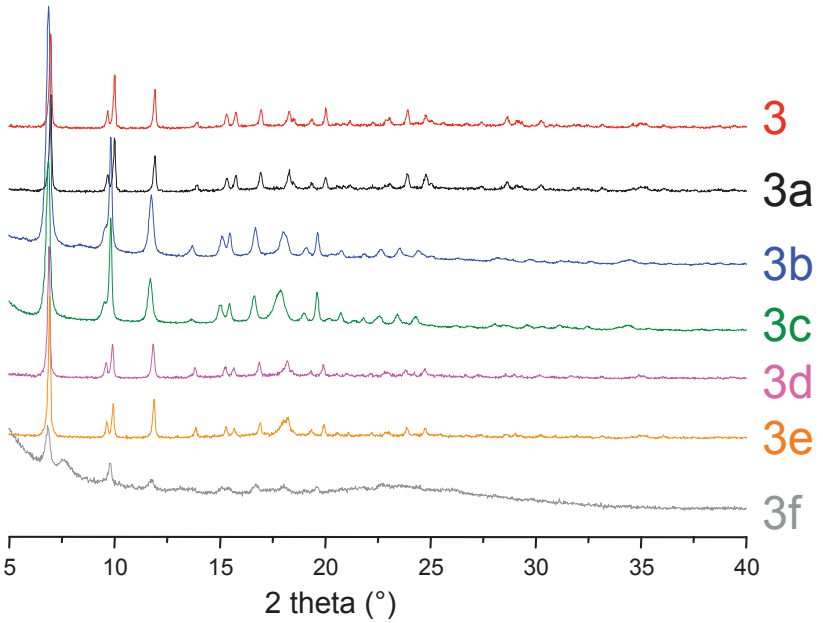

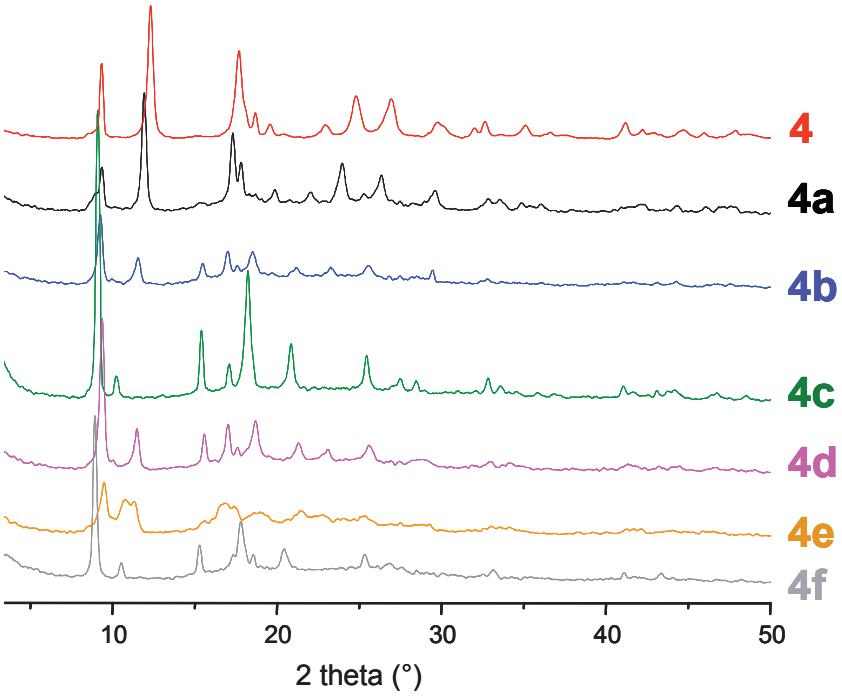
4
4a
4b
4c
4d
4e
4f
10
20
30
40
50
2 theta (°)

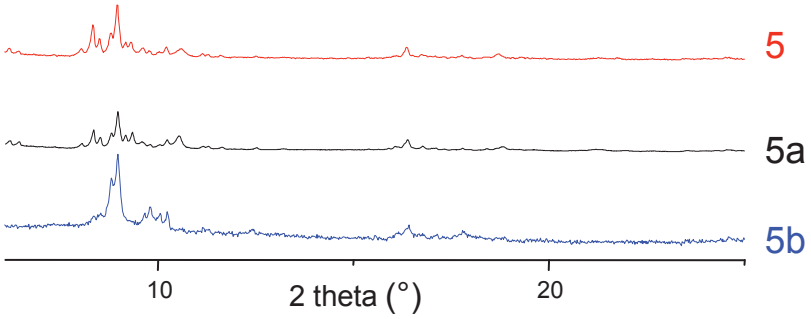
5
5a
5b
10
2 theta (°)
20

Publications

1.

Solvent free base catalysis and transesterifiation over basic functionalised Metal-Organic Frameworks, M. Savonnet, S. Aguado, U. Ravon, D. Bazer-Bachi, V. Lecocq, N. Bats, C. Pinel and D. Farrusseng, *Green Chem.*, **2009**, 11, 1729-1732.
Times Cited: 10

2.

Engineering of coordination polymers for shape selective alkylation of large aromatics and the role of defects, U. Ravon, M. Savonnet, S. Aguado, M. E. Domine, E. Janneau and D. Farrusseng, *Microporous Mesoporous Mater.*, **2010**, 129, 319-329.
Times Cited: 9

3.

Generic Postfunctionalization Route from Amino-Derived Metal-Organic Frameworks, M. Savonnet, D. Bazer-Bachi, N. Bats, J. Perez-Pellitero, E. Jeanneau, V. Lecocq, C. Pinel and D. Farrusseng*, J. Am. Chem. Soc.,* **2010**, 132, 4518-4519.
Times Cited: 14

4.

Evaluation of Energy Heterogeneity in Metal Organic Frameworks: Absence of Henry's Region in MIL-53 and MIL-68 Materials?, M. Pera-Titus, M. Savonnet and D. Farrusseng, *J. Phys. Chem. C,* **2010**, 114, 17665-17674.
Times Cited: 2

5.

Combinatorial Synthesis of Metal-Organic Frameworks libraries by Click-Chemistry,
M. Savonnet, E. Kockrick, A. Camarata, D. Bazer-Bachi, N. Bats, V.Lecocq, C. Pinel and D. Farrusseng, *New J. Chem.*, **2011**, DOI:10.1039/C1NJ20350A

6.

Tailoring MOFs for CO_2 capture: the amino-effect, J. G. Vitillo, M. Savonnet, G. Ricchiardi and S. Bordiga, *ChemsusChem.*, **2011,** *accepted.*

7.

Tailoring Metal-Organic Framework Catalysts by Click Chemistry: Synergistic Effect by Tandem Functionalization, M. Savonnet, A. Camarata, J. Canivet, D. Bazer-Bachi, N. Bats, V. Lecocq, C. Pinel and D. Farrusseng, *Angew. Chem., Int. Ed.,* **2011,** *submitted.*

Solvent free base catalysis and transesterification over basic functionalised Metal-Organic Frameworks†

Marie Savonnet,[a,b] Sonia Aguado,[a] Ugo Ravon,[a] Delphine Bazer-Bachi,[b] Vincent Lecocq,[b] Nicolas Bats,[b] Catherine Pinel[a] and David Farrusseng*[a]

Received 7th June 2009, Accepted 31st July 2009
First published as an Advance Article on the web 18th August 2009
DOI: 10.1039/b915291c

Metal-Organic Frameworks (post-)functionalised with nitrogen containing moieties undergo solvent free aza-Michael condensation and transesterification, surpassing molecular and functionalised MCM-type analogues.

Despite intensive efforts to develop new efficient, selective and recyclable solid base catalysts such as Layered Double Hydroxides (LDH),[1–3] hydrotalcite, KF and amino supported compounds, the development of green processes involving base catalysts remains a challenge.[4]

Thanks to their versatility, Metal-Organic Frameworks (MOF), which are at the frontier between zeolites and surface organometallic compounds, open new perspectives in heterogeneous catalysis.[4–6] In the context of base catalysis and the valorisation of large molecules, they possess two main assets: (i) a porous network which is usually large enough to accommodate molecules such as Fatty Acid Methyl Esters (FAMEs), and (ii) a degree of basicity and a hydrophilicity/hydrophobicity balance which can be tuned by (post)-functionalisation to adjust reactivities and adsorption properties, respectively. Direct functionalisation consists in selecting an already functional linker which is directly used in the synthesis through self-assembly, whereas post-functionalisation modifies the organic part of the solid by a chemical reaction which takes place within the porous framework. Amino-derived MOFs have been shown to be excellent platforms for the grafting of various synthons such as isocyanates and anhydride acids.[7,8,9,10]

The objective of this work is to explore functionalised MOF materials in an aim to perform transesterification of FAMEs and base catalysis in line with the principles of green catalysis.

Zinc carboxylate (IsoReticular Metal-Organic Framework IRMOF-3, **1a**) and triazolate ($ZnF(Am_2TAZ)$ (Am = amino, TAZ = triazolate), **2a**) were synthesised from aminoterephthalic acid using procedures described in ref. 11 and 12 and then tested in catalytic reactions. They both possess amino groups pointing to the channels which have pore openings of 7.4 and 4.6 Å for **1a** and **2a**, respectively (Fig. 1). Structural (X-ray diffraction, IR) and porous characterisation (N_2 physisorption at 77 K) results match with data reported in the literature (ESI†). Physisorption of CO_2 performed at 303 K, 1 atm reveals a threefold uptake (27.1 and 8.5 ml g^{-1}) for **1a** with respect to **2a**, which also corresponds to a much higher surface area for **1a** (S_{BET} = 623 m^2 g^{-1}).

In addition, both **1a** and **2a** were post-functionalised with pyridine groups in order to increase the hydrophobicity while maintaining a similar level of basicity (pK_a ~ 5 for aniline and pyridine). The grafting on solids **1a** and **2a** was performed by acylation with nicotinoyl chloride, yielding **1b** and **2b**, respectively (Fig. 1).

In a typical postsynthetic modification procedure, a suspension of **1a** (or **2a**) in DMF is treated with nicotinoyl chloride for 5 days at 100 °C, then filtered and washed three times with DMF to provide **1b** (or **2b**). Infrared analyses of **1a** and **1b** reveal a significant decrease in the two signals centred at 3500 and 3390 cm^{-1} corresponding to the stretching vibrational modes of $-NH_2$ species. The integration of these bands allows an estimation of ~50% functionalisation for IRMOF-3. The peak at 3070 cm^{-1},

[a]*Université Lyon 1, CNRS, UMR 5256, IRCELYON, Institut de recherches sur la catalyse et l'environnement de Lyon, 2 avenue Albert Einstein, F-69626, Villeurbanne, France.*
E-mail: david.farrusseng@ircelyon.univ-lyon1.fr
[b]*IFP-Lyon, BP 3, 69360, Solaize, France*

† Electronic supplementary information (ESI) available: Supplementary figures. See DOI: 10.1039/b915291c

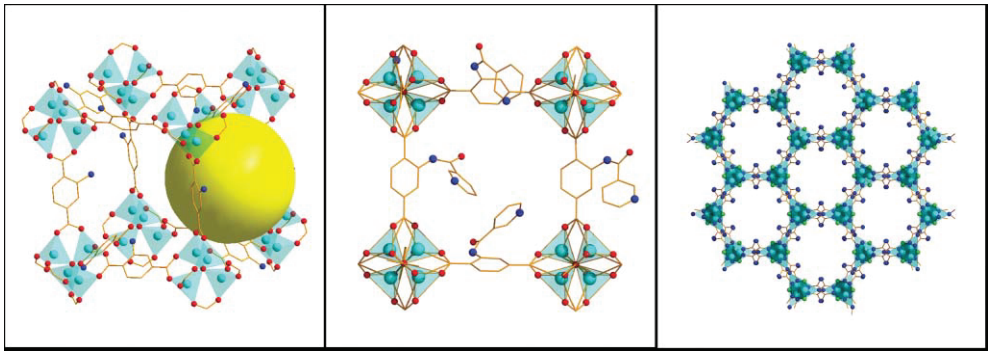

Fig. 1 Diagram of IRMOF-3 (left), functionalised IRMOF-3 (middle) and $ZnF(Am_2TAZ)$ (right) frameworks. The yellow balls indicate the size of the pore openings.

assigned to νArC-H, reveals the presence of the nicotinoyl group, while the absence of a signal at 3600 cm^{-1} indicates that there are no Zn-OH bonds.[6] Further proofs of grafting are revealed by ^{1}H NMR and mass spectrometry (MS) analysis of digested **1b** in DCl/D_2O/DMSO-d_6. The negative mode MS clearly shows a base peak at m/z 285.1 ($M\text{-}H^-$) corresponding to the grafted linker. In addition, aromatic shifts of the grafted compounds were assigned by COSY experiments (^{1}H–^{1}H) (δ = 7.71, 7.82, 8.20, 8.36, 8.88, 9.20 and 12.16 ppm) (Fig. 2). The ^{1}H integration indicates a grafting rate of ~60%, which is close to that obtained *via* infrared measurements. Although the washing routine with DMF removes unreacted nicotinoyl chloride, 0.3 molecules per unit cage still remain in the porous network (Fig. 2). The decrease of the microporous surface from 650 $m^2\ g^{-1}$ for **1a** to 180 $m^2\ g^{-1}$ for **1b** confirms a reduction in free available space provoked by the introduction of basic groups and the presence of residual acid in the pore, which might be the cause of the loss of crystallinity.

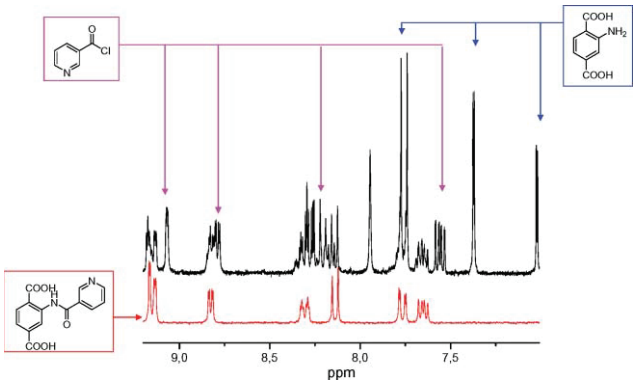

Fig. 2 ^{1}H-NMR of digested **1b** (top) and functionalised linker as reference (bottom).

In contrast, the crystallinity of the functionalised zinc triazolate (**2b**) is fully preserved. Unfortunately, the NMR quantification of the grafting rate cannot be performed on **2b** due to the absence of ^{1}H on the linker. A grafting rate of approximatively 60% was measured by elementary analysis based on the N and C contents. In addition, mass spectrometry analysis performed after digestion shows a signal at $m/z = 309$ corresponding to the doubly functionalised linker.

Catalytic materials were evaluated using aza-Michael reaction and simple transesterification as model reactions. Knoevenagel condensations are usually chosen as model reactions for evaluating base catalysts. However, the condensation liberates water which in our case could modify the structure of IRMOF-3.[13–15] In contrast, aza-Michael condensations do not liberate water and is appropriate to probe weak demanding base reactions. In addition, the aza-Michael reaction has found practical applications. The conjugate addition of amines to α,β-unsaturated compounds to form β-amino carbonyl compounds constitutes a key reaction in the synthesis of various complex natural products, antibiotics, β-amino alcohols and chiral auxillaries[16] (Fig. 3).

In an aim of probing the catalytic centres and getting rid of possible mass transfer limitations, ethyldecanoate was used as model compound for transesterification instead of bulkier triglycerides.

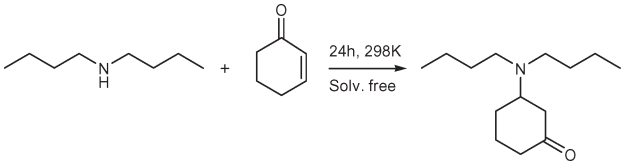

Fig. 3 Diagram of one example of the aza-Michael reaction. Reaction of dibutylamine with cyclohexen-1-one.

For comparison purposes, alkylamino-functionalised mesoporous ordered silica MCM-41 (Mobil Composition of Matter No.41)[17,18] (**3a**) and corresponding post-functionalised compounds[19] with 1.5% mol based on amino groups (**3b**) were prepared following the same procedure and then tested. Moreover, test reactions were carried out in homogeneous conditions with molecular analogues, namely aniline and pyridine which are the corresponding active centres for **1a**, **2a**, **3a** and **1b**, **2b**, **3b**, respectively.

Cyclic and acyclic aliphatic amines underwent 1,4-addition with different α,β-unsaturated compounds to afford the corresponding aza-Michael product without formation of byproduct (Table 1). The molecular catalysts *i.e.* aniline and pyridine show similar yields which is consistent with their very close pK_a, 4.6, and 5.2, respectively. Clearly, the functionalised MOF materials exhibit superior yields with regards to their molecular analogues and also with regards to MCM functionalised materials. Finally, highest yields are always found for post-functionalised materials **1b**, **2b** and **3b**, with respect to their parent forms **1a**, **2a** and **3a**. These self-consistent results point out the superiority of MOF catalysts over molecular and inorganic analogues. It has to be pointed out that the difference in yields according to the substrates results from the electrophilic character of the acceptor and the relative nucleophilicity of the donor. Highest yields are achieved for the most activated acceptor and/or the most nucleophilic donor.

For ethyldecanoate transesterification with MeOH (1:28), all MOF compounds reach 95% conversion after 24 h stirring at

Table 1 Catalytic results of aza-Michael reactions at room temperature based on 1.5 mol% on basic (aniline or pyridine type) groups and with a stoichiometry donor:acceptor of 1.0:1.1. The bold numbers indicate the highest yield obtained for each reaction.

	Yield (%)							
Substrates	Aniline	Pyridine	**1a**	**1b**	**2a**	**2b**	**3a**	**3b**
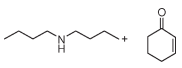	17	19	44	**47**	23	28	21	34
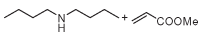	66	70	76	77	59	**79**	63	65
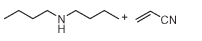	59	57	66	72	42	**85**	72	80
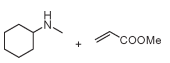	82	83	90	**94**	88	90	84	86
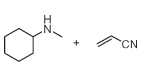	79	81	76	**94**	75	87	76	85
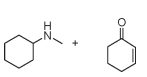	19	22	24	29	20	**33**	18	24

180 °C (1.5 mol% catalyst), which corresponds to equilibrium. Catalytic runs were carried out at lower temperature (130 °C) in order to discriminate activities between the various MOFs (Fig. 4). Here again, **1a** and **1b** show the highest catalytic activities, with a significant enhancement of the yield after post-functionalisation with pyridine (TOF of 3 h^{-1}). On the other hand, for the MCM catalyst, a decrease in activity was observed after functionalisation (Fig. 4, **3b**). No further reaction takes place after removing the catalysts from reaction mixture, indicating the absence of leaching. After filtration, the MOF catalysts can be re-used twice without any loss of activity.

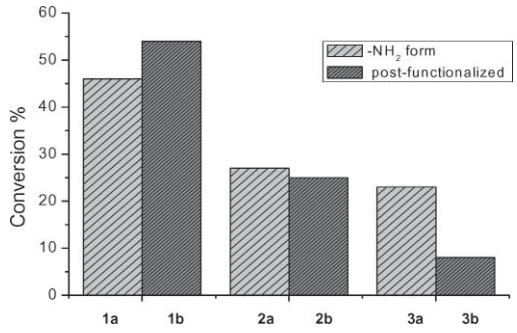

Fig. 4 Catalytic results of the transesterification of ethyldecanoate with MeOH (1:28) at 130 °C for 24 h.

The aza-Michael reaction does not require strong basic sites since it can proceed on pyridine polymers.[20] In contrast, stronger immobilized nitrogen bases such as guanidines are required for low temperature transesterification (*e.g.* 80 °C). However, weaker sites such as described herein are sufficient to perform the reaction in current process conditions (T = 190 °C, P ~ 30 bars).

We anticipate that the superiority of functionalised MOFs (**1b** and **2b**) against MCM analogue catalysts arises from the activation of the substrates *via* strong adsorption in the organic micropore framework whereas such confinement is not found in inorganic mesoporous MCM materials.

We report herein, for the first time, the application of functionalised Metal-Organic Frameworks to base catalysis. We believe that the development of post-functionalisation routes will make it possible to achieve tailor made materials that will create new breakthroughs in selective catalysis.

Experimental

Synthesis

All chemicals were used as received: *N*,*N*′-dimethylformamide, DMF (Aldrich, 99.8%), $Zn(NO_3)_2{\cdot}4H_2O$ (Merck, 98.5%), 2-aminoterephtalic acid (Alfa Aesar, 99%), nicotinoyl chloride hydrochloride (Aldrich, 97%), dichloromethane (Acros Organics, 99.99%), triethylamine (Riedel-de Haën, 99%), 4-(dimethylamino)pyridine DMAP (Aldrich, 99%), $ZnF_2{\cdot}4H_2O$ (Alfa Aesar, 98%), 3,5-diamino-1,2,4-triazole (Alfa Aesar, 98+%).

IRMOF-3 was prepared according to the procedure reported by Huang *et al.*:[11] 4.4 mL (31.6 mmol) of triethylamine was directly added to a DMF solution (80 mL) containing 2.4 g (8 mmol) of $Zn(NO_3)_2{\cdot}4H_2O$ and 0.66 g (4 mmol) of 2-aminoterephthalic acid under stirring at room temperature for 90 min. The powder was collected by repeated centrifugation and thorough DMF washing for three times. Then, they were dried at 130 °C under static air.[11]

$ZnF(Am_2TAZ)$ was prepared by placing a mixture of 0.2 g (2 mmol) of 3,5-diamino-1,2,4-triazole, 0.35 g (2 mmol) of $ZnF_2{\cdot}4H_2O$ and 10 mL of water into a 40 mL Teflon® lined autoclave. The resulting mixture was stirred for 5 min prior to sealing the autoclave. The autoclave was then placed in an oven and heated to 160 °C for 3.5 days.[12]

(Post-)functionalisation

All experiments were carried out under an inert atmosphere.

A sample of IRMOF-3 (0.85 g) activated at 250 °C for 12 h was suspended in dry, freshly distilled DMF and treated with one equivalent of nicotinoyl chloride (0.35 g) in the presence of an excess of distilled pyridine (5 mL) and DMAP (0.1 g) at 100 °C for five days. The resulting powder was collected by filtration, then thoroughly washed three times with DMF and dried under vacuum at 170 °C for 12 h. The same procedure was performed for the post-functionalisation of $ZnF(Am_2TAZ)$ and MCM-41-NH_2.

Catalytic reactions

Ethyldecanoate (Fluka, 99%), dibutylamine (Fluka, 99%), *N*-methylcyclohexylamine (Aldrich, 99%), methyl acrylate (aldrich, 99%), acrylonitrile (Aldrich, 99%), cyclohexen-1-one (Fluka, 98%), methanol (Aldrich, 99%), toluene (Chimie-Plus, 99%) and decane (Alfa Aesar, 99%) were used as received.

Aza-Michael reaction. The reaction of the donor group (5 mmol) with the acceptor group (5.5 mmol) in the presence of 1.5 mol% of catalyst based on the amino group was carried out at room temperature for 24 h.[3] After the reaction was completed and the catalyst filtered off, a sample of the filtrate was diluted in *n*-decane with 5% toluene as internal standard and analysed by gas chromatography (HP 6890 N equipped with a 30 m HP5 column).

Transesterification. Ethyldecanoate (2.5 mL) and methanol (10 mL) along with 1.5 mol% catalyst based on basic (amino or aniline) groups were made to react in a Teflon® lined stainless steel digestion bomb (TopIndustrie) for 24 h at 180 °C or 130 °C. After the reaction, the catalyst was recovered by filtration and a sample of the filtrate was diluted in CH_2Cl_2 and analysed by GC.

Acknowledgements

We thank Dr. A. Galarneau and M. F. Driole of the Institut Charles Gerhardt of Montpellier (France) for having provided us MCM-41 materials. We also thank A. Camarata and Dr. J. Pawlesa for the technical work, along with IRCELYON Scientific Services.

References

1 M. L. Kantam, A. Ravindra, C. V. Reddy, B. Sreedhar and B. M. Choudary, *Adv. Synth. Catal.*, 2006, **348**, 569–578.
2 V. P. Raje, R. P. Bhat and S. D. Samant, *Synlett*, 2006, **16**, 2676–2678.

3 M. L. Kantam, B. Neelima and C. V. Reddy, *J. Mol. Catal. A: Chem.*, 2005, **241**, 147–150.
4 D. Farrusseng and C. Mirodatos, in *Design of Heterogeneous Catalysts*, U. S. Ozkan, (Ed.), Wiley-VCH, 2009.
5 G. Ferey, *Chem. Soc. Rev.*, 2008, **37**, 191–214.
6 U. Ravon, M. E. Domine, C. Gaudillere, A. Desmartin-Chomel and D. Farrusseng, *New J. Chem.*, 2008, **32**, 937–940.
7 Z. Q. Wang and S. M. Cohen, *Angew. Chem., Int. Ed.*, 2008, **47**, 4699–4702.
8 P. Gamez, J. S. Costa, C. A. Black, O. Roubeau, S. J. Teat and J. Reedijk, *Eur. J. Inorg,. Chem.*, 2008, 1551–1554.
9 S. Cohen, E. M. Dugan, Z. Q. Wang, M. Okamura and A. Medina, *Chem. Commun.*, 2008, 3366–3368.
10 M. J. Rosseinsky, M. J. Ingleson, J. P. Barrio, J. B. Guilbaud and Y. Z. Khimyak, *Chem. Commun.*, 2008, 2680–2682.
11 L. M. Huang, H. T. Wang, J. X. Chen, Z. B. Wang, J. Y. Sun, D. Y. Zhao and Y. S. Yan, *Microporous Mesoporous Mater.*, 2003, **58**, 105–114.
12 A. M. Goforth, C.-Y. Su, R. Hipp, R. B. Macquart, M. D. Smith and H.-C. zur Loye, *J. Solid State Chem.*, 2005, **178**, 2518.
13 S. S. Kaye, A. Dailly, O. M. Yaghi and J. R. Long, *J. Solid State Chem.*, 2007, **129**, 14176.
14 S. Hausdorf, F. Baitalow, J. Seidel and F. Mertens, *J. Phys. Chem. A*, 2007, **111**, 4259–4266.
15 S. Hausdorf, J. Wagler, R. Mossig and F. Mertens, *J. Phys. Chem. A*, 2008, **112**, 7567–7576.
16 M. E. Jung, B. M. Trost and I. Fleming, *Comp. Org. Synth.*, 1991, **4**, 30.
17 D. Brunel, A. Cauvel, F. Fajula and F. Di Renzo, *Stud. Surf. Sci. Catal.*, 1995, **97**, 173–180.
18 A. Galarneau, D. Desplantier-Giscard, F. Di Renzo and F. Fajula, *Catal. Today*, 2001, **68**, 191–200.
19 D. Brunel, A. C. Blanc, A. Galarneau and F. Fajula, *Catal. Today*, 2002, **73**, 139–152.
20 S. D. Samant, V. P. Raje and R. P. Bhat, *Synlett*, 2006, **16**, 2676–2678.

Microporous and Mesoporous Materials 129 (2010) 319–329

Contents lists available at ScienceDirect

Microporous and Mesoporous Materials

journal homepage: www.elsevier.com/locate/micromeso

Engineering of coordination polymers for shape selective alkylation of large aromatics and the role of defects

Ugo Ravon [a], Marie Savonnet [a], Sonia Aguado [a], Marcelo E. Domine [a], Erwann Janneau [b], David Farrusseng [a,*]

[a] Université Lyon 1, CNRS, UMR 5256, IRCELYON, Institut de recherches sur la catalyse et l'environnement de Lyon, 2 Avenue Albert Einstein, F-69626 Villeurbanne, France
[b] Université Lyon 1, Laboratoire Multimatériaux et Interfaces, F-69622 Villeurbanne, France

ARTICLE INFO

Article history:
Received 13 April 2009
Accepted 3 June 2009
Available online 13 June 2009

Keywords:
Metal-organic frameworks
MOF-5
IRMOF
MIL-53
MOF-69
Shape selective catalysis

ABSTRACT

For economic and environmental reasons, there is a strong incentive to replace of homogeneous by green and efficient heterogeneous processes in catalysis. The Friedel-Crafts alkylation of aromatics is a marking example. Numbers of homogeneous catalysts (such as HF, H_2SO_3, and $AlCl_3$) have been replaced by H-form zeolites. However, large pore zeolite can not accommodate bulk aromatic molecules and/or alkylating agents avoiding the reaction to take place within the porous network. Due to their larger pore size, metal-organic frameworks (MOFs) open the doors to the alkylation of very large poly-aromatic compounds. We report different approaches for the design of acid shape selective MOFs. The first refers to a "zeolite mimetic" approach. It deals with the design of porous Zn or Al based MOF exhibiting bridging –OH species (MOF-69, MIL-53 Al) like those found in zeolites [Si–O(H)–Al]. The second approach aims at synthesizing MOF materials having structural defects to generate active catalytic centers. Two different synthetic strategies were investigated, either by fast precipitation or by the partial substitution of dicarboxylic by mono-carboxylic acid linkers. Acid centers have been characterized by solid ^{1}H NMR and Diffuse Reflectance IR. The mono-alkylation of biphenyl with *tert*-BuCl is achieved with 100% of para-selectivity, well superior to H-MOR and H-BEA reference zeolites.

1. Introduction

MOF materials can be regarded as a "new" class of catalytic materials at the frontier between active 3D inorganic frameworks like zeolites and surface organo-metallic compounds taking into account their porous structure and their accessible metallic nanoclusters, respectively. The possible organization and functionalization of active sites on the nanoscale provides the basis to develop materials specifically adapted to catalytic challenges like complex chemo-, regio- or stereo-selectivity. Although the later properties are still rarely reported for MOFs, the rapidly increasing studies on these materials with different design clearly demonstrate the versatility of metal-organic frameworks for catalysis [1,2]. MOF materials exhibiting paddle–wheel type nodes [3] have shown Lewis type catalytic activities such as cyanosilylation [4], terpene isomerization [5], alkene hydrogenation [6,7] and alcohol aerobic oxidation [8,9]. In addition, the organic moiety can be functionalized by reactive centers such as chiral basic groups [10] or metallo complexes [11].

For economic and environmental reasons, there is a strong incentive to replace of homogeneous by green and efficient heterogeneous processes in Catalysis. The alkylation of aromatics also known as Friedel-Crafts reaction is a marking example. Olefins, different types of alcohols, and also alkyl- and aryl-chlorides are applied as alkylating agents on a wide range of large scale processes in industry [12]. Numbers of strong mineral acids (such as HF, H_2SO_3, among others) and also Lewis acids (such as $AlCl_3$, $FeCl_3$, $ZnCl_2$, among others), commonly used as homogeneous catalysts for this reactions, have continuously been replaced by H-form zeolites [13]. Thus, the shape selective β-methylation of naphthalene with methanol over mordenite (0.64×0.70 nm) to produce mainly 2,6-dimethylnaphthalene is one of the major examples in acid catalysis [14]. The high selectivity to the β-mono-methylation and/or β-di-methylation is mainly due to the larger size of the 1- and 3-oriented products which strongly limits their diffusion through the porous systems of medium pore size zeolites. However, large pore zeolite can not accommodate bulky aromatic molecules and/or alkylating agents making the reaction impossible to take place within the porous network. Due to their larger pore size, metal-organic frameworks (MOFs) open the doors to the alkylation of very large poly-aromatic compounds. Recently, Horcajada et al. [15] have reported the catalytic activity of two different MIL-101 (Fe, Cr) for Friedel–Crafts benzylation. We have very recently shown in a short account that microporous zinc carboxylate frameworks show outstanding shape selectivity properties on similar alkylation type reactions [16].

* Corresponding author. Tel.: +33 4 72 44 53 65; fax: +33 4 72 44 53 9.
E-mail address: david.farrusseng@ircelyon.univ-lyon1.fr (D. Farrusseng).

1387-1811/$ - see front matter © 2009 Elsevier Inc. All rights reserved.
doi:10.1016/j.micromeso.2009.06.008

The first objective of this work is to explore different strategies to develop MOF materials exhibiting M–OH Brønsted sites for catalytic alkylation. Two main routes are investigated. The first route deals with the selection of MOF materials for which –OH groups are part of the structure as those found in H-form of zeolites. This solution can therefore be regarded as a design by zeolite mimetic approach (Fig. 1). The two compounds MIL-53(Al) [17] and MOF-69C [18] discovered by Ferey and co-workers, have been selected for testing. Both of them have well structurally identified hydroxyl groups as indicated in their formulae Al(OH)(bdc) and $Zn_3(OH)_2$(bdc), respectively. The compound MIL-53(Al) is built from infinite chains of corner-sharing $AlO_4(\mu_2\text{-}OH)_2$ while MOF-69C consists of chains of $ZnO_2(OH)_2$ tetrahedron and $ZnO_4(OH)_2$ octahedron and with μ_3-OH as bridging species. The second route aims at creating defaults in a MOF network leading to nodes that are coordinated to –OH terminal groups, instead to a linker as they should be in a perfect structure. Here also, two strategies have been investigated (Fig. 2). We have anticipated that a synthesis by very fast precipitation may lead to crystalline compounds for which a fraction of linkers are missing in the network while still maintaining a robust structure. The second strategy consists in synthesizing MOF materials from a mixture of poly-dentate and mono-dentate linkers which shall yield "defects" at the nodes which are adjacent to the mono-dentate linkers. Because, MOF-5 or IRMOF family materials do not contain –OH groups with respect to the pure crystalline structure, we have selected MOF-5 as parent material to create –OH species as structural defects.

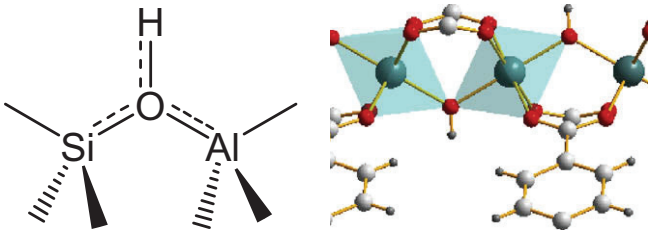

Fig. 1. MOF selection by zeolite mimetic approach. Scheme of Brønsted centers in zeolites showing μ_2 – bridging hydroxyl (left); Inorganic chain of MIL-53 showing μ_2 hydroxyl groups as potential acid centers (right).

A second objective is to address the properties of MOF for catalytic shape selectivity. Many metal-organic frameworks exhibit pore size and pore windows which exceed large pore zeolites such as beta (BEA) and mordenite (MOR). It is reasonable to envision that analogous shape selectivity effects can be also observed for MOF materials provided that the dimension of the micropores match well enough to discriminate between molecular sizes of different reagents, products or transition states involved in a particular process [19]. In this work, we have studied the alkylation of toluene and *tert*-butylbenzene, as well as larger aromatics such as naphthalene and biphenylene in order to better highlight pore-shape selectivity (Fig. 3). For the same reason, we reasoned that the *tert*-butyl group being much bulkier than the isopropyl usually studied, may be more suitable to observe larger degrees of shape selectivity. In this frame, the selection of IRMOF [20] and MOF-69 [21] materials were good candidates to investigate since their pore size can be tuned by selecting dicarboxylate ligands of different length.

2. Experimental

2.1. Synthesis

2.1.1. Solvothermal synthesis (MOF-5 solvo)

The synthesis of MOF-5 solvo was performed as reported by Sabo et al. [22]. Typically, 8.32 g (31.824 mmol) of $Zn(NO_3)_2{\cdot}4H_2O$ and 1.76 g (10.594 mmol) of 1,4-benzenedicarboxylic acid (H_2dbc) (Aldrich 99.7%), were dissolved in 100 ml of dried diethylformamide (DEF). The solution was heated at 100 °C in a Teflon-lined stainless-steel autoclave, the solid filtered off, washed and finally exchanged with $CHCl_3$ in argon flow. Finally, the material was evacuated and handled in a glove box for transferring in Schlenk type vessel.

2.1.2. Slow precipitation synthesis (MOF-5 basf)

The preparation of MOF-5 basf followed the procedure reported by Mueller et al. [23]. Typically, 3.22 g (10.8 mmol) of $Zn(NO_3)_2{\cdot}6H_2O$ (Riedel–Dehaën, pure) and 0.66 g (3.97 mmol) of H_2dbc were dissolved in 100 ml of DMF (Aldrich, 99.8% anhydrous and used as received). After 4 h of stirring at 130 °C, the solid was

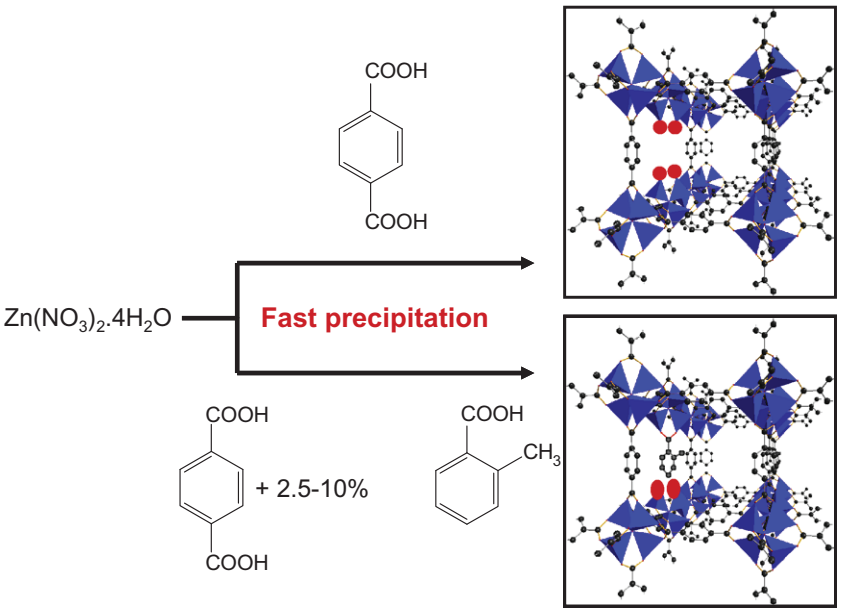

Fig. 2. Scheme of the two synthesis routes to generate structural defects; missing ligand (top), isomorphous substitution by a mono-carboxylic acid (bottom).

filtered off, washed three times with DMF and dried at 130 °C under vacuum during 3 h. It shall be pointed out that chemicals used here have different grade from the chemical used by the original authors. As a matter of fact, we do not claim that this sample, denoted hereafter MOF-5 basf, has the same properties than those reported in the original publication.

2.1.3. Fast precipitation synthesis (MOF-5 pre)

The precipitation method followed the recipe described by Huang et al. [24]. The precursors H_2(dbc) 0.66 g (3.97 mmol) and $Zn(NO_3)_2{\cdot}6H_2O$ 2.4 g (8.1 mmol) were solubilized in 80 ml of DMF (Aldrich, 99.8% anhydrous, used as received). The precipitation took place instantaneously at room temperature upon drop wise addition of 3 ml (31.6 mmol) of pure Et_3N (Riedel–Dehaën, pure). After 90 min of stirring, the white powder was filtered and washed three times with DMF. The samples were heated at 130 °C overnight under dry air flow. This procedure was extended to synthesize the isoreticular compounds IRMOF-3, Zn-MOF-8 and Zn-MOF-10 by using 2-aminoterephthalic acid, naphthalene 2,6-dicarboxylic acid and the biphenyl-4,4′-dicarboxylic acid, respectively [20].

A similar experimental procedure was applied to prepare a series of samples with an isomorphous substitution of di- by mono-carboxylate linkers. The precipitation takes place in a mixture of mono- and dicarboxylic acid, namely 2-methyl-toluic acid and H_2dbc (Fig. 2). Three samples were prepared by varying the di- to mono-carboxylic acid ratio from 2.5, 5 to 10 wt% in order to yield ZnMOF-5 (2.5), ZnMOF-5 (5) and ZnMOF-5 (10), respectively.

2.1.4. Synthesis of MOF-69 samples

The synthesis of MOF-69C, $Zn_3(OH)_2$(1,4-dbc)$_2{\cdot}$(DEF)$_2$, followed the method described by Loiseau et al. [18]. In a Teflon-lined stainless-steel bombs, H_2dbc (0.33 g, 1.99 mmol) and $Zn(NO_3)_2{\cdot}6H_2O$ (1.77 g, 5.96 mmol) were dissolved in 35 ml of DEF (Alfa Aesar, 99%). Deionized H_2O (1.17 ml) was added to the reaction solution, and the mixture was heated at 100 °C during 20 h. The crystals were collected and washed twice with DEF (30 ml) and acetone (30 ml). They were then dried at 100 °C in air. These experimental procedures were extended to the synthesis of MOF-69A, MOF-69B with 4,4′-biphenyl-dicarboxylic acid and 2,6-naphthalene-dicarboxylic acid as linkers, respectively.

2.1.5. Reference materials and catalysts

MIL-53(Al) was purchased from Aldrich (Basolite A100). The acid form of beta (H-BEA, Si/Al = 23) and mordenite (H-MOR, Si/Al = 10) zeolites were obtained from the commercial Na-forms (Fluka) by ammonium exchange following by calcination treatment. The ion exchange was carried out with 10 wt% solution of NH_4COOCH_3 in water at 80 °C during 4–5 h followed by calcination treatment at 550 °C during 3 h. This procedure was repeated twice. Both $AlCl_3$ (Aldrich 99.9%), and $ZnCl_2$ (Alfa Aesar, anhydrous, 98+%) were used as received and as reference Lewis acids. All MOF samples synthesized and used as catalysts in this study are summarized in Table 1.

2.2. Characterization

X-ray diffraction (XRD) patterns were recorded on Brucker D5005. The N_2 adsorption/desorption isotherms were measured on an ASAP 2010M from Micromeritics. Before the measurement, the sample was degassed for 3 h at 130 °C. The specific surface was determined by BET method, the pore volume by *t*-plot analysis, and the pore diameter by DFT. The samples were further characterized by TG/TD analysis with a Setaram – Type Setsys Evolution 12. Inductively Coupled Plasma (ICP) emission spectrometry was used for the analysis of the bulk chemical composition of

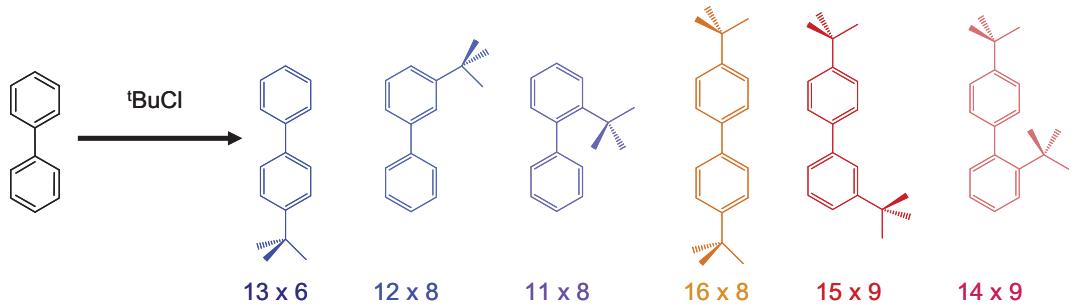

Fig. 3. Major products expected from the *tert*-butylation of biphenyl. Molecular size are indicated for 4-*tert*-butylbiphenylene, 3-*tert*-butyl-biphenylene, 2-*tert*-butyl-biphenylene, 4,4′-di*tert*-butyl-biphenylene, 3,4′-di*tert*-butyl-biphenylene, 2,4′-di*tert*-butyl-biphenylene (from left to right) Data were obtained with the software "CS Chem 3D-Pro Molecular Modeling and Analysis – 2001 CambridgeSoft" from the minimum energy configuration of each structure by performing the molecular dynamics calculations by the MM2 method.

Table 1
Summary of MOF samples synthesized and used as catalysts in this study.

Sample name	Basic structure	Linker	Synthesis method	Reference
MOF-5 solvo	MOF-5	H_2dbc	Solvothermal	[22]
MOF-5 basf	MOF-5	H_2dbc	Basf procedure	[23]
MOF-5 pre	MOF-5	H_2dbc	Fast precipitation	[24]
ZnMOF-5 (2.5)	MOF-5	H_2dbc + 2-methyl toluic acid (2.5%)	Fast precipitation	This study
ZnMOF-5 (5)	MOF-5	H_2dbc + 2-methyl toluic acid (5%)	Fast precipitation	This study
ZnMOF-5 (10)	MOF-5	H_2dbc + 2-methyl toluic acid (10%)	Fast precipitation	This study
MOF-69A	MOF-69	4,4′-Biphenyl-dicarboxylic acid	Solvothermal	This study
MOF-69B	MOF-69	2,6-Naphthalene-dicarboxylic acid	Solvothermal	This study
MOF-69C	MOF-69	H_2dbc	Solvothermal	[18]
IRMOF-3 pre	IRMOF-3	2-Aminoterephtahlic acid	Fast precipitation	This study
Zn-MOF-8	MOF-69	2,6-Naphthalene-dicarboxylic acid	Fast precipitation	This study
Zn-MOF-10	MOF-69	4,4′-Biphenyl-dicarboxylic acid	Fast precipitation	This study

the samples. DRIFT analysis was carried out on a Nicolet Magna 550 equipped with a MCT detector. The samples were loaded in a DRIFT Spectratech cell equipped with ZnSe windows. A thin layer of SiC sieved at 200–400 μm was first loaded to improve thermal exchange. Then SiC was cover up with the samples. Water desorption was followed by heating the cell to 220 °C under 50 ml min^{-1} of He. The cell was then cold down to room temperature and scans were performed in He flow. Solid state ^{1}H NMR analysis was carried out with a DX-400 Brucker in static conditions to allow quantification. Liquid ^{1}H NMR (Brucker Avance 250) was used to quantify the substitution of di- to mono-carboxylate for the samples ZnMOF-5 (2.5), (5) and (10). After the synthesis, the samples were digested in DCl/D_2O/DMSO-d_6 mixture, thus liberating the linkers in solution on the acid forms. The toluic acid was selected as mono-carboxylic acid because the methyl groups enable to distinguish chemical shifts between the two linkers. The integration of the characteristic signals of the two linkers allows the quantification of the respective amount of mono- and di-carboxylate linkers for the three samples.

2.3. Catalytic aromatic alkylation

Toluene (Ahimie-plus, 99%), biphenylene (Alfa Aesar, 99%), *tert*-butylbenzene (Alfa Aesar, 99%), naphthalene (Alfa Aesar, 99.6%), *n*-decane (Alfa Aesar, 99%), *tert*-butylchloride (*t*-BuCl) (Alfa Aesar 98+%) were used as received. The alkylation reactions were carried out in *n*-decane with an aromatic:*t*-BuCl molar ratio of 2:1. The catalytic sample (30 mg) was activated at 130 °C under 10^{-5} bar, unless specific conditions were given. As en example, a mixture of 1.7 g (18.8 mmol) of toluene, 0.851 g (9.2 mmol) of *t*-BuCl and 5.18 g of *n*-decane was placed in a 48 ml Teflon-lined autoclave (Top Industries) and heated to reaction temperature (100 °C or 170 °C) under stirring with autogeneous pressure. After 2 h of reaction, the solid was recovered by filtration at room temperature. The reaction mixtures were analyzed by gas chromatography with a HP 6890 N equipped with a HP-5 capillary column (30 m length). The toluene conversion was calculated by taking into account the initial concentration (100% excess). Identification of the different isomer configurations was performed by GC–MS (HP 6890 equipped with HP-5/HP-1 capillary columns, a HP 5973 quadrupolar detector – ionic impact at 70ev, and NIST02 library). In order to check that the reaction takes place in heterogeneous conditions leaching issues were investigated. Fresh reactants were added to the liquids recovered from reaction mixture and a new reaction run was performed.

3. Results

3.1. Structural characterization

The MOF-69C, $Zn_3(OH)_2(bdc)_2{\cdot}2DEF$, belongs to the rod-like type of metal open framework [25]. It consists of chains of $ZnO_2(OH)_2$ tetrahedrons and $ZnO_4(OH)_2$ octahedrons and μ_3-OH as bridging species (Fig. 4). MOF-69C exhibit 1D diamond-shaped channel with pores of diameter close to 0.85 nm. The XRD patterns reveal a mixture of mainly $Zn_3(OH)_2(bdc)_2{\cdot}2DEF$ (MOF-69C) and $Zn_3(OH)_2(bdc)_2{\cdot}DEF$ (Fig. 5). The latter is obtained after removing on molecule of DEF by heating at 170 °C in air. The powder-pattern can be indexed in a monoclinic unit-cell, space-group $P2_1/n$ [a = 17.590(2), b = 19.659(2), c = 11.992(1), β = 97.9(1)] with a volume of 4107.4(7) Å^3, similar to that of the parent compound. MOF-69A and MOF-69B, which are made from di-carboxybiphenylate and di-carboxynaphthalate linkers, respectively, are isostructural to MOF-69C [21,26]. Within these units, there are tetrahedral and octahedral Zn(II) centers bound to 4 and 2 carboxylate groups, respectively. For MOF-69A, the channel dimensions are of 12.2 Å along an edge and 16.6 Å along the diagonal.

The powder X-ray diffraction patterns of the samples MOF-5 solvo (see Ref. [22]), MOF-5 basf, and IRMOF-3 match very well with the IRMOF cubic structure (Fig. 6). For the samples prepared by precipitation, namely MOF-5 pre, ZnMOF-5 series with 2.5%,

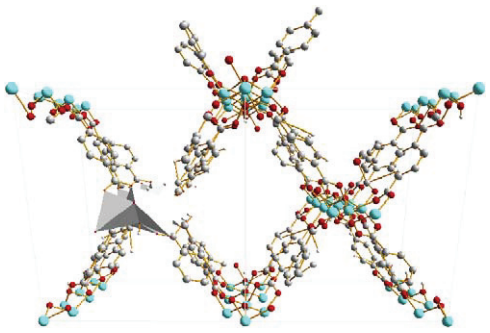

Fig. 4. MOF-69C rod-like porous structure (molecules of DEF omitted for clarity).

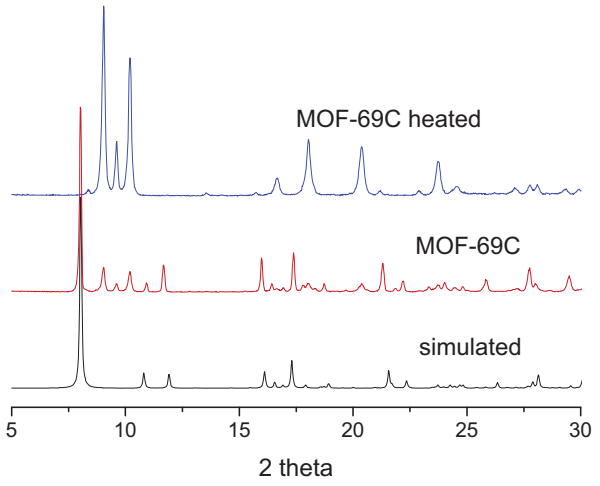

Fig. 5. Powder X-ray diffraction patterns of simulated MOF-69C (bottom), $Zn_3(OH)_2(bdc)_2{\cdot}2DEF$ (MOF-69C) (center), and of $Zn_3(OH)_2(bdc)_2{\cdot}DEF$ (top).

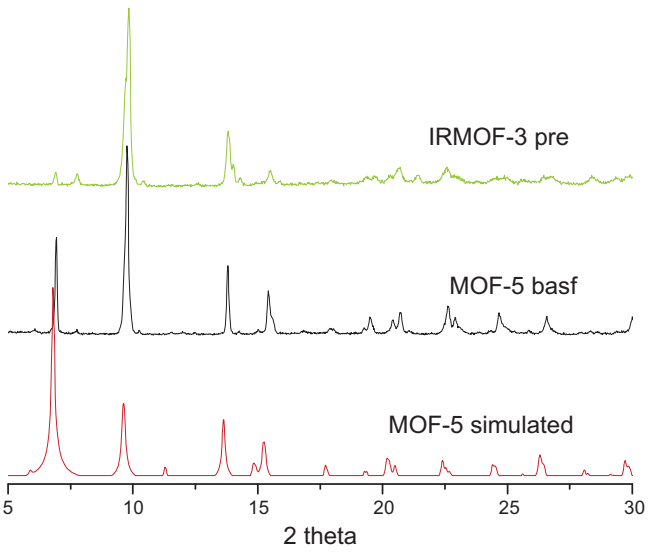

Fig. 6. Powder X-ray diffraction patterns of MOF-5 basf (center) and IRMOF-3 pre (top) samples compared with the simulated pattern (bottom).

5% and 10% of mono-carboxylic acid, XRD patterns do match with the cubic structure however with a much lower level of crystallinity. We also observe a net splitting of the peak at 9.6 (220) for MOF-5 pre which may indicate a distorted structure of lower symmetry according to Hafizovic et al. [27]. This split is sample depending and most of the time we can observe a non symmetrical peak instead such in the case of MOF-5 basf, ZnMOF-5 (2.5%, 5% and 10%). For the later series (Fig. 7), we can observe one additional signal at 8.9° which is relatively intense which upon heating at 130 °C gains of intensity. This phase can be attributed to $Zn(bdc)\cdot xH_2O$ (called N phase) which was identified by Thirumurugan et al. as the intermediate phase between $[Zn(H_2O)_2(bdc)]$ (VI) and $[Zn(H_2O)(bdc)]$ (VII) upon heating at moderate temperature [28].

The indexation of the X-ray powder-pattern of the samples Zn-MOF-8 and Zn-MOF-10 (data not shown) reveal that MOF-69 type phases have been obtained instead of expected IRMOF structures. For Zn-MOF-10 the cell parameters are 20.180(1), 18.562(1), 12.164(1), 90 95.34(5), 90 in space-group *C*2/*c*, which is identical to that of MOF-69B. The cell parameters for Zn-MOF-8 show similar values: 21.59(2), 20.88(4), 11.94(2), and 90 96.10(2), 90 and the systematic absences also suggest *C*2/*c* as a space-group. The synthesis of MOF-5 is known to be very sensitive to the conditions, especially regarding the water concentration in the media [29,30]. For instance, MOF-69C has been obtained by Loiseau et al. instead of the MOF-5 as initially expected [18]. Our finding indicates that this synthesis sensitivity is also found for the homologues IRMOF-8 and -10. The synthetic conditions applied here are more favourable for obtaining MOF-69 series against IRMOF structures.

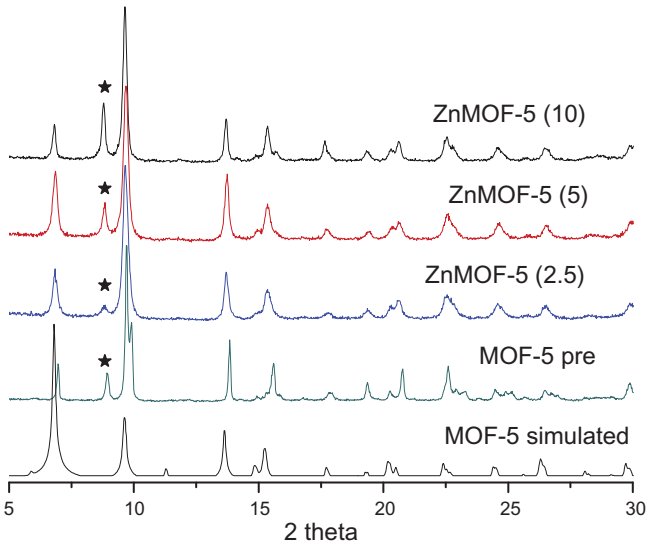

Fig. 7. Powder X-ray diffraction patterns of MOF-5 based samples prepared by precipitation (MOF-5 pre) and with increasing rate of mono-carboxylic acid ZnMOF-5 (2.5), (5), and (10), respectively. The symbol * indicates $Zn(bdc)\cdot xH_2O$ (N phase).

In order to characterize hydroxyl groups, short range DRIFT and ^{1}H NMR studies were carried out. From the DRIFT spectra (Fig. 8), we can clearly observe a common intense signal at about 3600 cm^{-1} for MOF-69C, MOF-5 pre, MOF-5 basf samples, and also for Zn-MOF-8. This signal can be attributed to Zn–OH species such as found in $Zn_5(OH)_4(bdc)_3\cdot 2DMF$ [31]. The presence of this –OH band is expected for MOF-69 samples since μ_3-OH specie is found in the structure. However, for pure IRMOF samples, this band should not appear. On other hand, the intensity of the hydroxyl band is much weaker for IRMOF-3 suggesting higher purity while the two intense signals centered at 3500 and 3390 cm^{-1} correspond to the both stretching and bending vibrational modes of $-NH_2$ species, respectively. The nature of the hydroxyl centers as characterized by DRIFT results are also confirmed by solid ^{1}H NMR studies. For MOF-69C, the intense and broad signal at −1 ppm can be assigned to Zn-(μ_3-OH)-Zn chains as reported in Loiseau et al. [18] (Fig. 9). Similarly, the presence of Zn–OH–Zn species is also revealed for MOF-5 samples in a much lower amount however (small peak at $\delta = -0.4$ ppm). Depending on the sample preparation, the peak integrations lead to μ_3-OH: bdc ratio from 10 to 25 for MOF-5 solvo and MOF-5 pre, respectively.

From XRD, DRIFT and ^{1}H NMR studies, we did not observe structural changes for IRMOF-3 upon air exposure, neither at long rand (phase transformation) or short range (hydroxyl groups) as also reported by Gascon and Kapteijn [32].

The partial substitution of the 1,4-benzene-di-carboxylate by mono-carboxylate linkers is followed by liquid ^{1}H NMR measurements after sample digestion (Fig. 10). The presence of the distinctive aromatic resonances at δ(ppm) = 7.21 (m, 2 H, H_{1-1}, H_{1-3}), 7.44 (t, 1 H, $^1J_{HH}$ = 6.5 Hz, H_{1-2}) and 7.72 (d, 1 H $^1J_{CH}$ = 6.5 Hz, H_{1-4}) indicates the presence of toluic acid in liquid phase which find its origin in the porous framework. Depending on the percentage of mono-carboxylic acid used in the synthesis, the peak integration reveals di-carboxylate: mono-carboxylate ratios between 1:17 and 1:53. As revealed by DRIFT, the substitution of di- to mono-carboxylate linkers is accompanied by additional signals in the hydroxyl region which could be additional Zn–OH species; the strongest being at 3580, and 3530 cm^{-1}. We also observe that for the sample with the lowest level of substitution (2.5) the intensities of the later IR bands are weaker.

In summary, DRIFT and ^{1}H NMR results confirm the presence of Zn–OH species in MOF-5 basf sample and MOF-5 prepared by precipitation that could, in principle, be addressed to Brønsted acid type. Pyridine adsorption measurements from room temperature to 200 °C followed by FTIR were carried out in order to characterize

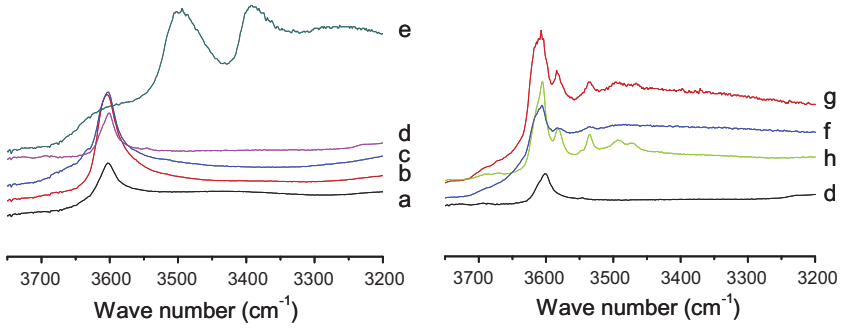

Fig. 8. DRIFT spectra recorded after drying at 220 °C under N_2 flow. Key: Zn-MOF-8 (a), MOF-5 basf (b), MOF-69C (c), MOF-5 pre (d), IRMOF-3 (e), ZnMOF-5 (2.5) (f), ZnMOF-5 (5) (g), ZnMOF-5 (10) (h).

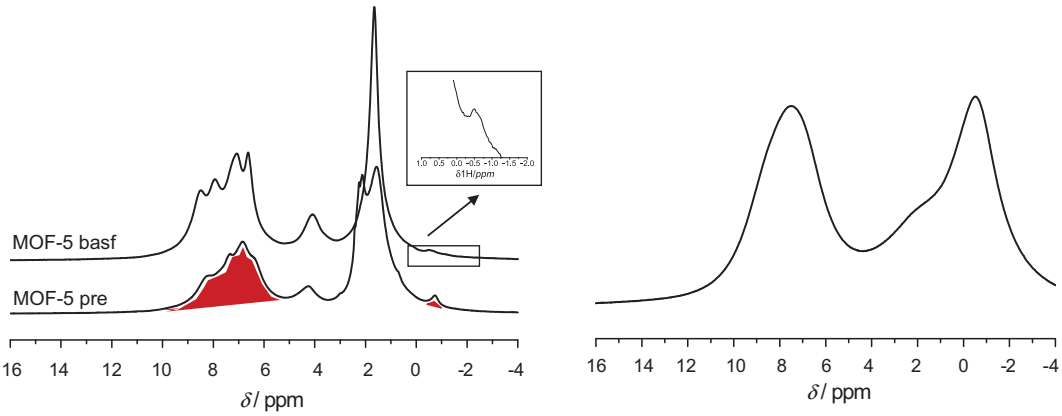

Fig. 9. Solid ^{1}H NMR of MOF-5 samples prepared by basf and precipitation methods (left) and MOF-69C (right).

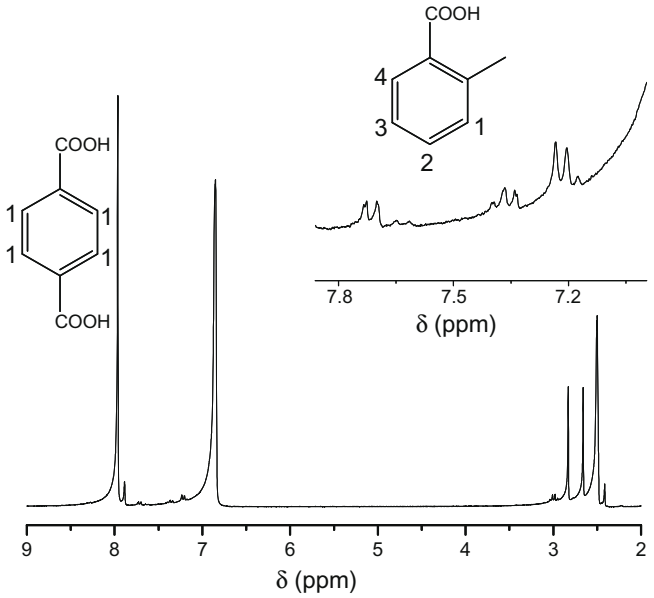

Fig. 10. Liquid ^{1}H NMR of digested ZnMOF-5 (2.5).

the nature and the strength of the acid sites. Any significant adsorptions were measured even at low temperature neither for MOF-5 pre nor for MIL-53 (Al). However, the adsorption of pyridine in low amount can not be ruled out since the signals could be masked by the intense bands of carboxylates. Although deeper investigations are requested to further characterize the acid centers, we can conclude that the acidity of identified Zn–OH is much weaker than surface hydroxides of reference oxides such as silica–alumina. For the same reason, the presence of certain amount of Lewis acid sites could not be ruled out.

3.2. Porous structure characterization

The results of N_2 physisorption experiments (Fig. 11) show that samples prepared either by precipitation or basf methods are microporous materials. Surface areas, micropore volumes and pore sizes are also reported in Table 2. The very high surface area (>2600 $m^2\ g^{-1}$) and micropore volume (>1.3 $cm^3\ g^{-1}$) of the MOF-5 sample prepared by solvothermal technique (MOF-5 solvo) are in good agreement with already reported values [33]. This demonstrates the high quality of the solids with respect to its structure since the presence of other non porous phases would result in a proportional decrease of the surface area and pore volumes. For the samples prepared by precipitation, surface areas, micropore volumes and pore sizes correspond to those reported elsewhere with similar preparation procedures for MOF-5 [24,27] and IR-MOF-8 [34]. Logarithmic plots (Fig. 11) show that for Zn-MOF-8 nitrogen adsorption occurs in two steps revealing two distinct pore sizes. Surprisingly, there are major surface area discrepancies between MOF-69 series. Because of structural similarity in terms of pore size and geometry with MIL-53, we would have expected much larger porous volume for MOF-69C. In contrast, their analogues with longer linkers, naphthyl (MOF-69B) and biphenyl (MOF-69A) carboxylates yield surface higher areas values.

3.3. Catalytic testing

Alkylations of aromatic compounds can be performed with either Brønsted or Lewis acid catalysts, the later being preferable

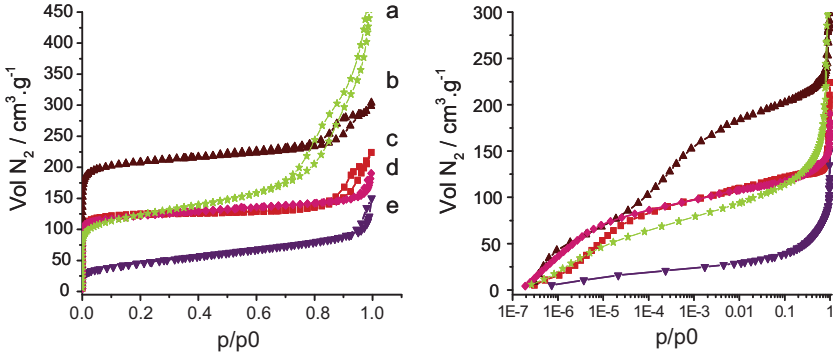

Fig. 11. N_2 adsorption/desorption isotherms at 77 K in log scale (left) and linear scale (right) for: H-BEA (a), Zn-MOF-8 (b), IRMOF-1 (c), IRMOF-3 (d) and Zn-MOF-10 (e).

Table 2
N_2 physisorption results.

Sample	Surface Area ($m^2\ g^{-1}$)[a]	Pore volume ($cm^3\ g^{-1}$)	Micropore volume ($cm^3\ g^{-1}$)[b]	Pore diameter (Å)[c]
MOF-5 solv	2600	0.3	1.31	–
MOF-5 basf	400	–	–	–
MOF-5 pre	450	0.32	0.18	8.8
MOF-69A	270	–	–	–
MOF-69B	970	–	–	–
MOF-69C	45	–	–	–
IRMOF-3	426	0.25	0.16	7.3
Zn-MOF-8	730	0.46	0.29	7.3/11.6
Zn-MOF-10	160	0.17	0.02	8.7
H-BEA	430	0.62	0.10	7.7

[a] From BET analysis.
[b] From *t*-plot analysis.
[c] From DFT analysis.

when linear alkyl-halides are used as alkylating agents [35]. Because the reactivity of alkylated aromatics are higher than the parent aromatics, both Brønsted and Lewis acids usually perform un-desired poly-alkylations. In order to limit this issue, the aromatic compound is commonly fed in high excess with respect to the alkylating agent, thus enhancing selectivity and workup operations [36]. In our case, we did consider that an aromatic: *tert*-BuCl ratio of 2:1 would be appropriate to highlight different behaviours of different catalysts towards the selective mono-alkylation while minimizing analytical issues due to the liberation of HCl.

The alkylation of four aromatic substrates, toluene, *tert*-butylbenzene, naphthalene and biphenylene has been carried out. For sake of conciseness and clarity, only the results on the alkylation of toluene and biphenylene are only reported here. The catalytic conversion of *tert*-butylbenzene gives similar insights than those obtained with the toluene while naphthalene is alkylated selectively in β-position (2-*tert*-butyl-naphtahlene as main mono-alkylated product) whatever the catalysts employed; thus hindering structure–activity relationships to be proposed. A first series of screening has been carried out at 170 °C, a relatively elevated temperature, in order to discriminate active from non active formulations (Table 3). Except for IRMOF-3 and MIL-53(Al), all other tested MOF samples convert toluene in the range of 70–80% which are intermediate values with respect to reference catalysts (H-BEA and $AlCl_3$). Note that the H-BEA sample is a non-dealuminated zeolite which contains moderate to strong Brønsted acidity and accompanied with Lewis centers. Furthermore, all MOF samples exhibit high selectivity to the less bulky para-oriented products (80–85%) slightly superior to H-BEA whereas $AlCl_3$ produces mixtures of ortho- and para-isomers in nearly equal ratio. The obtained results on the catalytic alkylation of biphenylene confirm the later trends. MOF samples, at the exception again of IRMOF-3 and MIL-53(Al), are as active as H-BEA zeolite and show exceptional selectivity to the para-isomer 4-*tert*-butylbiphenylene. Indeed, only traces of di-alkylated products (<1%) are detected whereas much higher selectivity to the ortho-oriented product and about 15% towards di-alkylated products are measured for H-BEA and $AlCl_3$.

After these preliminary tests, catalytic experiments at 100 °C were carried out in order to better discriminate the activity of MOF catalysts and also to better highlight shape selectivity properties. As a matter of fact, MOFs conversion values are now more spread (from 8% to 62%) (Table 4). At this temperature also, both IRMOF-3 and MIL-53(Al) are not active whatever activation procedures which were applied. We can see major activity differences on MOF-5 samples depending on the synthesis procedure. The most crystalline and porous MOF-5 (MOF-5 solvo) sample shows the lowest catalytic activity in contrast to all other MOF-5 type samples including the samples with mixture of mono- and di-carboxylate linkers (ZnMOF-5 samples). On the other hand, it appears that the generation of additional defects by mono-acid substitution (ZnMOF-5 samples) does not affect significantly catalytic performances with respect to MOF-5 sample prepared by precipitation (MOF-5 pre). We also observe significantly lower activities for MOF-69 type samples; the lowest activity being for MOF-69C which has also the lowest surface area. Surprisingly, Zn-MOF-8 and -10 show the highest catalytic activities, although they have similar structure than MOF-69B and MOF-69A, respectively. Kinetic studies confirm the ranking of MOF activities with Zn-

Table 3
Catalytic results for the *tert*-butylation of toluene and biphenylene at 170 °C after 6 h.

Catalyst	Toluene conversion	Selectivity			Biphenylene conversion	Selectivity		
		Para [a]	Ortho	Di [c]		Para [b]	Ortho	Di [c]
MOF-5 solvo	n.a.	–	–	–	n.a.	–	–	–
MOF-5 basf	73	84	16	0	n.a.	–	–	–
MOF-5 pre	73	82	18	0	37	90	6	4
IRMOF-3 [d]	0	–	–	–	0	–	–	–
Zn-MOF-8	86	84	16	0	38	97	3	0
Zn-MOF-10	86	82	18	0	39	99	1	0
MOF-69C	81	81	19	0	33	89	7	4
MIL-53(Al) [d]	0	–	–	–	0	–	–	–
H-BEA	90	72	28	0	70	66	18	16
H-MOR	n.a.	–	–	–	15	75	0	25
$AlCl_3$	64	46	54	0	64	50	35	15
$ZnCl_2$	8	77	23	0	n.a.	–	–	–

Selectivity [a] 4-*tert*-butyltoluene, [b] 4-*tert*-butylbiphenylene, [c] sum of di-alkylated products, [d] MIL-53 (Al) samples were tested as made or after being activated either at 220 °C under N_2 flow or at 170 °C under vacuum (10^{-5} mbar). In all cases, meta-isomers were not detected. However, the presence of minor quantity of meta-isomers can not be rule out. Key: n.a. not analyzed.

Table 4
Catalytic results for the *tert*-butylation of toluene and biphenylene at 100 °C after 2 h.

Catalyst	Toluene conversion	Selectivity			Biphenylene conversion	Selectivity		
		Para	Ortho	Di		Para	Ortho	Di
MOF-5 solvo	13	90	10	0	n.a.	–	–	–
MOF-5 basf	47	89	11	0	n.a.	–	–	–
MOF-5 pre	40	88	12	0	28	100	0	0
ZnMOF-5 (2.5)	30	85	15	0	n.a.	–	–	–
ZnMOF-5 (5)	46	86	14	0	n.a.	–	–	–
ZnMOF-5 (10)	36	86	14	0	n.a.	–	–	–
MOF-69C	8	90	10	0	n.a.	–	–	–
MOF-69A	15	89	11	0	n.a.	–	–	–
MOF-69B	23	90	10	0	n.a.	–	–	–
Zn-MOF-8	47	90	10	0	13	100	0	0
Zn-MOF-10	62	92	8	0	10	100	0	0
MIL-53 (Al)	0	–	–	–	n.a.	–	–	–
H-BEA	67	72	28	0	30	55	25	20
H-MOR	5	85	15	0	5	81	0	19
$AlCl_3$	n.a.	–	–	–	55	47	34	19

MOF-10 > MOF-5 pre > MOF-69C (Fig. 13). In contrast to the wide range of activities, selectivity values are very similar for all porous zinc carboxylates samples whatever their synthesis procedures. The para-selectivity for the toluene alkylation is plotted as a function of the conversion in Fig. 12. It clearly shows that high level of selectivity for zinc carboxylate frameworks can be maintained at high conversion in contrast to tested zeolites. Indeed, we note that H-BEA catalyst is much less selective with respect to Zn-MOF-10 with similar conversion. However, we must mention that selectivity for H-form zeolites, such as BEA and MOR can be enhanced by dealumination of samples in order to produce stronger Brønsted acid sites and extra framework Al species [37,38]. In addition, di- and poly-alkylation products as well as *trans*-alkylation products can be decreased in a large amount by a post-synthesis silanization treatment [39,40]. Thus, silanized H-MOR shows enhanced selectivity (90%, at 10% of conversion) to the corresponding mono-alkyl-isomer in the naphthalene alkylation with iso-propyl-bromide at 200 °C during 1 h [39]. In this sense, our results obtained for Zn-MOF-8 and Zn-MOF-10 in the naphthalene alkylation with *t*-BuCl at 170 °C during 2 h are readily comparable to those reported in literature using modified mordenite zeolites [39]. Thus, 100% of 2-*tert*-butylnaphthalene is produced at 42% and 23% of conversion when Zn-MOF-8 and Zn-MOF-10 are used as catalysts, respectively (data not shown).

The main outcome of the biphenylene alkylation is the 100% selectivity in the para-oriented product. It has to be emphasized also that reference catalysts (H-BEA, H-MOR, $AlCl_3$) yield high amount of di-alkylated products in contrast to MOF catalysts.

Isomerization test reactions have been performed to investigate product reactivity in the MOF. In absence of alkylaton agent, 4-*tert*-butyltoluene does not isomerize on MOF compounds at 100 °C in contrast to acid zeolites. It means that when the para-allkylation is performed in the course of the reaction the product does not react further, likely because of the weak acidity of investigated MOFs. This result may explain the superior selectivity of MOF materials. Summarizing, those results point out outstanding pore-shape selectivity properties of microporous zinc carboxylate open frameworks for large poly-aromatics.

3.4. Catalyst post characterization and leaching tests

After filtration and washing with *n*-decane under inert atmosphere, MOF-5 pre sample can be re-used without any loss of activity or selectivity. Solid ^{1}H NMR spectrum of used precipitated MOF-5 reveals the presence of a guest in the structure which can be assigned to $H_3O^+Cl^-$ (very intense peak at δ = 3.4 ppm). Indeed, very similar ^{1}H NMR spectra are obtained when concentrated HCl (36%) is added to fresh MOF-5 samples. We suggest that the HCl,

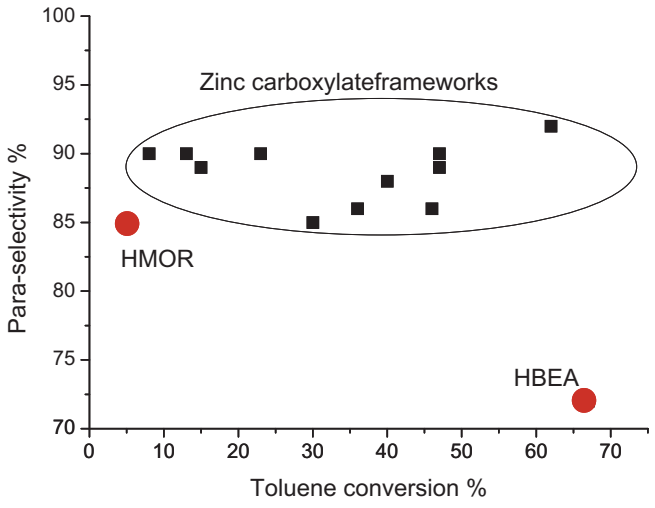

Fig. 12. Conversion-selectivity plot on toluene alkylations with *tert*-butyl chloride at 100 °C during 2 h.

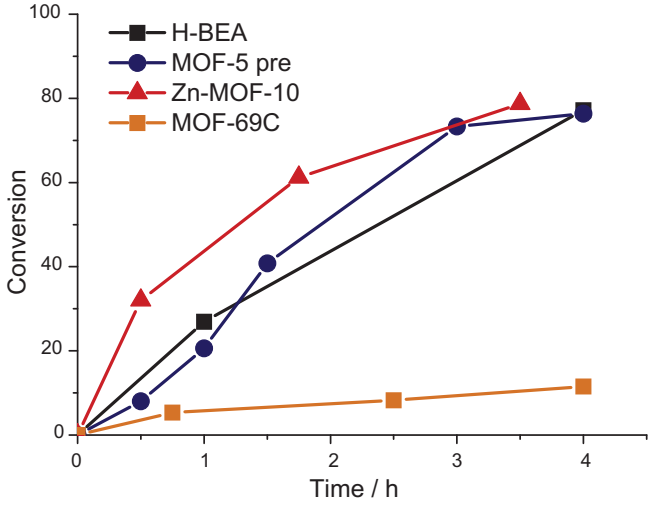

Fig. 13. Kinetic curves for different catalytic samples in the *tert*-butylation of toluene at 100 °C.

which is produced in the course of the reaction, is trapped into the framework, likely, at the oxygen containing nodes. The hydration of the sample, which provokes the rapid formation of $H_3O^+Cl^-$, arises from the sample cell which is not tight against ambient air. We believe that this aqueous HCl formation is responsible of a partial hydrolysis of the framework as indicated by a very broad peak at $\delta = 14$ ppm and the change of the XRD pattern (Fig. 14). Because the linkers from the solid framework are also made form aromatics species, we were wondering whether the alkylation could take place on the terephthalate linkers as well. Any data from solid NMR supports this hypothesis.

In order to check that the reaction takes place in heterogeneous conditions, leaching issues were investigated. Firstly, tests in absence of solid catalysts were carried out in same conditions and any conversions were measured. Secondly, reaction mixtures were filtered off after the completion of catalytic reactions, both solid catalyst and liquid being recovered separately. When a new reaction was started by adding fresh reactants to the recovered liquid, any additional conversion was detected. This is consistent with the fact that HCl is trapped into the framework making the filtrate HCl free. Finally, we have observed that the reaction takes place at 50 °C with precipitated MOF-5. In these conditions of pressure and temperature, IRMOF samples are likely not soluble in *n*-decane indicating that the reaction does not proceed in homogeneous phase.

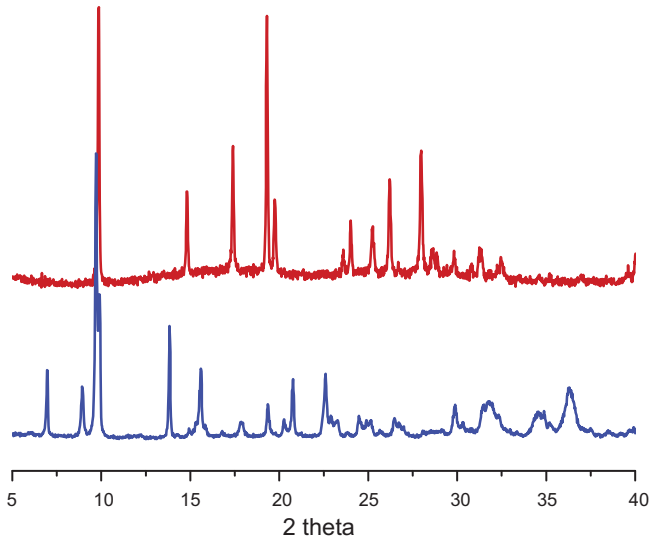

Fig. 14. Powder X-ray diffraction patterns of MOF-5 pre before (bottom) and after reaction (top).

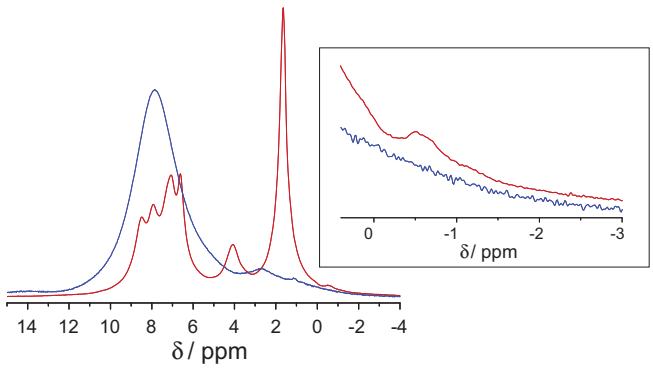

Fig. 15. Solid ^{1}H NMR post characterization after running the alkylation with toluene-d_8.

3.5. Post characterization of H–D exchange in the course of the reaction

In order to ascertain the key role of Zn–OH species in the catalytic properties of zinc carboxylate open frameworks, alkylation on toluene-d_8 was carried out with precipitated MOF-5 at 100 °C. After reaction, the sample was recovered as indicated above and characterized by solid state ^{1}H NMR measurements (Fig. 15). Apart the aromatic signal arising from the linker, we can observe a broad peak placed at $\delta = 3$ ppm which may be assigned to $DH_2O^+Cl^-$ trapped in the network. But more importantly, the characteristic Zn–O(H)–Zn peak at $\delta = 0.4$ ppm has disappeared suggesting an H–D exchange with the toluene-d_8 while the reaction takes place.

4. Discussion

The intriguing non activity of IRMOF-3 and the very low activity of pure MOF-5 (MOF-5 solvo with the highest surface area) clearly indicate the key role of Zn–OH species in the catalytic properties. Obviously, all samples exhibiting a sharp IR band at 3600 cm^{-1} are active whereas IRMOF-3 is not active. We suggest that the very low activity of pure MOF-5 arises from its partial hydrolysis in the reaction media which may contain about 0.02% of water (*tert*-butyl chloride was used as received). The ZnOH–ZnOD exchange in the course of the reaction when using toluene-d_8 also supports that Zn–OH species are the actual catalytic centers. Furthermore, the fact that there is no evidence of alkylations on the aromatic linkers, clearly suggests that the catalyst centers are bewared by the framework itself. Finally, we can rule out the role of Zn–Cl as catalytic species that would arise from structural modifications since kinetic studies show that MOF catalysts are active in the first minutes on operation in contrast to MIL-101(Cr) [15]. Furthermore, the poor activity of $ZnCl_2$ tested as a powder at 170 °C (only 8% conversion) confirms that $ZnCl_2$ is not the catalytic specie. We therefore conclude that Zn–OH species, that are part of the framework, are likely responsible from the catalytic activity of the zinc carboxylate open frameworks. The non activity of MIL-53(Al) may suggest that the acidity of bridging μ_2-OH is not strong enough to catalyze the reaction. Unfortunately, the adsorption of pyridine measured by IR did not allow a proper quantification of the acid site strength. On the other hand, preliminary molecular modeling results (DFT) [41] indicate a very low acidity of MIL-53(Al) which is in agreement with pyridine adsorption and catalytic results. On the other hand, the presence of uncoordinated Zn at the surface or at crystalline defects with Lewis feature can not be ruled out. These centers may also be involved in the reaction pathway. As a matter of fact, Horcajada et al. [15] proposed that benzylation of benzene over MIL-101(Fe) type materials could be catalyze on both Lewis and Brønsted acid sites.

Structural (X-ray diffraction, IR) and thermal (TDA, TGA) characterization data (not shown) for precipitated MOF-5 are in very good agreement with the results reported by Huang et al. [24] and Hafizovic et al. [27]. We also measured a 10% excess of Zn with respect to the theoretical formulae (elemental analysis and TGA), which leads to a global composition of $Zn_4O(bdc)\cdot 2H_2O + Zn(OH)_2$. According to Hafizovic et al. [27], zinc hydroxide nanoclusters that partly occupy the cavities could be responsible for the structure distortion evidenced by the splitting of the diffraction peak at 9.7. However, authors point out that other structural change would result in the same distortion. On the other hand, the ^{1}H NMR spectra obtained for different precipitated MOF-5 samples indicated the presence of 3–5% of Zn–OH–Zn species, like those found for $Zn_3(\mu_3OH)_2(bdc)_2\cdot 2DEF$ (MOF-69C). Phase transformation from MOF-5 to MOF-69C has been well characterized since very recently [29,30]. The later phase can be formed during the synthesis of

MOF-5, and is kinetically favoured in moisture conditions, as was the case in this study. Therefore, in addition to zinc hydroxide clusters, precipitated MOF-5 samples also contain Zn–(μ_3OH)–Zn chains in minor quantities, which could either, be a crystalline default of the cubic structure or non-XRD detectable MOF-69C microcrystallites. Finally, it was recently demonstrated that pure MOF-5 undergoes a rapid phase transformation under moist conditions to MOF-69C that is accompanied by a drastic decrease inaccessible porous volume [22,42].

They are many more Zn–OH–Zn species in MOF-69 samples than in MOF-5 type samples as confirmed by solid ^{1}H NMR studies. In addition, MOF-69A and B show comparable and higher surface areas than MOF-5 type samples, suggesting equal or even enhanced site accessibility. The fact that precipitated MOF-5 samples have superior activity than MOF-69 type samples, although they have a much lower number of sites, indicate that (i) Zn–μ_3OH–Zn species have a moderate activity and/or other kind of Zn–OH (as described above) exist in precipitated MOF-5 which are much more active. In summary, catalytic centers may arise either from Zn hydroxide clusters or from the presence of Zn–OH–Zn type species [i.e. $Zn_3(\mu_3OH)_2(bdc)_2{\cdot}2DEF$ found in MOF-69C], or structural defects as Zn–OH species formed at the synthesis step or upon water adsorption.

Obviously, the action of water content at the synthesis stage and/or the action of the moisture when handling the MOF-5 samples are responsible from the generation of structural defects as Zn–OH species. In addition to the later, the isomorphous substitution of di-carboxylate by mono-carboxylate linkers creates other types of Zn–OH species. Unfortunately, their characterization, quantification and role in catalysis are made difficult by the high sensitivity of MOF-5 against moisture.

The pore size distribution calculated by Horvath–Kawazoe or Density Functional Theory (DFT) methods can be only indicative values, since the principal interaction potentials of the adsorbate and the adsorbent are unknown and assumptions have to be made about the pore morphology. The numerical values of the pore diameters calculated from the DFT method (Table 5) are therefore not fully accurate but, more importantly, allow a comparison among members of a class of similar materials which presumably have the same interaction potentials. In order to complete the picture of MOF samples with regard to their porous properties, calculated sizes of cages and channel windows from structural data of pure crystals are reported in Table 5. For example, the window between the cages of IRMOF-1 have a van der Waals space that can accommodate a sphere with a diameter of approximately 7.8 Å, herein referred as the "free-space" diameter. In contrast to zeolite pore sizes, these numbers shall be interpreted with care for MOF materials, especially when one wants to correlate structural features and properties. Indeed, in addition to their general flexibility properties the aromatic rings of IRMOF can rotate thus making feasible the diffusion of larger guests [43,44].

From experimental and theoretical data, there is in principle no steric hindrance for mono-alkylated products to diffuse out of all porous solids, including H-BEA. Even very bulky products such as the di-alkylated product 4,4′-di-*t*-butylbiphenylene (16 × 8 Å) can be formed in large amounts in H-BEA [45–48]. Therefore, the shape selectivity properties observed for IRMOF sample can not arise from diffusion hindrance of the most bulky products since pore windows are even larger. For the reaction to take place we suggest that the biphenylene is absorbed in a specific manner to allow the formation of the transitions state for the para-oriented product. Once alkylated, it can not be activated in the same manner because of steric hindrance and double alkylation can not proceed.

Table 5
Theoretical cage and window sizes from structural data.

	Cage free space diameter (Å)	Window free space diameter (Å)
IRMOF-1[a]	15.1	7.8
IRMOF-8[a]	18.0	9.2
H-BEA[b]	6.6	6.1

[a] "Free-space" diameter refers to the diameter of the largest sphere that can fit in the cage or through the window when van der Waals radii are assumed for all frameworks atoms from Ref. [20].
[b] From Ref. [49].

5. Conclusions

The MOF design by a "zeolite" mimetic approach leads us to select microporous structures exhibiting bridging hydroxyls (MOF-69, MIL-53). By NMR and IR characterization, we have demonstrated the key role of Zn–OH species to generate catalytic properties. Although Zn–OH groups can be created by isomorphous substitution of di- by mono-carboxylate linkers, the impact on the catalytic performances can be hardly assessed. Indeed, MOF-5 prepared by precipitation, without taking special care to control neither water concentration nor moisture, already shows a few percent of Zn–OH as structural defects while the overall cubic structure is maintained.

This study illustrates the rational design of MOF to generate single site Brønsted acid catalysts. The construction by building block approach enables to regard MOF material as extended molecules. However, they are by essence solids. With this respect, they are quite similar to zeolites and thus there are accompanied with characterization issues such as the identification and quantification of defects. As clearly shown in this study, short range characterization shall be systematically carried out in order to identify actual catalytic centers. On the other hand, we believe that the engineering of structural defects in MOF materials may lead to the generation of a new class of catalysts with different acidity and hydrophobic properties than encountered in zeolites. In this sense, other alkylating agents of high industrial relevance and also much more catalyst demanding in terms of acidity strength, such as alcohols and alkenes, are now under study.

We have also demonstrated that MOFs can undergo 100% shape selective catalytic alkylations of large aromatics molecules. This discovery lead us to generate a new class of Brønsted acid MOFs which are more acid and can perform alkylation and isomerization at room temperature [41].

Acknowledgments

We thank C. Daniel and C. Lorenz for DRIFT and NMR investigations. We also thank Prof. S. Kaskel and Dr. A. Henschel for having provided high surface area MOF-5 samples.

References

[1] G. Ferey, Chemical Society Reviews 37 (2008) 191.
[2] D. Farrusseng, C. Mirodatos, in: U. Ozkan (Ed.), Handbook of Catalyst Design, Wiley-VCH, Weinheim, 2009.
[3] S. Vagin, A. Ott, B. Rieger, Chemie Ingenieur Technik 79 (2007) 767.
[4] K. Schlichte, T. Kratzke, S. Kaskel, Microporous and Mesoporous Materials 73 (2004) 81.
[5] L. Alaerts, E. Seguin, H. Poelman, F. Thibault-Starzyk, P.A. Jacobs, D.E. De Vos, Chemistry – A European Journal 12 (2006) 7353.
[6] W. Mori, T. Sato, T. Ohmura, C.N. Kato, T. Takei, Journal of Solid State Chemistry 178 (2005) 2555.
[7] W. Mori, S. Takamizawa, C.N. Kato, T. Ohmura, T. Sato, Microporous and Mesoporous Materials 73 (2004) 31.
[8] C.N. Kato, W. Mori, Comptes Rendus Chimie 10 (2007) 284.
[9] C.N. Kato, M. Ono, T. Hino, T. Ohmura, W. Mori, Catalysis Communications 7 (2006) 673.
[10] J.S. Seo, D. Whang, H. Lee, S.I. Jun, J. Oh, Y.J. Jeon, K. Kim, Nature 404 (2000) 982.
[11] K.S. Suslick, P. Bhyrappa, J.H. Chou, M.E. Kosal, S. Nakagaki, D.W. Smithenry, S.R. Wilson, Accounts of Chemical Research 38 (2005) 283.

[12] G.A. Olah, Friedel–Crafts Chemistry, Wiley, NY, 1973.
[13] J.S. Beck, A.D. Dandekar, T.F. Degnan, in: M. Guisnet, J.-P. Gilson (Eds.), Zeolites for Cleaner Technologies. Catalytic Science Series, vol. 3, Imperial College Press, London, 2002, p. 223.
[14] A. Corma, Journal of Catalysis 216 (2003) 298.
[15] P. Horcajada, S. Surble, C. Serre, D.Y. Hong, Y.K. Seo, J.S. Chang, J.M. Greneche, I. Margiolaki, G. Ferey, Chemical Communications (2007) 2820.
[16] U. Ravon, M.E. Domine, C. Gaudillère, A. Desmartin-Chomel, D. Farrusseng, New Journal of Chemistry 32 (2008) 937.
[17] F. Millange, C. Serre, G. Ferey, Chemical Communications (2002) 822.
[18] T. Loiseau, H. Muguerra, G. Ferey, M. Haouas, F. Taulelle, Journal of Solid State Chemistry 178 (2005) 621.
[19] E. Armengol, A. Corma, H. Garcia, J. Primo, Applied Catalysis, A: General 149 (1997) 411.
[20] M. Eddaoudi, J. Kim, N. Rosi, D. Vodak, J. Wachter, M. O'Keefe, O.M. Yaghi, Science 295 (2002) 469.
[21] N.L. Rosi, M. Eddaoudi, J. Kim, M. O'Keeffe, O.M. Yaghi, Angewandte Chemie, International Edition 41 (2002) 284.
[22] M. Sabo, A. Henschel, H. Froede, E. Klemm, S. Kaskel, Journal of Materials Chemistry 17 (2007) 3827.
[23] U. Mueller, M. Schubert, F. Teich, H. Puetter, K. Schierle-Arndt, J. Pastre, Journal of Materials Chemistry 16 (2006) 626.
[24] L.M. Huang, H.T. Wang, J.X. Chen, Z.B. Wang, J.Y. Sun, D.Y. Zhao, Y.S. Yan, Microporous and Mesoporous Materials 58 (2003) 105.
[25] N.L. Rosi, M. Eddaoudi, J. Kim, M. O'Keeffe, O.M. Yaghi, CrystEngComm 4 (2002) 401.
[26] N.L. Rosi, J. Kim, M. Eddaoudi, B. Chen, M. O'Keeffe, O.M. Yaghi, Journal of the American Chemical Society 127 (2005) 1504.
[27] J. Hafizovic, M. Bjorgen, U. Olsbye, P.D.C. Dietzel, S. Bordiga, C. Prestipino, C. Lamberti, K.P. Lillerud, Journal of the American Chemical Society 129 (2007) 3612.
[28] A. Thirumurugan, C.N.R. Rao, Journal of Material Chemistry 15 (2005) 3852.
[29] S. Hausdorf, F. Baitalow, J. Seidel, F. Mertens, Journal of Physical Chemistry A 111 (2007) 4259.
[30] S. Hausdorf, J. Wagler, R. Mossig, F. Mertens, Journal of Physical Chemistry A 112 (2008) 7567.
[31] J.H. Liao, T.J. Lee, C.T. Su, Inorganic Chemistry Communications 9 (2006) 201.
[32] J. Gascon, F. Kapteijn, Journal of Catalysis 261 (2009) 75.
[33] A.R. Millward, O.M. Yaghi, Journal of the American Chemical Society 127 (2005) 17998.
[34] Y.W. Li, R.T. Yang, Journal of the American Chemical Society 128 (2006) 726.
[35] K. Smith, G.M. Pollaud, I. Matthews, Green Chemistry (1999) 75.
[36] Y. Du, S. Liu, Y. Ji, Y. Zhang, F. Liu, Q. Gao, F.-S. Xiao, Catalysis Today 131 (2008) 70.
[37] R. Anand, R. Maheswari, K.U. Gore, B.B. Tope, Journal of Molecular Catalysis A: Chemical 193 (2003) 251.
[38] A.B. Halgeri, J. Das, Applied Catalysis, A: General 181 (1999) 347.
[39] P. Moreau, A. Finiels, P. Geneste, J. Solofo, Journal of Catalysis 136 (1992) 487.
[40] C.T. O'Connor, K.P. Möller, H. Manstein, Journal of Molecular Catalysis A: Chemical 181 (2002) 15.
[41] D. Farrusseng, submitted for publication.
[42] S. Kaye, A. Dailly, O.M. Yaghi, J. Long, Journal of the American Chemical Society 129 (2007) 14176.
[43] M.J. Rosseinsky, Microporous and Mesoporous Materials 73 (2004) 15.
[44] S. Kitagawa, K. Uemura, Chemical Society Reviews 34 (2005) 109.
[45] J. Horniakova, D. Mravec, J. Joffre, P. Moreau, Journal of Molecular Catalysis A: Chemical 185 (2002) 249.
[46] R. Millini, F. Frigerio, G. Bellussi, G. Pazzuconi, C. Perego, P. Pollesel, U. Romano, Journal of Catalysis 217 (2003) 298.
[47] D. Mravec, P. Zavadan, A. Kaszonyi, J. Joffre, P. Moreau, Applied Catalysis, A: General 257 (2004) 49.
[48] Y. Sugi, S. Tawada, T. Sugimura, Y. Kubota, T. Hanaoka, T. Matsuzaki, K. Nakajima, K. Kunimori, Applied Catalysis, A: General 189 (1999) 251.
[49] M.D. Foster, I. Rivin, M.M.J. Treacy, O.D. Friedrichs, Microporous and Mesoporous Materials 90 (2006) 32.

J|A|C|S COMMUNICATIONS

Published on Web 03/16/2010

Generic Postfunctionalization Route from Amino-Derived Metal−Organic Frameworks

Marie Savonnet,[†,‡] Delphine Bazer-Bachi,[‡] Nicolas Bats,[‡] Javier Perez-Pellitero,[‡] Erwann Jeanneau,[§] Vincent Lecocq,[‡] Catherine Pinel,[†] and David Farrusseng*[,†]

IRCELYON, Institut de recherches sur la catalyse et l'environnement de Lyon; Université Lyon 1 - UMR 5256 CNRS, 2 avenue Albert Einstein, F-69626 Villeurbanne Cedex, France, IFP-Lyon, BP n°3, 69360 Solaize, France, and Université Lyon 1, Centre de Diffractométrie, 69629 Villeurbanne Cedex, France

Received November 12, 2009; E-mail: david.farrusseng@ircelyon.univ-lyon1.fr

The secondary building unit (SBU) approach for engineering of metal−organic frameworks (MOFs) with tunable pore sizes is very attractive for designing practical properties such as separation by molecular sieving and shape-selective catalysis.[1] The conceptual approach used to increase the pore sizes of MOFs through the use of longer ligands has also been extended to the design of multifunctional MOFs bearing a functional group on the organic moiety. This is the case for IRMOF-3,[2] MOF-101(-Br),[3] and MIL-53(Al)-NH_2,[4] to name a few. However, this extension is not straightforward in practice.[5] Indeed, the chemistry of MOF network formation is very sensitive to the chemical reactivity and solubility of the functionalized linkers.[6] This is particularly the case for functions such as −OH, −COOH, and N-donating groups, which can interfere with the coordination chemistry associated with the assembly of the nodes.

When self-assembly fails in the synthesis of an MOF with functionalized linkers, the postfunctionalization of a parent MOF appears to be a very valuable alternative.[7] In fact, postsynthesis opens the door to advanced porous solid engineering by multiple synthesis steps[8] and, as a consequence, to the design of new types of adsorbents and catalysts. Postfunctionalization consists of modifying the organic part of the MOF by a chemical reaction that takes place within the porous framework. In this case, the parent MOF must possess accessible reactive functions. Similar issues have been resolved for MCM-like materials, for which various functionalization methods have been developed.[9] In a similar fashion to alkylamino-functionalized MCMs,[10] amino-derived MOFs such as IRMOF-3 and DMOF-NH_2[11] are excellent platforms for the grafting of various synthons such as aldehydes, isocyanates, and acid anhydrides. That said, the suitability, diversity and availability of such synthons can appear limited when one considers the ever-increasing demands for different functionalities and the ambitious projects imagined by chemists.

Valuable alternatives lie in the development of all kinds of generic postfunctionalization methods that are soft, do not liberate byproducts that may react or remain blocked in the pores, and enable grafting of a wide variety of chemical functions with high efficiency and selectivity. The Sharpless "click" reaction using Cu^I-catalyzed Huisgen cycloaddition of azides to alkynes fulfills all of these criteria.[12,13] The corresponding azide linkers are, however, highly unstable and not commercially available; this significantly limits the synthesis of MOFs bearing azide groups by self-assembly methods.

The objective of this work was to develop a one-pot, two-step functionalization method starting from already available amino-derived MOF compounds.[14] The first step involves an original method to convert a MOF in its amino form to the corresponding azide compound. Next, the desired functionalized material is obtained by "clicking" a synthon onto the azide without isolation of the intermediate.

The starting materials DMOF-NH_2 [Zn(bdc-NH_2)(DABCO)] (section S1 in the Supporting Information) and MIL-68(In)-NH_2 [In(OH)(bdc-NH_2)][15] (section S5) were selected as representative compounds. The former is a zero-dimensional-type MOF with a layered structure made of Zn carboxylate sheets supported by 1,4-diazabicyclo(2.2.2)octane (DABCO) pillars. It is representative of a large class of porous coordination polymers (PCPs).[16] On the other hand, MIL-68(In)-NH_2 belongs to another important class of MOFs characterized by a one-dimensional rod-shaped structure. This class has been reviewed by Yaghi et al.[17]

It should be noted that the usual route for preparing azide compounds from the corresponding amines via their diazonium salts cannot be applied here because DMOF-NH_2 dissolves under acidic conditions. Instead, we investigated another pathway that uses mild conditions and involves stable, nonexplosive compounds.[18]

Scheme 1. One-Pot, Two-Step Functionalization of DMOF-NH_2

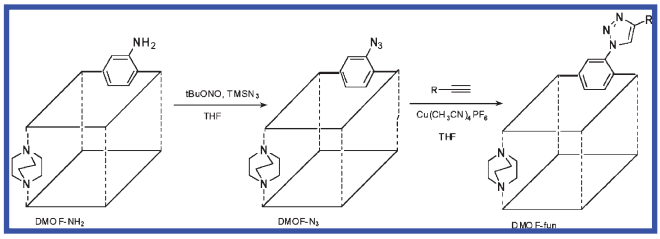

In a typical synthesis (Scheme 1), the freshly dried DMOF-NH_2 was treated with tBuONO and $TMSN_3$ in THF overnight at room temperature to produce the corresponding azide intermediate compound DMOF-N_3.[19] In the same vessel, the functionalized DMOF (DMOF-fun) was obtained by addition of excess phenylacetylene in the presence of $Cu^I(CH_3CN)_4PF_6$ followed by continuous stirring for 24 h (section S3). For characterization purposes, the synthesis was stopped after formation of the azide intermediate DMOF-N_3.

MIL-68(In)-NH_2 was modified by applying a similar procedure.[20] For sake of brevity, details are given in section S6 in the Supporting Information.

Clear proof of azide formation and the subsequent (3 + 2) cycloaddition was obtained by IR spectroscopy. The absorption band of DMOF-N_3 at 2123 cm^{-1} is characteristic of the N_3 asymmetric stretching vibration (section S3). In addition, unambiguous characterization and quantification were provided by liquid

[†] IRCELYON UMR 5256 CNRS.
[‡] IFP-Lyon.
[§] Université Lyon 1.

10.1021/ja909613e

^{1}H NMR analysis. Samples of DMOF-N_3 were digested and dissolved in dilute DCl/D_2O/DMSO-d_6 solution (Figure 1) and then analyzed by ^{1}H NMR spectroscopy, which confirmed the formation of the azide compound by the appearance of new aromatic signals (7.74−7.85 ppm, m, 3H, ArH). This coincided with the complete disappearance of the aromatic signals of the amine (7 ppm, d, 1H, J = 8.3 Hz; 7.4 ppm, s, 1H; 7.74 ppm, d, 1H, J = 8.3 Hz), thus indicating full conversion to the azide form. On the other hand, the aliphatic moiety was not affected by the reaction (section S3).

DMOF-fun obtained after the one-pot synthesis was characterized using identical techniques. Here again, the conversion to the final compound was complete after 24 h. IR analysis revealed the complete disappearance of the azide stretching band at 2123 cm^{-1} (section S3). The liquid ^{1}H NMR spectrum of DMOF-fun illustrates that the corresponding triazole derivative was formed as the unique product; aromatic shifts of the grafted compound were assigned by ^{1}H−^{1}H correlation spectroscopy (COSY) experiments (δ = 7.38, 7.49, 7.93, 8.04, 8.19, 9.15 ppm), and no azido or amino compound was detected (Figure 1). In addition, positive-mode mass spectrometry performed after digestion clearly showed a base peak at m/z 310 corresponding to the functionalized linker [2-(4-phenyl-1,2,3-triazol-1-yl)terephthalic acid]. The powder X-ray diffraction patterns indicated that the two-step reaction proceeded without loss of long-range order (section S3). We stress that the crystallinity of the parent DMOF-NH_2 is strongly affected by post-treatments such as solvent removal and/or solvent exchange (section S2).

Nitrogen physisorption experiments performed on the parent DMOF-NH_2 and DMOF-fun at 77 K revealed a decreases in the porous surface area (1320 to 244 m^2/g) and the microporous volume (0.54 to 0.08 cm^3/g) due to pore blocking (section S3).

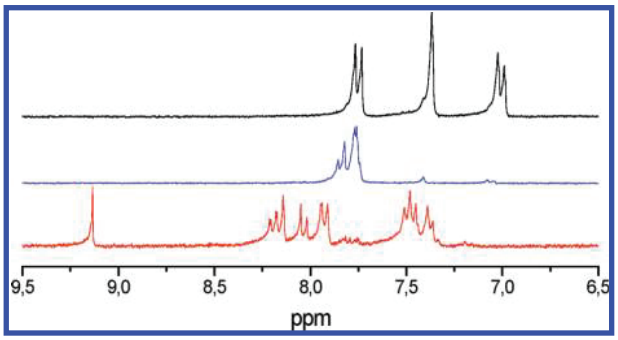

Figure 1. Liquid ^{1}H NMR spectra of digested materials: (top) DMOF-NH_2; (middle) DMOF-N_3; (bottom) DMOF-fun.

These investigations were also undertaken for the postfunctionalization of MIL-68(In)-NH_2, and the same results were obtained in terms of grafting rate (>90%), decrease in surface area (1260 to 120 m^2/g) and microporous volume (0.48 to 0.03 cm^3/g), and preservation of crystallinity (section S6).

Cycloaddition in azide-functionalized MOFs has recently been demonstrated for IRMOF-type compounds.[12] In this work, we have shown that direct functionalization from amino-derived MOFs is possible, provided that the pore cavity is large enough to accommodate a C_5 ring (section S3). The main advantage of this one-pot method is the ease of preparing amino-functionalized MOFs. To the best of our knowledge, five different structures based on 2-aminoterephthalic acid have been reported to date: IRMOF-3,[2] MIL-101-NH_2,[4] CAU-1,[21] DMOF-NH_2, and MIL-53(Al)-NH_2. The large library of amino acids also opens promising perspectives for new potential amino-functionalized MOFs as synthetic platforms. A second advantage is the softness of the method. Indeed, both reaction steps proceed at room temperature and do not liberate byproducts such as water, acids, or bases that could damage the structure by hydrolysis.[22] Finally, in contrast to the anhydride condensation method, which has a limited grafting yield (30−50%),[23] we have shown that this approach allows complete functionalization even for a bulky group. This is in line with molecular modeling results showing weak steric demand (section S3). Notably, the crystallite sizes of the two MOFs are ∼1 μm (section S1), whereas Wang et al.[11] used DMOF-NH_2 crystallites with diameters of 100 μm. We believe that the accessibility of reactants to the centers of the crystals arises from the very small size of the MOF crystallites.

However, this small size comes at the expense of a decrease in microporous volume. Thanks to the efficiency of the azide formation, the grafting rate can be controlled by adding phenylacetylene in default with respect to −NH_2 functions. For a grafting rate of 50% on MIL-68(In)-NH_2, the surface area decreased only by 55% (S_{BET} = 571 m^2/g), which is in line with other methods.[8]

In this study, controlled functionalization was performed with phenylacetylene as a proof of concept. A systematic study dealing with the grafting of moieties exhibiting different functions on diverse amino-MOF platforms will be reported soon. We believe that this method will allow the design of tailor-made catalysts with more complex functional groups.

Acknowledgment. We thank A. Camarata for the technical work, along with IRCELYON and IFP scientific services.

Supporting Information Available: Synthetic procedures, characterization data, and molecular modeling results. This material is available free of charge via the Internet at http://pubs.acs.org.

References

(1) (a) Férey, G. *Chem. Soc. Rev.* **2008**, *37*, 191. (b) Farrusseng, D.; Aguado, S.; Pinel, C. *Angew. Chem., Int. Ed.* **2009**, *48*, 7502.
(2) Eddaoudi, M.; Kim, J.; Rosi, N.; Vodak, D.; Wachter, J.; O'Keefe, M.; Yaghi, O. M. *Science* **2002**, *295*, 469.
(3) Eddaoudi, M.; Kim, J.; O'Keeffe, M.; Yaghi, O. M. *J. Am. Chem. Soc.* **2002**, *124*, 376.
(4) Bauer, S.; Serre, C.; Devic, T.; Horcajada, P.; Marrot, J.; Férey, G.; Stock, N. *Inorg. Chem.* **2008**, *47*, 7568.
(5) (a) Yang, C.; Wang, X. P.; Omary, M. A. *J. Am. Chem. Soc.* **2007**, *129*, 15454. (b) Kawano, M.; Kawamichi, T.; Haneda, T.; Kojima, T.; Fujita, M. *J. Am. Chem. Soc.* **2007**, *129*, 15418.
(6) Fischer, R. A.; Woll, C. *Angew. Chem., Int. Ed.* **2008**, *47*, 8164.
(7) Wang, Z. Q.; Cohen, S. M. *Chem. Soc. Rev.* **2009**, *38*, 1315.
(8) Wang, Z. Q.; Cohen, S. M. *Angew. Chem., Int. Ed.* **2008**, *47*, 4699.
(9) Wright, A. P.; Davis, M. E. *Chem. Rev.* **2002**, *102*, 3589.
(10) (a) Brunel, D. *Microporous Mesoporous Mater.* **1999**, *27*, 329. (b) Brunel, D.; Blanc, A. C.; Galarneau, A.; Fajula, F. *Catal. Today* **2002**, *73*, 139.
(11) Wang, Z. Q.; Tanabe, K. K.; Cohen, S. M. *Inorg. Chem.* **2009**, *48*, 296.
(12) Goto, Y.; Sato, H.; Shinkai, S.; Sada, K. *J. Am. Chem. Soc.* **2008**, *130*, 14354.
(13) (a) Gadzikwa, T.; Lu, G.; Stern, C. L.; Wilson, S. R.; Hupp, J. T.; Nguyen, S. T. *Chem. Commun.* **2008**, 5493. (b) Gadzikwa, T.; Farha, O. K.; Malliakas, C. D.; Kanatzidis, M. G.; Hupp, J. T.; Nguyen, S. T. *J. Am. Chem. Soc.* **2009**, *131*, 13613.
(14) Savonnet, M.; Bazer-Bachi, D.; Pinel, C.; Lecocq, V.; Bats, N.; Farrusseng, D. FR Patent 09/05.107, 2009.
(15) Savonnet, M.; Bazer-Bachi, D.; Pinel, C.; Lecocq, V.; Bats, N.; Farrusseng, D. 2009, FR Patent 09/05.101, 2009.
(16) (a) Kitagawa, S.; Tanaka, D. *Chem. Mater.* **2008**, *20*, 922. (b) Seki, K. *Langmuir* **2002**, *18*, 2441. (c) Kitagawa, S.; Kitaura, R.; Noro, S. *Angew. Chem., Int. Ed.* **2004**, *43*, 2334.
(17) Yaghi, O. M.; O'Keeffe, M.; Rosi, N. L.; Kim, J.; Eddaoudi, M.; Chen, B. L. *J. Am. Chem. Soc.* **2005**, *127*, 1504.
(18) Barral, K.; Moorhouse, A. D.; Moses, J. E. *Org. Lett.* **2007**, *9*, 1809.
(19) Savonnet, M.; Bazer-Bachi, D.; Pinel, C.; Lecocq, V.; Bats, N.; Farrusseng, D. FR Patent 09/04.521, 2009.
(20) Savonnet, M.; Bazer-Bachi, D.; Pinel, C.; Lecocq, V.; Bats, N.; Farrusseng, D. FR Patent 09/05.102, 2009.
(21) Ahnfeldt, T.; Guillou, N.; Gunzelmann, D.; Margiolaki, I.; Loiseau, T.; Férey, G.; Senker, J.; Stock, N. *Angew. Chem., Int. Ed.* **2009**, *48*, 5163.
(22) Savonnet, M.; Aguado, S.; Ravon, U.; Bazer-Bachi, D.; Lecocq, V.; Bats, N.; Pinel, C.; Farrusseng, D. *Green Chem.* **2009**, *11*, 1729.
(23) Tanabe, K. K.; Cohen, S. M. *Angew. Chem., Int. Ed.* **2009**, *48*, 7424.

JA909613E

Evaluation of Energy Heterogeneity in Metal−Organic Frameworks: Absence of Henry's Region in MIL-53 and MIL-68 Materials?

Marc Pera-Titus,* Marie Savonnet, and David Farrusseng

Université de Lyon, Institut de Recherches sur la Catalyse et l'Environnement de Lyon (IRCELYON), UMR 5256 CNRS - Université Lyon 1, 2, Av. A. Einstein, 69626 Villeurbanne Cedex, France

Received: May 25, 2010; Revised Manuscript Received: July 23, 2010

We present in this study a detailed thermodynamic analysis of N_2 adsorption at 77.4 K and low pressures in a series of metal−organic framework materials displaying different structures, pore textures, and framework flexibility. The energy heterogeneity of these materials has been quantified using a thermodynamic isotherm model developed in previous studies through two characteristic parameters. This formulation also allows the generation of an equation differing from the Dubinin−Astakhov isotherm that allows a proper description of gas adsorption at low pressures. Unlike zeolites or rigid coordination polymers, highly flexible MIL-53(Al) and MIL-68(In) materials are characterized by N_2 adsorption isotherms lacking of a characteristic Henry's region (linear trend) at low relative pressures. We argue about an unexpected promotion of energy heterogeneity on these materials due to sorbate-induced elastic deformation ascribed to compression tensions to explain this observation.

1. Introduction

A crucial step in the development of adsorption-based technologies is the ability to design and benchmark stable adsorbents with a convenient pore size, pore shape, and surface chemistry. Metal−organic frameworks (MOFs) and more extensively hybrid inorganic−organic coordination polymers have emerged as a new class of "nanoporous" materials to this aim, adding to already existing "classical" adsorbents (e.g., zeolites and carbons[1]).

MOFs are crystalline materials synthesized by self-assembly of organic ligands (linkers) and metal clusters, creating highly regular porous frameworks with different topologies, defined micro- and/or mesopores, and chemical functionalities that can be tuned by modifying the metal group or organic ligand. MOF materials can also be subjected to further postsynthetic modification,[2−4] whereby both the metal unit and the ligand can undergo heterogeneous chemical transformations while keeping the overall crystalline structure of the material. Several reviews have been recently published documenting a vast number of porous MOF structures with varying pore sizes and functionalities, as well as some outstanding adsorption and catalytic properties.[5−15]

The most widely studied MOFs and coordination polymers include the MIL series of Ferey and co-workers,[16−26] relying on stable divalent and trivalent 3d and 4f metal-based carboxylates, terephthalates, phosphates, and phosphonates; the isoreticular MOF (IRMOF) series of Yaghi and O'Keeffe;[27−32] and Cu-BTC or HKUST-1.[33] The original adsorption properties of these materials make them attractive for gas and liquid separation,[11,34] gas storage,[35] and control release.[36]

Unlike zeolites, characterized by relatively rigid frameworks and a high thermal stability ascribed to strong Si−O covalent bonds, MOF materials show an inherent structural flexibility due to their weaker bonds (e.g., Π−Π stacking, hydrogen bonds, and van der Waals interaction) promoting in some cases elastic guest accommodations. According to Kitagawa and co-workers,[37,38] such dynamic porous properties might promote a rich variety of guest-induced structural and reversible phase transitions upon gas adsorption and desorption (either amorphous-to-crystal or crystal-to-crystal transformations) not observed in rigid 3D frameworks. These transitions differ from a classical sorbate rearrangement reported in certain zeolite−guest systems such as *p*-xylene/silicalite-1. Another guest-related property of flexible MOFs is the dynamic rotation of bridging ligands, which might be reversibly affected by adsorption/desorption of guest molecules without involving geometrical changes.[38,39]

The above stated structural changes in flexible MOFs are at the origin of anomalous adsorption isotherm patterns (either in the presence of polar or nonpolar sorbates) such as the so-called "gate opening" and "breathing" phenomena. On the one hand, gate-opening phenomena are characterized by a large hysteresis loop between the adsorption and desorption curves due to an abrupt transition between a nonporous state and a porous crystalline phase promoted by guest accommodation. On the other hand, breathing phenomena are characterized by an abrupt expansion of the unit cell upon adsorption (the unit cell parameters can suffer variations >5 Å) due to guest-induced crystal-to-crystal transformations. A paradigmatic example of breathing phenomena can be found in the MIL-53 material, exhibiting an abrupt phase transition upon water[19] and CO_2[40] adsorption (and to a lesser extent upon adsorption of C1−C9 *n*-alkanes[41]), resulting in a ca. 38% unit cell expansion. This transition is accompanied by a prominent inflection in the CO_2 isotherm (S-shape) at about 6 bar and 304 K.[40] The difference in free energy between the low- and high-pressure phases (lp → hp) has been estimated to about 2.5 kJ/mol per unit cell for MIL-53(Cr,Al).[42] Serre et al.[43] have attributed the large breathing effect observed in the MIL-53 structure to strong guest−guest bonds along the tunnels created by the sorbate species, acting as a backbone for the onset of symmetrical interactions (usually with the interplay of OH surface groups) with two opposite chains of the framework.

The potential technological impact of MOF materials makes the development of suitable isotherm models for describing gas/

* Corresponding author. Phone: +33 (0) 472445368. Fax: +33 (0) 472445399. E-mail: marc.pera-titus@ircelyon.univ-lyon1.fr.

10.1021/jp104788p
Published on Web 09/20/2010

vapor adsoption imperative. By now, most of the studies dealing with adsorption properties of MOFs have been aimed at providing a materials screening and ranking for target separations. A series of simulation studies has also elucidated the main interactions and adsorption mechanisms in MOF materials, as well as the thermodynamic basis for double structural transitions in MOFs upon adsorption (see, for instance, refs 44−54). However, only a scarce number of studies have been reported to date discussing the suitability of transposing well-known concepts of gas/vapor adsorption in "robust" zeolites and activated carbons to hybrid polymer materials. This analysis appears to us crucial on the basis of the great elasticity of some MOF structures, as well as their ultrahigh specific surface areas, attaining values as high as 4000 m^2/g for MIL-100[22] and MOF-177.[30] These specificities pose obvious questions on the compatibility of the classical Brunauer−Emmett−Teller (BET) theory[55] for measuring specific surface areas on these materials, as well as the classical Dubinin−Radushkevich (DR) and Dubinin−Astakhov (DA) isotherms[56] usually applied to the description of gas adsorption in carbonaceous materials and zeolites. Both points are fundamental not only for a proper characterization of MOF materials but also for an accurate prediction of their adsorption (and surface diffusion) properties in industrially relevant separations.

This first point has been partially elucidated by Walton and Snurr[57] in a recent study. These authors have demonstrated that BET analysis provides consistent specific surface areas in a series of simulated IRMOF materials compared to accessible surface areas calculated geometrically from crystal structures, even if the dominating adsorption mechanism in MOFs is pore filling as in the case of zeolites or microporous carbons. However, no indication about the role of framework distortion effects on the measured BET surfaces was addressed.

This paper is aimed at providing a critical assessment on the second aforementioned point, namely, on the applicability of the DR and DA isotherms for describing gas/vapor adsorption in MOF materials, which to our knowledge has not been treated yet in detail. Moreover, this paper is also intended to provide a detailed analysis of energy heterogeneity in both robust and flexible MOFs using the original thermodynamic isotherm developed in previous studies from solution thermodynamics first principles[58,59] and validated for zeolite materials. Briefly, this formulation relies on a "scaling law" representation of the integral free energy of adsorption relative to saturation, $-\Psi/RT$, computed as a Kiselev integral, against the variable $Z = 1/-\ln(\Pi)$, being $\Pi = P/P_0$

$$-\frac{\Psi}{RT} = \int_\theta^1 -\ln(\Pi)\delta\theta \int_\theta^1 Z^{-1}\delta\theta = \frac{G^\circ}{1 + kZ^m} \quad (1)$$

with $G^\circ = -\Phi(P^\circ)/RT$ and $k = [-\ln(\Pi_k)]^m = Z_k^{-m}$, with $\Phi(P^\circ)$ being the surface potential at saturation pressure and Π_k the Π value accounting for a sorbate integral free energy relative to saturation equaling $G^\circ/2$.

Parameter m can be linked to the energy heterogeneity (or energy distribution) of the adsorbent, providing information about molecular packing in micropores. We have identified two different potential trends in the adsorption pattern of zeolites for a wide series of sorbates and temperatures, characterized each by two different m values (i.e., m_1 and m_2). Parameter m_1 has been linked to sorbate confining effects in zeolites.[60] In the case of parameter m_2, this can be linked to the characteristic α exponent of the DA isotherm at $\Pi > 0.01$ in a simple way ($\alpha = m - 1$),[58] providing information about the energy heterogeneity of the solid−guest system at high sorbate loadings.

In a further study,[61] we have proposed a modified version of eq 1, taking into account explicitly the contribution of both potential trends

$$-\frac{\Psi}{RT} = \int_\theta^1 Z^{-1}\delta\theta = \frac{G^o}{1 + \dfrac{\lambda_1\lambda_2}{\lambda_1 + \lambda_2}} \quad (2)$$

where $\lambda_1 = k_1 Z^{m_1}$ and $\lambda_2 = k_2 Z^{m_2}$, with $m_1 > m_2$ and $k_1 \gg k_2$ in the case of zeolites.

Equation 2 allows the derivation of two analytical expressions describing gas adsorption in two limiting pressure zones:

$$\theta = G^\circ k_1 \left(\frac{Z^{m_1+1}}{1 + k_1 Z^{m_1}}\right) \quad \text{for} \quad 1/\lambda_1 \le 1 \quad (3)$$

$$\theta = 1 - \frac{G^\circ}{k_1}\frac{m_1}{(m_1 - 1)}Z^{-(m_1-1)} - \frac{G^\circ}{k_2}\frac{m_2}{(m_2 - 1)}Z^{-(m_2-1)} \quad \text{for} \quad Z_\beta \ll Z < 1 \quad (4)$$

We have shown that eq 3, accomplished at relative pressures $<10^{-3}$ for a great variety of zeolite−guest systems, includes implicitly Henry's region (linear trend between the surface coverage and pressure) in zeolites. In the case of eq 4, this expression can be simplified into eq 5 for relative pressures >0.1, being formally equivalent to a McLaurin development of the DA isotherm (see ref 61 for further details).

$$\theta = 1 - \frac{G^\circ}{k_2}\frac{m_2}{(m_2 - 1)}Z^{-(m_2-1)} \quad (5)$$

Keeping these ideas in mind, this themodynamic formulation will be used here to compare the adsorption pattern of robust and flexible MOF materials to that of zeolites at low pressures, as an attempt to characterize in detail Henry's region. The set of eqs 3−5 will be used for a comprehensive characterization of Henry's region in MOF materials through the evaluation of the heterogeneity of the system at low pressures, overcoming the intrinsic limitations of the DA isotherm in this region. We will also discuss in detail the structure-related variation of energy heterogeneity of relatively elastic MOF materials.

2. Materials and Methods

2.1. Chemicals. All chemicals were used as received without any further purification: zinc nitrate tetrahydrate, $Zn(NO_3)_2 \cdot 4H_2O$ (Merck, 98.5%); zinc nitrate hexahydrate, $Zn(NO_3)_2 \cdot 6H_2O$ (Riedel-de-Haën, pure); indium nitrate, $In(NO_3) \cdot 4H_2O$ (Alfa Aesar, 99.99%); aluminum chloride hexahydrate, $AlCl_3 \cdot 6H_2O$ (Sigma-Aldrich, 98%); 2-aminoterephthalic acid, NH_2-bdc (Alfa Aesar, 99.0%); terephthalic acid, bdc (Sigma Aldrich, 98%); 1,4-diazabicyclo[2.2.2] octane, DABCO (Sigma-Aldrich, 98.0%); triethylamine, Et_3N (Riedel-de-Haën, pure); sodium hydroxyde, NaOH (Sigma-Aldrich, 98%); *N*,*N*′-dimethylformamide, DMF (Sigma-Aldrich, 99.8%); dichloromethane, CH_2Cl_2 (Acros Organics, 99.99%); THF (Sigma-Aldrich, 99.0%); methanol, MeOH (Sigma-Aldrich, 99%).

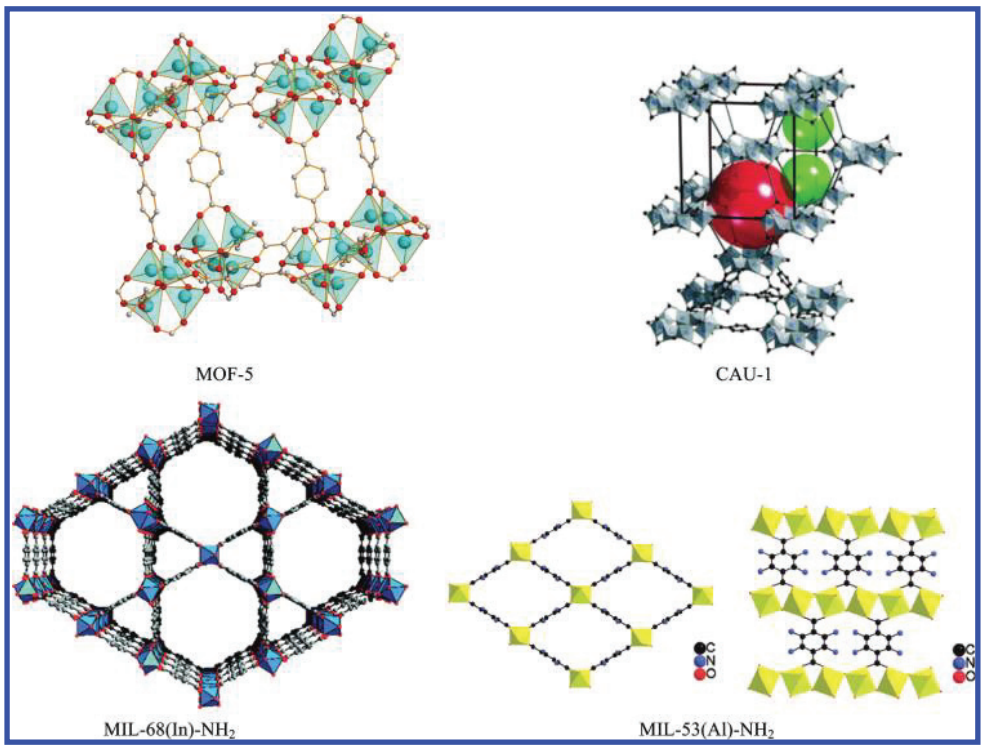

Figure 1. Structure of the MOF materials prepared in this study.

TABLE 1: Main Structural and Textural Properties of the MOF Materials Prepared in This Study and Zeolites Used as Reference Materials

MOF denomination	structure	pore channel	pore size	cell parameters	molecular weight (g/mol)	BET surface area (m^2/g)	pore volume (cm^3/g)	references
MOF-5	3D	3D	8 Å	cubic ($Fm\bar{3}m$) $a = b = c = 25.67$ Å	813	450	0.32	this study
CAU-1	3D	3D	10 Å + 4.5 Å	tetragonal ($I4/mmm$) $a = b = 1.835$ Å, $c = 1.777$ Å	803	810	0.42	this study
MIL-68(In)-NH_2	3D	1D	6 Å + 17 Å	orthorhombic ($Cmcm$) $a = 21.774$ Å, $b = 37.677$ Å, $c = 7.233$ Å	311	1260	0.58	this study
MIL-53(Al)-NH_2	3D	1D	8.5 Å	monoclinic system (Cc) $a = 19.702$ Å, $b = 7.764$ Å, $c = 6.592$ Å	223	1155	0.57	this study
NaY (Si/Al = 25)	3D	3D	7.4 + 12 Å	cubic system ($Fd\bar{3}m$) $a = b = c = 24.345$ Å	2172	337	0.099	BAM[a]
HZSM-5 (Si/Al = 500)	3D	3D	5.3 + 5.5 Å	orthorhombic system ($Pnma$) $a = 20.090$ Å, $b = 19.738$ Å, $c = 13.142$ Å	6056	∼350	∼0.20	62

[a] Data supplied by the Federal Institute for Materials Research and Testing (BAM, Unter den Eichen 87, 12205-Berlin, Germany).

2.2. Materials Synthesis and Characterization. Four different MOF structures were solvothermally synthesized following well-established protocols reported in the literature: "MOF-5-like", CAU-1, MIL-68(In)-NH_2, and MIL-53(Al)-NH_2. The synthesis protocols, as well as the final structures obtained (see Figure 1), are described below. Table 1 summarizes the main structural and textural properties of these materials.

2.2.1. "MOF-5-like" Material. The MOF-5-like material (simply referred hereinafter as MOF-5) was prepared according to a procedure reported by Mueller et al.[63] Typically, 8.32 g (31.824 mmol) of $Zn(NO_3)_2 \cdot 4H_2O$ and 1.76 g (10.594 mmol) of 1,4-benzenedicarboxylic acid (H_2dbc) (Sigma-Aldrich 99.7%) were dissolved in 100 mL of dried diethylformamide (DEF). The solution was heated at 100 °C in a Teflon-lined autoclave, the solid filtered off, washed, and finally exchanged with $CHCl_3$ under Ar flow. Finally, the material was evacuated and stored in a glovebox.

The MOF-5 framework (cubic system, $Fm3m$ space group with $a = b = c = 25.67$ Å[64]) consists of Zn_4O tethrahedral subunits linked in octahedral arrays by bdc groups to form a porous material with channel windows of about 8 Å. The Zn edges of the tetrahedra are bridged by six carboxylate groups forming octahedral nodes, linked to one another with 1,4-phenylene groups of the bdc linker, resulting in a 3D cubic network. Further information about the characterization of our MOF-5-like material can be found in ref 65.

2.2.2. CAU-1. CAU-1 was synthesized from 2-aminotereph-thalic acid using the procedure described in ref 66. A mixture of aluminum chloride (1.513 mmol) and NH_2-bdc (0.521 mmol) was suspended in MeOH (10 mL) and heated at 125 °C for 5 h. After filtration, a yellow microcrystalline product was obtained. The crystals were washed three times with MeOH and with DMF at 160 °C and then soaked in dichloromethane for 24 h. After drying at room temperature, the mass of dried CAU-1 obtained was 90 mg.

The CAU-1 framework (tetragonal system, $I4/mmm$ space group, $a = b = 1.835$ Å, $c = 1.777$ Å) is built up from a pseudobody-centered-cubic arrangement of 8-ring building blocks $\{Al_8(OH)_4(OCH_3)_8\}^{12+}$ linked by 12 aminoterephthalate ions. The wheel-shaped 8-rings are built from corner- and edge-sharing AlO_6 octahedra through hydroxide and methoxide groups. The Al(III) is coordinated to three carboxylate oxygen atoms, one hydroxide, and two methoxide ions. Each wheel is connected to 12 other units by aminoterephthalate linkers with four linkers in the plane of the 8-rings as well as four above and below the ring. Hence, a 3D microporous framework is

formed with two types of cages, distorted octahedral and distorted tetrahedral, with effective diameters of 10 and 4.5 Å, respectively.

2.2.3. MIL-68(In)-NH$_2$. MIL-68(In)-NH_2 has been prepared following the protocol presented in a recent patent.[67] It was obtained by precipitation reaction in a Pyrex beaker (capacity 100 mL) of a mixture of 4.82 mL (4.14 mmol) of 0.86 M indium nitrate in DMF and 10.06 mL (3.32 mmol) of 0.33 M 2-aminoterephthalic acid (NH_2-bdc) in DMF. The reaction mixture was stirred for 5 min, and then, 4.83 mL (6.67 mmol) of 1.38 M dabco in DMF was added. The reaction mixture was stirred for 2 h at room temperature. The obtained precipitate was washed with DMF at 160 °C and soaked in CH_2Cl_2 for 24 h. The mass of dried MIL-68(In)-NH_2 obtained was 0.88 g.

The MIL-68(In)-NH_2 framework (orthorhombic system, *Cmcm* space group, $a = 21.774$ Å, $b = 37.677$ Å, $c = 7.233$ Å) is built up from infinite straight chains of metal-centered $InO_4(OH)_2$ octahedra connected to each other through the NH_2-dbc ligands, generating 1D channels. The octahedral units are linked together via two hydroxyl groups located in *trans* positions, two adjacent octahedra also being connected via the carboxylate functions. These corner-sharing octahedral species MO_6 form a network of three- and six-membered windows, generating two types of channels with diameter openings of 6 and 17 Å, respectively, for the triangular and hexagonal rings.

2.2.4. MIL-53(Al)-NH$_2$. The synthesis of MIL-53(Al)-NH_2 was adapted from the procedure described in ref 68. 2-Aminoterephthalic acid (NH_2-bdc, 0.66 mmol) was suspended in water (28 mL, 1.55 mmol) in a 40 mL Teflon-lined SS digestion bomb. Then, 1.10 mL (0.44 mmol) of a 0.4 M aluminum chloride solution and 0.56 mL (0.22 mmol) of a 0.4 M NaOH solution were added. The reaction mixture was heated for 24 h without stirring at 110 °C. The final precipitate was washed with deionized water and DMF at 160 °C and then soaked in CH_2Cl_2 for 24 h. After drying at 80 °C, the mass of dried MIL-53(Al)-NH_2 obtained was 0.4 g.

The MIL-53(Al)-NH_2 framework (monoclinic system, *Cc* space group, $a = 19.702$ Å, $b = 7.764$ Å, $c = 6.592$ Å) is built up from chains of corner-sharing Al(III) octahedra connected by μ_2-OH and carboxylate groups. These chains are connected by aminoterephthalate ions to form a 1D rhomboedral-shape channel system. The combination of these chains allows the formation of three different 3D frameworks. In MIL-53 (as), the tunnels (7.3 Å × 7.7 Å) are occupied by disordered NH_2-bdc template molecules. The total removal of the template upon heating at 275 °C generates the MIL-53(ht) form showing empty pores of 8.5 Å × 8.5 Å. The reversible adsorption of water at room temperature gives rise to MIL-53(lt) with channel dimensions of 2.6 Å × 13.6 Å. Here, the MIL-53(Al)NH_2(lt) framework was prepared.

2.3. Adsorption Measurements. The MOF materials prepared in this study were characterized by N_2 adsorption at 77.4 K using a BELSORP max porosimeter. In the low-pressure region ($\Pi < 10^{-2}$), the adsorption measurements were carried out by doses of 3−6 cm^3(STP)/g with equilibrium times in the range 1620−3600 s. Care was taken of the absence of diffusional limitations in the adsorption measurements, especially at low pressure. Prior to the gas adsorption/desorption tests, the samples were subjected to an outgassing protocol under secondary vacuum at 100−200 °C for 12−48 h to remove adsorbed moisture and vapors. Helium was used as backfill gas to measure the freespace volume of the cell before the N_2 adsorption measurements. BET specific surfaces were determined from

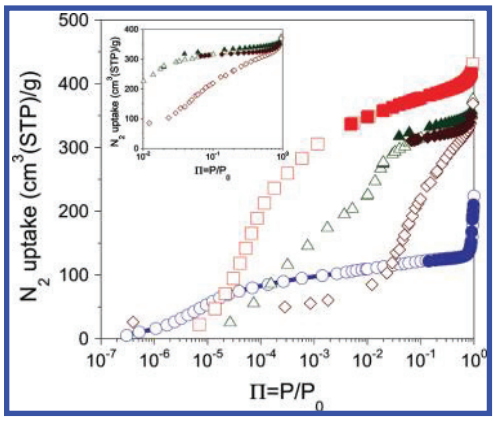

Figure 2. Adsorption isotherms of N_2 at 77.4 K on MOF-5 (○), CAU-1 (□), MIL-68(In)-NH_2 (△), and MIL-53(Al)-NH_2 (◇).

recorded adsorption data at $0.05 \leq \Pi \leq 0.25$, while the pore volume was determined from the N_2 adsorbed volume at $\Pi = 0.99$.

2.4. Calculation Details. The relevant parameters of the thermodynamic isotherm were obtained by fitting eq 2 to experimental N_2 adsorption data at 77.4 K. To improve the quality of the fittings, eq 2 was reduced to the following simplified expressions accounting for the low and high pressure domains

Low pressure region:

$$-\frac{\Psi}{RT} = \frac{G^\circ}{1 + (Z/Z_k)^{m_1}} \tag{6}$$

High pressure region:

$$-\frac{\Psi}{RT} = \frac{G^\circ}{k_2} Z^{-m_2} \tag{7}$$

with $Z_k = 1/-\ln(\Pi_k) = k_1^{-1/m_1}$ being the Z value corresponding to a sorbate integral free energy relative to saturation equaling $G^\circ/2$. Equation 6 can be rewritten as follows

$$\left(\frac{G^\circ}{-\Psi/RT} - 1\right) = \left(\frac{Z}{Z_k}\right)^{m_1} = kZ^{m_1} \tag{8}$$

The set of parameters in eq 6 (m_1, Z_k) and eq 7 (m_2, k_2) were fitted using a least-squares nonlinear optimization method based on the Levenberg−Marquardt algorithm by comparison of predicted and experimental pure adsorption data. The parameter G° has been kept constant in the fittings, its value being computed directly from the *raw* isotherms through the integral

$$G^\circ = \int_0^1 -\ln(\Pi)\delta\theta = \int_0^1 Z^1 \delta\theta \tag{9}$$

3. Results and Discussion

3.1. N_2 Adsorption/Desorption Patterns in MOFs. Figure 2 shows the N_2 adsorption/desorption isotherms at 77.4 K obtained on the MOF materials synthesized in this study. In good keeping with the adsorption pattern of zeolites, MOF-5 and CAU-1 "robust" frameworks show a sharp adsorption trend at relatively low N_2 pressures (type I isotherm), the first adsorption loadings being obtained for relative pressures $<10^{-5}$. The adsorption/desorption curves are entirely reversible, as is

usually the case encountered in zeolites in the absence of integranular condensation.

In the case of MIL-53(Al)-NH_2 material, however, a subtle step can be observed at $P/P_0 \sim 2 \times 10^{-3}$, suggesting a guest-induced structural transformation. This idea is reinforced by the intense adsorption/desorption hysteresis loop observed for this material. A hysteresis loop is also observed for MIL-68(In)-NH_2 but is less pronounced. These irreversibilities can be tentatively attributed to breathing of both flexible MIL-53 and MIL-68 frameworks upon N_2 adsorption, leading to a sorbate-induced phase transition involving partial swelling of the structures due to guest accommodation. This hysteresis provides a first evidence of the energy heterogeneity of the adsorption centers in these frameworks compared to "robust" structures due to a structural modification upon adsorption.

3.2. Applicability of the DA Isotherm to the Description of Gas Adsorption in MOFs. The DA equation, originally derived by Dubinin and co-workers from the volume filling theory of micropores (TVFM) for "robust solids" assuming a Polanyi's adsorption potential, A, relates the surface coverage of the sorbate with the relative pressure by a "temperature-invariant" potential function including three characteristic parameters, i.e., $E°$, α, and β.[56,69]

$$\theta = \exp\left\{-\left[\frac{A}{\beta E°}\right]^{\alpha}\right\} = \exp\left\{-\left[-\frac{RT}{\beta E°}\ln(\Pi)\right]^{\alpha}\right\} \quad (10)$$

where α is a characteristic exponent (α = 2 in the case of the DR isotherm), $E°$ is the adsorption energy, and β is the so-called "affinity coefficient", being usually taken as a constant characteristic of the sorbate and being used as a scaling factor to bring the characteristic curves of different sorbates into coincidence with that or a reference one (e.g., benzene in the case of activated carbons).

The characteristic α exponent (usually in the range 1.0−2.5 for zeolites) and the adsorption energy, $E°$, of the DA isotherm can be linked to the degree of surface heterogeneity of the material (e.g., presence of surface impurities, sites of different energies, different micropore sizes) through the formulation of Gaussian (or one-parameter Weibull) distribution functions.[69] We expect here that the energy heterogeneity of the adsorption sites of a material can also be ascribed, at least partially, to a sorbate-induced elastic deformation, either attributed to local flexibility or to the bistability of the structure.

Equation 10 can be transformed for plotting into eq 11

$$\ln[-\ln(\theta)] = D + \alpha \ln[-\ln(\Pi)] \quad (11)$$

where $D = \alpha\ln(RT/\beta E°)$. The DA plot of $\ln[-\ln(\theta)]$ against $\ln[-\ln(\Pi)]$ should be a straight line having an intercept equal to D, while from the slope, the value of the characteristic α exponent is obtained.

Figure 3 shows the fitting of eq 11 to N_2 adsorption data at 77.4 K for the collection of MOF materials prepared in this study, as well as the two zeolites (NaY and ZSM-5) used here as reference materials. As can be deduced from Figure 3A, irrespective of the material, the DA isotherm fails to predict the adsorption behavior at low pressures ($\Pi < 0.1$). As a matter of fact, differentiated linear trends with different slopes can be clearly sorted out in this region. According to the classification proposed by Marsh and Rand,[70] this observation suggests A-type deviations at low pressures from the DA predicted pattern for both zeolites and MOFs. In the case of zeolites, however, the

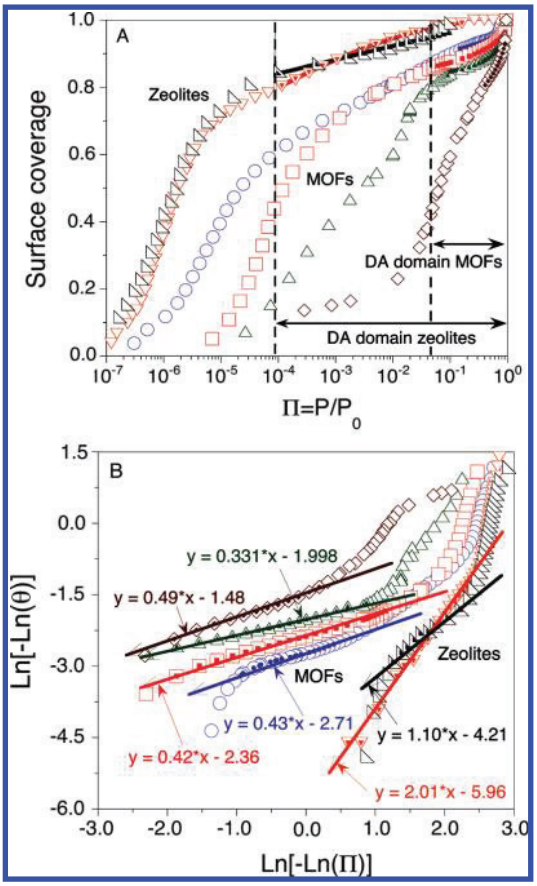

Figure 3. Adsorption isotherms of N_2 at 77.4 K on MOF-5 (○), CAU-1 (□), MIL-68(In)-NH_2, (△) MIL-53(Al)-NH_2 (◇), and reference materials NaY (▽) and HZSM-5 (left-pointing triangles). The straight curves on top reflect the range of applicability of the DA isotherm for MOFs and zeolites, while the straight lines on bottom correspond to the fittings of the DA isotherm (eq 7) at high relative pressures.

domain of application of eq 7 can be extended to relative pressures up to 10^{-4} (see Figure 3B), about 3 orders of magnitude higher than that of CAU-1. In any case, as can be deduced from Figure 3, the DA isotherm is not applicable in Henry's region, this appearing in the case of N_2 adsorption at 77.4 K in an extremely narrow range of low relative pressures, usually less than one decade.

3.3. Energy Heterogeneity in MOFs. The fact that the DA equation does not completely describe the adsorption behavior in MOFs and zeolites at low pressures can be explained in terms of different energy heterogeneities of the materials as a function of pressure. As a matter of fact, as can be inferred from the fittings plotted in Figure 3B, the slopes obtained for zeolites NaY and HZSM-5 are much higher than those corresponding to the MOF materials considered here. This suggests that, at high loadings, adsorption centers in MOFs are more heterogeneous than those in zeolites upon adsorption, namely, molecular confinement in MOFs alters the energy distribution of the material (in the case of N_2 essentially nonspecific) to a higher extent than in the case of zeolites.

More insight about the energy heterogeneity level of MOF materials can be gained by means of the thermodynamic isotherm formulation defined by eq 2. Figure 4 shows the thermodynamic representations obtained for the different MOF materials considered here, while Table 2 collects the main data obtained from the fittings. In all cases, two different potential trends can be distinguished, in good keeping with the results plotted in Figure 3B, matching the general qualitative behavior

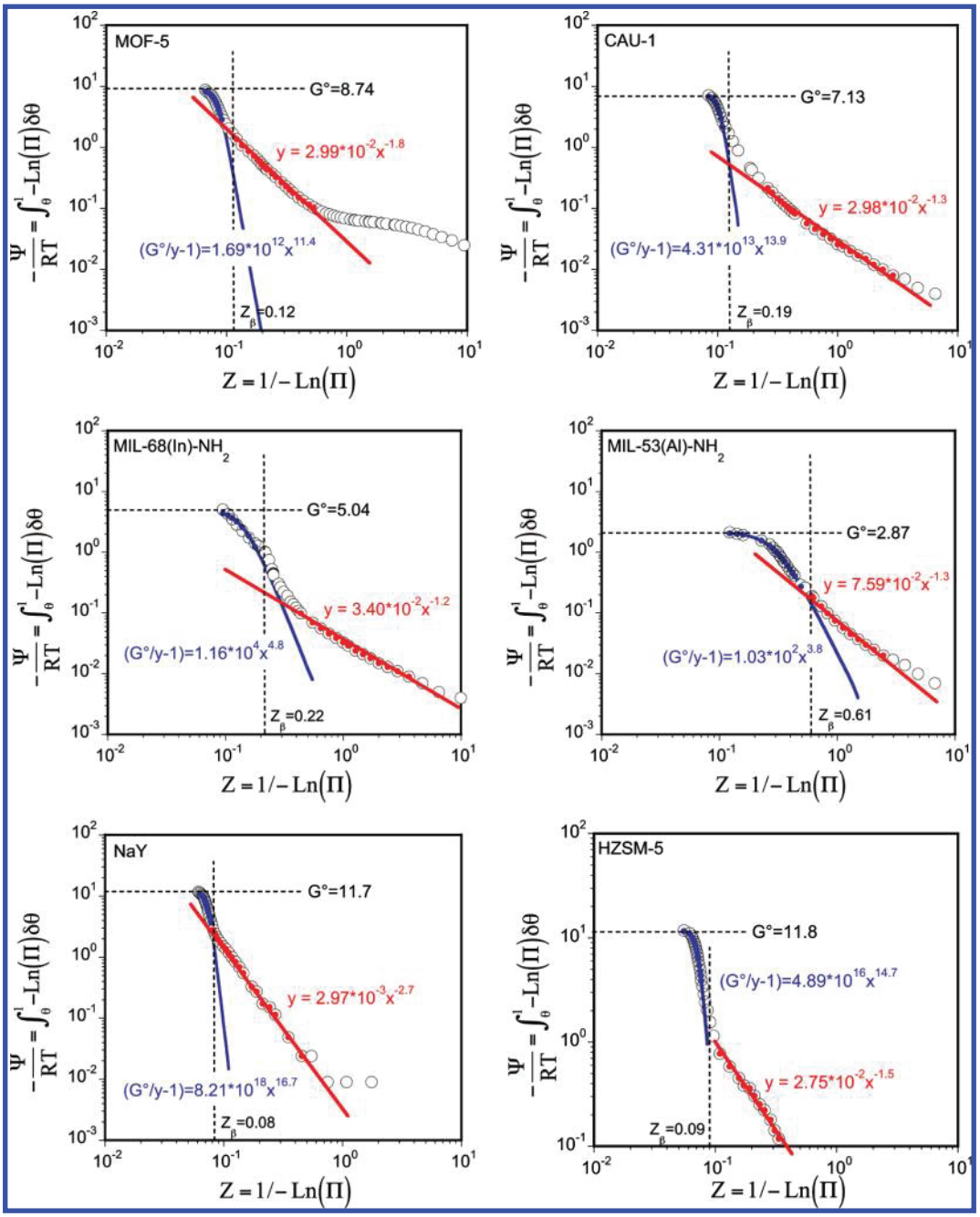

Figure 4. Representations of the thermodynamic isotherm (eq 2) for N_2 adsorption at 77.4 K on the collection of MOF materials prepared in this study and zeolites NaY and HZSM-5. The straight lines correspond to the fittings of eqs 6 and 7, respectively, at low and high relative pressures.

TABLE 2: Fitted Parameters of the Thermodynamic Isotherm Corresponding to the First and Second Potential Zones for Some MOF Materials and Reference Zeolites

				first potential trend			second potential trend		
notation	sorbate	T (K)	$G°$	m_1	Z_k	k_1	m_2	k_2	references
MOF-5	N_2	77.4	8.74	11.4 ± 0.6	$(8.5 \pm 0.1) \times 10^{-2}$	$(1.7 \pm 0.5) \times 10^{12}$	1.8 ± 0.1	$(2.9 \pm 0.1) \times 10^{2}$	this study
CAU-1	N_2	77.4	7.13	13.8 ± 0.6	$(1.0 \pm 0.1) \times 10^{-1}$	$(4 \pm 1) \times 10^{13}$	1.3 ± 0.1	$(2.9 \pm 0.1) \times 10^{2}$	this study
MIL-68In-NH_2	N_2	77.4	5.04	4.8 ± 0.1	$(1.4 \pm 0.2) \times 10^{-1}$	$(1.1 \pm 0.5) \times 10^{4}$	1.2 ± 0.1	$(1.5 \pm 0.2) \times 10^{2}$	this study
MIL-53Al-NH_2	N_2	77.4	2.87	3.6 ± 0.1	$(3.0 \pm 0.3) \times 10^{-1}$	$(1.0 \pm 0.5) \times 10^{2}$	1.3 ± 0.1	$(3.8 \pm 0.5) \times 10^{1}$	this study
NaY (Si/Al = 25)	N_2	77.4	11.71	16.7 ± 0.5	$(7.4 \pm 0.1) \times 10^{-2}$	$(8 \pm 1) \times 10^{18}$	2.7 ± 0.1	$(4 \pm 1) \times 10^{3}$	BAM[a]
HZSM-5 (Si/Al = 500)	N_2	77.4	11.80	15 ± 3	$(7.3 \pm 0.1) \times 10^{-2}$	$(4.9 \pm 0.7) \times 10^{16}$	1.5 ± 0.1	$(7 \pm 1) \times 10^{2}$	62

[a] Data supplied by the Federal Institute for Materials Research and Testing (BAM, Unter den Eichen 87, 12205-Berlin, Germany).

observed for zeolites. Both potential trends can be characterized by two different m slope values (i.e., m_1 and m_2) in such a way that $m_1 > m_2$, suggesting a different pore filling pattern at the early stage of adsorption and at high loadings.

For all the MOF materials tested, the m_2 values show similar values, lying in the narrow range 1.2−1.8, these values being comparable to those obtained in zeolites. In the case of parameter m_1, the most rigid MOFs, i.e., MOF-5 and CAU-1, show values slightly lower than those measured on zeolites NaY and HZSM-5 but keeping consistent with what is expected for a rigid material with relatively homogeneous adsorption strengths. In contrast, in the case of MIL-53(Al)-NH_2 and MIL-68(In)-NH_2 materials, much lower values for parameter m_1 are obtained ($m_1 < 5$). These low values are classically attributed to sites displaying different adsorption strengths, as is usually the case of carbon materials (see ref 58 for further information). In contrast, we attribute the higher degree of heterogeneity of the MIL materials considered here to their comparably more flexible structures, especially in the case of MIL-53(Al)-NH_2, as evidenced from the broad hysteresis loop between the N_2 adsorption/desorption curves even at cryogenic temperatures (see Figure 2). In the case of MIL-68(In)-NH_2, with a more robust framework than that for MIL-53(Al)-NH_2 and thus less susceptible to breathing phenomena, we cannot exclude a source of heterogeneity ascribed to a much higher number of potential adsorption sites with comparable adsorption strengths (see Figure 1) but subjected to a different order pattern (i.e., entropy effects).

As we have discussed in a previous study,[58] parameter m_1 provides a picture of the energy heterogeneity of the *raw* material for a given type of sorbate−sorbent interaction (e.g., nonspecific). In contrast, parameter m_2 provides information about the energy heterogeneity of the adsorbent partially filled with the sorbate, being subjected to sorbate−sorbate interactions that might alter the inherent heterogeneity of the material. We have already demonstrated that the DA isotherm is intrinsically consistent with eq 1 (and eq 2), the characteristic α exponent of this isotherm being linked to parameter m_2 of the thermodynamic isotherm by the expression $m_2 = \alpha + 1$), but not to parameter m_1. As we have stated above, the consistency between both isotherms vanishes at low relative pressures ($\Pi < 0.1$ in MOFs and $\Pi < 0.01$ for zeolites), reflecting the intrinsic limitations of the DA equation at reduced loadings. The fundamental relationship between parameters m_2 and α is confirmed by the results presented in Table 2. This expression confirms the underlying dependence of the α exponent of the DA isotherm on the energy heterogeneity of a microporous system.

The narrow domain of application of the DA isotherm to the description of vapor adsorption in MOF materials, limited in practice to $\Pi > 0.1$, can be broadened using the set of eqs 3 and 4 deduced from the thermodynamic isotherm formulation, accounting for, respectively, the low- and high-pressure adsorption domains. Figure 5 shows the fittings of both equations to the experimental N_2 adsorption data at 77.4 K using the m and k parameter values obtained from the corresponding representations of the thermodynamic isotherm. In all cases, the isotherms represent accurately the experimental data both at low and high pressures, improving the description level of the original DA isotherm and modified versions of this isotherm with adequate low-pressure corrections.[71−73]

3.4. Compressive Tensions in MOFs. In the previous section, we have advanced the hypothesis of an effect of framework distortion, most probably due to a phase transition, on the promotion of the heterogeneous character of MIL-68(In)-NH_2 and MIL-53(Al)-NH_2 materials upon N_2 adsorption at 77.4 K. Our purpose here is to rationalize the much higher elastic deformation of these materials compared to MOF-5 and CAU-1

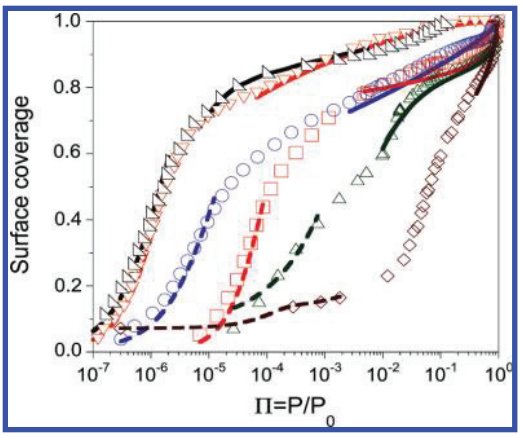

Figure 5. Adsorption isotherms of N_2 at 77.4 K on MOF-5 (○), CAU-1 (□), MIL-68(In)-NH_2 (△) MIL-53(Al)-NH_2 (◇), and reference materials NaY (▽) and HZSM-5 (left-pointing triangles). The dashed and straight lines correspond to the fittings of eqs 3 and 4, respectively, for the low and high relative pressures domains.

and conventional zeolites triggered by the presence of comparably higher structural stresses.

On the guidance of the recent study reported by Neimark et al.,[74] the tension exerted by a sorbate on the adsorbent framework, σ, can be computed from the variation of the grand thermodynamic potential (or surface potential within the framework of solution thermodynamics) of the sorbate with the unit cell volume at a given temperature and constant chemical potential, that is

$$\sigma = -\frac{\delta\Phi}{\delta V_c}\bigg|_{T,\mu} \tag{12}$$

The surface potential can be computed by eq 13 (see ref 58)

$$\frac{\Phi}{q_M RT} = -\int_0^{\Pi} \theta\delta\,\ln(\Pi) = -\int_0^{Z} \frac{\theta}{Z^2}\delta Z < 0 \tag{13}$$

At low pressures ($1/_1 \leq 1$), the surface potential can be computed introducing eq 3 into eq 13

$$\frac{\Phi}{q_M RT} = -\frac{G^\circ}{m_1}\ln(1 + k_1 Z^{m_1}) \tag{14}$$

Introducing eq 14 into eq 12, an expression can be obtained accounting for the stress experienced by the solid at low pressures as a function of the parameters G°, m_1, and k_1 of the thermodynamic isotherm adsorption parameters

$$\sigma = RT\frac{q_M G^\circ}{m_1}\frac{\delta[\ln(1 + k_1 Z^{m_1})]}{\delta V_c} = RT\frac{q_M G^\circ}{m_1}\frac{Z^{m_1}}{(1 + k_1 Z^{m_1})}\frac{\delta k_1}{\delta V_c}_{T,Z} < 0 \tag{15}$$

In the derivation of eq 15, we have implicitly assumed that the unit cell volume variation does not affect the saturation loading of the material (weak assumption for sufficiently low relative pressures).

Equation 15 reflects that, since $\delta k_1/\delta V_c < 0$, the framework tension is negative at low pressures, causing sample contraction

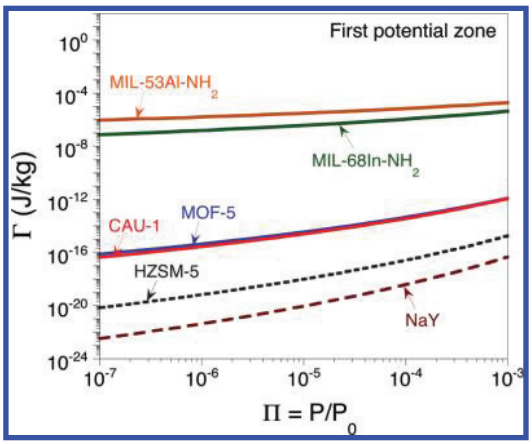

Figure 6. Evolution of parameter Γ, ascribed to the compression tension for a constant $\delta k_1/\delta V_c$, as a function of the relative pressure for the different MOF solids and zeolites tested in this study.

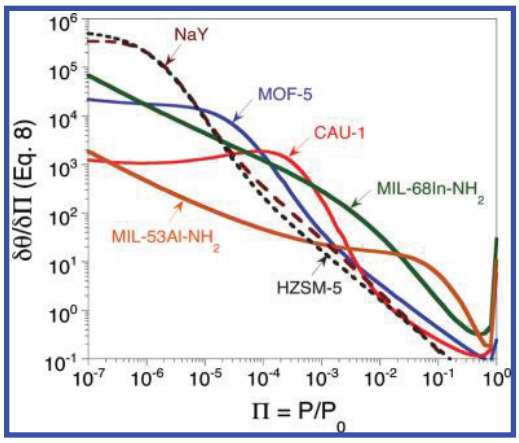

Figure 7. Evolution of the slope of the isotherms plotted in Figure 4 for the different MOFs and zeolites obtained by fitting of eq 10 as a function of the relative pressure.

upon adsorption. Taking into account that the derivative $\delta k_1/\delta V_c$ is hardly measurable, a parameter Γ can be defined from eq 15 as a measure of the compression stress of the framework

$$\Gamma(T,Z) \equiv \frac{\delta\Phi/\delta V_c|_{T,Z}}{\delta k_1/\delta V_c|_{T,Z}} = RT\frac{q_M G^\circ}{m_1}\frac{Z^{m_1}}{(1+k_1 Z^{m_1})} > 0 \quad (16)$$

Figure 6 plots the evolution of parameter Γ computed from eq 16 as a function of the relative pressure for low pressures, corresponding to the first potential zone of the thermodynamic isotherm (i.e., $\Pi < 10^{-3}$), for the collection of MOF solids and reference zeolites considered in this study. In all cases, the parameter Γ increases with the applied pressure, reflecting higher compressive tensions. It is noteworthy that, when comparing the trends observed for the different solids, much higher Γ values for MIL-type materials are obtained unlike the other MOF and zeolite solids (up to 17 orders magnitude difference!). Although the elastic coefficients of MOF materials are unknown, these allowing the translation of surface tensions into deformations following the standard elastic theory (Young equation in the case of linear deformation), we feel entitled to propose that sorbate-induced framework deformation, most probably linked to a phase transition, is at the basis of the observed heterogeneity of MIL-68(In)-NH_2 and MIL-53(Al)-NH_2 solids, involving abnormally low m_1 parameter values.

3.5. Nature of Henry's Region in MOFs at Low Pressures: Nonlinear Trends in Flexible Materials. It is generally accepted that, at low sorbate loadings, the adsorption isotherm for a given sorbate−sorbent system, regardless of its form, can be linearized to a Henry's-type linear isotherm with a characteristic slope or Henry's coefficient, H, reflecting the magnitude of the sorbate−sorbent interaction and confinement level of the sorbate

$$H = \lim_{q\to 0}\frac{\delta\theta}{\delta\Pi} \quad (17)$$

One of the characteristics of gas/vapor adsorption in zeolites is the presence of sharp adsorption trends at low pressures (usually $<10^{-4}$ for N_2 adsorption at 77.4 K, see Figure 2 and Table 2). As a consequence, Henry's region is usually found in an extremely reduced pressure interval, this interval being displaced to higher pressures for weaker adsorbents. This translates into a displacement of this region to the plateau zone in the representation of the thermodynamic isotherm.

Figure 7 plots the evolution of the slope of the adsorption curves, $\delta\theta/\delta\Pi$, against the relative pressure for the four MOF materials prepared in this study and reference zeolites NaY and ZSM-5. The experimental slopes can be successfully reproduced and resolved using the following expression derived from the thermodynamic isotherm (see ref 60 for further details)

$$\frac{\delta\theta}{\delta\Pi} = \frac{1}{\Pi\ln^2(\Pi)}\frac{\delta\theta}{\delta Z} = \frac{G^\circ\lambda_1\lambda_2}{\Pi\ln^2(\Pi)}\frac{(m_2\lambda_1+m_1\lambda_2)}{(\lambda_1+\lambda_2+\lambda_1\lambda_2)^2} \quad (18)$$

One interesting characteristic of Figure 7 is the absence of linear trends typical of Henry's region at low pressures in the case of MIL-53(Al)-NH_2 and MIL-68(In)-NH_2 materials. Contrary to what would be expected from our experience gathered on zeolite adsorption, eq 11 predicts a monotonous increase of the slope, practically linear, for relative pressures $<10^{-6}$. As a matter of fact, this pressure value can usually be considered as a threshold value for the beginning of Henry's (linear) region in zeolites.[60] Note also that the extrapolation of eq 18 to relative pressures $<10^{-9}$ for MIL-68(In)-NH_2 and MIL-53(Al)-NH_2 materials does not predict the presence of a "true" linear trend, the slope increasing monotonously while reducing the pressure. We attribute this observation to the structural deformation on these materials ascribed to high surface tensions, providing higher energy heterogeneity compared to "robust" MOF-5 and CAU-1 materials and zeolites NaY and HZSM-5. We have already demonstrated in a previous publication[60] that linear trends in Henry's region (constant slope) are only possible as long as $m_1 > 12$ for a high range of k_1 values, as is usually the case encountered in zeolites.

Interestingly, eq 18 admits lower and upper bounds for the existence of a linear Henry's region in gas adsorption as a function of the relative values of parameters m_1 and k_1 for a given sorbent but irrespective of parameters m_2 and k_2 and G°. Figure 8 plots the bounds predicted by eq 18, as well as the threshold pairs [m_1, k_1] for the MOF solids and zeolites considered here. As can be observed, MOF-5, CAU-1, and zeolites NaY and HZSM-5 appear in the linear zone, confirming the presence of a linear trend in Henry's region (constant slope) in Figure 7. In contrast, the MIL-type materials slightly overcome the upper bound, appearing as a consequence in a

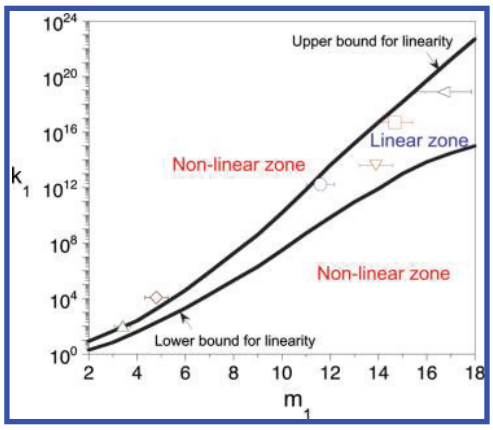

Figure 8. Evolution of parameter Γ, ascribed to the compression tension for a constant $\delta k_1/\delta V_c$, as a function of the relative pressure for the different MOF solids and zeolites tested in this study. Calculations: $G° = 10$, $m_2 = 2.0$, $k_2 = 3000$.

nonlinear region. This is mainly due to the abnormally low m_1 values for these materials ascribed to their high energy heterogeneity, being therefore at the origin of their unexpected lack of linear trend in Henry's adsorption domain.

4. Conclusions

In this study, we have shown that the DA isotherm fails to reproduce successfully N_2 adsorption data at 77.4 K in MOF materials for relative pressures <0.1. This inherent limitation can be overcome using the thermodynamic isotherm characterized by eq 2. Rigid MOF materials show comparable energy heterogeneity to that usually observed in zeolites, characterized by $m_1 > 10$. In the case of MIL-68(In)-NH_2 and MIL-53(Al)-NH_2 materials, showing flexible frameworks, sorbate-induced framework deformation appears to promote energy heterogeneity, the materials showing unexpectedly low m_1 values (<5). This fact appears to be at the origin of a lack of a "true" linear Henry's region at low pressures, as is usually found (and often postulated *a priori*) in zeolites and other "robust" microporous materials.

Glossary

$E°$	Characteristic energy of the DA isotherm ($J \cdot mol^{-1}$)
$G°$	Integral free energy of the sorbate at $P°$, eqs 1−5
H	Henry's constant, eq 17
k	Parameter in eqs 1−5
m	Exponent in eqs 1−5
$P°$	Saturation pressure (Pa)
P	Pressure (Pa)
q_M	Saturation loading ($mol \cdot kg^{-1}$)
R	Gas constant (8.314 $J \cdot mol^{-1} \cdot K^{-1}$)
T	Temperature (K)
V_c	Unit cell volume ($m^3 \cdot kg^{-1}$)
Z	$1/-\ln(\Pi)$

Greek Symbols

α	Exponent in the DA isotherm
β	Affinity coefficient in the DA isotherm
σ	Tension exerted by the sorbate to the solid ($J \cdot kg^{-1}$ solid)
Φ	Surface potential of the sorbate ($J \cdot kg^{-1}$ solid)
Γ	Parameter defined by eq 16 ($J \cdot kg^{-1}$ solid)
λ	kZ^m
Π	$P/P°$
Π_k	Π value corresponding to the disipation of $G°/2$
θ	Surface coverage
Ψ	Integral Gibbs free energy relative to saturation ($J \cdot kg^{-1}$)

Subscripts

1, 2	First and second zone in the thermodynamic isotherm

Acronyms

DA	Dubinin−Astakhov isotherm
DR	Dubinin−Radhuskevitch isotherm
TVFM	Theory of volume filling in micropores

References and Notes

(1) Yang, R. T. *Adsorbents: Fundamentals and Applications*; John Wiley & Sons: Hoboken, NJ, 2003.
(2) Jones, S. C.; Bauer, C. A. *J. Am. Chem. Soc.* **2009**, *131*, 12516.
(3) Hoskins, B. F.; Robson, R. J. *J. Am. Chem. Soc.* **1990**, *112*, 1546.
(4) Wang, Z.; Cohen, S. M. *J. Am. Chem. Soc.* **2007**, *129*, 12368.
(5) James, S. L. *Chem. Soc. Rev.* **2003**, *32*, 276.
(6) Kitagawa, S.; Kitaura, R.; Noro, S. *Angew. Chem., Int. Ed.* **2004**, *43*, 2334.
(7) Ockwig, N. W.; Delgado-Friedrichs, O.; O'Keeffe, M.; Yaghi, O. M. *Acc. Chem. Res.* **2005**, *38*, 176.
(8) Ferey, G.; Mellot-Draznieks, C.; Serre, C.; Millange, F. *Acc. Chem. Res.* **2005**, *38*, 217.
(9) Ferey, G.; Serre, C. *Chem. Soc. Rev.* **2009**, *38*, 1380.
(10) Düren, T.; Bae, Y.-S.; Snurr, R. Q. *Chem. Soc. Rev.* **2009**, *38*, 1237.
(11) Li, J.-R.; Kuppler, R.-J.; Zhou, H.-C. *Chem. Soc. Rev.* **2009**, *38*, 1477.
(12) Murray, L. J.; Dinc, M.; Long, J. R. *Chem. Soc. Rev.* **2009**, *38*, 1294.
(13) Farrusseng, D.; Aguado, S.; Pinel, C. *Angew. Chem., Int. Ed.* **2009**, *48*, 7502.
(14) Lee, J. Y.; Farha, O. K.; Roberts, J.; Scheidt, K. A.; Nguyen, S. T.; Hupp, J. T. *Chem. Soc. Rev.* **2009**, *38*, 1450.
(15) Ma, L.; Abney, C.; Lin, W. *Chem. Soc. Rev.* **2009**, *38*, 1248.
(16) Livage, C.; Egger, C.; Ferey, G. *Chem. Mater.* **2001**, *13*, 410.
(17) Livage, C.; Guillou, N.; Marrot, J.; Ferey, G. *Chem. Mater.* **2001**, *13*, 4387.
(18) Barthelet, K.; Marrot, J.; Riou, D.; Ferey, G. *Angew. Chem., Int. Ed.* **2002**, *41*, 281.
(19) Serre, C.; Millange, F.; Thouvenot, C.; Nogues, M.; Marsolier, G.; Loueur, D.; Ferey, G. *J. Am. Chem. Soc.* **2002**, *124*, 13519.
(20) Barthelet, K.; Adil, K.; Millange, F.; Serre, C.; Riou, D.; Ferey, G. *J. Mater. Chem.* **2003**, *13*, 2208.
(21) Riou-Cavellec, M.; Lesaint, C.; Nogues, M.; Greneche, J. M.; Ferey, G. *Inorg. Chem.* **2003**, *42*, 5669.
(22) Guillou, N.; Livage, C.; van Beek, W.; Nogues, M.; Ferey, G. *Angew. Chem., Int. Ed.* **2003**, *42*, 644.
(23) Guillou, N.; Livage, C.; Drillon, M.; Ferey, G. *Angew. Chem., Int. Ed.* **2003**, *42*, 5314.
(24) Devic, T.; Serre, C.; Auderbrand, N.; Marrot, J.; Ferey, G. *J. Am. Chem. Soc.* **2005**, *127*, 12788.
(25) Ferey, G.; Mellot-Draznieks, C.; Serre, C.; Millange, F.; Dutour, J.; Surble, S.; Margiolaki, I. *Science* **2005**, *307*, 2040.
(26) Serre, C.; Mellot-Draznieks, C.; Surble, S.; Audebrand, N.; Filinchuk, Y.; Ferey, G. *Science* **2007**, *315*, 1828.
(27) Rowsell, J. L. C.; Yaghi, O. M. *Microporous Mesoporous Mater.* **2004**, *73*, 3.
(28) Eddaoudi, M.; Kim, J.; Rosi, N.; Vodak, D.; Wachter, J.; O'Keeffe, M.; Yaghi, O. M. *Science* **2002**, *205*, 469.
(29) Millward, A. R.; Yaghi, O. M. *J. Am. Chem. Soc.* **2005**, *127*, 17998.
(30) Walton, K. S.; Millward, A. R.; Dubbeldam, D.; Frost, H.; Low, J. J.; Yaghi, O. M.; Snurr, R. Q. *J. Am. Chem. Soc.* **2008**, *130*, 406.
(31) Rowsell, J. L. C.; Yaghi, O. M. *J. Am. Chem. Soc.* **2006**, *128*, 1304.
(32) Wong-Foy, A. G.; Matzger, A. J.; Yaghi, O. M. *J. Am. Chem. Soc.* **2006**, *128*, 3494.
(33) Chui, S. S. Y.; Lo, S. M. F.; Charmant, J. P. H.; Orpen, A. G.; Williams, I. D. *Science* **1999**, *283*, 1148.
(34) Alaerts, L.; Kirschhock, C. E. A.; Maes, M.; van der Veen, M. A.; Finsy, V.; Depla, A.; Martens, J. A.; Baron, G. V.; Jacobs, P. A.; Denayer, J. E. M.; de Vos, D. E. *Angew. Chem., Int. Ed.* **2007**, *46*, 4293.
(35) Murray, L. J.; Dinca, M.; Long, J. R. *Chem. Soc. Rev.* **2009**, *38*, 1294.
(36) McKinlay, A. C.; Xiao, B.; Wragg, D. S.; Wheatley, P. S.; Megson, I. L.; Morris, R. E. *J. Am. Chem. Soc.* **2008**, *130*, 10440.

(37) Kitagawa, S.; Uemura, K. *Chem. Soc. Rev.* **2005**, *34*, 109.
(38) Bureekaew, S.; Shimomura, S.; Kitagawa, S. *Sci. Technol. Adv. Mater.* **2008**, *9*, 1.
(39) Horike, S.; Matsuda, R.; Tanaka, D.; Matsubara, S.; Mizuno, M.; Endo, K.; Kitagawa, S. *Angew. Chem., Int. Ed.* **2006**, *45*, 7226.
(40) Bourrelly, S.; Llewellyn, P. L.; Serre, C.; Millange, F.; Loiseau, T.; Ferey, G. *J. Am. Chem. Soc.* **2005**, *127*, 13519.
(41) Trung, T. K.; Trens, P.; Tanchoux, N.; Bourrelly, S.; Llewellyn, P. L.; Loera-Serna, S.; Serre, C.; Loiseau, T.; Fajula, F.; Ferey, G. *J. Am. Chem. Soc.* **2008**, *130*, 16926.
(42) Coudert, F.-X. Jeffroy, M. Fuchs, A. H. Boutin, A. Mellot-Draznieks, C. *J. Am. Chem. Soc.* **2008**, *130*, 14294.
(43) Serre, C.; Bourrelly, S.; Vimont, A.; Ramsahye, N. A.; Maurin, G.; Llewellyn, P. L.; Daturi, M.; Filinchuk, Y.; Leynaud, O.; Barnes, P.; Ferey, G. *Adv. Mater.* **2007**, *19*, 2246.
(44) Düren, T.; Sarkisov, L.; Yaghi, O. M.; Snurr, R. Q. *Langmuir* **2004**, *20*, 2683.
(45) Sagara, T.; Klassen, J.; Ganz, E. *J. Chem. Phys.* **2004**, *121*, 12543.
(46) Sarkisov, L.; Düren, T.; Snurr, R. Q. *Mol. Phys.* **2004**, *102*, 211.
(47) Mellot-Draznieks, C.; Serre, C.; Surble, S.; Audebrand, N.; Ferey, G. *J. Am. Chem. Soc.* **2005**, *127*, 16273.
(48) Garberoglio, G.; Skoulidas, A. I.; Johnson, J. K. *J. Phys. Chem. B* **2005**, *109*, 13094.
(49) Ramsahye, N. A.; Maurin, G.; Bourrelly, S.; Llewellyn, P. L.; Devic, T.; Serre, C.; Loiseau, T.; Ferey, G. *Adsorption* **2005**, *13*, 461.
(50) Yang, Q. Y.; Zhong, C. L. *J. Phys. Chem. B* **2006**, *110*, 17776.
(51) Yang, Q. Y.; Zhong, C. L. *ChemPhysChem* **2006**, *7*, 1417.
(52) Skoulidas, A. I.; Sholl, D. S. *J. Am. Chem. Soc.* **2007**, *129*, 8552.
(53) Salles, F.; Ghoufi, A.; Maurin, G.; Bell, R. G.; Mellot-Draznieks, C.; Ferey, G. *Angew. Chem., Int. Ed.* **2008**, *47*, 8487.
(54) Özgür Yazaydin, A.; Benin, A. I.; Faheem, A.; Jakubczak, P.; Low, J. J.; Willis, R. R.; Snurr, R. Q. *Chem. Mater.* **2009**, *21*, 1425.
(55) Brunauer, S.; Emmett, P. H.; Teller, E. *J. Am. Chem. Soc.* **1938**, *60*, 309.
(56) Dubinin, M. M. Astakhov, V. A. Radushkevich, L. V. *Physical Adsorption of Gases and Vapors in Micropores, Progress and Membrane Science*; Academic Press: New York, 1975; Vol. 9.
(57) Walton, K. S.; Snurr, R. Q. *J. Phys. Chem. B* **2005**, *109*, 15760.
(58) Llorens, J.; Pera-Titus, M. *J. Colloid Interface Sci.* **2009**, *331*, 302.
(59) Llorens, J.; Pera-Titus, M. *Colloids Surf., A* **2009**, *350*, 63.
(60) Pera-Titus, M.; Llorens, J. *Appl. Surf. Sci.* **2010**, *256*, 5305.
(61) Pera-Titus, M. *J. Colloid Interface Sci.* **2010**, *345*, 410.
(62) Nakai, K.; Sonoda, J.; Yoshida, M.; Hakuman, M.; Naono, H. *Adsorption* **2007**, *13*, 351.
(63) Mueller, U.; Schubert, M.; Teich, F.; Puetter, H.; Schierle-Arndt, K.; Pastre, J. *J. Mater. Chem.* **2006**, *16*, 626.
(64) Li, H.; Eddaoudi, M.; O'Keeffe, M.; Yaghi, O. M. *Nature* **1999**, *402*, 276.
(65) Ravon, U.; Savonnet, M.; Aguado, S.; Domine, M. E.; Janneau, E.; Farrusseng, D. *Microporous Mesoporous Mater.* **2010**, *129*, 319.
(66) Ahnfeldt, T.; Guillou, N.; Gunzelmann, D.; Margiolaki, I.; Loiseau, T.; Férey, G.; Senker, J.; Stock, N. *Angew. Chem., Int. Ed.* **2009**, *48*, 5163.
(67) Savonnet, M.; Bazer-Bachi, D.; Pinel, C.; Lecocq, V.; Bats, N.; Farrusseng, D. Patent Pending FR 09/05.101.
(68) Bauer, S.; Serre, C.; Devic, T.; Horcajada, P.; Marrot, J.; Férey, G.; Stock, N. *Inorg. Chem.* **2008**, *47*, 7568.
(69) Stoeckli, F. *Adsorpt. Sci. Technol.* **1993**, *10*, 3.
(70) Marsh, H.; Rand, B. *J. Colloid Interface Sci.* **1970**, *33*, 101.
(71) Sundaram, N. *Langmuir* **1993**, *9*, 1568A.
(72) Kapoor, A.; Ritter, J. A.; Yang, R. T. *Langmuir* **1989**, *5*, 1118.
(73) Mahle, J. J. *Carbon* **1997**, *35*, 432.
(74) Neimark, A. V.; Coudert, F.-X.; Boutin, A.; Fuchs, A. *J. Phys. Chem. Lett.* **2010**, *1*, 445.

JP104788P

NJC

View Online
Dynamic Article Links

Cite this: DOI: 10.1039/c1nj20350a

www.rsc.org/njc

PAPER

Combinatorial synthesis of metal–organic frameworks libraries by click-chemistry†

Marie Savonnet,[ab] Emanuel Kockrick,[a] Aurélie Camarata,[a] Delphine Bazer-Bachi,[b] Nicolas Bats,[b] Vincent Lecocq,[b] Catherine Pinel[a] and David Farrusseng*[a]

Received (in Montpellier, France) 19th April 2011, Accepted 16th June 2011
DOI: 10.1039/c1nj20350a

A key to address advanced MOF materials suitable for more sophisticated applications is to add functionalities of greater complexity in a controlled manner. We report a generic and original post-synthetic modification method starting from amino derived MOFs. The first step consists in converting the amino group into azide (N_3). Without isolation nor purification, the desired functionalized material is obtained by grafting the corresponding alkyne using "Click Chemistry". This work reports for the first time the synthesis of a two-dimensional combinatorial library of 24 functionalized MOFs. We also show that the grafting yield can be controlled from 10 to 100%. Finally, we compare the effect of the grafting yield on the porous volume of (1D) and (3D)MOF porous structures.

Introduction

Metal–organic frameworks (MOFs) are porous crystalline materials composed of cationic systems that behave like nodes with polytopic organic ligands acting as spacers;[1,2] these materials are often viewed as a new class of zeolites due to their porous structure.

One solution for synthesizing advanced MOFs suitable for more specialized and sophisticated applications is the controlled addition of more complex functionalities into the porous network. If the physical environment of the pores and the cavities within MOFs can be modified, the interactions with guest species can in turn be adapted, thereby fine-tuning the chemical reactivity.[3] That said, the introduction of reactive chemical functions by self-assembly methods is not a trivial task and cannot be generalized to all MOFs.[4] Various synthetic strategies have been employed with the aim of achieving MOF post-functionalization, as detailed in extensive reviews by Cohen *et al.*[5–8] Post-synthetic modification (PSM) using covalent-type grafting methods has undergone outstanding progress in recent years.[9] A versatile approach toward multi-functional MOFs was developed so far by Cohen and coworkers using a variety of functional anhydrides.[6]

In this study, we present an alternative method of PSM[10] that can be applied to all kinds of MOFs over a very wide range of pore size (micro to meso), chemical stability (low to high) and structural flexibility, using a great variety of grafted chemical functions (acidic, coordinative, basic, aromatic, aliphatic and hydrophilic) (Fig. 1). To the best of our knowledge, this is the first report dealing with the synthesis of a multi-dimensional combinatorial library of functionalized MOFs. The impact of the grafting rate between the porous volumes of 1D and 3D channeled structures is also compared for the first time.

Five aminoterephthalate-containing MOFs exhibiting different structural and chemical features were selected (Fig. 1). These five parent MOFs are DMOF-NH_2 (**1**) (Zn(bdc-NH_2)-(DABCO)),[8] MIL-68(In)-NH_2 (**2**) (In(OH)(bdc-NH_2)),[11] CAU-1 (**3**) ($Al_4(OH)_2(OCH_3)_4(NH_2\text{-bdc})_3$),[12] MIL-53(Al)-$NH_2$ (**4**) (Al(OH)(bdc-NH_2))[13,14] and MIL-101(Fe)-NH_2 (**5**) ($Fe_3O(solv)_3Cl(bdc\text{-}NH_2)_3$) (solv = H_2O, DMF).[13] For DMOF-NH_2, MIL-101(Fe)-NH_2 and MIL-53(Al)-NH_2, crystallite sizes are of about 0.2–0.6 μm whereas crystallite sizes are significantly smaller for MIL-53(In)-NH_2 and CAU-1 as observed by SEM (see ESI†). DMOF-NH_2 and CAU-1 exhibit the smallest pore size (6 Å and 4–10 Å, respectively) and MIL-101 the largest (29–34 Å).[15] In terms of the pore network, MIL-53 and MIL-68 have monodirectional channels (1D), whereas the other materials have a 3D pore structure. Some of the MOFs selected present chemical features that may interfere with grafting processes, namely CAU-1, which exhibits hydroxy and methoxy bridging groups, as well as MIL-68(In)-NH_2 and MIL-53(Al)-NH_2, which are built from inorganic nodes with hydroxyl bridging groups. In addition, the trinuclear nodes of MIL-101(Fe)-NH_2 show uncoordinated centers as well as terminating Cl and OH. DMOF-NH_2 is built from carboxylate layers pillared with DABCO that weakly

[a] *IRCELYON, University of Lyon, CNRS, 2, Av. Albert Einstein, Villeurbanne, F-69626, France. E-mail: david.farrusseng@ircelyon.univ-lyon1.fr; Fax: +33(4)7244536*
[b] *IFP Energies nouvelles, Catalysis and Separation Division, Rond-point de l'échangeur de Solaize, BP 3, 69360 Solaize, France*
† Electronic supplementary information (ESI) available. See DOI: 10.1039/c1nj20350a

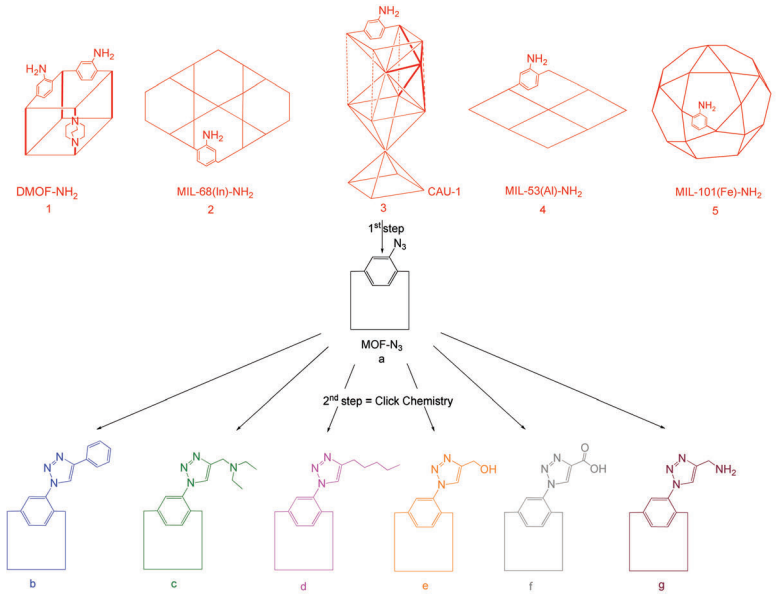

Fig. 1 Strategy for the generation of functionalized MOFs.

coordinate to the Zn paddlewheel. This confers a certain degree of flexibility to DMOF-NH_2[16] but lowers its chemical stability (it is easily soluble in acidic or basic media). By contrast, MIL-53(Al)-NH_2 is barely soluble in aqueous acidic solution. The MIL-53 structure allows large breathing phenomena upon external stimuli.

Results

The post-modification of the MOFs proceeds as previously described[10] and has been applied to all cases described herein. In a typical synthesis, the freshly-dried amino-MOF is treated with tBuONO and $TMSN_3$ in THF for one night at room temperature to produce the corresponding azide intermediate MOF (**1a**, **2a**, **3a**, **4a**, **5a**). In the same vessel, functionalized MOF is obtained by adding an appropriate amount of alkyne in the presence of $Cu^I(CH_3CN)_4PF_6$, followed by continuous stirring for 24 h. Extensive washings were carried out to remove the copper catalyst from the solids. The post-modification yield, also called PSM degree, can be controlled by the amount of alkynes added (default or excess).

Liquid ^{1}H NMR analysis was carried out in order to obtain unambiguous quantifications of the degree of post-modification. The samples derived from parent MOFs (**1**), (**2**), (**3**) and (**5**) were digested and dissolved in dilute DCl/D_2O/DMSO-d_6 solution, whereas the compounds derived from (**4**) required dissolution in DCl/D_2O/DMSO-d_6 followed by NaOD/D_2O/DMSO-d_6 because of their high chemical stability. It was verified that the digestion of (**4**) in HF/DMSO-d_6 leads to the same conclusions[7] (see S17, ESI†). Table 1 reports the degree of modification for the five parent MOFs, *i.e.*, the conversion of $-NH_2$ to $-N_3$ and that of $-N_3$ to the corresponding functional triazolate when a large excess of alkynes are used. Due to the very broad peaks and the low resolution obtained in ^{1}H NMR for MIL-101(Fe) systems containing paramagnetic iron species, only one grafting reaction was conducted as proof of concept. For this system, the calculations of grafting rates by peaks integration were not possible.

One can see that the complete conversion of the amino to the azide can be achieved for all types of MOFs. This first step of functionalization is already highly relevant to obtain MOF-bearing nitrene groups through photoactivation.[6] The kinetics of the conversion of (**1**), (**2**), (**3**), (**4**) and (**5**) was followed by ^{1}H NMR analysis (Fig. 2). We have observed that for an equal excess of $TMSN_3$, the kinetics are much slower for MIL-68(In)-NH_2 (**2**) and MIL-53(Al)-NH_2 (**4**) than for the other parent MOFs. This likely arises from their 1D porous structure, which limits the diffusion rate of $TMSN_3$ to the center of the crystallites. Nevertheless, a contraction of the channels cannot be ruled out for the MIL-53 structure. For MIL-68(In)-NH_2 (**2**) and MIL-53(Al)-NH_2 (**4**), a larger excess of $TMSN_3$ shall therefore be used in order to allow complete conversion in a few hours.

Conversely, the apparent kinetics is faster for 3D porous structures with high porous volume, such as MIL-101(Fe)-NH_2 (**5**). While DMOF-NH_2 (**1**) was completely converted to (**1a**) after 12 h, for equal ratio (**5a**) was formed within only 30 min.

One can also see that the Huygens [3 + 2] addition reaction generally proceeds very well; for most of the systems, full conversion is achieved for the second step. That said, complete functionalization for DMOF-NH_2 (**1**) and CAU-1 (**3**) is achieved even with bulky groups, while a lower degree of modification is obtained for the 1D rod-shaped structured materials, MIL-68(In)-NH_2 (**2**) and MIL-53-Al-NH_2 (**4**). Here again, a larger excess of alkynes has been used for (**2**) and (**4**) to favor the reaction. To obtain fully-functionalized (**1d**), the alkyne : MOF ratio is 8.5 : 1 *versus* 68 : 1 for (**2d**) (see Table S1, ESI†). It has to be pointed out that DMOF-NH_2 (**1**) cannot be

Table 1 Degrees of post-modification (%) of amino-MOFs with different alkynes. Measured by liquid ^{1}H NMR analysis

	(a) $TMSN_3$	(b) 	(c) 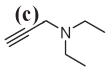	(d) 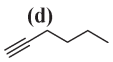	(e) 	(f) 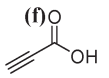	(g) 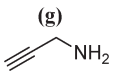
DMOF-NH_2 (**1**)	>99	>99	>99	>99	>99	Dissolution[b]	[a]
MIL-68(In)-NH_2 (**2**)	>99	80 ± 2	45 ± 2	>99	>99	68 ± 2	>99
CAU-1 (**3**)	>99	>99	>99	>99	>99	>99	[a]
MIL-53(Al)-NH_2 (**4**)	>99	82 ± 3	55 ± 3	60 ± 2	>99	55 ± 2	[a]
MIL-101(Fe)-NH_2 (**5**)	>99	>99	[a]	[a]	[a]	[a]	[a]

[a] Not performed. [b] The solid dissolves in the media.

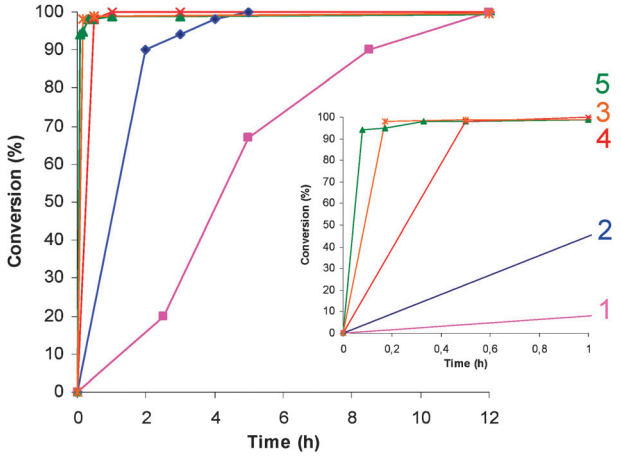

Fig. 2 Kinetics of conversion of (**1**), (**2**), (**3**), (**4**) and (**5**). The $TMSN_3$: MOF ratio is 6, 38, 17, 78 and 6, respectively.

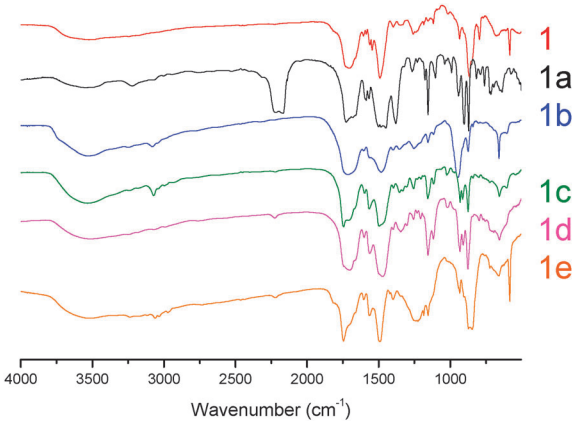

Fig. 3 FTIR spectra of (**1**), (**1a**), (**1b**), (**1c**), (**1d**) and (**1e**).

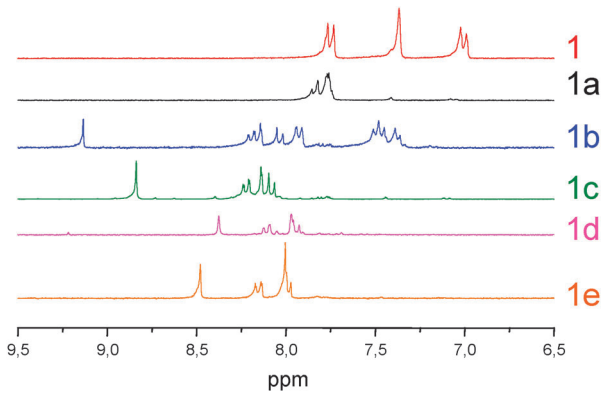

Fig. 4 ^{1}H NMR enlargement in the aromatic region of digested (**1**), (**1a**), (**1b**), (**1c**), (**1d**) and (**1e**).

functionalized with a propiolic acid derivative (**f**), since the starting solid dissolves when the acid is added. In addition, we have observed that partial loss of the long-range order occurred for (**2f**) and (**3f**).

Partial substitution of the carboxylate linker with the propriolate could be responsible for this loss of crystallinity. These results are consistent with the lower chemical stability of (**1**), (**2**), and (**3**) as found in sample digestions. For the sake of brevity, proofs of characterization are detailed for DMOF series (**1a**), (**1b**), (**1c**), (**1d**), (**1e**), and (**1f**), while details for the post-modification of (**2**), (**3**), (**4**) and (**5**) are given in the ESI.†

A clear proof of azide formation and the subsequent (3 + 2) cycloaddition was obtained by IR spectroscopy (Fig. 3). The appearance of the IR absorption band at 2123 cm^{-1} is characteristic of the N_3 asymmetric stretching vibration of DMOF-N_3 (**1a**). Its complete disappearance after the cycloaddition step is a proof of total conversion to the final compound (**1b**), (**1c**), (**1d**) or (**1e**).

Liquid ^{1}H NMR allows us to confirm these results on a quantitative manner. The spectrum of digest DMOF-N_3 (**1a**) reveals the formation of the corresponding azide compound through the appearance of new aromatic signals (7.73–7.83 ppm, m, ArH). This coincides with the complete disappearance of the aromatic signals of DMOF-NH_2 (**1**) (7.15 ppm, d, 1H, J = 8.3 Hz; 7.44 ppm, s, 1H; 7.8 ppm, d, 1H, J = 8.3 Hz) (Fig. 4), thus indicating full conversion to the azide form. After the cycloaddition step, new aromatic shifts of the post-modified compounds (**1b**), (**1c**), (**1d**) and (**1e**) confirm that the corresponding triazole derivative is formed as the sole product. Moreover the proton of the triazole moiety has a chemical shift in the range 8.5–9.5 depending on the nature of the alkynyl group. This enables straightforward quantification while providing a visible indicator that the reactions have proceeded, in contrast to condensation reactions, for which the degree of conversion is usually more difficult to identify.

Except when propiolic acid (which can interact with the inorganic node) was used, powder X-ray diffraction (PXRD) confirmed that the long-range order was preserved for all post-modified MOFs as present in Table 1 (see ESI†), even for post-modified DMOF compounds (Fig. 5), which are

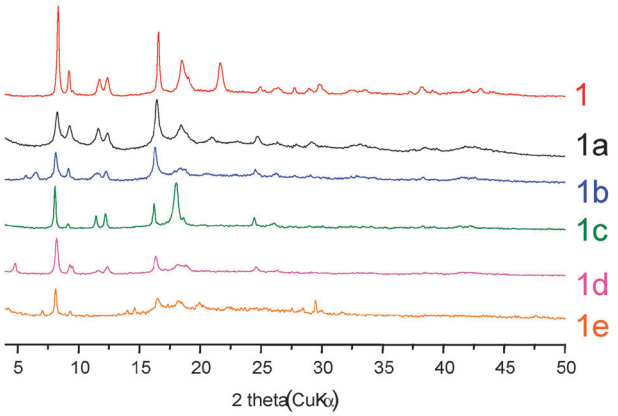

Fig. 5 PXRD patterns of (**1**), (**1a**), (**1b**), (**1c**), (**1d**) and (**1e**).

based on the most fragile of the structures considered. This preservation of the long-range order arises from the softness of this method, which allows its application to all kinds of amino-MOFs. Indeed, both reaction steps proceed at room temperature and do not liberate byproducts such as water, acids or bases that could damage the structure.[7,17]

The impact of the grafting rate with (**b**) on the porous volume was studied for both channeled (MIL-68) and 3D (CAU-1) porous structures. All samples underwent desorption at only 100 °C prior to N_2 physisorption at 77 K. This soft degassing procedure is required in order to prevent the azide from decomposing. As shown by the N_2 adsorption isotherms of (**2**) and (**3**) and of the modified samples (Fig. 6 and 7), an increased degree of modification leads to lowered microporous volume. It can nevertheless be seen that the isotherms maintain their type I shape, which indicates that microporosity is maintained whatever the degree of PSM.

Fig. 8 illustrates the impact of the degree of modification with (**b**) on the apparent BET surface area measurements of MIL-68(In)-N_3 (**2a**) and CAU-1-N_3 (**3a**). The progressive introduction of the 4-phenyl-1,2,3-triazolate moiety into the porous network reduces the surface area and microporous volume in the same manner for both MOFs (see Table S3, ESI†).

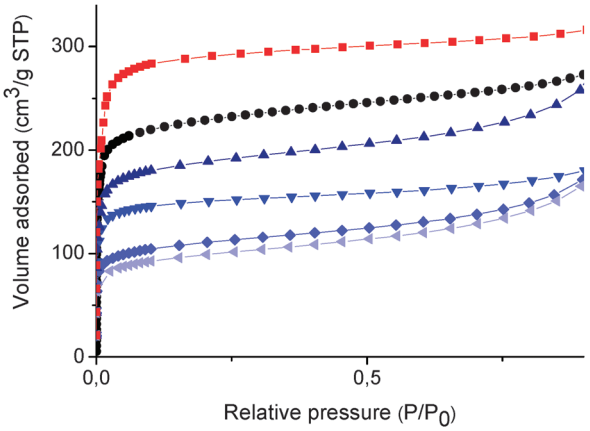

Fig. 6 Effect of the degree of modification with phenylacetylene (**b**) on N_2 adsorption isotherms of MIL-68(In)-NH_2 (**2**) (■), MIL-68(In)-N_3 at 0% (●), corresponding to (**2a**); at 10% (▲); at 20% (▼); at 50% (◆) and at 80% (◀).

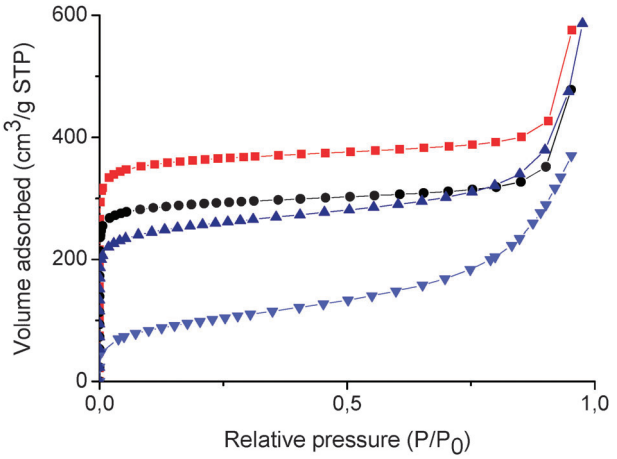

Fig. 7 Effect of the degree of modification with phenylacetylene (**b**) on N_2 adsorption isotherms of CAU-1 (**3**) (■); at 0% (●), corresponding to (**3a**); at 20% (▲); and at 100% (▼).

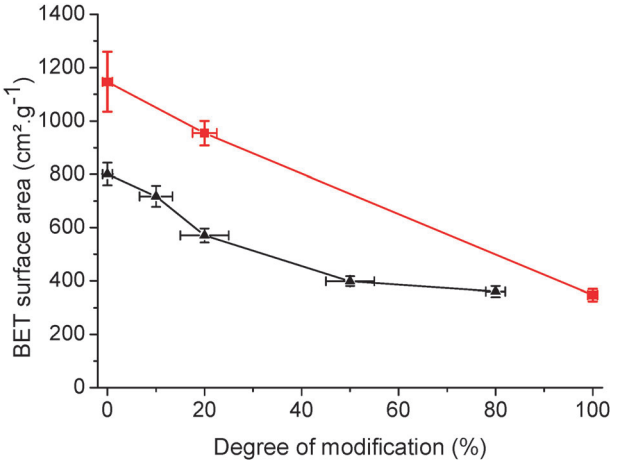

Fig. 8 Effect of the degree of modification with phenylacetylene (**b**) on apparent BET surface areas of MIL-68(In)-N_3 (**2a**) (▲) and CAU-1-N_3 (**3a**) (■).

For both porous structures, the apparent surface area decreases linearly as a function of the degree of modification. Once full conversion is achieved, the surface areas have decreased by a factor of about 2.5 to 3 with respect to the parent azide-MOF (from 800 to 360 m g^{-1} for MIL-68 and from 1150 to 350 m^2 g^{-1} for CAU-1). Similar results are obtained when the evolution of the microporous volume is considered (see ESI†).

Discussion

This generic PSM method makes it possible to generate multi-dimensional libraries of original MOFs that could not be obtained by traditional solvothermal synthesis. The classic, most common method of creating new functional MOFs is to focus on the synthesis by self-assembly from pre-functionalized linkers, ultimately using high-throughput (HT) methods.[2,18,19] Although this approach regularly provides outstanding new materials, it is not very appropriate when, for instance, one seeks to engineer a functional MOF for a given catalytic application.

It is, in fact, usually difficult to predict whether a functional MOF will be obtained by self-assembly, and numerous synthesis trials are usually required to provide an adequate number of new well-defined MOFs. For practical applications, it is more efficient to start from already-available amino-MOF platforms and to then insert functionalities by PSM. This study demonstrates that a very high success rate (>90%) can be achieved in producing porous coordination polymers of diverse properties, including adsorption and catalysis. In addition, this generic method presents the advantage of being easily implemented for the parallel synthesis of a large library of MOFs using conventional automated workstations. Of equal importance is the robustness of this technique: not every member of the MOF library would require complete solid characterization, since PSM is successfully achieved in all cases. The PSM degree can be easily measured if desired by using liquid NMR after sample digestion. This method is therefore of high practical value and will allow the acceleration of MOF testing by HT methods for the development of catalysts or adsorbents.

In addition to its practical advantages, this novel PSM procedure presents several benefits for the engineering of MOF catalysts: (1) the softness of the method places almost no restriction on the choice of amino-MOFs, (2) the grafted moieties can possess reactive functional groups such as acid or base, and (3) the grafting rate can be precisely controlled by adjusting the MOF : alkyne ratio. It is therefore possible to engineer MOF catalysts in a rational manner, considering multiple independent factors, with an initial MOF structure that is appropriate in terms of its pore size or other intrinsic functions, and with various new functions to be inserted in optimized percentages. Thanks to the strict control of synthetic conditions, the precise optimization of these parameters can be achieved.

In conclusion, this original PSM technique provides a high level of control for the engineering of tailor-made catalysts. It should also enable the preparation of diverse libraries of functional porous solids with a high degree of reliability for HT testing in catalysis and adsorption applications, while opening new doors for the design of catalysts that combine different antagonistic functions in a confined area, providing a synthetic tool to one of the key challenges in catalysis.

Experimental

General

All chemicals were used as received without any further purification from commercial suppliers.

^{1}H NMR analysis

All NMR spectra were recorded with the same automated procedure for routine analysis on a Bruker Avance 250 spectrometer operating at 250 MHz for ^{1}H. Spectra are calibrated using the deuterium signals of DMSO. Approximately 5 mg of (**1**), (**2**), (**3**) and (**5**) derivate samples were digested and dissolved in 0.45 mL of DMSO-d_6 and 0.05 mL of dilute DCl (35% DCl in D_2O). Approximately 5 mg of (**4**) derivate samples were dissolved by using DCl/D_2O/DMSO-d_6 followed by 0.05 mL of dilute NaOD (in D_2O). Due to their high chemical stability, (**4**) derivate samples were also digested in HF/DMSO-d_6 and the same results were obtained.

XRD analysis

Powder X-ray diffraction patterns were recorded using a Bruker D5005 diffractometer (Bragg–Brentano geometry, graphite monochromator, Cu Kα radiation) and a Bruker D8 ADVANCE diffractometer (Bragg–Brentano geometry, Cu Kα radiation, 50 kV, 35 mA, λ = 0.154184 nm).

Gas sorption analysis

N_2 isotherms were carried out at 77 K using a BELSORP-max (BEL Japan). (**2**), (**3**) and (**4**) were degassed for one night at 180 °C under vacuum, while (**1**) and (**5**) were degassed for one night at 120 °C under vacuum. All derivatives of (**1**), (**2**), (**3**), (**4**) and (**5**) were degassed for one night at 100 °C under vacuum.

Infrared spectroscopy

IR spectra were recorded on a Fourier Transform Vector 22 Bruker spectrometer in KBr pellets in the 400–4000 cm^{-1} region.

Synthesis of parent amino-MOFs

DMOF-NH_2 (**1**) and MIL-68(In)-NH_2 (**2**), CAU-1 (**3**) were synthesized as described previously.[10,13]

The synthesis of MIL-53(Al)-NH_2 (**4**) was adapted from the procedures described in ref. 18. 2-Aminoterephthalic acid (NH_2-bdc, 0.120 g, 0.66 mmol) was suspended in water (28 mL, 1.55 mmol) in a 40 mL Teflon®-lined stainless steel digestion bomb. 1.10 mL (0.44 mmol) of a 0.4 M $AlCl_3{\cdot}6H_2O$ solution and 0.56 mL (0.22 mmol) of a 0.4 M NaOH solution were added. The reaction mixture was heated for 24 h without stirring at 110 °C. The resulting precipitate was washed with water and DMF at 160 °C, and then soaked in CH_2Cl_2 for 24 h. After drying at 80 °C in air, the mass of dried MIL-53(Al)-NH_2 obtained was 0.1 g.

MIL-101(Fe)-NH_2 (**5**) was synthesized from amino-terephthalic acid using a procedure described in ref. 18. A mixture of $FeCl_3{\cdot}6H_2O$ (1.0812 g, 4.00 mmol) and NH_2-bdc (0.3623 g, 1.65 mmol) was suspended in DMF (24 mL) and heated at 110 °C for 24 h. After filtration, a brown microcrystalline product was obtained. The crystals were washed three times with DMF and three times with dichloromethane. After drying at room temperature under vacuum, the mass of dried MIL-101(Fe)-NH_2 obtained was 0.72 g.

Experimental conditions for generic post-functionalization

In a typical synthesis, the freshly-dried amino-MOF (80 mg) is treated with tBuONO and $TMSN_3$ in THF for one night at room temperature to produce the corresponding intermediate azide compound, azide-MOF. In the same vessel, functionalized MOF is obtained by adding an excess of alkynes in the presence of $Cu^I(CH_3CN)_4PF_6$ in THF, with the mixture continuously stirred for 24 h. The alkynes used in this study are phenylacetylene (**b**), diethylpropargylamine (**c**), hexyne (**d**), propargyl alcohol (**e**), propiolic acid (**f**) and propargylamine (**g**).

After decantation, the supernate was removed. The solid was washed three times by THF (×8 mL) and three times by CH_2Cl_2 (×8 mL) in order to remove unreactive substrates. The solid was then dried under vacuum at room temperature to yield the final compound.

Acknowledgements

The authors thank IRCELYON and IFP Energies Nouvelles Scientific Services. The authors also thank Prof N. Stock and T. Ahnfeldt (Christian-Albrechts Universität zu Kiel, Germany) for providing a sample of CAU-1.

Notes and references

1 M. O'Keeffe, M. Eddaoudi, H. Li, T. Reineke and O. M. Yaghi, *J. Solid State Chem.*, 2000, **152**, 3–20; N. L. Rosi, M. Eddaoudi, J. Kim, M. O'Keeffe and O. M. Yaghi, *CrystEngComm.*, 2002, 401–404; G. Ferey, *Chem. Mater.*, 2001, **13**, 3084–3098; G. Férey, *J. Solid State Chem.*, 2000, **152**, 37–48; M. J. Rosseinsky, *Microporous Mesoporous Mater.*, 2004, **73**, 15–30; M. Eddaoudi, D. B. Moler, H. L. Li, B. L. Chen, T. M. Reineke, M. O'Keeffe and O. M. Yaghi, *Acc. Chem. Res.*, 2001, **34**, 319–330; J. P. Zhang and X. M. Chen, *J. Am. Chem. Soc.*, 2008, **130**, 6010–6017; B. Wang, A. P. Cote, H. Furukawa, M. O'Keeffe and O. M. Yaghi, *Nature*, 2008, **453**, 207–211; S. Kaskel, *Porous Metal–Organic Frameworks*, Wiley-VCH Verlag GmbH, 2008; D. J. Tranchemontagne, J. L. Mendoza-Cortes, M. O'Keeffe and O. M. Yaghi, *Chem. Soc. Rev.*, 2009, **38**, 1257–1283; S. Kitagawa, R. Kitaura and S. Noro, *Angew. Chem., Int. Ed.*, 2004, **43**, 2334; J. L. C. Rowsell and O. M. Yaghi, *Microporous Mesoporous Mater.*, 2004, **73**, 3; G. Ferey, *Chem. Soc. Rev.*, 2008, **37**, 191–214; S. Horike, S. Shimomura and S. Kitagawa, *Nat. Chem.*, 2009, **1**, 695–704; A. U. Czaja, N. Trukhan and U. Muller, *Chem. Soc. Rev.*, 2009, **38**, 1284–1293.

2 R. Banerjee, A. Phan, B. Wang, C. Knobler, H. Furukawa, M. O'Keeffe and O. M. Yaghi, *Science*, 2008, **319**, 939–943.

3 A. Corma, M. Iglesias and F. Sanchez, *Catal. Lett.*, 1995, **32**, 313–318; A. Corma, M. Iglesias, C. Delpino and F. Sanchez, *J. Organomet. Chem.*, 1992, **431**, 233–246; A. Corma, M. Iglesias, C. Delpino and F. Sanchez, *J. Chem. Soc., Chem. Commun.*, 1991, 1253–1255; S. J. M. Thomas, *ChemCatChem.*, 2010, **2**, 127–132; J. M. Thomas and R. Raja, *Acc. Chem. Res.*, 2008, **41**, 708–720; M. D. Jones, R. Raja, J. M. Thomas, B. F. G. Johnson, D. W. Lewis, J. Rouzaud and K. D. M. Harris, *Angew. Chem., Int. Ed.*, 2003, **42**, 4326–4331; J. M. Thomas, T. Maschmeyer, B. F. G. Johnson and D. S. Shephard, *J. Mol. Catal. A: Chem.*, 1999, **141**, 139–144; M. E. Davis, *Nature*, 2002, **417**, 813–821.

4 M. Kawano, T. Kawamichi, T. Haneda, T. Kojima and M. Fujita, *J. Am. Chem. Soc.*, 2007, **129**, 15418–15419.

5 S. Cohen, E. M. Dugan, Z. Q. Wang, M. Okamura and A. Medina, *Chem. Commun.*, 2008, 3366–3368; S. M. Cohen, *Chem. Sci.*, 2010, **1**, 32–36; E. Dugan, Z. Q. Wang, M. Okamura, A. Medina and S. M. Cohen, *Chem. Commun.*, 2008, 3366–3368; T. Gadzikwa, O. K. Farha, C. D. Malliakas, M. G. Kanatzidis, J. T. Hupp and S. T. Nguyen, *J. Am. Chem. Soc.*, 2009, **131**, 13613–13615; T. Gadzikwa, G. Lu, C. L. Stern, S. R. Wilson, J. T. Hupp and S. T. Nguyen, *Chem. Commun.*, 2008, 5493–5495; Y. Goto, H. Sato, S. Shinkai and K. Sada, *J. Am. Chem. Soc.*, 2008, **130**, 14354–14355; K. K. Tanabe, Z. Q. Wang and S. M. Cohen, *J. Am. Chem. Soc.*, 2008, **130**, 8508–8517; Z. Q. Wang and S. M. Cohen, *J. Am. Chem. Soc.*, 2007, **129**, 12368–12369; Z. Q. Wang and S. M. Cohen, *Angew. Chem., Int. Ed.*, 2008, **47**, 4699–4702; Z. Q. Wang and S. M. Cohen, *Chem. Soc. Rev.*, 2009, **38**, 1315–1329.

6 S. J. Garibay, Z. Q. Wang, K. K. Tanabe and S. M. Cohen, *Inorg. Chem.*, 2009, **48**, 7341–7349.

7 C. Volkringer and M. C. Seth, *Angew. Chem., Int. Ed.*, 2010, **49**, 4644–4648.

8 Z. Q. Wang, K. K. Tanabe and S. M. Cohen, *Inorg. Chem.*, 2009, **48**, 296–306.

9 K. K. Tanabe and S. M. Cohen, *Chem. Soc. Rev.*, 2011, **40**, 498–519; H. Sato, R. Matsuda, K. Sugimoto, M. Takata and S. Kitagawa, *Nat. Mater.*, 2010, **9**, 661–666; S. Aguado, J. Canivet and D. Farrusseng, *J. Mater. Chem.*, 2011, **21**, 7582–7588; J. Canivet, S. Aguado, C. Daniel and D. Farrusseng, *ChemCatChem.*, 2011, **3**, 675–678; A. D. Burrows, *CrystEngComm.*, 2011, **13**, 3623–3642.

10 M. Savonnet, D. Bazer-Bachi, N. Bats, J. Perez-Pellitero, E. Jeanneau, V. Lecocq, C. Pinel and D. Farrusseng, *J. Am. Chem. Soc.*, 2010, **132**, 4518–4519.

11 M. Savonnet, D. Bazer-Bachi, C. Pinel, V. Lecocq, N. Bats and D. Farrusseng, *FR Pat.*, 09/05.1012009.

12 T. Ahnfeldt, N. Guillou, D. Gunzelmann, I. Margiolaki, T. Loiseau, G. Ferey, J. Senker and N. Stock, *Angew. Chem., Int. Ed.*, 2009, **48**, 5163–5166.

13 S. Bauer, C. Serre, T. Devic, P. Horcajada, J. Marrot, G. Ferey and N. Stock, *Inorg. Chem.*, 2008, **47**, 7568–7576.

14 T. Loiseau, C. Serre, C. Huguenard, G. Fink, F. Taulelle, M. Henry, T. Bataille and G. Ferey, *Chem.–Eur. J.*, 2004, **10**, 1373.

15 G. Ferey, C. Mellot-Draznieks, C. Serre, F. Millange, J. Dutour, S. Surble and I. Margiolaki, *Science*, 2005, **309**, 2040–2042.

16 D. N. Dybtsev, H. Chun and K. Kim, *Angew. Chem., Int. Ed.*, 2004, **43**, 5033–5036.

17 M. Savonnet, S. Aguado, U. Ravon, D. Bazer-Bachi, V. Lecocq, N. Bats, C. Pinel and D. Farrusseng, *Green Chem.*, 2009, **11**, 1729–1732.

18 S. Bauer, C. Serre, T. Devic, P. Horcajada, J. Marrot, G. Ferey and N. Stock, *Inorg. Chem.*, 2008, **47**, 7568–7576.

19 P. M. Forster, N. Stock and A. K. Cheetham, *Angew. Chem., Int. Ed.*, 2005, **44**, 7608–7611.

DOI: 10.1002/cssc.200((will be filled in by the editorial staff))

Tailoring MOFs for CO_2 capture: the amino-effect

Jenny G. Vitillo,*[a] Marie Savonnet,[b] Gabriele Ricchiardi[a] and Silvia Bordiga[a]

((Dedication, optional))

The carbon dioxide capture from power plant flues is one of the strategies adopted to decrease the anthropogenic greenhouse gases emissions. In order to lower the cost associated to the regeneration of amine-based scrubbers systems, one of the envisaged strategies is the grafting of amines on high surface area supports and in particular on metal-organic frameworks (MOFs). In this study, the interaction between CO_2 and aliphatic and aromatic amines has been characterized by quantum mechanical methods (MP2), focusing the attention both on species already reported in MOFs and on new amine-based linkers in order to direct MOFs synthesis and functionalization. The calculations also indicate as the CO_2 modes are quite independent on the adsorption energy when the interaction is carried out by the organic linker.

Introduction

The increase in the greenhouse gases concentration in the terrestrial atmosphere is one of the grand problems of the present century, not only on the environmental point of view. It is in fact nowadays clear that a strict relationship exists between the carbon dioxide and methane atmospheric concentrations and the air-temperature.[1, 2] In particular, from the analysis of the Vostok and Dome C stations data, it is evident as any change in the CO_2 and CH_4 concentration is always followed, with a certain delay, by a proportional change in the air-temperature. The sheer increase in the atmospheric carbon dioxide concentration, evidenced from the data recorded at the Mauna Loa observatory,[3] has then caused a big alarm for their trend but even more for the recorded absolute CO_2 concentration values: these data in fact indicate as in 2009 the CO_2 concentration amounted to about 390 ppm, that is one third larger than the highest value measured over the past 740,000 years, period interested by ice ages and warm periods. The duty to find a solution to invert this trend and mitigate its consequences is then mandatory. However, if on one hand is important to reduce the greenhouse gas emissions by increasing the energy efficiency of the existing technologies and by adopting less-CO_2 emitting energy sources, a more practical and direct approach to solve the problem is the CO_2 capture approach. In this context, two strategies can be adopted: (i) capturing the atmospheric CO_2 (DAC, direct air capture), in order to reduce the concentration of the CO_2 already present in the atmosphere;[4-8] (ii) capturing the CO_2 present in the flue gases, to avoid any increase in its concentration by reducing the CO_2 anthropogenic emissions. In particular, as the second approach is concerned, the main stream of the research is concentrated in the design of processes for CO_2 capture in power plants based on the combustion of fossil fuels, that account for the 86% of the total anthropogenic greenhouse gas emissions.[9, 10] The capture processing can be placed before or after the combustion of the fuel and then characterized by sensitively different working pressure and temperature. In fact, whereas in a post-combustion process the temperature is only slightly different from RT and the pressure is around 1 bar, for the pre-combustion purification the temperature can be as high as 400°C with pressures sensitively larger than the atmospheric one.[11] The materials used as CO_2 scrubbers are then sensitively different for the two technologies: it is then important to stress for which kind of technology the capturing materials are optimized for. Another important difference between the pre- and the post-combustion processes are the gases involved in: the post-combustion capture, in fact, can be approximately seen as a CO_2/N_2 separation, being essentially an air purification from CO_2, whereas the pre-combustion technology is in a first approximation a H_2/CO_2 separation, if applied in a natural gas plant.[9]

Although promising, the pre-combustion methods are expected to have just a limited application in the short and middle term, being the pre-existing infrastructure fundamentally of post-combustion type. It is then evident as, despite the importance of creating new and more efficient methods for the CO_2 capture, the improvement of the performances of the post-combustion technology would be a more beneficial and more applicable solution to the greenhouse gas problem in the immediate. In particular, between the envisaged CO_2 capture technologies, the

[a] *Dr. J. G. Vitillo, Dr. G. Ricchiardi, Prof. S. Bordiga*
Dipartimento di Chimica IFM and NIS Centre of Excellence,
Università di Torino, INSTM UdR Università
Via Pietro Giuria 7, 10125 Torino, Italia
Fax: (+39) 0116707855
E-mail: jenny.vitillo@unito.it

[b] *Dr. M. Savonnet,*
IRCELYON
University-Lyon, CNRS
2, Av. Albert Einstein, 69626 Villeurbanne Cedex, France

Supporting information for this article is available on the WWW under http://www.chemsuschem.org or from the author.

amine–based scrubbing is the most mature and used in post-combustion air purification processes. Nevertheless, although employed on industrially scale for over 50 years because of its high separation efficiency and its ability to work in a wet environment, the amines technology suffers a number of drawbacks[9, 12] besides the amines flammable, corrosive and toxic nature.[13, 14] These drawbacks are related to the amines sensitivity to oxidation and to the great energy penalty associated with their regeneration, problems that evidently have a strong impact on the cost of the process. In particular, the regeneration energy accounts for the 25-40% of the power generated in the plant, a cost that is difficultly sustainable and that is one order of magnitude larger than the thermodynamic minimum energy penalty,[9] meaning that has a big potential of improvement. The reasons of a so large energy cost are associated to the large stability of the carbamate and carboxylate species formed upon the reaction with CO_2 but also to the presence of a great amount of water (the solvent). Actually, the presence of water, because of its high thermal capacity, requires the wasting of a large amount of heat to bring the amine solution to the regeneration temperatures (80-140°C). Fifty years of research have allowed to identify different ways to improve the performances of the amine technology, by lowering the stability of the reacted species or avoiding the presence of the solvent.[15] For what concerns the latter, a stratagem is to disperse the amines on high surface area supports and many studies employing almost all classes of materials have been already reported, e.g. zeolites,[16] mesoporous siliceous materials,[12, 15, 17-19] xerogels,[20] polymers[21] and MOFs.[22-31] High cyclability, high CO_2 uptake and the thermal stability in the range for the regeneration of the system (25-140°C) are the necessary requirements for the industrial use of an amino-supported material as CO_2 scrubbers. They can be assured by three main features:[12] (i) the presence of a covalent bond between the group bearing the amine functionalities and the support; (ii) high amine loadings (>6 mmol N/g);[32] (iii) moisture resistance. Between the different classes of supports, MOFs are receiving a great interest[26, 28, 33-36] because of their flexibility in synthesis that allows not only to easily change the pore topology but also the chemical composition of the framework, allowing to tune at the molecular level the affinity of the material toward CO_2 in terms of adsorption capacity and selectivity. It is then not surprising that the CO_2 capacities of MOFs are between the largest reported so far[37, 38] and that they have shown promising performances also in separation processes, as CO_2/N_2 (postcombustion),[37, 39, 40] CO_2/H_2 (precombustion),[39] CO_2/CO (steel industry)[41] and CO_2/CH_4 (natural gas sweetening)[26, 37, 39, 42, 43] separations.

It has been claimed as the presence of nitrogen atoms[44, 45] and in particular the functionalization by amino groups[22, 28, 31, 33-36] is a valuable way to increase the MOFs affinity toward CO_2, with benefits on the adsorbed quantities and on the separation selectivities. Nevertheless, small attention is in general paid on the difference of the amines nature present in the framework and on their different affinity and ability to bind CO_2. Both aromatic and aliphatic amines have been dispersed in MOFs. For what concerns aromatic amines,[22, 28-31, 34] they are in general introduced in the framework during the synthesis, by using linkers bearing a $–NH_2$ functionality. Aliphatic amines, on the contrary, are introduced in the MOF frameworks with post-synthesis reactions involving (i) the open metal centers[24, 25] or (ii) a pre-existing aromatic $–NH_2$ groups.[46, 47] In the first case the amine is coordinated by the metal center, whereas in the second case the aromatic amino-group is converted in a functional group bearing an aliphatic amine by using aziridine reactions[46] or the click-on chemistry,[47] with the advantage over (i) that a chemical bond between the MOF and the amine exists, assuring the stability of the grafted species. During the past years, quantum mechanical studies on the interaction between CO_2 and amines were mainly targeted to the use of supercritical CO_2 as alternative to toxic organic solvents in a large number of industrial applications,[48-51] and in particular as dispersion media in the synthesis of polymeric materials as polyurethane.[51, 52] In this case, the possibility to use only low molecular weight monomers, that is CO_2 as a reactant with an amine and an alcohol,[51, 53] avoiding the use of diisocyanate is particularly appealing on the economic and environmental point of view.[54-56] Studies have been also performed on the interaction between CO_2 and polymers.[21, 48-50] Only recently, some works concerning the interaction between CO_2 and MOFs have appeared.[28, 45, 57-60] In particular, Vogiatzis et al.[45] have reported a very detailed study on the CO_2 interaction with N-containing organic heterocycles to be used as MOF linkers. However, although the existence of infrared studies aimed to verify the effect of the presence of amino groups on CO_2 vibrational modes,[22, 29, 31, 51] a corresponding computational work was still lacking. In this work, the possibility to tune the CO_2 affinity for MOFs has been studied at the MP2 level by considering the CO_2 interaction with the cluster models reported in Scheme 1. The possibility to correlate the binding energies with the changes in the CO_2 geometry and vibrations has been also investigated. In a first step, the interaction with benzene-1,4-dicarboxylic acid has been considered because it represents the basic linker in most MOFs;[25, 28, 31, 34] two cluster models have been adopted: benzene (**1**) and benzene-1,4-dicarboxylic acid (**1'**). Three different types of amino-functionalities have been then considered: (i) aromatic amines,[22, 28-31, 34] (ii) aliphatic amines as part of the substituent group on the ring,[46, 47] (iii) aliphatic amines grafted on an open metal center.[24, 25] For what concerns the aromatic amines, aniline (**2**), 2-amino-1,4-benzenedicarboxylic acid (**2'**), 1,2-amino-benzene (**3**), and adenine (**14**) have been used. The **3** model has been adopted also in order to study the contemporary interaction of CO_2 with two $-NH_2$ groups: in fact, the random distribution of the $-NH_2$ substituents in the MOF frameworks makes likely the presence of $-NH_2$ pairs in the material (although belonging to two different rings). Aliphatic amines introduced by aziridation has been modeled with N-phenyl-1,2-ethanediamine (**4**). 4-methylamino-1,2,3-triazole (**5**), 4-methylamino-1,2,3-triazol-1-phenyl (**5'**), 4-dimethylaminomethylene-1,2,3-triazole-1-phenyl (**6**), 4-diethylaminomethylene-1,2,3-triazole-1-phenyl (**7**) have been adopted as models for possible aliphatic amines grafted by means of click-on reactions. These models have been adopted I order to study the adsorption on primary and tertiary amines and the dependence of the CO_2 affinity on the dimension of the N-substituents. Ethylenediamine grafted on 3-Zn-di-1,2,3-triazole (**10**) has been used as model for ethylenediamine in interaction with open metals in MOFs. For comparison, the two adducts have been also simulated separately (**8** and **9**), in order to quantify the benefit of the introduction of the amine (if any) in the MOF. Other functionalities as $-N_3$ (azidebenzene, **11**), $-NO_2$ (nitrobenzene, **12**),[26, 31] and -Br (bromobenzene, **13**)[26, 31] have been considered and their energetics compared to the amines ones. In the end, the interaction of CO_2 with Al-OH (**16**),[22, 40] Ga-OH (**17**),[61] and In-OH (**18**)[61] hydroxyls, often present as competitive adsorption sites in MOFs have been studied. The interaction with silanol (**15**) has been also taken into account as rough model of the most energetic species in silicalite, because of the experimental use of the CO_2 modes in silicalite as reference for the CO_2 shift.[62]

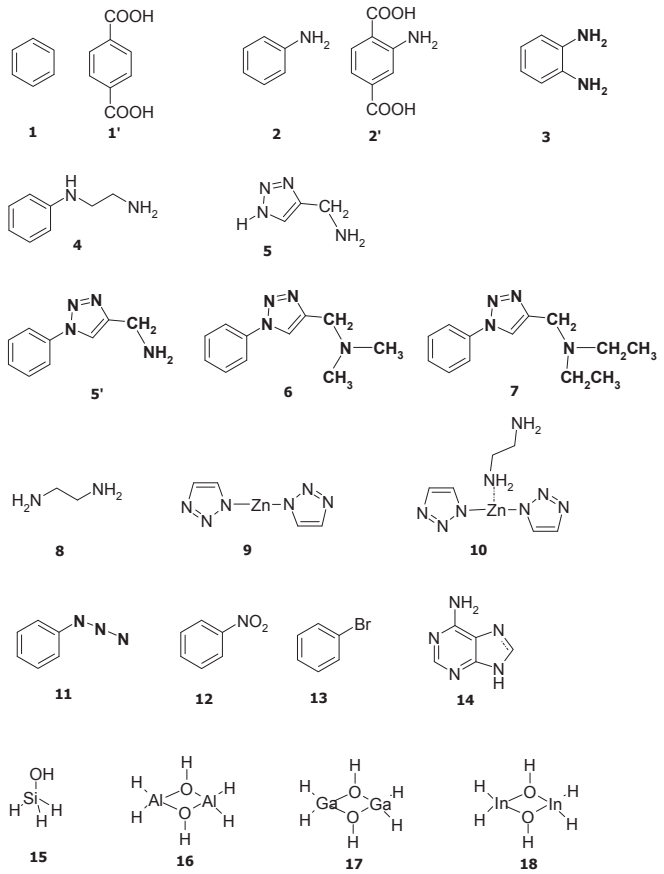

Scheme 1.

Results and Discussion

Carbon dioxide molecule

Carbon dioxide is a linear molecule with a $D_{\infty h}$ symmetry ($d_{C\text{-}O}$ = 1.170 Å at MP2/TZV2p, close to the experimental value of 1.163 Å). The large charge separation in the C=O bonds (q_C = -2q_O = 0.735449 *e*, MP2/TZV2p) is responsible of the significant quadrupole moment of the molecule.[63] The quadrupolar shape of the CO_2 electrostatic potential (ESP) with a positive doughnut in the C plane and two negative lobes on the molecular axis is evident in the map reported in Figure 1. In particular, if the molecule is aligned along the *z* axis, the components of the electrostatic quadrupole are $\Theta_{xx} = \Theta_{yy} = -1/2\Theta_{zz} = 1.3924$ Debye · Å (MP2/TZV2p, traceless tensor, referred to the molecular center of mass coincident with the coordinate origin and in the Buckingham notation). Because of its quadrupolar nature, CO_2 can act both as a Lewis acid and a Lewis base:[63] on purely electrostatic basis for the interaction with negative charges the minimum configuration geometry would be characterized by a side-on geometry in order to allow the interaction through C,[64] whereas interactions with positive centers would involve one of the oxygen atoms in a end-on geometry.[62] As observed for other quadrupolar molecule,[65] also for CO_2 an higher polarization of the molecule is expected for interaction involving the lobes of the molecule and then interaction with positive centers. This would not necessary imply a larger adsorption enthalpy, whereas a larger shift of the vibrational stretching frequencies of the molecule is expected. Moreover, a larger polarization of the molecule would have a beneficial effect on the CO_2-CO_2 interaction and then in facilitating the adsorption process itself after the nucleation.[66]However, because of the large role played also by dispersion forces, in order to maximize its adsorption energy, the CO_2 adsorption in materials happens in general through the contemporaneous interaction of the C atom with a negatively charged/lone pair of the adsorptive and of one or both the O atoms with positive ESP region.

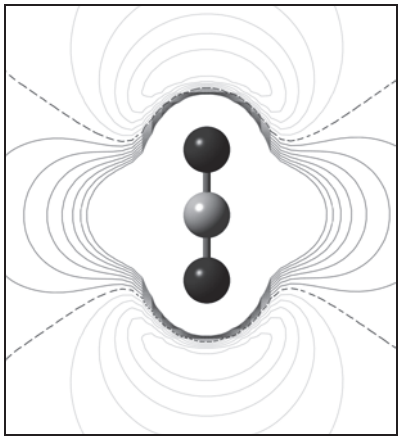

Figure 1. Electrostatic potential map of CO_2 molecule in the plane of the atoms, as obtained at the MP2/TZV2p level. Solid black, dashed black and solid grey lines correspond to positive, zero and negative potentials respectively, in the range between -0.028 a.u. and +0.028 a.u., separated by 0.004 a.u.. Dimensions of the rectangle: 7.5×6.8 Å.

Carbon dioxide is characterized by three vibrational modes: $\tilde{\nu}_1$ that corresponds to the IR-inactive symmetric stretching mode, $\tilde{\nu}_2$, the doubly degenerated bending vibration and $\tilde{\nu}_3$, the asymmetric stretching mode. Upon the interaction with the materials these modes are just slightly shifted, also when highly charged species are present.[62] It is possible to have an idea on the geometry of interaction (side-on or end-on) from the shift of the CO_2 infrared spectrum and then on the nature of the species (Lewis acid or base) directly involved in the interaction (see Table 1). Nevertheless, the presence of a negative charge, although leaving identical (and elongated) the two C=O bonds, causes a change in the ∠OCO angle: this corresponds to the decrease of the $\tilde{\nu}_3$ mode and to the removal of the degeneracy for the $\tilde{\nu}_2$ mode. This results spectroscopically to an increase of the asymmetric stretching mode. On the contrary, in the case of adsorption on a positive charge the molecule is still linear but the two C=O bond are no more identical: the C-O adjacent to the cation increases slightly whereas the other C-O bond decreases of almost the same amount.

Table 1. Sign of the vibrational mode shift for CO_2 adsorption on point charges.

	Positive charges[62]	Negative charges[64]
$\Delta\tilde{\nu}_1$	<0	>0
$\Delta\tilde{\nu}_2$	>0	<0 and > 0
$\Delta\tilde{\nu}_3$	>0	<0

Structure and stability of carbon dioxide complexes

The atoms coordinates as obtained from the optimization of the isolated clusters and of the corresponding CO_2 adducts are

reported in the Supporting Information. Different minima can be individuated for the adsorption of CO_2 on the clusters reported in Scheme 1. In particular, more than one geometry of interaction was considered for the **2**, **4**, **5**, **5'**, **12** and **14** clusters. Being the main purpose of the present study to understand the effect of the introduction in MOFs on the reactivity of the amino groups, these adducts and they were the ones considered in the following, also when they are only local minima (only when in the discussion also the other minima will be taken into account, they will be labeled with the letter a to avoid misunderstanding). The structures of the adducts that will constitute the main topic of the following discussion are reported in Figure 2 and their main geometrical and energetic parameters are reported in Table 2. In Table S1, a more exhaustive summary of the results obtained for all the adducts is presented. In Table S2, the optimized structures and the corresponding labels are shown for the adducts omitted in Figure 2.

Table 2. Average deformation of the CO_2 bond lengths [Å] and angle [°] in the CO_2 adducts with the molecules reported in Scheme 1, distances between the clusters and the carbon of CO_2 and between the clusters and the one of the CO_2 oxygens [Å], and BSSE-corrected binding energies [kJ mol-1] calculated at the MP2/TZV2p level of theory.

system	$\overline{\Delta(C=O)}$[a]	$\Delta\angle OCO$[a]	r(C-X)[b]	r(O-X)[b]	BE[c]
1	0.0004	1.0	3.290	3.416	9.1
1'	0.0005	0.4	3.215	3.250	9.9
2a	0.0005	1.4	2.982	3.323	13.7
2'	0.0004	0.8	3.135	3.144	8.8
3	0.0000	1.7	2.967	2.592	16.2
4a	0.0002	2.6	2.930	2.910	11.3
5a	0.0001	2.4	2.952	2.572	13.0
5'a	0.0005	2.8	2.959	3.039	14.3
6	0.0008	4.1	2.807	2.514	17.1
7	0.0009	3.8	2.908	2.644	15.4
8	0.0003	3.1	2.896	3.300	11.5
9	0.0007	6.0	2.669	2.220	28.2
10	0.0001	2.8	2.939	2.634	12.2
11	0.0003	0.4	3.144	3.107	10.7
12a	0.0003	0.5	3.137	3.095	9.5
13	0.0004	0.7	3.197	3.147	9.5
14a	0.0000	3.1	2.852	2.341	12.6
15	-0.0003	1.9	2.802	3.039	9.5
16	-0.0005	1.0	3.769	2.175	11.2
17	-0.0003	0.6	3.641	2.250	9.4
18	-0.0004	1.0	3.868	2.296	8.8

[a] Calculated values for the unperturbed CO_2 at the MP2/TZV2p: d(C=O) = 1.1702 Å, $\angle$OCO = 180°C. [b] r(C-X) (and r(O-X)) represents the shortest distance between the carbon atom (one of the oxygens) of CO_2 and one atom of the cluster. For the clusters containing a $-NH_2$ directly interacting with CO_2, r(C-X) coincides with the distance from the N atom of the amino group.

It is evident that in all the adducts, the interaction between CO_2 and the clusters is obtained through both the carbon and at least one of the oxygens. This was expected because of the Lewis acid-base nature of CO_2 and it is asked by the need to increase its adsorption energy. Moreover, this agrees with previous calculations[45, 51, 57, 58] and with the geometry of interaction expected on the basis of the electrostatic potential (ESP) maps of the isolated clusters (reported in Figure S1 in the Supporting information): side-on for the **1-15** adducts and end-on for the **9** and **16-18** ones. The usefulness of the ESP maps in predicting the different stability of CO_2 adducts has been reported in a previous study concerning the interaction between CO_2 and N-containing heterocycles.[45] Also in the CO_2/**9** where a strong positive Zn^{2+} center is present, a side-on geometry was obtained because of the high negative potential on the N=N pair of the triazolate ring in **9**, responsible of the low $r_{C\text{-}X}$ value. For what concerns the **16**, **17** and **18** complexes an end-on configuration was evidenced for CO_2 with respect to the H atom of the hydroxyl group. This geometry is different with respect to the one evidenced for the interaction with Si-OH in the **15** adduct, where CO_2 is side on with respect to the hydroxyl. This dissimilarity can be ascribed to the different negative-positive ESP balance in the O-H couple in these four hydroxyl species. In fact, whereas in the case of Si-OH the O and H sites are characterized by an almost equal value of the ESP, in the case of the Al-OH, Ga-OH and In-OH the positive potential on the H is in absolute value larger than the negative potential on the oxygen atom indicating a proton-like behavior of the H atom in **16**, **17** and **18** whereas for silanol the hydroxyl is expected to act as a Lewis acid-base couple, thus justifying the different geometry of adsorption observed for the silanol. The strength of the interaction decreases in the order Al > Si~Ga > In, accordingly to the $r_{O\text{-}H}$ (Al < Ga < In, see Table 2). Being possible in some cases (e.g. MIL-53) to synthesize isostructural Al-, Ga- and In-based MOFs with hydroxyl species, these calculations indicate as an higher affinity toward CO_2 is expected for the Al-MOFs.

As the interaction with arenes is concerned (**1**, **1'**, **2a**, **2'**, **3**, **11**, **12a**, **13**, **14a**), in all the adducts CO_2 is oriented parallel to ring because of the π ···quadrupole interaction but in none of them it is placed on the center of the ring: when a polar group is present on the ring as substituent, the global minimum is always the result of a direct interaction of CO_2 with the group, the relative orientation of CO_2 with respect to the ring changing case by case because results from the attempt to maximize the BE.[57, 58] This holds also in the case of benzene (**1**) where CO_2 is slightly displaced from the center of mass of C_6H_6, in order to allow the oxygen to interact with one of the positively charged H of the benzene. This is in disagreement with previous calculations conducted at a lower level of approximation (PW91/DNP)[57, 58] that indicated a more symmetric geometry for the CO_2/C_6H_6 system. For what concerns aniline, the BE[c] obtained is close to that reported in refs. [51, 58] (14.3 at MP2/aug-cc-pVDZ and 11.9 kJ mol^{-1} at MP2/6-311+G(2d,2p)//PW91/DNP) but lower to that reported in ref. [28] (20 kJ mol^{-1}), that however was not corrected for the BSSE, that is not negligible in interactions where the dispersion component is majority (compare the corrected and uncorrected BE values reported in Table S1 in the Supporting Information).

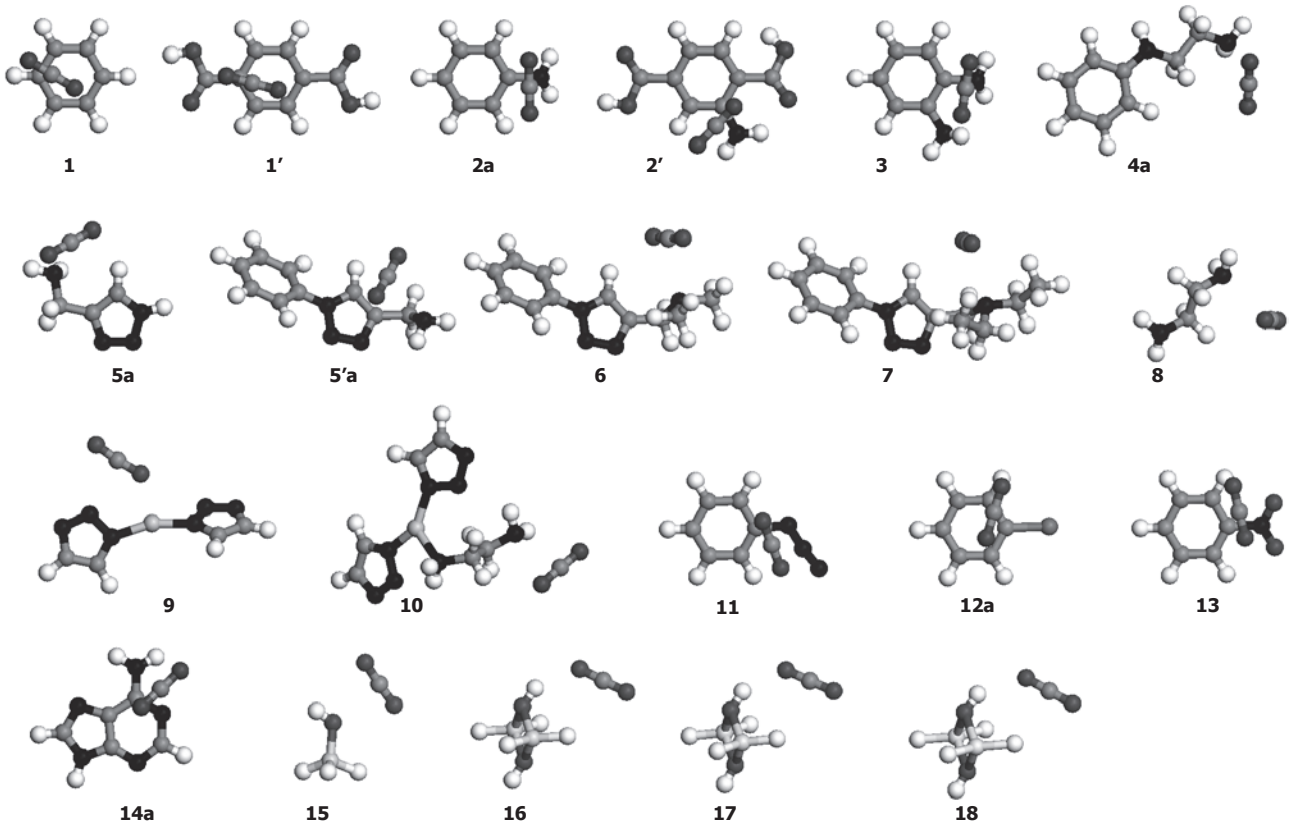

Figure 2. Geometries as obtained by optimization at the MP2/TZV2p level for all the CO_2 adducts considered in this study. The atoms are represented as spheres with the gray code: N (black) > O > C > Br > Zn > Si > Al > Ga > In > H (white).

The BE^c was always larger than that obtained for benzene for both electron-acceptor (-COOH, **1'**, $-N_3$, **11**, $-NO_2$, **12**, and -Br, **13**) and electron-donor ($-NH_2$, **2**, **3**) substituents. This was a further proof that the interaction does not involve only the π orbitals of the arene, because in this case a decrease in the BE^c would be observed for electron-acceptor substituents. The lower BE^c obtained in **2'** is due to the larger deformation energy (DE) obtained for this adduct (3.4 vs. 0.1 kJ mol^{-1}): if the DE energy is considered, the interaction energy results of 12.2 kJ mol^{-1} that is larger than that obtained for **1** and **1'** but lower than that obtained for **2** (**2** > **2'** > **1'** > **1**). In fact in **2'** the ESP on the N atom of the $-NH_2$ group is less negative than in **2** because of the presence of the electron acceptor –COOH group on the ring. The same effect is observed if N are introduced as heteroatom in the ring as in adenine (**14**). In this case the BE^c for the CO_2/NH_2 interaction would be of only 11.6 kJ mol^{-1} (**14a** adduct, see Table 2). It is important to stress that **2'** is the actual linker present in most amino-MOFs that have been claimed in literature to possess an higher affinity for CO_2 with respect to the unfunctionalised ones. This higher affinity has been verified in literature for MIL-53(Al) by means of calorimetric (30 vs. 50[28] kJ mol-1 for the MIL-53(Al) and amino-MIL-53(Al) at the lower coverage), and chromatographic measurements (20.1 vs. 38.4[22] kJ mol^{-1}) and it has been associated to a direct interaction between the $-NH_2$ and the CO_2 molecule. This would be supported by the present calculations if the BE^c for **1** and **2** are concerned. However, if the larger clusters **1'** and **2'** are considered, it is evident as this hypothesis is no more valid being the BE of **2'** even lower than that of **1'** (8.8 vs. 9.9 kJ mol^{-1}). That is the calculations indicate that the presence of aromatic amines would be even detrimental on the CO_2 adsorption enthalpies in terephtalate-based materials. Moreover, although in the amino-functionalised MOFs the CO_2 would be located on the $-NH_2$ group, the larger increase in the affinity toward CO_2 of MIL-53(Al)-NH_2 would be more related to an increased polarity of the whole MOF walls or in the reduction of the internal pore diameter because of the presence of this functional groups than in a local effect. The clusters here studied are a first approximation of the actual linker in the MOF. In fact, first of all, in a metal-organic framework, additional effects, both electronic and steric will come into play, and full periodic calculations on model materials will be necessary to investigate for instance, how steric hindrance might affect the accessibility of the adsorption sites and their interaction with CO_2.[57] This is even more important in breathing materials as MIL-53 is. An estimate of the energetic contribution coming from the pore can be evaluated in a first approximation by comparing the GCMC calculated adsorption enthalpies of CO_2 in the "narrow pores" and the "large pores" configuration of MIL-53(Al)[67] that amounts to 37 and 17 kJ mol^{-1}, respectively). Their difference would account for almost the whole difference between the BE^c obtained for the present model (9.9 kJ mol^{-1}) and the experimental value (30 kJ mol^{-1}) for MIL-53(Al).

However, it is also interesting to note that when two aromatic $-NH_2$ functionalities are present on the ring (**3**), the BE is increased by about the 20%. This is due on one hand to the increase of the ESP values on the ring, because of the well known additive effect on the ESP with respect to the number of substituents on the ring.[57, 68, 69] On the other hand, the presence of a $-NH_2$ pair allows the contemporaneous interaction of CO_2 through C with the N atom of one $-NH_2$ and through one O with the H atoms of the second $-NH_2$. The interaction of CO_2 with the H atoms of the amino-group of aniline (**2b** cluster) is only slightly less energetic than that with the nitrogen atom (11.8 vs. 13.7 kJ

mol^{-1}). This means that if a –NH_2 pair is present, the adsorption enthalpy could be significantly increased with respect to a single –NH_2 and then to an unfunctionalised MOFs. The presence of this pair is possible because of the random distribution of the amino-functionalities in the MOFs. A rough estimation of the probability to have –NH_2 pairs in MIL-53(Al)-NH_2 by using a simple stochastic model has allowed to guess that the 33% of the –NH_2 group in this material are involved in a pair (see Supporting Information for details). Their presence would allow to explain the complex dependence of the isosteric heat q_{iso} on the CO_2 coverage observed experimentally for MIL-53(Al)-NH_2[28] that would not be easily explainable if a single site of adsorption is considered. In fact, whereas for MIL-53(Al) q_{iso} resulted to be completely independent on the coverage being its value fixed at 30 kJ mol^{-1} in the 0-1 bar pressure range, in MIL-53(Al)-NH_2 its behavior was completely different. If the effect of the presence of the amino would be simply the substitution of the **1'** linker with the **2'**, the expected effect would be a shift of the q_{iso} horizontal line to higher/lower values. On the contrary, in MIL-53(Al)-NH_2 q_{iso} is decreasing with the pressure starting from 50 kJ mol^{-1} for zero coverage and crossing the MIL-53(Al) curve for CO_2/NH_2 molar ratio of only 0.15 that is in conditions far from the saturation of the –NH_2 group by CO_2. On the basis of the present calculations the larger q_{iso} observed for CO_2/NH_2 < 0.15 would be ascribable to the interaction with the -NH_2 pairs (that can be then estimated to involve the 30% of the total –NH_2 groups that is a value very close to the percentage calculated on the basis of stochastic considerations), whereas for larger coverage the interaction with single –NH_2 functionalities would allow to obtained lower q_{iso} than that obtained in the unfunctionalised material. Summarizing, it would be the presence of –NH_2 pair and not of the single –NH_2 functionalities the responsible for the larger CO_2 affinity observed experimentally for 2-amino-1,4-benzenedicarboxylate based materials with respect to the corresponding benzene-1,4-dicarboxylate ones.

If the interaction with aliphatic amines (**4**-**8**, **10**) is concerned, the BE significantly changes with the system considered. If the aliphatic amine is grafted directly to the ring (**4**) the BE^c for the CO_2 interaction with -NH_2 was even lower than that obtained for the corresponding aromatic amine in **2** (11.3 kJ mol^{-1}). This was unexpected because of the higher basicity of aliphatic amines than of aromatic ones.[51] However, the BE and the geometrical parameters in CO_2/**4** are identical to those obtained for the isolated ethylenediamine (**8**) and then its chemical reactivity toward CO_2 is expected to be maintained unalterated after the grafting in the MOF, that could then act as a dry dispersing agent. On the contrary, if the ethylenediamine is grafted in MOF by coordinating it to an open metal center, the amine would be strongly polarised by the interaction with the cation (compare the ESP for **8** and **10** in Figure S2): a larger affinity but also an increased chemical reactivity toward CO_2 (formation of carbamate) with respect to the isolated molecule is expected in this case. In fact, the CO_2 binding energy in this case results to be of 12.2 kJ mol^{-1}. However, this BE^c is significantly lower than that calculated for the CO_2 adsorption on the bare cation (**9**, 28.2 kJ mol^{-1}). This is in disagreement to what observed experimentally: for example in ref. [24] a q_{iso} of 21 kJ mol^{-1} has been obtained for CO_2 adsorption on Cu-BTTri (a material with open Cu^{2+} centers) that results to be increased to 90 kJ mol^{-1}[24] after the grafting of ethylenediamine. Nevertheless, the difference between the calculated and experimental values can be reasonably ascribed to the chemical reaction of CO_2 with ethylenediamine, that is not taken into account in the model. The great stability predicted for the grafted ethylenediamine on the Zn^{2+} center in **10** (BE^c = 152.8 kJ mol^{-1}) is in accordance to the observed great thermal stability of these grafted species.[24, 25] The calculated BE^c for water on the metal center amounts to 108.6 kJ mol^{-1}, that is significantly lower that that predicted for the amine, property that would makes this system interesting on the practical point of view.

An alternative way to introduce aliphatic amines in MOFs is by using a click-on reaction. Following the procedure reported in ref. [47], the amine species would be linked to the terephtalic of the MOF through a triazolate. Three possible species have been here considered: a primary amine (-CH_2-NH_2 in **5**, **5'**) and two tertiary amines with a different dimension of the substituents on the N atom (–CH_2-$N(CH_3)_2$ in **6** and –CH_2-$N(CH_2CH_3)_2$ in **7**) in order to verify the effect of the dimension of the substituents on the BE. In these **5**-**7** clusters, two competitive adsorption sites exist on the basis of the ESP maps: the –NH_2 group of the aliphatic amine and the N=N pair on the triazolate ring. Between these two sites, the N=N resulted to possess a lower affinity for CO_2 in all the clusters but for **5**. However, in this case the largest stability of the N=N adduct was in big part due to the great involvement in the interaction of the H^+ proton of the N-H group (cluster **5b** in Figure S2) that is no more present in the larger cluster **5'** because substituted by the benzene ring (capping atom of the model). The –NH^+ group is also responsible of the large BE^c (22.1 kJ mol^{-1}, MP2/TZVPP) obtained in ref. [45] for imidazopyridamine. This hydrogen is in fact characterized by a sensitively higher positive potential with respect of the H atom in benzene. In fact in the corresponding adsorption on the N=N pair in **5'**, CO_2 prefers a pure side on configuration, with the C equidistant from the two N of the pair and the CO_2 oriented perpendicular to the ring (cluster **5'**b in Figure S2) in order to minimize the repulsion between the O atoms and the N=N pair. The dimension of the groups linked to the N atom of the amine has not a monotone influence on the ESP (and then on the BE^c). In fact, whereas an increase in the ESP values is obtained by substituting the primary amine –CH_2-NH_2 of **5'** with the tertiary amine –CH_2-$N(CH_3)_2$ of **6**, no further benefit is obtained by considering bulkier substituent as verified for –CH_2-$N(CH_2CH_3)_2$ (**7**). The reactivity of the amino functionalities are then in the order: **6** (CH_3) > **5'** (H) > **7** (CH_2CH_3). This trend is in accordance with the $r_{C\text{-}N}$ distances as listed in Table 2 but it is opposite with respect to what observed for calculations on aliphatic amines where the BE^c increases with the dimension of the substituents on the N atom going from ETA to TBA.[51] For what concerns the BE^c, it is worth noticing that an increase in the BE^c is observed from **5** to **5'**. This behavior is opposite to what observed for the other functionalities, where the introduction in MOFs (that is increasing the cluster size) causes a decrease in the CO_2 affinity of the group.

In Figure 3, the BE^c is reported as function of $r_{O\text{-}X}$ for **9**, **16**, **17** and **18** that is for the clusters were a predominance of the oxygen contribution can be evidenced and of $r_{C\text{-}X}$ for all the other systems. Also the data related to the **4b** and **14b** adducts characterized by a strong interaction between one of the CO_2 oxygen and the proton of the –NH group of the support are reported in the Figure 3. As a general statement, it is evident from his picture that when the interaction between CO_2 and the support is driven by one of the oxygen the distance of coordination is significantly lower that in the case of carbon. The larger distances observed in the latter case are ascribable to the large electronic repulsion due to the presence of the oxygen atoms on the both side of carbon that prevents small distances of coordination. From this picture it is evident as if the **9** and **14b** clusters are neglected, the BEs slightly changes being all in the interval between 8.8 (for the aromatic amine in 2-amino-terephatalate) and 17.1 kJ mol^{-1} (for the aliphatic tertiary amine of 4-

dimethylaminomethylene-1,2,3-triazole-1-phenyl). A sensitively larger BE^c is obtained when a charged species as a cation is in interaction with CO_2 as in **9**. This is in agreement with what stated in ref. [58], where the highest BE were obtained for the interaction of CO_2 with the acid H atom of the –COOH and -SO_3H groups (14.5 and 16.2 kJ/mol at the MP2/6-311+G(2d,2p) level). As a general observation, when the dispersion forces constitute the main contribution to the BE^c, the binding energies do not exceed 15 kJ/mol also if other functionalities than amines are considered. For what concerns the aliphatic amines, the BE^c are larger than those calculated for the aromatic amines as average, as expected for the well-known larger basicity of the aliphatic amines with respect to the aromatic ones. However, in order to avoid the chemical reaction between the material and CO_2 an aromatic amine would be preferable. The calculations predict that the adsorption enthalpy for an aromatic amine can be close to that of an aliphatic amine, being the two largest BE^c obtained for an aromatic (**3**) and an aliphatic amine (**6**) almost coincident. Nevertheless, it is important to stress as **3** is a model for just special positions in the MOFs synthesized so far whereas the aliphatic amine **6** would represent a "regular" site.

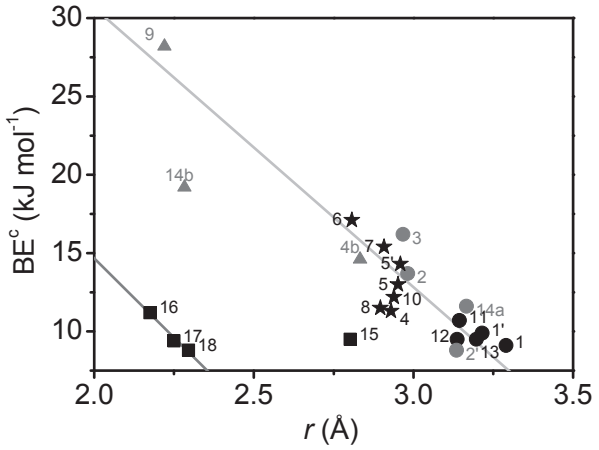

Figure 3. BE^c dependence on the CO_2 – cluster distance for CO_2 adducts. The different scatters refer to the different subsets: arenes (black circles), aromatic (gray circles), aliphatic amines (stars), hydroxyls (squares) and cationic species (triangles).

From the plot reported in Figure 3, it is evident as BE^c does not have a general dependence on the cluster-CO_2 distance (R^2 = 0.18 for a linear fit). Nevertheless, if the adducts are separated in two sets, a linear behavior can be evidenced, the first of this set constituted by almost all the clusters (**1-7**, **9-13**, **14a**, y = -17.83 *x* + 68.31, with R^2 = 0.87), whereas the second one is formed by the adducts with the Al-, Ga- and In-OH species (*y* = -20.24 *x* + 55.14 , with R^2 = 0.97). For what concerns the BE^c dependence on the deformation of the CO_2 molecule (both bond lengths and angle) an even more spread plot was obtained (not reported for the sake of brevity). As a general trend, a larger deformation of CO_2 corresponds to a larger affinity of the system towards CO_2 but a simple relationship between these quantities can not be evidenced.

Vibrational modes

Besides some exceptions, the CO_2 BEs are almost coincident also for quite different systems. On the basis of the present calculations it would be difficult to predict what would be the preferential adsorption site in materials where more than one functionalities is present at the same time. In many MOFs as MIL-68 and MIL-53, hydroxyl groups are present in the structure and can reasonable constitute competitive adsorption sites with respect to the linker: if the BEs are concerned, in terephtalate and 2-amino-terephtalate-based materials the adsorption would essentially involve the hydroxyl groups. If the corresponding enthalpy are considered (see Table 3), on the contrary, whereas for In-OH the adsorption energy is so low that they are expected to coordinate CO_2 only at higher coverage, Al-OH species can constitute competitive adsorption sites with respect to the linker in MIL-53(Al) and MIL-53-(Al)-NH_2. In order to help the understanding of the adsorption mechanism, other techniques have to be used in combination with calorimetry. In particular, infrared spectroscopy can represent a useful tool to have a quick insight on the nature of the sites involved in the interaction from the shift of CO_2 modes (see Table 1). Nevertheless, because these shifts often do not allow an univocal identification of these sites (see below), this information can be more easily derived from the shift of the MOF vibrations.

Table 3. Calculated dissociation energy, adsorption enthalpy [kJ mol^{-1}], and shifts of the CO_2 vibrational modes [cm^{-1}] with respect to the gas phase for the adducts reported in Figure 2 (MP2/TZVp level). All the energetic values are BSSE corrected.

system	D_0^c	ΔH^c	$\Delta\tilde{\nu}_2$ [a]	$\Delta\tilde{\nu}_1$ [a]	$\Delta\tilde{\nu}_3$ [a]
1	7.6	5.4	-2/-14	-1	-3
2a	11.6	9.7	-2/-16	1	-1
3	13.9	12.2	1/-17	1	0
4	9.2	7.4	4/-25	0	-2
5a	10.3	8.9	3/-22	0	-1
8	9.2	7.6	5/-28	0	-2
11	9.5	7.2	-5/-11	-1	-3
12a	7.9	5.8	-5/-8	-1	-3
13a	8.3	5.8	-4/-13	-1	-4
14a					
15	7.4	5.6	4/-12	2	3
16	8.6	6.9	-1/12	3	5
17	7.3	5.3	-5/19	2	3
18	6.4	4.5	-1/-5	3	4

[a] Calculated vibrational modes for isolated CO_2 in the gas phase: $\tilde{\nu}_2$ = 640.9, $\tilde{\nu}_1$ = 1310.8 and $\tilde{\nu}_3$ = 2368.3 cm^{-1}.

In Table 3 the shift of the CO_2 vibrational modes is reported as calculated for a subset of the adducts under study. From a quick look at this table is evident as very similar spectra are expected for different materials, independently on the adsorption energy. In fact, it was not possible to identify a simple relation between the CO_2 shifts and BE^c. This agrees with what can be concluded from the analysis of Table 4 where a review of the CO_2 modes as reported in literature for its adsorption on different MOFs is presented: for example it is evident as the spectra obtained on UiO-66 MOFs prepared with different linker are

almost identical. Coming back to the calculated data reported in Table 3, it is evident as whereas $\tilde{\nu}_1$ and $\tilde{\nu}_3$ are almost unchanged with respect to the free molecule, $\tilde{\nu}_2$ results to be split in two components where one remains close to the gas phase value ($|\Delta\tilde{\nu}_2| \leq 5$ cm^{-1}) whereas the other is redshifted of some tens of cm^{-1}. The larger sensitivity of the $\tilde{\nu}_2$ with respect to the most common used $\tilde{\nu}_3$ has been observed experimentally for the interaction of CO_2 with polymers.[21] The greater sensitivity of $\tilde{\nu}_2$ has also been demonstrated in studies on the CO_2 solubility in liquids.[70, 71] In such a kind of systems, the width of the ν_2 band can be also used to estimate the strength of interaction between CO_2 and polymers.[21] Unfortunately this region of the spectrum is complicated by the presence of the $^{13}CO_2$ bending modes that being only 20 cm^{-1} redshifted with respect to the $^{12}CO_2$ ones makes more difficult the determination of the actual shift: the vibration of the $^{13}CO_2$ in the gas phase can be superimposed to that corresponding to the adsorbed $^{12}CO_2$.

Table 4. Review of the CO_2 vibrational frequencies [cm^{-1}] as obtained experimentally for its adsorption on MOFs at room temperature in different pressure *P* conditions [mbar]. The frequencies for the two most abundant CO_2 isotopes in the gas phase and the frequencies reported for $^{12}CO_2$ after the adsorption in silicalite and polystyrene are also reported.

system	*P*	$\tilde{\nu}_2$	$\tilde{\nu}_1$	$\tilde{\nu}_3$
Gas ($^{12}CO_2$)[62]		667.3	1388.3	2349.3
Gas ($^{13}CO_2$)[72]		649	1334	2283
Silicalite[62, 73]	< 1	662		2341
PS[21]		657.2		2334.9
UiO-66[31]	0.72			2340
UiO-66-NH_2[31]	0.72			2337
UiO-66-NO_2[31, 74]	0.72	685, 669, 659, 649		2339
UiO-66-Br[31, 74]	0.72	684, 669, 662, 657, 649		2338
MIL-53(Cr)[75, 76]	11	669, 662, 650		2335
MIL-53(Al)[75]		661, 649		
MIL-53(Al)-NH_2[29]	200	669, 667, 661, 655, 649		2334
IRMOF-3[22, 29]		669, 667, 653		
HKUST-1				2333
CPO-27-Mg				2353
Ni-DBM-BPy[77]	2000	661, 645		2333

By carefully looking at the $\Delta\tilde{\nu}_3$ values reported in Table 3, it is evident as although this mode is only slightly shifted it can provide indications on the CO_2 adsorption site, as anticipated. In fact, as expected on the basis of what stated in Table 1, CO_2 results to be: (i) blueshifted in interactions where the "oxygen component" is the majoritary component (as for the interaction with the N=N pair in **5** or with the hydroxyls), (ii) redshifted if the "carbon component" is playing the main role (as in the clusters representing the organic component of the material), (iii) it is not perturbed if these two components are balancing each other as for **3** where although a relatively high BE^c the predicted $\Delta\tilde{\nu}_3$ is null. This observation is important because it would represent an easy way to understand by which kind of site the adsorption is carried out and which is the geometry of CO_2 with respect to it. However, $\Delta\tilde{\nu}_3$ is in general so small that if more than one site is contemporaneously interacting with the same CO_2 molecule it would be difficult to correctly understand what is going on.

A more clear indication would come from the shift of the functional group modes. For what concerns the $-NH_2$ stretching modes, the calculations indicate that if the amino group is directly interacting with CO_2 both its symmetric and asymmetric stretching modes would be redshifted of about –10 cm^{-1}: -10 and –10 cm^{-1} in **2**, -8 and –8 cm^{-1} in **4**, -9 and –8 cm^{-1} in **5** and -9 and –8 cm^{-1} in **8** (a negligible shift for the not interacting NH_2 is also predicted in **8**). Also in **3** the two asymmetric stretching frequencies are redshifted of –5 and –9 cm^{-1}, whereas for the symmetric modes a shift of –5 cm^{-1} was calculated. These shifts agree with those observed experimentally by Farbos et al.[51] for the symmetric stretching mode of $-NH_2$ in aromatic amine in supercritical CO_2 at 80 bar and 40°C: -9 cm^{-1} for aniline, -15 cm^{-1} for 1,4-benzene-diamine and of –7 cm^{-1} for 1,3-benzene-diamine. Shifts of the same order of magnitude are expected for the $-N_3$ (-7 cm^{-1}, **11**) and $-NO_2$ (-3/+3 cm^{-1}, **13**) groups.

If the sites involved directly in the interaction with CO_2 would be hydroxyl species, even larger shifts of their modes are expected: $\Delta\tilde{\nu}_{OH}$ of –12 (**15**), -44 (**16**), -30 (**17**), and –26 (**18**) cm^{-1} have been calculated. These values are of the same order of magnitude of the $\Delta\tilde{\nu}_{OH}$ reported in refs. [75, 76] for CO_2 adsorption in MIL-53(Cr) (-19 cm^{-1}).

In order to allow the comparison between the calculated CO_2 vibrational frequencies and those reported experimentally for MOFs, it is important to remind as in the case of the adsorption on microporous materials, it is not correct to take as reference for the unperturbed molecule the gas phase value for $\tilde{\nu}_3$ because of the large matrix effect due to the confinement.[62] For this reason, the $\tilde{\nu}_3$ value observed in silicalite, because of its apolar framework is in general taken as reference.[59, 62, 78] However, although lacking of cations, silicalite is not lacking of possible adsorption sites represented by silanols. By looking at the data reported in Table 3 it is evident that although the low interaction, a silanol would be able to shift upwards the $\tilde{\nu}_3$ mode of +3 cm^{-1}. On the basis of that, the reference value for the unperturbed CO_2 in a microporous matrix would be of 2338 cm^{-1} and for this purpose will be adopted in the following. This value is even in larger agreement with that calculated for unperturbed CO_2 in Ref. [62]. By considering this as the reference value, a $\Delta\tilde{\nu}_3 > 0$ was reported for UiO-66 (+2 cm^{-1}), UiO-66-NO_2 (+1) and CPO-27-Mg (+15) as expected for the interaction with –OH (**15**-**18** clusters), -NO_2 (**12**) and open metal cations (**9**) respectively. Unexpectedly for MIL-53(Cr) a $\Delta\tilde{\nu}_3 < 0$ was observed in apparent contrast with the contemporaneous shift of the hydroxyls modes that would ask for a $\Delta\tilde{\nu}_3 > 0$. However, this contradiction is ascribable to the completely different arrangement of CO_2 in MIL-53 material in their narrow pore conformation (verified at lower CO_2 coverage): in fact, molecular mechanics calculations performed on a periodic model[67] indicates that in this case, because of the suitable distance between the two hydroxyls rows on the opposite sides of the pore, CO_2 would be able to interact contemporaneously with two -OH. Only at pressure higher than 6 bar, that is when the adsorption is carried out by the larger pore conformer a blue shit of the stretching mode would be observable.

Conclusions

Different functional groups have been tested for their affinity toward CO_2 by means of quantum-mechanical calculations. As a

general remarks if strongly polarizing sites are absent, the BEs are only slightly dependent on the system considered. For the systems considered the BEs in this case were all comprises in the interval between 8.8 (for the aromatic amine in 2-amino-terephatalate) and 17.1 kJ mol^{-1} (for the aliphatic tertiary amine of 4-dimethylaminomethylene-1,2,3-triazole-1-phenyl). If on the contrary highly polarizing species as open cations (e.g. Zn^{2+} or H^+) are present, the affinity of these systems easily overcome that of other sites. It is not accidental that the two largest BE belongs to 3-Zn-di-1,2,3-triazole and adenine where CO_2 is adsorbed on a Zn^{2+} and H^+ cation respectively. In general a side-on geometry of interaction for CO_2 is observed independently on the predominant negative/positive values of the electrostatic potential on the cluster. This was related to the low BEs that would result CO_2 results to have the tendency to adsorb both by the C and at least one O in order to maximize the energetics. On this basis it can be predicted that the CO_2 geometry of interaction with materials is the side-on one. This is opposite what happens in gas phase for the interaction with bare positive or negative charges. This hypothesis was confirmed on the basis of literature data that indicate that always the interaction the CO_2 bending mode is always followed by the spitting of the degenerate bending mode in two separate components.

For what concerns the amines, a large variety of species have been considered in this study, chosen between those already reported in literature and by proposing some new functionalities. The cluster calculations allowed to confirm the larger affinity towards CO_2 of aliphatic amines with respect to aromatic amines as average, as expected on the basis of their larger basicity. In particular, between the amino species studied the 4-dimethylaminomethylene-1,2,3-triazole-1-phenyl is predicted to be able to improve the MOF affinity toward CO_2 in separation/adsorption processes with respect to similar systems proposed in literature up to now. For what concerns the use of infrared spectroscopy as methods to characterize the CO_2 adsorption in materials the calculations indicates as the stretching modes are quite insensitive to the adsorption energy being shifted of just some cm^{-1} whereas a larger difference between the signals obtained can be obtained by looking at the bending CO_2 modes or, even better, to the shift of the functional groups involved in the interaction. IR is not able to discriminate between the different adsorption sites present on the organic linker as predicted by the calculations (same spectra for different materials): IR is useful to detect if chemical fixation happens but not to discriminate different organic sites although of different adsorption energy. In the end, on the basis of the present calculations an attempts to assign the adsorption sites in different MOFs has been made on the basis of the experimental isosteric heats and spectroscopical signals. The present calculations also indicate as–NH_2 pairs occasionally occurring in amino-terephatalate based MOFs, as the sites actually responsible for the improved performances of MIL-53(Al)-NH_2, one of the most studied material for CO2 adsorption and separation, with respect of the unfunctionalised MIL-53(Al).

Experimental Section

Computational methods. The calculations have been performed with the *Gaussian 09* software package.[79] All the systems under study have been optimized by means of the post-Hartree Fock perturbative Møller-Plesset method truncated at second-order (MP2) [80] in the frozen-core approximation. The use of MP2 was necessary because of the significant role of the dispersion forces in the interaction.[28, 45, 60] The inadequacy of less expensive DFT methods, was verified by applying the B3-LYP method to a subset of the complexes here studied. For the hydrogen atoms, the standard Pople basis set supplemented by diffuse and polarizability functions 6-31+G(d,p) has been adopted.[81, 82] For In, an effective core potential (ECP) has been used to replace the innermost core electrons whereas the outermost core orbitals has been treated utilizing a double-ζ contraction[83, 84] (Lanl2DZ). The C, N, O, Br, Si, Al and Ga elements have been modeled by means of the fully optimized triple-ζ valence basis sets proposed by Ahlrichs *et al*.[85] with polarization (TZVp). The C, N, O and Br basis set has been augmented by two sets of polarization functions derived from the original ones following an even-tempered recipe that is by substituting the polarization orbital in the basis set with two orbitals, having respectively the coefficient doubled and halved with respect to the parent orbital. The so obtained basis sets will be indicated as TZV2p in the following. Geometry optimization has been carried out by means of the Berny optimization algorithm with analytical gradient. The thresholds were set to 0.000450 and 0.000300 a.u. for the maximum and the rms forces respectively; and to 0.001800 and 0.001200 a.u. for the maximum and rms atomic displacements, respectively. A (99,590) pruned grid was used (i.e. 99 radial points and 590 angular points per radial point). No symmetry constraints have been imposed.

Harmonic frequencies have been obtained by analytically determining the second derivatives of the energy with respect to the Cartesian nuclear coordinates and then transforming them to mass-weighted coordinates. No scaling factor has been adopted. The dissociation energy from the ground state (D_0) of the adducts was calculated from the corresponding dissociation energy from the potential energy minimum D_e by including the zero point energies (ZPE) of reactants and products. The ZPE was calculated in the harmonic approximation. The enthalpy variations ($^{\Delta H}_{ads}$) at standard conditions (298.15 K and 1 atm) were derived from the reaction energies including the ZPE and temperature corrections. The temperature corrections were computed using the standard expressions for an ideal gas in the canonical ensemble. No scaling factors were adopted. All the energetic data have been corrected for the basis set superposition error (BSSE) following the a posteriori method proposed by Boys and Bernardi[86] as implemented in *Gaussian 09*. The BSSE corrected energetic values are signalized by a c superscript and were obtained from the computed *Y* values as $Y^c = Y$ - BSSE.

Acknowledgements

Financial support by European VI framework through STREP project MOFCAT Contract number: NMP4-CT-2006-033335 and by European VII framework through STREP project NANOMOF Contract number: FP7-NMP-2008-LARGE-2 are gratefully acknowledged. Prof. A. Zecchina is acknowledged for fruitful discussions.

Keywords: Carbon dioxide fixation, Amines, Metal-organic frameworks, Density functional calculations, supercritical solvent.

[1] ((Reference 1, Example: a) A. Author, B. Coauthor, *ChemSusChem* **2008**, *1*, 1-10; b) A. Author, B. Coauthor, *Angew. Chem.* **2006**, *118*, 1-5; *Angew. Chem. Int. Ed.* **2006**, *45*, 1-5.))

[2] ((Reference 2.))

[3] …

Received: ((will be filled in by the editorial staff))
Published online: ((will be filled in by the editorial staff))

Entry for the Table of Contents (Please choose one layout)

Layout 1:

FULL PAPER

((Text for Table of Contents))

((Insert TOC Graphic here))

((Author(s), Corresponding Author(s))*

Page No. – Page No.

((Title))

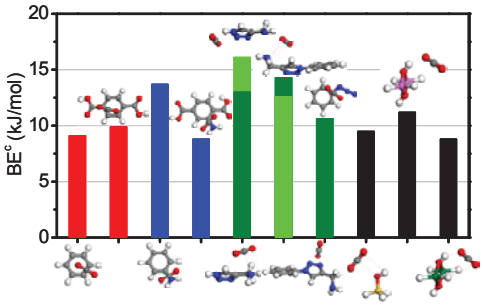

Layout 2:

FULL PAPER

((Insert TOC Graphic here))

((Author(s), Corresponding Author(s))*

Page No. – Page No.

((Title))

((Text for Table of Contents))

[1] EPICA, *Nature* **2004**, *429*, 623.
[2] J. R. Petit, et al., *Nature* **1999**, *399*, 429.
[3] C. D. Keeling, T. P. Whorf, Carbon Dioxide Research Group del Scripps Institution of Oceanography (SIO), *University of California, La Jolla, California USA 92093-0444*, (http://cdiac.esd.ornl.gov/ftp/maunaloa.
[4] D. W. Keith, M. Ha-Duong, J. K. Stolaroff, *Clim. Change* **2006**, *74*, 17.
[5] K. S. Lackner, *Sci.Am.* **2010**, *302*, 66.
[6] V. Nikulshina, A. Steinfeld, *Chem. Eng. J.* **2009**, *155*, 867.
[7] M. C. MacCracken, *Environ. Res. Lett.* **2009**, *4*.
[8] K. S. Lackner, *Eur. Phys. J.-Spec. Top.* **2009**, *176*, 93.
[9] D. M. D'Alessandro, B. Smit, J. R. Long, *Angew. Chem.-Int. Edit.* **2010**, *49*, 6058.

[10] S. R. Caskey, A. G. Wong-Foy, A. J. Matzger, *J. Am. Chem. Soc.* **2008**, *130*, 10870.
[11] A. L. Goodman, L. A. Campus, K. T. Schroeder, *Energy Fuels* **2005**, *19*, 471.
[12] J. C. Hicks, J. H. Drese, D. J. Fauth, M. L. Gray, G. G. Qi, C. W. Jones, *J. Am. Chem. Soc.* **2008**, *130*, 2902.
[13] M. Nainar, A. Veawab, *Ind. Eng. Chem. Res.* **2009**, *48*, 9299.
[14] A. Veawab, P. Tontiwachwuthikul, A. Chakma, *Ind. Eng. Chem. Res.* **1999**, *38*, 3917.
[15] R. Serna-Guerrero, E. Da'na, A. Sayari, *Ind. Eng. Chem. Res.* **2008**, *47*, 9406.
[16] R. Srivastava, D. Srinivas, P. Ratnasamy, *Appl. Catal. A* **2005**, *289*, 128.
[17] X. C. Xu, C. S. Song, J. M. Andresen, B. G. Miller, A. W. Scaroni, *Energy Fuels* **2002**, *16*, 1463.
[18] R. Srivastava, D. Srinivas, P. Ratnasamy, *J. Catal.* **2005**, *233*, 1.
[19] R. Srivastava, D. Srinivas, P. Ratnasamy, *Micropor. Mesopor. Mater.* **2006**, *90*, 314.
[20] A. Dibenedetto, C. Pastore, C. Fragale, M. Aresta, *ChemSusChem* **2008**, *1*, 742.
[21] S. G. Kazarian, M. F. Vincent, F. V. Bright, C. L. Liotta, C. A. Eckert, *J. Am. Chem. Soc.* **1996**, *118*, 1729.
[22] S. Couck, J. F. M. Denayer, G. V. Baron, T. Remy, J. Gascon, F. Kapteijn, **2009**, *131*, 6326.
[23] J. L. Song, Z. F. Zhang, S. Q. Hu, T. B. Wu, T. Jiang, B. X. Han, *Green Chem.* **2009**, *11*, 1031.
[24] A. Demessence, D. M. D'Alessandro, M. L. Foo, J. R. Long, *J. Am. Chem. Soc.* **2009**, *131*, 8784.
[25] Y. K. Hwang, et al., *Angew. Chem.-Int. Edit.* **2008**, *47*, 4144.
[26] A. Phan, C. J. Doonan, F. J. Uribe-Romo, C. B. Knobler, M. O'Keeffe, O. M. Yaghi, *Acc. Chem. Res.* **2009**, *43*, 58.
[27] R. Vaidhyanathan, S. S. Iremonger, K. W. Dawson, G. K. H. Shimizu, *Chem. Commun.* **2009**, 5230.
[28] B. Arstad, H. Fjellvag, K. O. Kongshaug, O. Swang, R. Blom, *Adsorption* **2008**, *14*, 755.
[29] J. Gascon, U. Aktay, M. D. Hernandez-Alonso, G. P. M. van Klink, F. Kapteijn, *J. Catal.* **2009**, *261*, 75.
[30] S. Bauer, C. Serre, T. Devic, P. Horcajada, J. Marrot, G. Ferey, N. Stock, *Inorg. Chem.* **2008**, *47*, 7568.
[31] M. Kandiah, et al., **2010**, accepted.
[32] P. J. E. Harlick, A. Sayari, *Ind. Eng. Chem. Res.* **2006**, *45*, 3248.
[33] M. J. Ingleson, J. P. Barrio, J. B. Guilbaud, Y. Z. Khimyak, M. J. Rosseinsky, *Chem. Commun.* **2008**, 2680.
[34] J. L. C. Rowsell, O. M. Yaghi, *J. Am. Chem. Soc.* **2006**, *128*, 1304.
[35] O. M. Yaghi, M. O'Keeffe, N. W. Ockwig, H. K. Chae, M. Eddaoudi, J. Kim, *Nature* **2003**, *423*, 705.
[36] M. Eddaoudi, J. Kim, N. Rosi, D. Vodak, J. Wachter, M. O'Keeffe, O. M. Yaghi, *Science* **2002**, *295*, 469.
[37] A. R. Millward, O. M. Yaghi, *J. Am. Chem. Soc.* **2005**, *127*, 17998.
[38] P. L. Llewellyn, S. Bourrelly, C. Serre, Y. Filinchuk, G. Férey, **2006**, *45*, 7751.
[39] E. Neofotistou, C. D. Malliakas, P. N. Trikalitis, *Chem.-Eur. J.* **2009**, *15*, 4523.
[40] A. Comotti, S. Bracco, P. Sozzani, S. Horike, R. Matsuda, J. Chen, M. Takata, Y. Kubota, S. Kitagawa, *J. Am. Chem. Soc.* **2008**, *130*, 13664.
[41] H. Kim, Y. Kim, M. Yoon, S. Linn, S. M. Park, G. Seo, K. Kim, *J. Am. Chem. Soc.* **2010**, *132*, 12200.
[42] M. Xue, Y. Liu, R. M. Schaffino, S. C. Xiang, X. J. Zhao, G. S. Zhu, S. L. Qiu, B. L. Chen, *Inorg. Chem.* **2009**, *48*, 4649.
[43] M. Tagliabue, D. Farrusseng, S. Valencia, S. Aguado, U. Ravon, C. Rizzo, A. Corma, C. Mirodatos, *Chem. Eng. J.* **2009**, *155*, 553.
[44] H. Hayashi, A. P. Cote, H. Furukawa, M. O'Keeffe, O. M. Yaghi, *Nat. Mater.* **2007**, *6*, 501.
[45] K. D. Vogiatzis, A. Mavrandonakis, W. Klopper, G. E. Froudakis, *ChemPhysChem* **2009**, *10*, 374.
[46] O. M. Yaghi, *FY 2009 Annual Progress Report, DOE Hydrogen Program* **2009**.
[47] M. Savonnet, D. Bazer-Bachi, N. Bats, J. Perez-Pellitero, E. Jeanneau, V. Lecocq, C. Pinel, D. Farrusseng, *J. Am. Chem. Soc.* **2010**, *132*, 4518.
[48] C. A. Eckert, B. L. Knutson, P. G. Debenedetti, *Nature* **1996**, *383*, 313.
[49] J. F. Brennecke, *Nature* **1997**, *389*, 333.
[50] O. S. Fleming, S. G. Kazarian, *Polymer Processing with Supercritical Fluids*, Wiley-VCH Verlag GmbH & Co. KGaA, **2006**.
[51] B. Farbos, T. Tassaing, *Phys. Chem. Chem. Phys.* **2009**, *11*, 5052.
[52] B. Renault, E. Cloutet, H. Cramail, T. Tassaing, M. Besnard, *J. Phys. Chem. A* **2007**, *111*, 4181.
[53] W. McGhee, D. Riley, K. Christ, Y. Pan, B. Parnas, *J. Org. Chem.* **1995**, *60*, 2820.
[54] J. E. Bara, D. E. Camper, D. L. Gin, R. D. Noble, *Acc. Chem. Res.* **2009**, *43*, 152.
[55] J. E. Bara, T. K. Carlisle, C. J. Gabriel, D. Camper, A. Finotello, D. L. Gin, R. D. Noble, *Ind. Eng. Chem. Res.* **2009**, *48*, 2739.
[56] D. Camper, J. E. Bara, D. L. Gin, R. D. Noble, *Ind. Eng. Chem. Res.* **2008**, *47*, 8496.
[57] A. Torrisi, C. Mellot-Draznieks, R. G. Bell, *J. Chem. Phys.* **2009**, *130*.
[58] A. Torrisi, C. Mellot-Draznieks, R. G. Bell, *J. Chem. Phys.* **2010**, *132*, 044705.
[59] L. Valenzano, B. Civalleri, S. Chavan, G. Turnes Palomino, C. Otero Areán, S. Bordiga, **2010**, *114*, 11185.
[60] B. Arstad, R. Blom, O. Swang, *J. Phys. Chem. A* **2007**, *111*, 1222.
[61] C. Volkringer, et al., **2008**, *47*, 11892.
[62] B. Bonelli, B. Civalleri, B. Fubini, P. Ugliengo, C. Otero Areán, E. Garrone, **2000**, *104*, 10978.
[63] P. Raveendran, Y. Ikushima, S. L. Wallen, *Accounts Chem. Res.* **2005**, *38*, 478.
[64] J. M. Weber, H. Schneider, *J. Chem. Phys.* **2004**, *120*, 10056.
[65] J. G. Vitillo, A. Damin, A. Zecchina, G. Ricchiardi, *J. Chem. Phys.* **2006**, *124*.
[66] J. Zhou, Q. Wang, Q. Sun, P. Jena, X. S. Chen, *Proc. Natl. Acad. Sci. U.S.A.* **2010**.
[67] N. A. Ramsahye, G. Maurin, S. Bourrelly, P. L. Llewellyn, T. Devic, C. Serre, T. Loiseau, G. Ferey, **2007**, *13*, 461.
[68] A. D. Hunter, V. Mozol, S. D. Tsai, *Organometallics* **1992**, *11*, 2251.
[69] J. G. Vitillo, E. Groppo, S. Bordiga, S. Chavan, G. Ricchiardi, A. Zecchina, *Inorg. Chem.* **2009**, *48*, 5439.
[70] C. Heald, *Proc. R. Soc.* **1962**, *A268*, 89.
[71] J. C. Dobrowolski, M. H. Jamroz, *J. Mol. Struct.* **1992**, *275*, 211.
[72] T. Shimanouchi, *Tables of Molecular Vibrational Frequencies Consolidated Vol. I*, National Bureau of Standards, **1972**.
[73] S. K. Wirawan, D. Creaser, *Micro. Meso. Mat.* **2006**, *91*, 196.
[74] F. Bonino, private communication.
[75] A. Vimont, A. Travert, P. Bazin, J. C. Lavalley, M. Daturi, C. Serre, G. Ferey, S. Bourrelly, P. L. Llewellyn, *Chem. Commun.* **2007**, 3291.
[76] S. Bourrelly, P. L. Llewellyn, C. Serre, F. Millange, T. Loiseau, G. Ferey, **2005**, *127*, 13519.
[77] J. T. Culp, A. L. Goodman, D. Chirdon, S. G. Sankar, C. Matranga, *J. Phys. Chem. C* **2010**, *114*, 2184.
[78] M. Armandi, E. Garrone, C. O. Arean, B. Bonelli, **2009**, *10*, 3316.
[79] M. J. Frisch, et al., Revision B.05 ed., Gaussian, Inc., Wallingford CT, **2004**.
[80] C. Møller, M. S. Plesset, **1934**, *46*, 618.
[81] T. Clark, J. Chandrasekhar, G. W. Spitznagel, P. v. R. Schleyer, *J. Comp. Chem.* **1983**, *4*, 294.
[82] M. J. Frisch, J. A. Pople, J. S. Binkley, *J. Chem. Phys.* **1984**, *80*, 3265.
[83] W. R. Wadt, P. J. Hay, **1985**, *82*, 284.
[84] P. J. Hay, W. R. Wadt, **1985**, *82*, 270.
[85] A. Schäfer, C. Huber, R. Ahlrichs, *J. Chem. Phys.* **1994**, *100*, 5829.
[86] S. F. Boys, F. Bernardi, *Mol. Phys.* **1970**, *19*, 553.

DOI: 10.1002/anie.200((will be filled in by the editorial staff))

Tailoring Metal-Organic Framework Catalysts by Click Chemistry: Synergistic Effect by Tandem Functionalization

*Marie Savonnet, Aurélie Camarata, Jerome Canivet, Delphine Bazer-Bachi, Nicolas Bats, Vincent Lecocq, Catherine Pinel and David Farrusseng**

Metal-organic frameworks (MOFs) are porous crystalline materials composed of cationic metal systems that behave like nodes with polytopic organic ligands acting as spacers.[1] These materials are often viewed as a new class of zeolites due to their porous structure. MOFs of the most recent generation present molecular recognition properties[2] originating from their considerable dynamic flexibility[3], which is usually under the control of host-guest interactions. It is acknowledged that MOFs could ultimately mimic enzymes using a "locking" concept favoring high chemo-, regio- and enantioselectivity.[4] MOFs could indeed be viewed as potential "artificial enzymes" combining several properties in a concerted fashion at the nanometer scale. Fairly few MOFs bear more than one reactive function, however. The catalytic properties of these materials have, to date, essentially relied on the features of the inorganic nodes.[5] For example, inorganic clusters with unsaturated coordination (such as HKUST-1) or bridging hydroxyl groups (such as MIL-53) have been shown to perform Lewis [6] and Brønsted type catalysis [7] respectively.

One solution for synthesizing advanced MOFs suitable for specialized and sophisticated applications is the controlled addition of more complex functionalities into the porous network. Through this functionalization, if the physical environment of the pores and the cavities within the MOFs can be modified, the interactions with guest species can in turn be adapted, thereby fine-tuning the chemical reactivity.[8] However, the introduction of reactive chemical functions by self-assembly methods is not a trivial task and cannot be generalized to all MOFs.[9] Various synthetic strategies have been employed with the aim of achieving MOF post-functionalization, as detailed in extensive reviews by Cohen *et al*.[10] Post-synthetic modification (PSM) using covalent-type grafting methods has undergone outstanding progress during the last five years.[11] We have recently reported an original PSM method starting from amino derived MOFs.[12] The first step consists in converting the amino groups on the framework walls into their analogous azido (N_3). Without isolation nor purification, the desired triazolyl functionalized MOF materials are obtained by grafting the corresponding alkyne using "clik chemistry" (Figure 1). Using two different MOFs templates, the DMOF [Zn(2-amino-terephthalate)(dabco)] (dabco = 1,4-diazabicyclo[2.2.2]octane) and the IHM-2 [In(OH)(2-amino-terephthalate)], we showed that this novel PSM method presents key benefits for the engineering of MOF: i) the softness of the method allows no restriction on the choice of starting amino-MOFs and ii) the grafting yield can be controlled by adjusting the MOF:alkyne ratio.

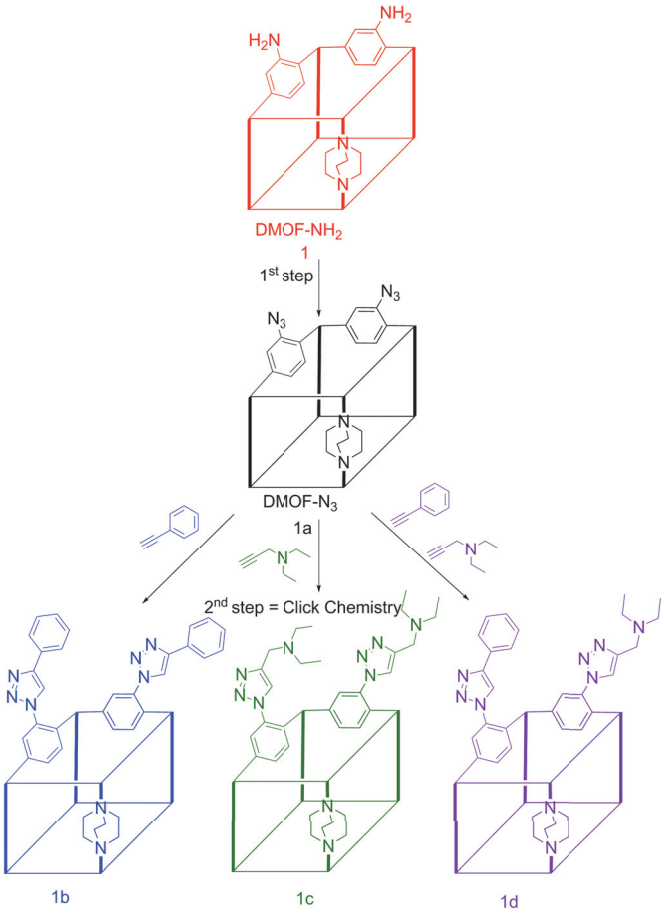

Figure 1. Synthesis of MOF catalysts by "click chemistry"

Despite intensive efforts to develop new efficient, selective and recyclable solid base catalysts such as Layered Double Hydroxides (LDH),[13] hydrotalcite, KF and amine supported compounds, the development of green processes involving basic catalysts remains a challenge.[14]

In this contribution, we demonstrate that PSM by "click chemistry" enables the engineering of MOFs for application in base catalysis. The controlled post-modification of the frameworks introducing basic and/or hydrophobic features allows a rational

[*] A. Camarata, Dr. J. Canivet, Dr. C. Pinel, Dr. D. Farrusseng
IRCELYON, University of Lyon 1
CNRS, 2 avenue Albert Einstein
F-69626, Villeurbanne Cedex
Fax: (+33) 4 72 44 53 99
E-mail: david.farrusseng@ircelyon.univ-lyon1.fr

M. Savonnet, Dr. D. Bazer-Bachi, Dr. N. Bats, Dr. V. Lecocq
IFP Energies Nouvelles
BP n°3, 69360, Solaize, France

[**] We thank IRCELYON and IFP Scientific Services.

Supporting information for this article is available on the WWW under http://www.angewandte.org or from the author.

design of catalytic MOFs for the transesterification reaction.[15] We show for the first time that outstanding synergistic catalytic effect can be obtained by an optimal formulation of our functionalized material.

The base-catalyzed model reaction considered here is the transesterification of ethyldecanoate in methanol (Scheme 1).

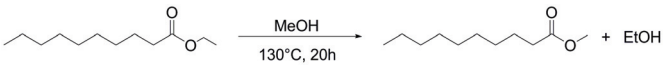

Scheme 1. Transesterification of ethyldecanoate in methanol

For this reaction to proceed efficiently, both substrates must be co-adsorbed into the MOF and MeOH should be activated by a base in order to favour the nucleophilic attack on the carbonyl group. The DMOF parent structure was selected as the starting platform since it contains neither Lewis nor Brønsted acid groups that could have a catalytic effect. Two different functional groups were selected for post-modification: a 1,2,3-triazolyl substituted with phenyl, corresponding to **b** compounds, or tertiary amine at the 4-position, corresponding to **c** compounds (Figure 1). They are obtained by reacting the DMOF-N_3 (**1a**) with phenylacetylene to give **1b** and with propargylamine to give **1c**. The former **1b** presents moderate basicity originating from the triazolyle group (pKa ≈ 1,2) as well as strong hydrophobicity, whereas the latter **1c** is a much stronger base (pKa ≈ 11 for alkylamines). A bifunctionalized MOF modified with **b** groups (phenyl) and then subsequently modified with **c** groups (tertiary amine) on the remaining azido sites was obtained and hereafter denoted **1d**. The degree of modification of the MOF catalysts is given in Table 1.

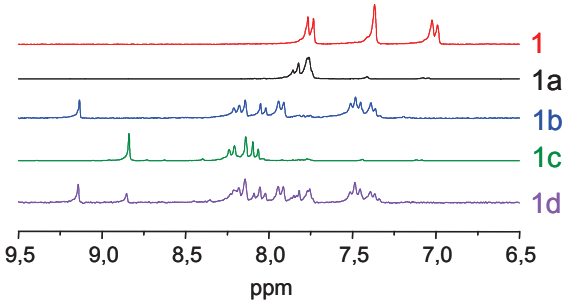

Figure 2. ^{1}H NMR of digested **1**, **1a**, **1b, 1c** and **1d** compounds

Clear proof of the azide formation and of the subsequent full (3+2) cycloaddition can be characterized by liquid ^{1}H NMR on a quantitative manner (figure 2). The spectrum of digested DMOF-N_3 (**1a**) reveals the formation of the azido corresponding compound through the appearance of new aromatic signals (7.73-7.83 ppm). This coincides with the complete disappearance of the aromatic signals of DMOF-NH_2 (**1**) at 7.15 ppm, 7.44 ppm and 7.8 ppm, thus indicating almost full conversion to the azido form. After the cycloaddition step, new aromatic shifts of the post-modified compounds **1b** and **1c** confirm that the corresponding triazole derivative is formed as the sole product. The post-digestion ^{1}H NMR spectrum of **1d** shows contributions of both **b** and **c** and also of the remaining azide in a 30:30:40 ratio (see Table 1).

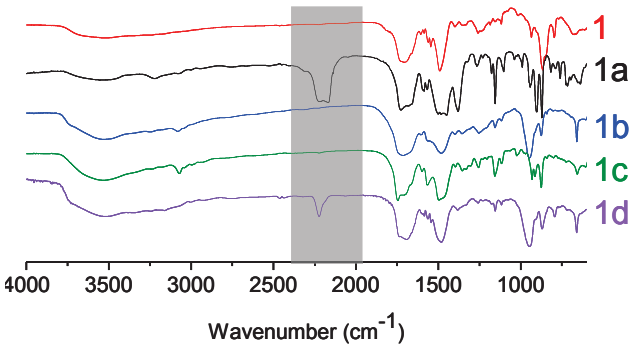

Figure 3. FT-IR of **1**, **1a**, **1b, 1c** and **1d** compounds

IR spectroscopy studies confirm these results (Figure 3). The appearance of the IR absorption band at 2123 cm^{-1} is characteristic of the N_3 asymmetric stretching vibration of DMOF-N_3 **1a**. In the cases of **1b**, **1c**, its disappearance after the cycloaddition step is proof of almost total conversion to the final compound. In the case of **1d** ,the less intense $-N_3$ signal is well in line with the partial conversion as quantified by ^{1}H NMR (see table 1). Despite solvent effects on DMOF structure and crystallinity,[12, 16] powder X-ray diffraction patterns (PXRD) indicates that long-range order is preserved for all samples (Figure 4).

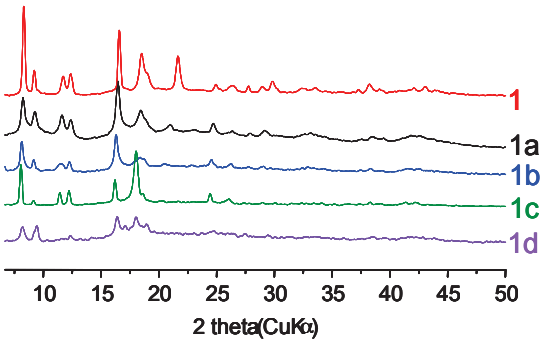

Figure 4. Powder XRD patterns of **1**, **1a**, **1b, 1c** and **1d** compounds

Following similar methodology, samples with variable degree of modification were prepared. They are obtained by adjusting the amount of alkyne reactants, phenylacetylene or diethyl-propargylamine, with respect to **1a**. There are denoted hereafter **1b-15**, **1b-40** and **1b-80** for degrees of modification with **b** groups (phenyl) of 15%, 40% and 80% respectively, and **1c-40**, **1c-85** for degrees of modification with **c** groups (tertiary amine) of 40% and 85% respectively. Synthesis details and characterization can be found in the supporting information.

These DMOF catalysts were involved in the transesterification of ethyldecanoate with methanol and all the catalytic results are summarized in the Table 1. It is worthy to note that the transesterification conversion obtained using the unmodified DMOF-NH_2 (**1**) as catalyst is not higher than that obtained without catalyst (c.a. 10%, entries 1 and 2).

Table 1. Transesterification conversion of functionalized MOFs and reference catalysts [a]

Entry	Catalyst	b (%)	c (%)	conversion (%)
1	**none**	-	-	10
2	**1**	-	-	10
3	**1b-40**	40	-	48
4	**1b-40** [b]	40	-	0
5	**1b-80**	80	-	82
6	**1c-40**	-	40	21
7	**1c-85**	-	85	28
8	**1d**	**30**	**30**	**84**
9	$Cu(ACN)_4PF_6$ [c]	-	-	32
10	$Cu(OAc)_2$ [c]	-	-	40
11	**linker b** [c]	100	-	30
12	**linker c** [c]	-	100	21

[a] Conditions: ethyldecanoate (2.5 mL) is allowed to react in methanol (10 mL) using 20 mg of DMOF catalyst (~0.03 mmol MOF, c.a 0.06 mmol $–NH_2$) at 130°C for 20h [b] 2-ethyl-1-butanol is used instead of methanol [c] Homologue catalysts used under homogenous conditions (scheme 2); 0.3 mmol of catalyst are used.

The figure 5 illustrates also how the degree of modification affects ethyldecanoate conversion in the case of the monofunctionalized materials. It appears that the activity of these DMOF materials increases linearly with the degree of modification. The syntheses and tests were performed twice for **1b-80** in order to verify experimental reproducibility; both times the ethyldecanoate conversion was approximately 80% (Table 1, entry 5).

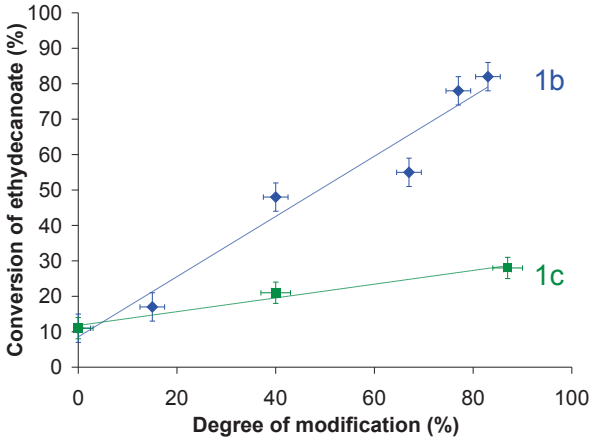

Figure 5. Effect of the degree of modification for **1b** (♦) and **1c** (■) on ethyldecanoate conversion at 130°C after 20 h

The DMOF grafted with **c** groups could have been expected to show better activity based on the higher basic strength of the trialkylamine compared to that of the phenyl substituent. Surprisingly, the introduction of hydrophobic functions via **b** exhibits a more beneficial effect on catalytic activity. Furthermore, the corresponding organic functionalized linker found in **1b** and **1c,** respectively **linker b** (dimethyl-2-(4-phenyl-1H-1,2,3-triazol-1-yl)-terephthalate) and **linker c** (dimethyl-2-(4-diethylaminomethyl-1H-1,2,3-triazol-1-yl)-terephthalate), were synthesized (Scheme 2).

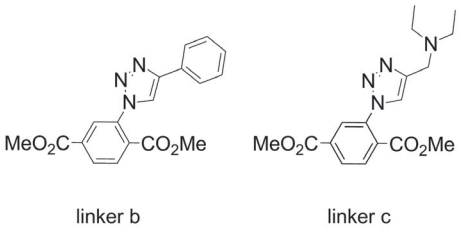

Scheme 2. Molecular homologues of the catalysts **1b** and **1c**.

The **linker b** and the **linker c** were tested in the transesterification reaction under homogeneous conditions and show moderate activity compared to the corresponding grafted MOFs with conversions of 30% and 21% respectively (Table 1, entries 11 and 12) against 82% for **1b-80** (entry 5) and 28% for **1c-85** (entry 7). These results confirm the moderate activity of the triazolyl group itself.

In contrast, the tandem post-modified **1d** shows outstanding performances compared to the monofunctionalized DMOF samples. Although **1d** contains only 30% of **b** and 30% of **c**, 84% conversion was achieved (entry 8). Under similar reaction conditions, using **1b-40** and **1c-40** with similar degree of modification, the conversion only reached 48% and 21%, respectively (entries 3 and 6). This superior activity can be attributed to a synergistic effect resulting from the combination of both basic and hydrophobic groups at molecular level.

In order to assess our hypothesis of a synergistic basic-hydrophobic effect, liquid adsorption isotherms with an ethyldecanoate/isooctane mixture were investigated for **1** and for **1b-40**, containing 40% of 4-phenyl-1,2,3-triazolyl functions (Figure 6).

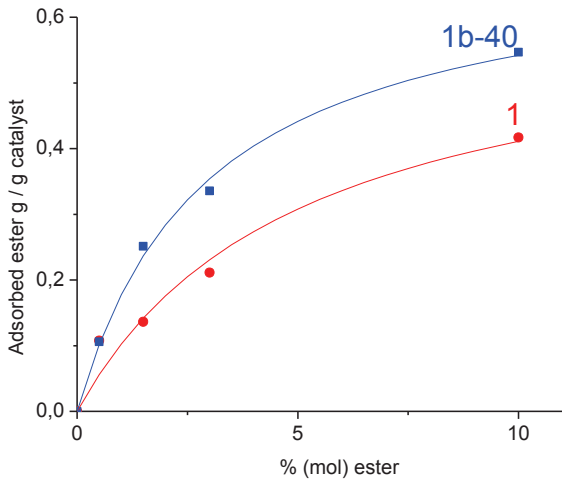

Figure 6. Liquid adsorption isotherms of ethyldecanoate in the ethyldecanoate/isooctane mixture for **1** (●) and **1b-40** (■)

These adsorption measurements confirm the stronger hydrophobicity of the latter material. Consequently, we suggest that the higher apparent activity of **1b** compared to **1c** should be due to a more appropriate co-adsorption ratio of both substrates inside the pores on the more hydrophobic MOF. Hence, **1d** with a tandem functionalization reaches an optimal basic/hydrophobic balance to perform the reaction.

Moreover, the use of a bulky primary alcohol in the transesterification reaction has been also used to confirm that the reaction takes place into the porous system and not only at the surface.[15b] The transesterification with 2-ethyl-1-butanol, which is a much bulkier substrate than methanol, was carried out using the MOF **1b-40**. As shown in the table 1, no conversion was obtained in 2-ethyl-1-butanol against 48% in MeOH (entry 4). This clearly indicates that the reaction proceeds into the pores framework when MeOH is used, whereas the reaction does not take place in the case of a bulky alcohol due to the molecular sieving property of the MOF.

Powder XRD shows that DMOF materials remain mostly crystalline after catalysis although peak broadening is observed (Figure S6). As discussed previously, it may arise from the intrinsic flexibility of the DMOF structure.[12, 16] Most important, under catalytic conditions the robustness of the solid towards leaching was investigated. When the catalyst is filtered off, the reaction does not proceed any longer. As far as the elemental analyses performed on our samples show the presence of 1 to 2 wt% of Cu in the solids, we investigated the effect of copper on our catalytic system. According to the molecular formula of the functionalized MOFs and to the catalyst quantity used in the reaction, the amount of copper present in our tests corresponds to 0.002-0.004 mmol. Although the exact nature and oxidation state of the copper is not known, it might be possible that some of the copper remain as $Cu^{I}(ACN)_4PF_6$ in the pore after the click chemistry and may act as a catalyst.[17] Control experiments carried out with 0,3 mmol of $Cu(ACN)_4PF_6$ or $Cu(OAc)_2$, corresponding to 100 times more Cu than really contained in our MOFs, show a catalytic activity lower than that obtained using our functionalized DMOF (Table 1).

In conclusion, we were able in a single framework to successively introduce new basic catalytic centers (amino groups) and hydrophobic groups (phenyl groups) in order to enhance the catalytic activity of our solid. Thanks to the strict control of the synthetic conditions, the precise optimization of these parameters can be achieved. In the case of the transesterification of ethyldecanoate with methanol, the best activity is obtained using tandem post-modification involving at each step a low degree of modification. The resulting bifunctionalized MOF provides an optimized balance between catalytic activity, through the basicity, and substrates co-adsorption, through the hydrophobicity. More generally, this post-functionalization methodology based on an original "one-pot" click chemistry enables the engineering of MOF catalysts in a rational manner, considering multiple independent factors and starting from an initial MOF structure that is appropriate in terms of pore size or intrinsic functionalities.[18] This opens new perspective for the rational design of multifunctional solid catalysts.

Experimental Section

The synthesis procedure and the method of post-functionalization for DMOF-NH_2 (**1**) to give **1b**, **1c** and **1d** are described in details in the Supporting Information.

All catalytic measurements for the transesterification reaction were carried out in a Teflon®-lined stainless steel digestion bomb (TopIndustrie) under stirring. Ethyldecanoate (2.5 mL) and methanol (10 mL) were made to react in the presence of 20 mg catalyst for 20 h at 130°C. After the reaction, the catalyst was recovered by filtration, and a sample of the filtrate was diluted in CH_2Cl_2 and analyzed by gas chromatography (HP 6890N equipped with a 30 m HP5 column). Carbon mass balances always exceeded 97%.

Received: ((will be filled in by the editorial staff))
Published online on ((will be filled in by the editorial staff))

Keywords: metal-organic frameworks · post-synthesis · click chemistry · coordination polymers · heterogeneous catalysis ·

[1] a) M. O'Keeffe, M. Eddaoudi, H. Li, T. Reineke, O. M. Yaghi, *J. Solid State Chem.* **2000**, *152*, 3; b) N. L. Rosi, M. Eddaoudi, J. Kim, M. O'Keeffe, O. M. Yaghi, *CrystEngComm* **2002**, 401; c) G. Ferey, *Chem. Mater.* **2001**, *13*, 3084; d) G. Férey, *J. Solid State Chem.* **2000**, *152*, 37; e) R. Banerjee, A. Phan, B. Wang, C. Knobler, H. Furukawa, M. O'Keeffe, O. M. Yaghi, *Science* **2008**, *319*, 939; f) M. J. Rosseinsky, *Microporous Mesoporous Mater.* **2004**, *73*, 15; g) M. Eddaoudi, D. B. Moler, H. L. Li, B. L. Chen, T. M. Reineke, M. O'Keeffe, O. M. Yaghi, *Acc. Chem. Res.* **2001**, *34*, 319; h) J. P. Zhang, X. M. Chen, *J. Am. Chem. Soc.* **2008**, *130*, 6010; i) B. Wang, A. P. Cote, H. Furukawa, M. O'Keeffe, O. M. Yaghi, *Nature* **2008**, *453*, 207; j) S. Kaskel, in *Handbook of Porous Solids*, Wiley-VCH Verlag GmbH, **2008**.

[2] a) R. Matsuda, R. Kitaura, S. Kitagawa, Y. Kubota, R. V. Belosludov, T. C. Kobayashi, H. Sakamoto, T. Chiba, M. Takata, Y. Kawazoe, Y. Mita, *Nature* **2005**, *436*, 238; b) S. Horike, R. Matsuda, D. Tanaka, S. Matsubara, M. Mizuno, K. Endo, S. Kitagawa, *Angew. Chem., Int. Ed.* **2006**, *45*, 7226; c) S. Bureekaew, S. Shimomura, S. Kitagawa, *Sci. Technol. Adv. Mater.* **2008**, *9*, 12.

[3] a) J. A. R. Navarro, E. Barea, A. Rodriguez-Dieguez, J. M. Salas, C. O. Ania, J. B. Parra, N. Masciocchi, S. Galli, A. Sironi, *J. Am. Chem. Soc.* **2008**, *130*, 3978; b) S. Horike, S. Shimomura, S. Kitagawa, *Nature Chem.* **2009**, *1*, 695; c) S. Kitagawa, M. Kondo, *Bull. Chem. Soc. Jpn.* **1998**, *71*, 1739.

[4] a) D. Farrusseng, S. Aguado, C. Pinel, *Angew. Chem., Int. Ed.* **2009**, *48*, 7502; b) J. Lee, O. K. Farha, J. Roberts, K. A. Scheidt, S. T. Nguyen, J. T. Hupp, *Chem. Soc. Rev.* **2009**, *38*, 1450; c) K. P. Lillerud, U. Olsbye, M. Tilset, *Top. Catal.* **2010**, *53*, 859; d) D. Bradshaw, J. B. Claridge, E. J. Cussen, T. J. Prior, M. J. Rosseinsky, *Acc. Chem. Res.* **2005**, *38*, 273; e) D. Bradshaw, T. J. Prior, E. J. Cussen, J. B. Claridge, M. J. Rosseinsky, *J. Am. Chem. Soc.* **2004**, *126*, 6106; f) C. J. Kepert, T. J. Prior, M. J. Rosseinsky, *J. Am. Chem. Soc.* **2000**, *122*, 5158.

[5] A. Corma, H. Garcia, F. X. Llabres i Xamena, *Chem. Rev.* **2010**, *110*, 4606.

[6] a) L. Alaerts, E. Seguin, H. Poelman, F. Thibault-Starzyk, P. A. Jacobs, D. E. De Vos, *Chem.-Eur. J.* **2006**, *12*, 7353; b) K. Schlichte, T. Kratzke, S. Kaskel, *Microporous Mesoporous Mater.* **2004**, *73*, 81; c) A. Dhakshinamoorthy, M. Alvaro, H. Garcia, *Chem.-Eur. J.* **2010**, *16*, 8530.

[7] U. Ravon, G. Chaplais, C. Chizallet, B. Seyyedi, F. Bonino, S. Bordiga, N. Bats, D. Farrusseng, *ChemCatChem* **2010**, *2*, 1235.

[8] a) A. Corma, M. Iglesias, F. Sanchez, *Catal. Lett.* **1995**, *32*, 313; b) A. Corma, M. Iglesias, C. Delpino, F. Sanchez, *J. Organomet. Chem.* **1992**, *431*, 233; c) A. Corma, M. Iglesias, C. Delpino, F. Sanchez, *J. Chem. Soc.-Chem. Commun.* **1991**, 1253; d) S. J. M. Thomas, *Chemcatchem* **2010**, *2*, 127; e) J. M. Thomas, R. Raja, *Acc. Chem. Res.* **2008**, *41*, 708; f) M. D. Jones, R. Raja, J. M. Thomas, B. F. G. Johnson, D. W. Lewis, J. Rouzaud, K. D. M. Harris, *Angew. Chem., Int. Ed.* **2003**, *42*, 4326; g) J. M. Thomas, T. Maschmeyer, B. F. G. Johnson, D. S. Shephard, *J. Mol. Catal.* **1999**, *141*, 139; h) M. E. Davis, *Nature* **2002**, *417*, 813.

[9] a) C. Yang, X. P. Wang, M. A. Omary, *J. Am. Chem. Soc.* **2007**, *129*, 15454; b) M. Kawano, T. Kawamichi, T. Haneda, T. Kojima, M. Fujita, *J. Am. Chem. Soc.* **2007**, *129*, 15418.

[10] a) S. Cohen, E. M.Dugan, Z. Q. Wang, M. Okamura, A. Medina, *Chem. Commun.* **2008**, 3366; b) S. M. Cohen, *Chemical Science* **2010**, *1*, 32; c) E. Dugan, Z. Q. Wang, M. Okamura, A. Medina, S. M. Cohen, *Chem. Commun.* **2008**, 3366; d) S. J. Garibay, Z. Q. Wang, K. K. Tanabe, S. M. Cohen, *Inorg. Chem.* **2009**, *48*, 7341; e) K. K. Tanabe, Z. Q. Wang, S. M. Cohen, *J. Am. Chem. Soc.* **2008**, *130*, 8508; f) C. Volkringer, M. C. Seth *Angew. Chem., Int. Ed.* **2010**, *49*, 4644; g) Z. Q. Wang, S. M. Cohen, *J. Am. Chem. Soc.* **2007**, *129*, 12368; h) Z. Q. Wang, S. M. Cohen, *Angew. Chem., Int. Ed.* **2008**, *47*, 4699; i) Z. Q. Wang, S. M. Cohen, *Chem. Soc. Rev.* **2009**, *38*, 1315; j) Z. Q. Wang, K. K. Tanabe, S. M. Cohen, *Inorg. Chem.* **2009**, *48*, 296.

[11] a) S. Aguado, J. Canivet, D. Farrusseng, *J. Mater. Chem.* **2011**, *21*, 7582; b) T. Ahnfeldt, D. Gunzelmann, T. Loiseau, D. Hirsemann, J.

Senker, G. Ferey, N. Stock, *Inorg. Chem.* **2009**, *48*, 3057; c) J. Canivet, S. Aguado, C. Daniel, D. Farrusseng, *ChemCatChem* **2011**, *3*, 675; d) C. J. Doonan, W. Morris, H. Furukawa, O. M. Yaghi, *J. Am. Chem. Soc.* **2009**, *131*, 9492; e) M. J. Ingleson, J. P. Barrio, J. B. Guilbaud, Y. Z. Khimyak, M. J. Rosseinsky, *Chem. Commun.* **2008**, 2680; f) M. Savonnet, S. Aguado, U. Ravon, D. Bazer-Bachi, V. Lecocq, N. Bats, C. Pinel, D. Farrusseng, *Green Chem.* **2009**, *11*, 1729; g) X. Zhang, F. X. Llabrés i Xamena, A. Corma, *J. Catal.* **2009**, *265*, 155.

[12] M. Savonnet, D. Bazer-Bachi, N. Bats, J. Perez-Pellitero, E. Jeanneau, V. Lecocq, C. Pinel, D. Farrusseng, *J. Am. Chem. Soc.* **2010**, *132*, 4518.

[13] a) M. L. Kantam, A. Ravindra, C. V. Reddy, B. Sreedhar, B. M. Choudary, *Adv. Synth. Catal.* **2006**, *348*, 569; b) V. P. R. Raje, R. P. Bhat, S. D. Samant, *Synlett* **2006**, *16*, 2676; c) M. L. Kantam, B. Neelima, C. V. Reddy, *J. Mol. Catal. A Chem.* **2005**, *241*, 147.

[14] a) A. Corma, H. Garcia, *Adv. Synth. Catal.* **2006**, *348*, 1391; b) F. Figueras, M. L. Kantam, B. M. Choudary, *Curr. Org. Chem.* **2006**, *10*, 1627; c) A. Martin, V. N. Kalevaru, *Chemcatchem* **2010**, *2*, 1504; d) Y. C. Sharma, B. Singh, J. Korstad, *Fuel* **2011**, *90*, 1309.

[15] a) C. Chizallet, S. Lazare, D. Bazer-Bachi, F. Bonnier, V. Lecocq, E. Soyer, A. A. Quoineaud, N. Bats, *J. Am. Chem. Soc.* **2010**, *132*, 12365; b) J. S. Seo, D. Whang, H. Lee, S. I. Jun, J. Oh, Y. J. Jeon, K. Kim, *Nature* **2000**, *404*, 982.

[16] D. N. Dybtsev, H. Chun, K. Kim, *Angew. Chem., Int. Ed.* **2004**, *43*, 5033.

[17] M. B. Smith, J. March, in *March's Advanced Organic Chemistry*, John Wiley & Sons, Inc., **2006**, pp. 1419.

[18] O. M. Yaghi, M. O'Keeffe, N. W. Ockwig, H. K. Chae, M. Eddaoudi, J. Kim, *Nature* **2003**, *423*, 705.

Entry for the Table of Contents (Please choose one layout)

Metal-Organic Frameworks

Marie Savonnet, Emanuel Kockrick, Aurélie Camarata, Delphine Bazer-Bachi, Nicolas Bats, Vincent Lecocq, Catherine Pinel and David Farrusseng*

_____ Page – Page

Tailoring Metal-Organic Framework Catalysts by Click Chemistry: Synergistic Effect by Tandem Functionalization

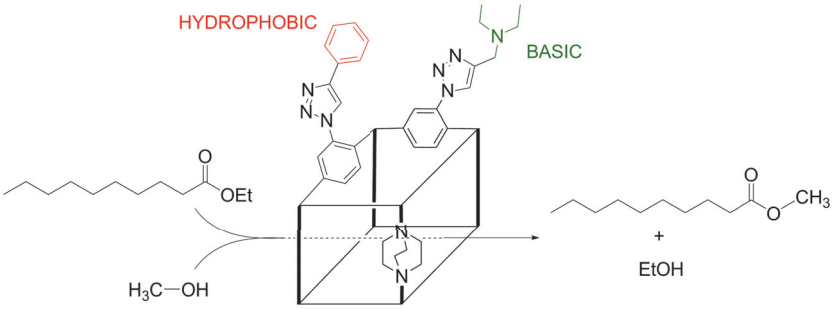

Click reaction into MOFs is an efficient tool to engineer its intrinsic properties and give new opportunities for catalyst design at molecular level. We successively introduce new basic catalytic centers and modify their environment by addition of hydrophobic groups. The resulting bifunctionalized MOF provides an optimized balance between basicity and hydrophobicity and shows outstanding performance for the transesterification reaction.

RESUME en français

Les MOFs résultent de l'organisation de polyèdres métalliques reliés par des molécules organiques chélatantes pour former un réseau poreux. La construction de solides hybrides organiques/inorganiques permet d'imaginer un très grand nombre de matériaux aux propriétés structurales et physico-chimiques variées. Le confinement du substrat dans une structure rigide, associé à des propriétés particulières des clusters métalliques ainsi qu'à des parois pouvant être fonctionnalisées, fournissent un environnement catalytique unique, plaçant les MOF à la frontière entre les espèces types zéolites et les enzymes. Cependant, il existe aujourd'hui très peu de MOFs possédant plus d'une fonction catalytique. Néanmoins, les propriétés catalytiques des MOFs peuvent être améliorées de façons non négligeables grâce aux méthodes de post-fonctionalisation. Dans ce travail, nous reportons le développement d'une méthode de post-fonctionnalisation originale des amino-MOFs. La première étape consiste à convertir la fonction amine en fonction azoture. Puis, sans isolation ni purification, le MOF fonctionnalisé est obtenu par « Click Chemistry » en ajoutant l'alcyne correspondant. Cette méthode peut être appliquée à tous les types d'amino-MOFs et à quasi toutes les fonctions chimiques que l'on souhaite greffer. Une large librairie de nouveaux matériaux a ainsi été obtenue et complètement caractérisée. Cette méthode a aussi été utilisée pour créer des MOFs catalytiques à façon pour une réaction de transesterification, ainsi que pour l'investigation de nouvelles applications plus fines (niches industrielle).

TITRE en anglais

Synthesis and catalytic activity of acid/basic Metal Organic frameworks

RESUME en anglais

MOFs result from the association of metallic clusters connected by organic linkers to form a net. It is acknowledged that ultimately MOFs could mimic "enzymes" using "molecular recognition" concept to allow high chemio-, regio-, enantio-selectivity. We could indeed anticipate MOFs as potential "artificial enzymes" that can combine several properties at the nanometer scale in a concerted fashion. However to date, the number of MOFs with more than one reactive "catalytic" function is rather scarce. A key to address advanced MOF materials suitable for more sophisticated applications is to add functionalities of greater complexity in a controlled manner. The ability to modify the chemical environment of the cavities within MOFs would allow tuning of the interactions with guest species, and serve as a route to tailor the chemical reactivity of the framework. However, the introduction of reactive chemical functions by self-assembly methods is not a trivial task.

In this work, we report an original PSM method starting from amino derived MOFs. The first step consists in converting the amino group into azide (N_3). Without isolation nor purification, the desired functionalized material is obtained by grafting the corresponding alkyne using "Clik Chemistry". This method can be applied to all kind of amino-MOFs and to all kind of grafted chemical functions. A diverse library of original MOFs was synthesized and characterized. Finally, this method was used to engineer catalytic MOFs for the transesterification of ethyldecanoate with methanol or to investigate applications in specialized industrial niches.

DISCIPLINE

Catalyse et Chimie-Physique des matériaux

MOTS-CLES: metal organic frameworks • post-synthesis • click chemistry • catalysis •

INTITULE ET ADRESSE DE L'U.F.R. OU DU LABORATOIRE :

IRCELYON, 2 avenue Albert Einstein, 69626, Villeurbanne cedex

IFP Energies nouvelles, Rond-point de l'échangeur de Solaize, BP 3, 69360, Solaize

III.3.4 Reactivity of hydroxyl groups

Among the few MOFs possessing bridging OH groups, the most famous is the 2-dimensional MIL-53 formulated as $M^{III}(OH)(bdc)$ where M^{III} can be Al, Cr [130], Ga [131] or Fe [132] . The postsynthetic modification of this inorganic linker, in contrast with the functionalization of organic ligands, is much less studied but must be highlighted as an alternative method, related to the OH reactivity in mesoporous silicates.

Starting from the MIL-53(Al), Meilikhov and coworkers used the highly reactive 1,1'-ferrocenediyl-dimethylsilane to perform the sylilation of the OH group, bridging AlO_6 octahedra, under solvent-free gas-phase conditions in order to form the oxydimethyl(ferrocenyl)silane analogue [133] (Figure III-9). According to ^2H MAS NMR experiments, 25% of the hydroxyl groups were modified following the protocol. Intensity variations were found in the PXRD data which were attributed to the pore filling but TG analysis showed no weight loss up to decomposition temperature of the network itself, indicating a strong binding of the ferrocenyl silane to the framework.

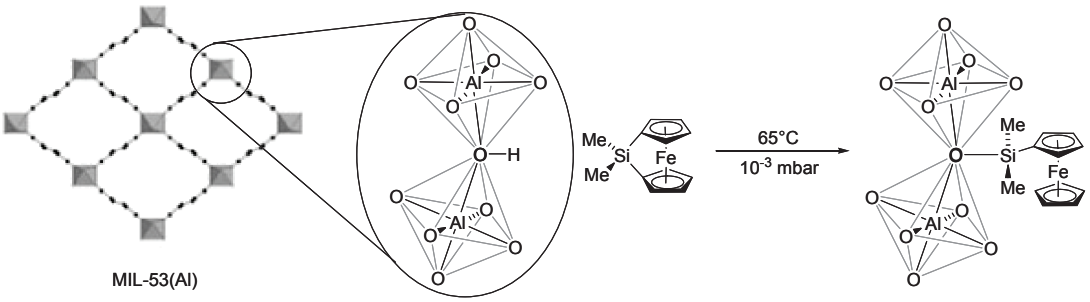

Figure III-9 : Silylation of OH bridging groups in the MIL-53(Al).

III.3.5 Chemical modification by "Click Chemistry"

The "Click Chemistry" was introduced by Sharpless and coworkers in 2001 and consists on the azide alkyne Huisgen cycloaddition, i.e. the reaction of an alkyne with azido-functionalized compound catalyzed by copper(I) species to form a triazole heterocycle [134] . It proceeds efficiently even at micromolar concentrations of reactants with high yields and high specificity in the presence of various functional groups. The first important application of this reaction in polymer chemistry is undeniably the synthesis of functionalized polymers (either end-functionalized or side-functionalized). Numerous examples of macromolecular

derivative is formed as the sole product. The post-digestion ^{1}H NMR spectrum of **1h** shows contributions of both **b** and **c** and also of the remaining azide in a 30:30:40 ratio.

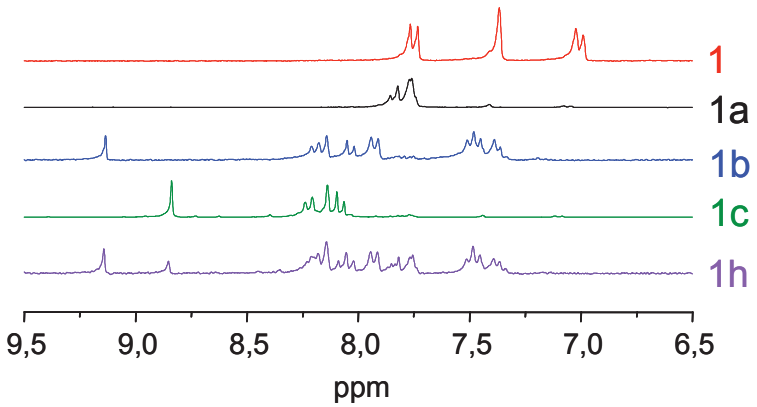

Figure II-3 : ^{1}H NMR enlargement in the aromatic region of digested 1, 1a, 1b, 1c and 1h

IR spectroscopy studies confirm these results (Figure II-4). The appearance of the IR absorption band at 2123 cm^{-1} is characteristic of the N_3 asymmetric stretching vibration of DMOF-N_3 **1a**. In the cases of **1b** and **1c**, its disappearance after the cycloaddition step is proof of almost total conversion to the final compound. In the case of **1h**, the less intense –N_3 signal is well in line with the partial conversion as quantified by ^{1}H NMR. Despite solvent effects on DMOF crystallinity [20, 21], powder X-ray diffraction patterns (PXRD) indicates that long-range order is preserved for all samples (Figure II-5).

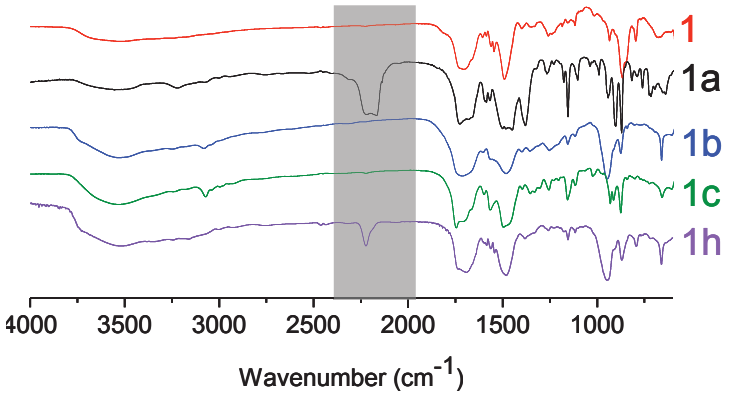

Figure II-4 : FT-IR of 1, 1a, 1b, 1c and 1h

J|A|C|S COMMUNICATIONS

Published on Web 03/16/2010

Generic Postfunctionalization Route from Amino-Derived Metal−Organic Frameworks

Marie Savonnet,[†,‡] Delphine Bazer-Bachi,[‡] Nicolas Bats,[‡] Javier Perez-Pellitero,[‡] Erwann Jeanneau,[§] Vincent Lecocq,[‡] Catherine Pinel,[†] and David Farrusseng*[,†]

IRCELYON, Institut de recherches sur la catalyse et l'environnement de Lyon; Université Lyon 1 - UMR 5256 CNRS, 2 avenue Albert Einstein, F-69626 Villeurbanne Cedex, France, IFP-Lyon, BP n°3, 69360 Solaize, France, and Université Lyon 1, Centre de Diffractométrie, 69629 Villeurbanne Cedex, France

Received November 12, 2009; E-mail: david.farrusseng@ircelyon.univ-lyon1.fr

The secondary building unit (SBU) approach for engineering of metal−organic frameworks (MOFs) with tunable pore sizes is very attractive for designing practical properties such as separation by molecular sieving and shape-selective catalysis.[1] The conceptual approach used to increase the pore sizes of MOFs through the use of longer ligands has also been extended to the design of multifunctional MOFs bearing a functional group on the organic moiety. This is the case for IRMOF-3,[2] MOF-101(-Br),[3] and MIL-53(Al)-NH_2,[4] to name a few. However, this extension is not straightforward in practice.[5] Indeed, the chemistry of MOF network formation is very sensitive to the chemical reactivity and solubility of the functionalized linkers.[6] This is particularly the case for functions such as −OH, −COOH, and N-donating groups, which can interfere with the coordination chemistry associated with the assembly of the nodes.

When self-assembly fails in the synthesis of an MOF with functionalized linkers, the postfunctionalization of a parent MOF appears to be a very valuable alternative.[7] In fact, postsynthesis opens the door to advanced porous solid engineering by multiple synthesis steps[8] and, as a consequence, to the design of new types of adsorbents and catalysts. Postfunctionalization consists of modifying the organic part of the MOF by a chemical reaction that takes place within the porous framework. In this case, the parent MOF must possess accessible reactive functions. Similar issues have been resolved for MCM-like materials, for which various functionalization methods have been developed.[9] In a similar fashion to alkylamino-functionalized MCMs,[10] amino-derived MOFs such as IRMOF-3 and DMOF-NH_2[11] are excellent platforms for the grafting of various synthons such as aldehydes, isocyanates, and acid anhydrides. That said, the suitability, diversity and availability of such synthons can appear limited when one considers the ever-increasing demands for different functionalities and the ambitious projects imagined by chemists.

Valuable alternatives lie in the development of all kinds of generic postfunctionalization methods that are soft, do not liberate byproducts that may react or remain blocked in the pores, and enable grafting of a wide variety of chemical functions with high efficiency and selectivity. The Sharpless "click" reaction using Cu^I-catalyzed Huisgen cycloaddition of azides to alkynes fulfills all of these criteria.[12,13] The corresponding azide linkers are, however, highly unstable and not commercially available; this significantly limits the synthesis of MOFs bearing azide groups by self-assembly methods.

The objective of this work was to develop a one-pot, two-step functionalization method starting from already available amino-derived MOF compounds.[14] The first step involves an original method to convert a MOF in its amino form to the corresponding azide compound. Next, the desired functionalized material is obtained by "clicking" a synthon onto the azide without isolation of the intermediate.

The starting materials DMOF-NH_2 [Zn(bdc-NH_2)(DABCO)] (section S1 in the Supporting Information) and MIL-68(In)-NH_2 [In(OH)(bdc-NH_2)][15] (section S5) were selected as representative compounds. The former is a zero-dimensional-type MOF with a layered structure made of Zn carboxylate sheets supported by 1,4-diazabicyclo(2.2.2)octane (DABCO) pillars. It is representative of a large class of porous coordination polymers (PCPs).[16] On the other hand, MIL-68(In)-NH_2 belongs to another important class of MOFs characterized by a one-dimensional rod-shaped structure. This class has been reviewed by Yaghi et al.[17]

It should be noted that the usual route for preparing azide compounds from the corresponding amines via their diazonium salts cannot be applied here because DMOF-NH_2 dissolves under acidic conditions. Instead, we investigated another pathway that uses mild conditions and involves stable, nonexplosive compounds.[18]

Scheme 1. One-Pot, Two-Step Functionalization of DMOF-NH_2

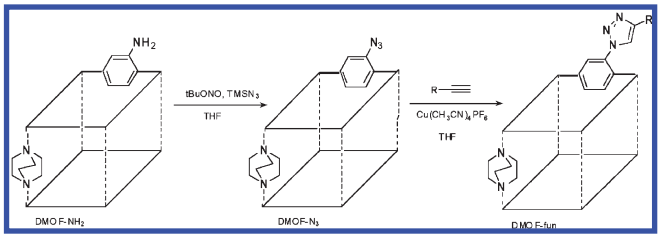

In a typical synthesis (Scheme 1), the freshly dried DMOF-NH_2 was treated with tBuONO and $TMSN_3$ in THF overnight at room temperature to produce the corresponding azide intermediate compound DMOF-N_3.[19] In the same vessel, the functionalized DMOF (DMOF-fun) was obtained by addition of excess phenylacetylene in the presence of $Cu^I(CH_3CN)_4PF_6$ followed by continuous stirring for 24 h (section S3). For characterization purposes, the synthesis was stopped after formation of the azide intermediate DMOF-N_3.

MIL-68(In)-NH_2 was modified by applying a similar procedure.[20] For sake of brevity, details are given in section S6 in the Supporting Information.

Clear proof of azide formation and the subsequent (3 + 2) cycloaddition was obtained by IR spectroscopy. The absorption band of DMOF-N_3 at 2123 cm^{-1} is characteristic of the N_3 asymmetric stretching vibration (section S3). In addition, unambiguous characterization and quantification were provided by liquid

[†] IRCELYON UMR 5256 CNRS.
[‡] IFP-Lyon.
[§] Université Lyon 1.

10.1021/ja909613e

^{1}H NMR analysis. Samples of DMOF-N_3 were digested and dissolved in dilute DCl/D_2O/DMSO-d_6 solution (Figure 1) and then analyzed by ^{1}H NMR spectroscopy, which confirmed the formation of the azide compound by the appearance of new aromatic signals (7.74−7.85 ppm, m, 3H, ArH). This coincided with the complete disappearance of the aromatic signals of the amine (7 ppm, d, 1H, J = 8.3 Hz; 7.4 ppm, s, 1H; 7.74 ppm, d, 1H, J = 8.3 Hz), thus indicating full conversion to the azide form. On the other hand, the aliphatic moiety was not affected by the reaction (section S3).

DMOF-fun obtained after the one-pot synthesis was characterized using identical techniques. Here again, the conversion to the final compound was complete after 24 h. IR analysis revealed the complete disappearance of the azide stretching band at 2123 cm^{-1} (section S3). The liquid ^{1}H NMR spectrum of DMOF-fun illustrates that the corresponding triazole derivative was formed as the unique product; aromatic shifts of the grafted compound were assigned by ^{1}H−^{1}H correlation spectroscopy (COSY) experiments (δ = 7.38, 7.49, 7.93, 8.04, 8.19, 9.15 ppm), and no azido or amino compound was detected (Figure 1). In addition, positive-mode mass spectrometry performed after digestion clearly showed a base peak at m/z 310 corresponding to the functionalized linker [2-(4-phenyl-1,2,3-triazol-1-yl)terephthalic acid]. The powder X-ray diffraction patterns indicated that the two-step reaction proceeded without loss of long-range order (section S3). We stress that the crystallinity of the parent DMOF-NH_2 is strongly affected by post-treatments such as solvent removal and/or solvent exchange (section S2).

Nitrogen physisorption experiments performed on the parent DMOF-NH_2 and DMOF-fun at 77 K revealed a decreases in the porous surface area (1320 to 244 m^2/g) and the microporous volume (0.54 to 0.08 cm^3/g) due to pore blocking (section S3).

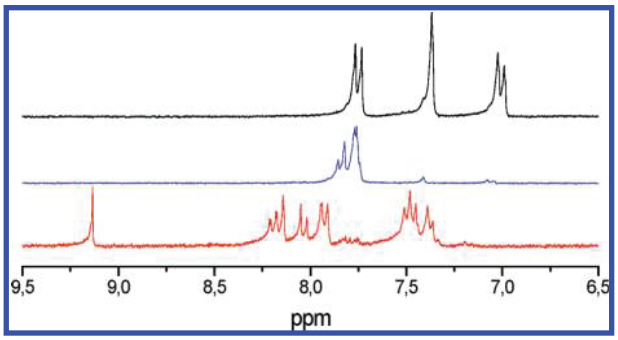

Figure 1. Liquid ^{1}H NMR spectra of digested materials: (top) DMOF-NH_2; (middle) DMOF-N_3; (bottom) DMOF-fun.

These investigations were also undertaken for the postfunctionalization of MIL-68(In)-NH_2, and the same results were obtained in terms of grafting rate (>90%), decrease in surface area (1260 to 120 m^2/g) and microporous volume (0.48 to 0.03 cm^3/g), and preservation of crystallinity (section S6).

Cycloaddition in azide-functionalized MOFs has recently been demonstrated for IRMOF-type compounds.[12] In this work, we have shown that direct functionalization from amino-derived MOFs is possible, provided that the pore cavity is large enough to accommodate a C_5 ring (section S3). The main advantage of this one-pot method is the ease of preparing amino-functionalized MOFs. To the best of our knowledge, five different structures based on 2-aminoterephthalic acid have been reported to date: IRMOF-3,[2] MIL-101-NH_2,[4] CAU-1,[21] DMOF-NH_2, and MIL-53(Al)-NH_2. The large library of amino acids also opens promising perspectives for new potential amino-functionalized MOFs as synthetic platforms. A second advantage is the softness of the method. Indeed, both reaction steps proceed at room temperature and do not liberate byproducts such as water, acids, or bases that could damage the structure by hydrolysis.[22] Finally, in contrast to the anhydride condensation method, which has a limited grafting yield (30−50%),[23] we have shown that this approach allows complete functionalization even for a bulky group. This is in line with molecular modeling results showing weak steric demand (section S3). Notably, the crystallite sizes of the two MOFs are ∼1 μm (section S1), whereas Wang et al.[11] used DMOF-NH_2 crystallites with diameters of 100 μm. We believe that the accessibility of reactants to the centers of the crystals arises from the very small size of the MOF crystallites.

However, this small size comes at the expense of a decrease in microporous volume. Thanks to the efficiency of the azide formation, the grafting rate can be controlled by adding phenylacetylene in default with respect to −NH_2 functions. For a grafting rate of 50% on MIL-68(In)-NH_2, the surface area decreased only by 55% (S_{BET} = 571 m^2/g), which is in line with other methods.[8]

In this study, controlled functionalization was performed with phenylacetylene as a proof of concept. A systematic study dealing with the grafting of moieties exhibiting different functions on diverse amino-MOF platforms will be reported soon. We believe that this method will allow the design of tailor-made catalysts with more complex functional groups.

Acknowledgment. We thank A. Camarata for the technical work, along with IRCELYON and IFP scientific services.

Supporting Information Available: Synthetic procedures, characterization data, and molecular modeling results. This material is available free of charge via the Internet at http://pubs.acs.org.

References

(1) (a) Férey, G. *Chem. Soc. Rev.* **2008**, *37*, 191. (b) Farrusseng, D.; Aguado, S.; Pinel, C. *Angew. Chem., Int. Ed.* **2009**, *48*, 7502.
(2) Eddaoudi, M.; Kim, J.; Rosi, N.; Vodak, D.; Wachter, J.; O'Keefe, M.; Yaghi, O. M. *Science* **2002**, *295*, 469.
(3) Eddaoudi, M.; Kim, J.; O'Keeffe, M.; Yaghi, O. M. *J. Am. Chem. Soc.* **2002**, *124*, 376.
(4) Bauer, S.; Serre, C.; Devic, T.; Horcajada, P.; Marrot, J.; Férey, G.; Stock, N. *Inorg. Chem.* **2008**, *47*, 7568.
(5) (a) Yang, C.; Wang, X. P.; Omary, M. A. *J. Am. Chem. Soc.* **2007**, *129*, 15454. (b) Kawano, M.; Kawamichi, T.; Haneda, T.; Kojima, T.; Fujita, M. *J. Am. Chem. Soc.* **2007**, *129*, 15418.
(6) Fischer, R. A.; Woll, C. *Angew. Chem., Int. Ed.* **2008**, *47*, 8164.
(7) Wang, Z. Q.; Cohen, S. M. *Chem. Soc. Rev.* **2009**, *38*, 1315.
(8) Wang, Z. Q.; Cohen, S. M. *Angew. Chem., Int. Ed.* **2008**, *47*, 4699.
(9) Wright, A. P.; Davis, M. E. *Chem. Rev.* **2002**, *102*, 3589.
(10) (a) Brunel, D. *Microporous Mesoporous Mater.* **1999**, *27*, 329. (b) Brunel, D.; Blanc, A. C.; Galarneau, A.; Fajula, F. *Catal. Today* **2002**, *73*, 139.
(11) Wang, Z. Q.; Tanabe, K. K.; Cohen, S. M. *Inorg. Chem.* **2009**, *48*, 296.
(12) Goto, Y.; Sato, H.; Shinkai, S.; Sada, K. *J. Am. Chem. Soc.* **2008**, *130*, 14354.
(13) (a) Gadzikwa, T.; Lu, G.; Stern, C. L.; Wilson, S. R.; Hupp, J. T.; Nguyen, S. T. *Chem. Commun.* **2008**, 5493. (b) Gadzikwa, T.; Farha, O. K.; Malliakas, C. D.; Kanatzidis, M. G.; Hupp, J. T.; Nguyen, S. T. *J. Am. Chem. Soc.* **2009**, *131*, 13613.
(14) Savonnet, M.; Bazer-Bachi, D.; Pinel, C.; Lecocq, V.; Bats, N.; Farrusseng, D. FR Patent 09/05.107, 2009.
(15) Savonnet, M.; Bazer-Bachi, D.; Pinel, C.; Lecocq, V.; Bats, N.; Farrusseng, D. 2009, FR Patent 09/05.101, 2009.
(16) (a) Kitagawa, S.; Tanaka, D. *Chem. Mater.* **2008**, *20*, 922. (b) Seki, K. *Langmuir* **2002**, *18*, 2441. (c) Kitagawa, S.; Kitaura, R.; Noro, S. *Angew. Chem., Int. Ed.* **2004**, *43*, 2334.
(17) Yaghi, O. M.; O'Keeffe, M.; Rosi, N. L.; Kim, J.; Eddaoudi, M.; Chen, B. L. *J. Am. Chem. Soc.* **2005**, *127*, 1504.
(18) Barral, K.; Moorhouse, A. D.; Moses, J. E. *Org. Lett.* **2007**, *9*, 1809.
(19) Savonnet, M.; Bazer-Bachi, D.; Pinel, C.; Lecocq, V.; Bats, N.; Farrusseng, D. FR Patent 09/04.521, 2009.
(20) Savonnet, M.; Bazer-Bachi, D.; Pinel, C.; Lecocq, V.; Bats, N.; Farrusseng, D. FR Patent 09/05.102, 2009.
(21) Ahnfeldt, T.; Guillou, N.; Gunzelmann, D.; Margiolaki, I.; Loiseau, T.; Férey, G.; Senker, J.; Stock, N. *Angew. Chem., Int. Ed.* **2009**, *48*, 5163.
(22) Savonnet, M.; Aguado, S.; Ravon, U.; Bazer-Bachi, D.; Lecocq, V.; Bats, N.; Pinel, C.; Farrusseng, D. *Green Chem.* **2009**, *11*, 1729.
(23) Tanabe, K. K.; Cohen, S. M. *Angew. Chem., Int. Ed.* **2009**, *48*, 7424.

JA909613E

Evaluation of Energy Heterogeneity in Metal−Organic Frameworks: Absence of Henry's Region in MIL-53 and MIL-68 Materials?

Marc Pera-Titus,* Marie Savonnet, and David Farrusseng

Université de Lyon, Institut de Recherches sur la Catalyse et l'Environnement de Lyon (IRCELYON), UMR 5256 CNRS - Université Lyon 1, 2, Av. A. Einstein, 69626 Villeurbanne Cedex, France

Received: May 25, 2010; Revised Manuscript Received: July 23, 2010

We present in this study a detailed thermodynamic analysis of N_2 adsorption at 77.4 K and low pressures in a series of metal−organic framework materials displaying different structures, pore textures, and framework flexibility. The energy heterogeneity of these materials has been quantified using a thermodynamic isotherm model developed in previous studies through two characteristic parameters. This formulation also allows the generation of an equation differing from the Dubinin−Astakhov isotherm that allows a proper description of gas adsorption at low pressures. Unlike zeolites or rigid coordination polymers, highly flexible MIL-53(Al) and MIL-68(In) materials are characterized by N_2 adsorption isotherms lacking of a characteristic Henry's region (linear trend) at low relative pressures. We argue about an unexpected promotion of energy heterogeneity on these materials due to sorbate-induced elastic deformation ascribed to compression tensions to explain this observation.

1. Introduction

A crucial step in the development of adsorption-based technologies is the ability to design and benchmark stable adsorbents with a convenient pore size, pore shape, and surface chemistry. Metal−organic frameworks (MOFs) and more extensively hybrid inorganic−organic coordination polymers have emerged as a new class of "nanoporous" materials to this aim, adding to already existing "classical" adsorbents (e.g., zeolites and carbons[1]).

MOFs are crystalline materials synthesized by self-assembly of organic ligands (linkers) and metal clusters, creating highly regular porous frameworks with different topologies, defined micro- and/or mesopores, and chemical functionalities that can be tuned by modifying the metal group or organic ligand. MOF materials can also be subjected to further postsynthetic modification,[2−4] whereby both the metal unit and the ligand can undergo heterogeneous chemical transformations while keeping the overall crystalline structure of the material. Several reviews have been recently published documenting a vast number of porous MOF structures with varying pore sizes and functionalities, as well as some outstanding adsorption and catalytic properties.[5−15]

The most widely studied MOFs and coordination polymers include the MIL series of Ferey and co-workers,[16−26] relying on stable divalent and trivalent 3d and 4f metal-based carboxylates, terephthalates, phosphates, and phosphonates; the isoreticular MOF (IRMOF) series of Yaghi and O'Keeffe;[27−32] and Cu-BTC or HKUST-1.[33] The original adsorption properties of these materials make them attractive for gas and liquid separation,[11,34] gas storage,[35] and control release.[36]

Unlike zeolites, characterized by relatively rigid frameworks and a high thermal stability ascribed to strong Si−O covalent bonds, MOF materials show an inherent structural flexibility due to their weaker bonds (e.g., Π−Π stacking, hydrogen bonds, and van der Waals interaction) promoting in some cases elastic guest accommodations. According to Kitagawa and co-workers,[37,38] such dynamic porous properties might promote a rich variety of guest-induced structural and reversible phase transitions upon gas adsorption and desorption (either amorphous-to-crystal or crystal-to-crystal transformations) not observed in rigid 3D frameworks. These transitions differ from a classical sorbate rearrangement reported in certain zeolite−guest systems such as *p*-xylene/silicalite-1. Another guest-related property of flexible MOFs is the dynamic rotation of bridging ligands, which might be reversibly affected by adsorption/desorption of guest molecules without involving geometrical changes.[38,39]

The above stated structural changes in flexible MOFs are at the origin of anomalous adsorption isotherm patterns (either in the presence of polar or nonpolar sorbates) such as the so-called "gate opening" and "breathing" phenomena. On the one hand, gate-opening phenomena are characterized by a large hysteresis loop between the adsorption and desorption curves due to an abrupt transition between a nonporous state and a porous crystalline phase promoted by guest accommodation. On the other hand, breathing phenomena are characterized by an abrupt expansion of the unit cell upon adsorption (the unit cell parameters can suffer variations >5 Å) due to guest-induced crystal-to-crystal transformations. A paradigmatic example of breathing phenomena can be found in the MIL-53 material, exhibiting an abrupt phase transition upon water[19] and CO_2[40] adsorption (and to a lesser extent upon adsorption of C1−C9 *n*-alkanes[41]), resulting in a ca. 38% unit cell expansion. This transition is accompanied by a prominent inflection in the CO_2 isotherm (S-shape) at about 6 bar and 304 K.[40] The difference in free energy between the low- and high-pressure phases (lp → hp) has been estimated to about 2.5 kJ/mol per unit cell for MIL-53(Cr,Al).[42] Serre et al.[43] have attributed the large breathing effect observed in the MIL-53 structure to strong guest−guest bonds along the tunnels created by the sorbate species, acting as a backbone for the onset of symmetrical interactions (usually with the interplay of OH surface groups) with two opposite chains of the framework.

The potential technological impact of MOF materials makes the development of suitable isotherm models for describing gas/

* Corresponding author. Phone: +33 (0) 472445368. Fax: +33 (0) 472445399. E-mail: marc.pera-titus@ircelyon.univ-lyon1.fr.

10.1021/jp104788p
Published on Web 09/20/2010

vapor adsoption imperative. By now, most of the studies dealing with adsorption properties of MOFs have been aimed at providing a materials screening and ranking for target separations. A series of simulation studies has also elucidated the main interactions and adsorption mechanisms in MOF materials, as well as the thermodynamic basis for double structural transitions in MOFs upon adsorption (see, for instance, refs 44−54). However, only a scarce number of studies have been reported to date discussing the suitability of transposing well-known concepts of gas/vapor adsorption in "robust" zeolites and activated carbons to hybrid polymer materials. This analysis appears to us crucial on the basis of the great elasticity of some MOF structures, as well as their ultrahigh specific surface areas, attaining values as high as 4000 m^2/g for MIL-100[22] and MOF-177.[30] These specificities pose obvious questions on the compatibility of the classical Brunauer−Emmett−Teller (BET) theory[55] for measuring specific surface areas on these materials, as well as the classical Dubinin−Radushkevich (DR) and Dubinin−Astakhov (DA) isotherms[56] usually applied to the description of gas adsorption in carbonaceous materials and zeolites. Both points are fundamental not only for a proper characterization of MOF materials but also for an accurate prediction of their adsorption (and surface diffusion) properties in industrially relevant separations.

This first point has been partially elucidated by Walton and Snurr[57] in a recent study. These authors have demonstrated that BET analysis provides consistent specific surface areas in a series of simulated IRMOF materials compared to accessible surface areas calculated geometrically from crystal structures, even if the dominating adsorption mechanism in MOFs is pore filling as in the case of zeolites or microporous carbons. However, no indication about the role of framework distortion effects on the measured BET surfaces was addressed.

This paper is aimed at providing a critical assessment on the second aforementioned point, namely, on the applicability of the DR and DA isotherms for describing gas/vapor adsorption in MOF materials, which to our knowledge has not been treated yet in detail. Moreover, this paper is also intended to provide a detailed analysis of energy heterogeneity in both robust and flexible MOFs using the original thermodynamic isotherm developed in previous studies from solution thermodynamics first principles[58,59] and validated for zeolite materials. Briefly, this formulation relies on a "scaling law" representation of the integral free energy of adsorption relative to saturation, $-\Psi/RT$, computed as a Kiselev integral, against the variable $Z = 1/-\ln(\Pi)$, being $\Pi = P/P_0$

$$-\frac{\Psi}{RT} = \int_\theta^1 -\ln(\Pi)\delta\theta \int_\theta^1 Z^{-1}\delta\theta = \frac{G^\circ}{1 + kZ^m} \quad (1)$$

with $G^\circ = -\Phi(P^\circ)/RT$ and $k = [-\ln(\Pi_k)]^m = Z_k^{-m}$, with $\Phi(P^\circ)$ being the surface potential at saturation pressure and Π_k the Π value accounting for a sorbate integral free energy relative to saturation equaling $G^\circ/2$.

Parameter m can be linked to the energy heterogeneity (or energy distribution) of the adsorbent, providing information about molecular packing in micropores. We have identified two different potential trends in the adsorption pattern of zeolites for a wide series of sorbates and temperatures, characterized each by two different m values (i.e., m_1 and m_2). Parameter m_1 has been linked to sorbate confining effects in zeolites.[60] In the case of parameter m_2, this can be linked to the characteristic α exponent of the DA isotherm at $\Pi > 0.01$ in a simple way ($\alpha = m - 1$),[58] providing information about the energy heterogeneity of the solid−guest system at high sorbate loadings.

In a further study,[61] we have proposed a modified version of eq 1, taking into account explicitly the contribution of both potential trends

$$-\frac{\Psi}{RT} = \int_\theta^1 Z^{-1}\delta\theta = \frac{G^o}{1 + \dfrac{\lambda_1\lambda_2}{\lambda_1 + \lambda_2}} \quad (2)$$

where $\lambda_1 = k_1 Z^{m_1}$ and $\lambda_2 = k_2 Z^{m_2}$, with $m_1 > m_2$ and $k_1 \gg k_2$ in the case of zeolites.

Equation 2 allows the derivation of two analytical expressions describing gas adsorption in two limiting pressure zones:

$$\theta = G^\circ k_1 \left(\frac{Z^{m_1+1}}{1 + k_1 Z^{m_1}}\right) \quad \text{for} \quad 1/\lambda_1 \le 1 \quad (3)$$

$$\theta = 1 - \frac{G^\circ}{k_1}\frac{m_1}{(m_1 - 1)}Z^{-(m_1-1)} - \frac{G^\circ}{k_2}\frac{m_2}{(m_2 - 1)}Z^{-(m_2-1)} \quad \text{for} \quad Z_\beta \ll Z < 1 \quad (4)$$

We have shown that eq 3, accomplished at relative pressures $<10^{-3}$ for a great variety of zeolite−guest systems, includes implicitly Henry's region (linear trend between the surface coverage and pressure) in zeolites. In the case of eq 4, this expression can be simplified into eq 5 for relative pressures >0.1, being formally equivalent to a McLaurin development of the DA isotherm (see ref 61 for further details).

$$\theta = 1 - \frac{G^\circ}{k_2}\frac{m_2}{(m_2 - 1)}Z^{-(m_2-1)} \quad (5)$$

Keeping these ideas in mind, this themodynamic formulation will be used here to compare the adsorption pattern of robust and flexible MOF materials to that of zeolites at low pressures, as an attempt to characterize in detail Henry's region. The set of eqs 3−5 will be used for a comprehensive characterization of Henry's region in MOF materials through the evaluation of the heterogeneity of the system at low pressures, overcoming the intrinsic limitations of the DA isotherm in this region. We will also discuss in detail the structure-related variation of energy heterogeneity of relatively elastic MOF materials.

2. Materials and Methods

2.1. Chemicals. All chemicals were used as received without any further purification: zinc nitrate tetrahydrate, $Zn(NO_3)_2 \cdot 4H_2O$ (Merck, 98.5%); zinc nitrate hexahydrate, $Zn(NO_3)_2 \cdot 6H_2O$ (Riedel-de-Haën, pure); indium nitrate, $In(NO_3) \cdot 4H_2O$ (Alfa Aesar, 99.99%); aluminum chloride hexahydrate, $AlCl_3 \cdot 6H_2O$ (Sigma-Aldrich, 98%); 2-aminoterephthalic acid, NH_2-bdc (Alfa Aesar, 99.0%); terephthalic acid, bdc (Sigma Aldrich, 98%); 1,4-diazabicyclo[2.2.2] octane, DABCO (Sigma-Aldrich, 98.0%); triethylamine, Et_3N (Riedel-de-Haën, pure); sodium hydroxyde, NaOH (Sigma-Aldrich, 98%); *N*,*N*′-dimethylformamide, DMF (Sigma-Aldrich, 99.8%); dichloromethane, CH_2Cl_2 (Acros Organics, 99.99%); THF (Sigma-Aldrich, 99.0%); methanol, MeOH (Sigma-Aldrich, 99%).

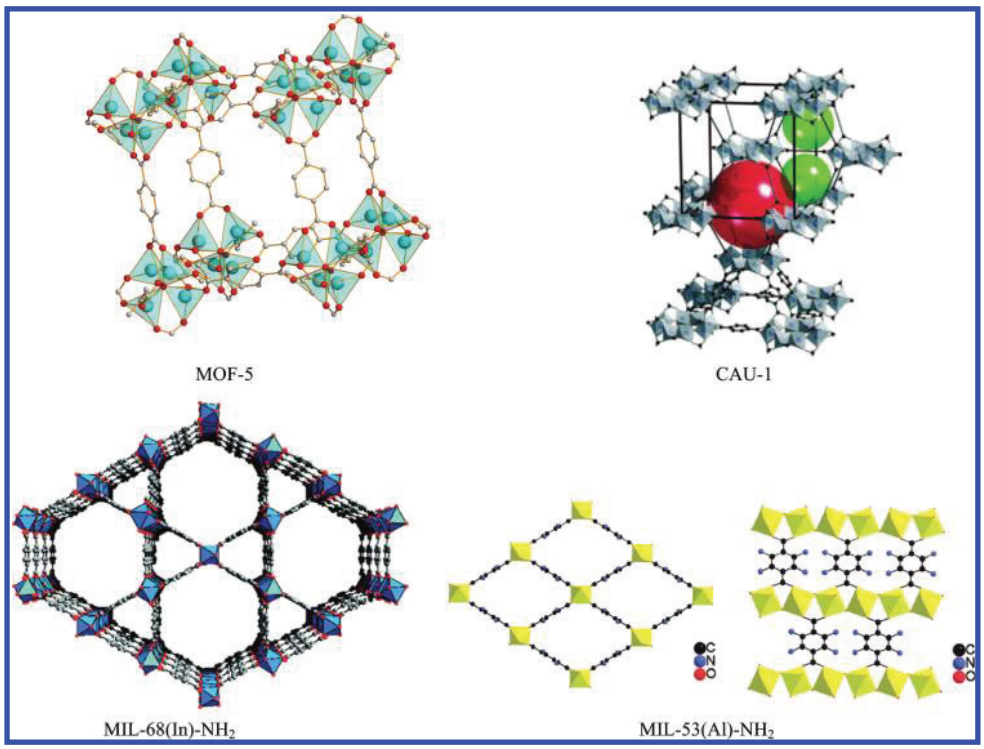

Figure 1. Structure of the MOF materials prepared in this study.

TABLE 1: Main Structural and Textural Properties of the MOF Materials Prepared in This Study and Zeolites Used as Reference Materials

MOF denomination	structure	pore channel	pore size	cell parameters	molecular weight (g/mol)	BET surface area (m^2/g)	pore volume (cm^3/g)	references
MOF-5	3D	3D	8 Å	cubic ($Fm\bar{3}m$) $a = b = c = 25.67$ Å	813	450	0.32	this study
CAU-1	3D	3D	10 Å + 4.5 Å	tetragonal ($I4/mmm$) $a = b = 1.835$ Å, $c = 1.777$ Å	803	810	0.42	this study
MIL-68(In)-NH_2	3D	1D	6 Å + 17 Å	orthorhombic ($Cmcm$) $a = 21.774$ Å, $b = 37.677$ Å, $c = 7.233$ Å	311	1260	0.58	this study
MIL-53(Al)-NH_2	3D	1D	8.5 Å	monoclinic system (Cc) $a = 19.702$ Å, $b = 7.764$ Å, $c = 6.592$ Å	223	1155	0.57	this study
NaY (Si/Al = 25)	3D	3D	7.4 + 12 Å	cubic system ($Fd\bar{3}m$) $a = b = c = 24.345$ Å	2172	337	0.099	BAM[a]
HZSM-5 (Si/Al = 500)	3D	3D	5.3 + 5.5 Å	orthorhombic system ($Pnma$) $a = 20.090$ Å, $b = 19.738$ Å, $c = 13.142$ Å	6056	~350	~0.20	62

[a] Data supplied by the Federal Institute for Materials Research and Testing (BAM, Unter den Eichen 87, 12205-Berlin, Germany).

2.2. Materials Synthesis and Characterization. Four different MOF structures were solvothermally synthesized following well-established protocols reported in the literature: "MOF-5-like", CAU-1, MIL-68(In)-NH_2, and MIL-53(Al)-NH_2. The synthesis protocols, as well as the final structures obtained (see Figure 1), are described below. Table 1 summarizes the main structural and textural properties of these materials.

2.2.1. "MOF-5-like" Material. The MOF-5-like material (simply referred hereinafter as MOF-5) was prepared according to a procedure reported by Mueller et al.[63] Typically, 8.32 g (31.824 mmol) of $Zn(NO_3)_2 \cdot 4H_2O$ and 1.76 g (10.594 mmol) of 1,4-benzenedicarboxylic acid (H_2dbc) (Sigma-Aldrich 99.7%) were dissolved in 100 mL of dried diethylformamide (DEF). The solution was heated at 100 °C in a Teflon-lined autoclave, the solid filtered off, washed, and finally exchanged with $CHCl_3$ under Ar flow. Finally, the material was evacuated and stored in a glovebox.

The MOF-5 framework (cubic system, $Fm3m$ space group with $a = b = c = 25.67$ Å[64]) consists of Zn_4O tethrahedral subunits linked in octahedral arrays by bdc groups to form a porous material with channel windows of about 8 Å. The Zn edges of the tetrahedra are bridged by six carboxylate groups forming octahedral nodes, linked to one another with 1,4-phenylene groups of the bdc linker, resulting in a 3D cubic network. Further information about the characterization of our MOF-5-like material can be found in ref 65.

2.2.2. CAU-1. CAU-1 was synthesized from 2-aminotereph-thalic acid using the procedure described in ref 66. A mixture of aluminum chloride (1.513 mmol) and NH_2-bdc (0.521 mmol) was suspended in MeOH (10 mL) and heated at 125 °C for 5 h. After filtration, a yellow microcrystalline product was obtained. The crystals were washed three times with MeOH and with DMF at 160 °C and then soaked in dichloromethane for 24 h. After drying at room temperature, the mass of dried CAU-1 obtained was 90 mg.

The CAU-1 framework (tetragonal system, $I4/mmm$ space group, $a = b = 1.835$ Å, $c = 1.777$ Å) is built up from a pseudobody-centered-cubic arrangement of 8-ring building blocks $\{Al_8(OH)_4(OCH_3)_8\}^{12+}$ linked by 12 aminoterephthalate ions. The wheel-shaped 8-rings are built from corner- and edge-sharing AlO_6 octahedra through hydroxide and methoxide groups. The Al(III) is coordinated to three carboxylate oxygen atoms, one hydroxide, and two methoxide ions. Each wheel is connected to 12 other units by aminoterephthalate linkers with four linkers in the plane of the 8-rings as well as four above and below the ring. Hence, a 3D microporous framework is

formed with two types of cages, distorted octahedral and distorted tetrahedral, with effective diameters of 10 and 4.5 Å, respectively.

2.2.3. MIL-68(In)-NH$_2$. MIL-68(In)-NH_2 has been prepared following the protocol presented in a recent patent.[67] It was obtained by precipitation reaction in a Pyrex beaker (capacity 100 mL) of a mixture of 4.82 mL (4.14 mmol) of 0.86 M indium nitrate in DMF and 10.06 mL (3.32 mmol) of 0.33 M 2-aminoterephthalic acid (NH_2-bdc) in DMF. The reaction mixture was stirred for 5 min, and then, 4.83 mL (6.67 mmol) of 1.38 M dabco in DMF was added. The reaction mixture was stirred for 2 h at room temperature. The obtained precipitate was washed with DMF at 160 °C and soaked in CH_2Cl_2 for 24 h. The mass of dried MIL-68(In)-NH_2 obtained was 0.88 g.

The MIL-68(In)-NH_2 framework (orthorhombic system, *Cmcm* space group, $a = 21.774$ Å, $b = 37.677$ Å, $c = 7.233$ Å) is built up from infinite straight chains of metal-centered $InO_4(OH)_2$ octahedra connected to each other through the NH_2-dbc ligands, generating 1D channels. The octahedral units are linked together via two hydroxyl groups located in *trans* positions, two adjacent octahedra also being connected via the carboxylate functions. These corner-sharing octahedral species MO_6 form a network of three- and six-membered windows, generating two types of channels with diameter openings of 6 and 17 Å, respectively, for the triangular and hexagonal rings.

2.2.4. MIL-53(Al)-NH$_2$. The synthesis of MIL-53(Al)-NH_2 was adapted from the procedure described in ref 68. 2-Aminoterephthalic acid (NH_2-bdc, 0.66 mmol) was suspended in water (28 mL, 1.55 mmol) in a 40 mL Teflon-lined SS digestion bomb. Then, 1.10 mL (0.44 mmol) of a 0.4 M aluminum chloride solution and 0.56 mL (0.22 mmol) of a 0.4 M NaOH solution were added. The reaction mixture was heated for 24 h without stirring at 110 °C. The final precipitate was washed with deionized water and DMF at 160 °C and then soaked in CH_2Cl_2 for 24 h. After drying at 80 °C, the mass of dried MIL-53(Al)-NH_2 obtained was 0.4 g.

The MIL-53(Al)-NH_2 framework (monoclinic system, *Cc* space group, $a = 19.702$ Å, $b = 7.764$ Å, $c = 6.592$ Å) is built up from chains of corner-sharing Al(III) octahedra connected by μ_2-OH and carboxylate groups. These chains are connected by aminoterephthalate ions to form a 1D rhomboedral-shape channel system. The combination of these chains allows the formation of three different 3D frameworks. In MIL-53 (as), the tunnels (7.3 Å × 7.7 Å) are occupied by disordered NH_2-bdc template molecules. The total removal of the template upon heating at 275 °C generates the MIL-53(ht) form showing empty pores of 8.5 Å × 8.5 Å. The reversible adsorption of water at room temperature gives rise to MIL-53(lt) with channel dimensions of 2.6 Å × 13.6 Å. Here, the MIL-53(Al)NH_2(lt) framework was prepared.

2.3. Adsorption Measurements. The MOF materials prepared in this study were characterized by N_2 adsorption at 77.4 K using a BELSORP max porosimeter. In the low-pressure region ($\Pi < 10^{-2}$), the adsorption measurements were carried out by doses of 3−6 cm^3(STP)/g with equilibrium times in the range 1620−3600 s. Care was taken of the absence of diffusional limitations in the adsorption measurements, especially at low pressure. Prior to the gas adsorption/desorption tests, the samples were subjected to an outgassing protocol under secondary vacuum at 100−200 °C for 12−48 h to remove adsorbed moisture and vapors. Helium was used as backfill gas to measure the freespace volume of the cell before the N_2 adsorption measurements. BET specific surfaces were determined from

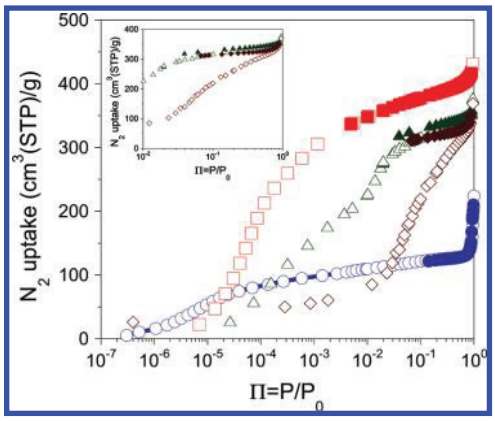

Figure 2. Adsorption isotherms of N_2 at 77.4 K on MOF-5 (○), CAU-1 (□), MIL-68(In)-NH_2 (△), and MIL-53(Al)-NH_2 (◇).

recorded adsorption data at $0.05 \leq \Pi \leq 0.25$, while the pore volume was determined from the N_2 adsorbed volume at $\Pi = 0.99$.

2.4. Calculation Details. The relevant parameters of the thermodynamic isotherm were obtained by fitting eq 2 to experimental N_2 adsorption data at 77.4 K. To improve the quality of the fittings, eq 2 was reduced to the following simplified expressions accounting for the low and high pressure domains

Low pressure region:

$$-\frac{\Psi}{RT} = \frac{G^\circ}{1 + (Z/Z_k)^{m_1}} \tag{6}$$

High pressure region:

$$-\frac{\Psi}{RT} = \frac{G^\circ}{k_2} Z^{-m_2} \tag{7}$$

with $Z_k = 1/-\ln(\Pi_k) = k_1^{-1/m_1}$ being the Z value corresponding to a sorbate integral free energy relative to saturation equaling $G^\circ/2$. Equation 6 can be rewritten as follows

$$\left(\frac{G^\circ}{-\Psi/RT} - 1\right) = \left(\frac{Z}{Z_k}\right)^{m_1} = kZ^{m_1} \tag{8}$$

The set of parameters in eq 6 (m_1, Z_k) and eq 7 (m_2, k_2) were fitted using a least-squares nonlinear optimization method based on the Levenberg−Marquardt algorithm by comparison of predicted and experimental pure adsorption data. The parameter G° has been kept constant in the fittings, its value being computed directly from the *raw* isotherms through the integral

$$G^\circ = \int_0^1 -\ln(\Pi)\delta\theta = \int_0^1 Z^1 \delta\theta \tag{9}$$

3. Results and Discussion

3.1. N_2 Adsorption/Desorption Patterns in MOFs. Figure 2 shows the N_2 adsorption/desorption isotherms at 77.4 K obtained on the MOF materials synthesized in this study. In good keeping with the adsorption pattern of zeolites, MOF-5 and CAU-1 "robust" frameworks show a sharp adsorption trend at relatively low N_2 pressures (type I isotherm), the first adsorption loadings being obtained for relative pressures $<10^{-5}$. The adsorption/desorption curves are entirely reversible, as is

usually the case encountered in zeolites in the absence of integranular condensation.

In the case of MIL-53(Al)-NH_2 material, however, a subtle step can be observed at $P/P_0 \sim 2 \times 10^{-3}$, suggesting a guest-induced structural transformation. This idea is reinforced by the intense adsorption/desorption hysteresis loop observed for this material. A hysteresis loop is also observed for MIL-68(In)-NH_2 but is less pronounced. These irreversibilities can be tentatively attributed to breathing of both flexible MIL-53 and MIL-68 frameworks upon N_2 adsorption, leading to a sorbate-induced phase transition involving partial swelling of the structures due to guest accommodation. This hysteresis provides a first evidence of the energy heterogeneity of the adsorption centers in these frameworks compared to "robust" structures due to a structural modification upon adsorption.

3.2. Applicability of the DA Isotherm to the Description of Gas Adsorption in MOFs. The DA equation, originally derived by Dubinin and co-workers from the volume filling theory of micropores (TVFM) for "robust solids" assuming a Polanyi's adsorption potential, A, relates the surface coverage of the sorbate with the relative pressure by a "temperature-invariant" potential function including three characteristic parameters, i.e., $E°$, α, and β.[56,69]

$$\theta = \exp\left\{-\left[\frac{A}{\beta E°}\right]^{\alpha}\right\} = \exp\left\{-\left[-\frac{RT}{\beta E°}\ln(\Pi)\right]^{\alpha}\right\} \quad (10)$$

where α is a characteristic exponent (α = 2 in the case of the DR isotherm), $E°$ is the adsorption energy, and β is the so-called "affinity coefficient", being usually taken as a constant characteristic of the sorbate and being used as a scaling factor to bring the characteristic curves of different sorbates into coincidence with that or a reference one (e.g., benzene in the case of activated carbons).

The characteristic α exponent (usually in the range 1.0−2.5 for zeolites) and the adsorption energy, $E°$, of the DA isotherm can be linked to the degree of surface heterogeneity of the material (e.g., presence of surface impurities, sites of different energies, different micropore sizes) through the formulation of Gaussian (or one-parameter Weibull) distribution functions.[69] We expect here that the energy heterogeneity of the adsorption sites of a material can also be ascribed, at least partially, to a sorbate-induced elastic deformation, either attributed to local flexibility or to the bistability of the structure.

Equation 10 can be transformed for plotting into eq 11

$$\ln[-\ln(\theta)] = D + \alpha \ln[-\ln(\Pi)] \quad (11)$$

where $D = \alpha\ln(RT/\beta E°)$. The DA plot of $\ln[-\ln(\theta)]$ against $\ln[-\ln(\Pi)]$ should be a straight line having an intercept equal to D, while from the slope, the value of the characteristic α exponent is obtained.

Figure 3 shows the fitting of eq 11 to N_2 adsorption data at 77.4 K for the collection of MOF materials prepared in this study, as well as the two zeolites (NaY and ZSM-5) used here as reference materials. As can be deduced from Figure 3A, irrespective of the material, the DA isotherm fails to predict the adsorption behavior at low pressures ($\Pi < 0.1$). As a matter of fact, differentiated linear trends with different slopes can be clearly sorted out in this region. According to the classification proposed by Marsh and Rand,[70] this observation suggests A-type deviations at low pressures from the DA predicted pattern for both zeolites and MOFs. In the case of zeolites, however, the

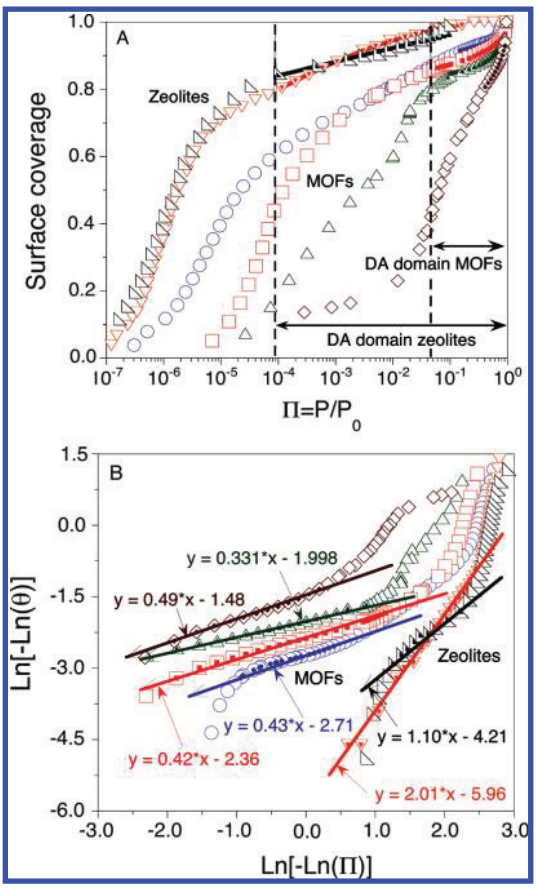

Figure 3. Adsorption isotherms of N_2 at 77.4 K on MOF-5 (○), CAU-1 (□), MIL-68(In)-NH_2, (△) MIL-53(Al)-NH_2 (◇), and reference materials NaY (▽) and HZSM-5 (left-pointing triangles). The straight curves on top reflect the range of applicability of the DA isotherm for MOFs and zeolites, while the straight lines on bottom correspond to the fittings of the DA isotherm (eq 7) at high relative pressures.

domain of application of eq 7 can be extended to relative pressures up to 10^{-4} (see Figure 3B), about 3 orders of magnitude higher than that of CAU-1. In any case, as can be deduced from Figure 3, the DA isotherm is not applicable in Henry's region, this appearing in the case of N_2 adsorption at 77.4 K in an extremely narrow range of low relative pressures, usually less than one decade.

3.3. Energy Heterogeneity in MOFs. The fact that the DA equation does not completely describe the adsorption behavior in MOFs and zeolites at low pressures can be explained in terms of different energy heterogeneities of the materials as a function of pressure. As a matter of fact, as can be inferred from the fittings plotted in Figure 3B, the slopes obtained for zeolites NaY and HZSM-5 are much higher than those corresponding to the MOF materials considered here. This suggests that, at high loadings, adsorption centers in MOFs are more heterogeneous than those in zeolites upon adsorption, namely, molecular confinement in MOFs alters the energy distribution of the material (in the case of N_2 essentially nonspecific) to a higher extent than in the case of zeolites.

More insight about the energy heterogeneity level of MOF materials can be gained by means of the thermodynamic isotherm formulation defined by eq 2. Figure 4 shows the thermodynamic representations obtained for the different MOF materials considered here, while Table 2 collects the main data obtained from the fittings. In all cases, two different potential trends can be distinguished, in good keeping with the results plotted in Figure 3B, matching the general qualitative behavior

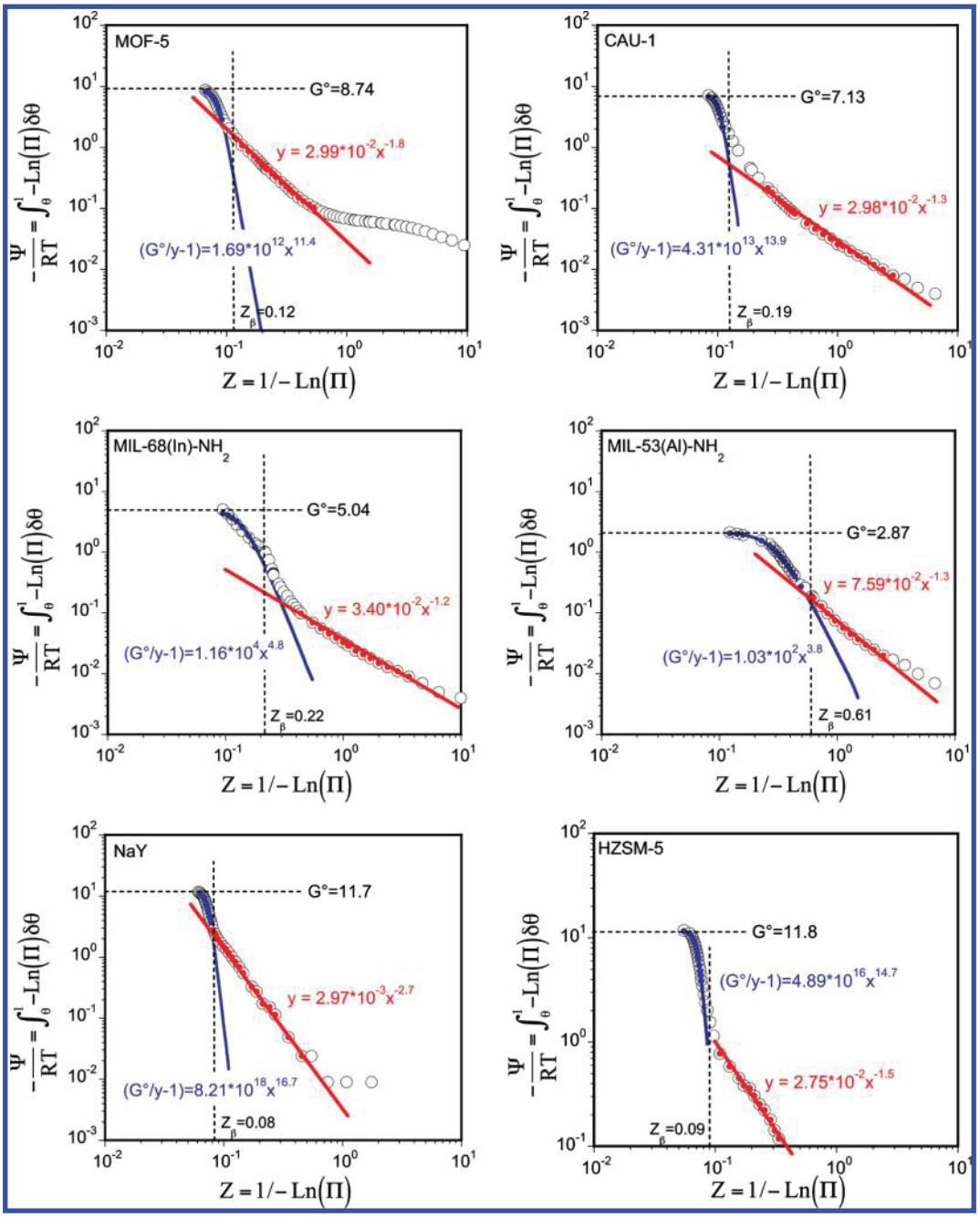

Figure 4. Representations of the thermodynamic isotherm (eq 2) for N_2 adsorption at 77.4 K on the collection of MOF materials prepared in this study and zeolites NaY and HZSM-5. The straight lines correspond to the fittings of eqs 6 and 7, respectively, at low and high relative pressures.

TABLE 2: Fitted Parameters of the Thermodynamic Isotherm Corresponding to the First and Second Potential Zones for Some MOF Materials and Reference Zeolites

				first potential trend			second potential trend		
notation	sorbate	T (K)	$G°$	m_1	Z_k	k_1	m_2	k_2	references
MOF-5	N_2	77.4	8.74	11.4 ± 0.6	$(8.5 \pm 0.1) \times 10^{-2}$	$(1.7 \pm 0.5) \times 10^{12}$	1.8 ± 0.1	$(2.9 \pm 0.1) \times 10^{2}$	this study
CAU-1	N_2	77.4	7.13	13.8 ± 0.6	$(1.0 \pm 0.1) \times 10^{-1}$	$(4 \pm 1) \times 10^{13}$	1.3 ± 0.1	$(2.9 \pm 0.1) \times 10^{2}$	this study
MIL-68In-NH_2	N_2	77.4	5.04	4.8 ± 0.1	$(1.4 \pm 0.2) \times 10^{-1}$	$(1.1 \pm 0.5) \times 10^{4}$	1.2 ± 0.1	$(1.5 \pm 0.2) \times 10^{2}$	this study
MIL-53Al-NH_2	N_2	77.4	2.87	3.6 ± 0.1	$(3.0 \pm 0.3) \times 10^{-1}$	$(1.0 \pm 0.5) \times 10^{2}$	1.3 ± 0.1	$(3.8 \pm 0.5) \times 10^{1}$	this study
NaY (Si/Al = 25)	N_2	77.4	11.71	16.7 ± 0.5	$(7.4 \pm 0.1) \times 10^{-2}$	$(8 \pm 1) \times 10^{18}$	2.7 ± 0.1	$(4 \pm 1) \times 10^{3}$	BAM[a]
HZSM-5 (Si/Al = 500)	N_2	77.4	11.80	15 ± 3	$(7.3 \pm 0.1) \times 10^{-2}$	$(4.9 \pm 0.7) \times 10^{16}$	1.5 ± 0.1	$(7 \pm 1) \times 10^{2}$	62

[a] Data supplied by the Federal Institute for Materials Research and Testing (BAM, Unter den Eichen 87, 12205-Berlin, Germany).

observed for zeolites. Both potential trends can be characterized by two different m slope values (i.e., m_1 and m_2) in such a way that $m_1 > m_2$, suggesting a different pore filling pattern at the early stage of adsorption and at high loadings.

For all the MOF materials tested, the m_2 values show similar values, lying in the narrow range 1.2−1.8, these values being comparable to those obtained in zeolites. In the case of parameter m_1, the most rigid MOFs, i.e., MOF-5 and CAU-1, show values slightly lower than those measured on zeolites NaY and HZSM-5 but keeping consistent with what is expected for a rigid material with relatively homogeneous adsorption strengths. In contrast, in the case of MIL-53(Al)-NH_2 and MIL-68(In)-NH_2 materials, much lower values for parameter m_1 are obtained ($m_1 < 5$). These low values are classically attributed to sites displaying different adsorption strengths, as is usually the case of carbon materials (see ref 58 for further information). In contrast, we attribute the higher degree of heterogeneity of the MIL materials considered here to their comparably more flexible structures, especially in the case of MIL-53(Al)-NH_2, as evidenced from the broad hysteresis loop between the N_2 adsorption/desorption curves even at cryogenic temperatures (see Figure 2). In the case of MIL-68(In)-NH_2, with a more robust framework than that for MIL-53(Al)-NH_2 and thus less susceptible to breathing phenomena, we cannot exclude a source of heterogeneity ascribed to a much higher number of potential adsorption sites with comparable adsorption strengths (see Figure 1) but subjected to a different order pattern (i.e., entropy effects).

As we have discussed in a previous study,[58] parameter m_1 provides a picture of the energy heterogeneity of the *raw* material for a given type of sorbate−sorbent interaction (e.g., nonspecific). In contrast, parameter m_2 provides information about the energy heterogeneity of the adsorbent partially filled with the sorbate, being subjected to sorbate−sorbate interactions that might alter the inherent heterogeneity of the material. We have already demonstrated that the DA isotherm is intrinsically consistent with eq 1 (and eq 2), the characteristic α exponent of this isotherm being linked to parameter m_2 of the thermodynamic isotherm by the expression $m_2 = \alpha + 1$), but not to parameter m_1. As we have stated above, the consistency between both isotherms vanishes at low relative pressures ($\Pi < 0.1$ in MOFs and $\Pi < 0.01$ for zeolites), reflecting the intrinsic limitations of the DA equation at reduced loadings. The fundamental relationship between parameters m_2 and α is confirmed by the results presented in Table 2. This expression confirms the underlying dependence of the α exponent of the DA isotherm on the energy heterogeneity of a microporous system.

The narrow domain of application of the DA isotherm to the description of vapor adsorption in MOF materials, limited in practice to $\Pi > 0.1$, can be broadened using the set of eqs 3 and 4 deduced from the thermodynamic isotherm formulation, accounting for, respectively, the low- and high-pressure adsorption domains. Figure 5 shows the fittings of both equations to the experimental N_2 adsorption data at 77.4 K using the m and k parameter values obtained from the corresponding representations of the thermodynamic isotherm. In all cases, the isotherms represent accurately the experimental data both at low and high pressures, improving the description level of the original DA isotherm and modified versions of this isotherm with adequate low-pressure corrections.[71−73]

3.4. Compressive Tensions in MOFs. In the previous section, we have advanced the hypothesis of an effect of framework distortion, most probably due to a phase transition, on the promotion of the heterogeneous character of MIL-68(In)-NH_2 and MIL-53(Al)-NH_2 materials upon N_2 adsorption at 77.4 K. Our purpose here is to rationalize the much higher elastic deformation of these materials compared to MOF-5 and CAU-1

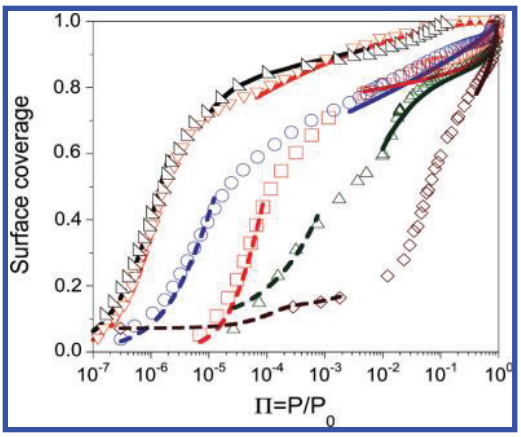

Figure 5. Adsorption isotherms of N_2 at 77.4 K on MOF-5 (○), CAU-1 (□), MIL-68(In)-NH_2 (△) MIL-53(Al)-NH_2 (◇), and reference materials NaY (▽) and HZSM-5 (left-pointing triangles). The dashed and straight lines correspond to the fittings of eqs 3 and 4, respectively, for the low and high relative pressures domains.

and conventional zeolites triggered by the presence of comparably higher structural stresses.

On the guidance of the recent study reported by Neimark et al.,[74] the tension exerted by a sorbate on the adsorbent framework, σ, can be computed from the variation of the grand thermodynamic potential (or surface potential within the framework of solution thermodynamics) of the sorbate with the unit cell volume at a given temperature and constant chemical potential, that is

$$\sigma = -\frac{\delta\Phi}{\delta V_c}\bigg|_{T,\mu} \tag{12}$$

The surface potential can be computed by eq 13 (see ref 58)

$$\frac{\Phi}{q_M RT} = -\int_0^{\Pi} \theta\delta\,\ln(\Pi) = -\int_0^{Z} \frac{\theta}{Z^2}\delta Z < 0 \tag{13}$$

At low pressures ($1/_1 \leq 1$), the surface potential can be computed introducing eq 3 into eq 13

$$\frac{\Phi}{q_M RT} = -\frac{G^\circ}{m_1}\ln(1 + k_1 Z^{m_1}) \tag{14}$$

Introducing eq 14 into eq 12, an expression can be obtained accounting for the stress experienced by the solid at low pressures as a function of the parameters G°, m_1, and k_1 of the thermodynamic isotherm adsorption parameters

$$\sigma = RT\frac{q_M G^\circ}{m_1}\frac{\delta[\ln(1 + k_1 Z^{m_1})]}{\delta V_c} = RT\frac{q_M G^\circ}{m_1}\frac{Z^{m_1}}{(1 + k_1 Z^{m_1})}\frac{\delta k_1}{\delta V_c}_{T,Z} < 0 \tag{15}$$

In the derivation of eq 15, we have implicitly assumed that the unit cell volume variation does not affect the saturation loading of the material (weak assumption for sufficiently low relative pressures).

Equation 15 reflects that, since $\delta k_1/\delta V_c < 0$, the framework tension is negative at low pressures, causing sample contraction

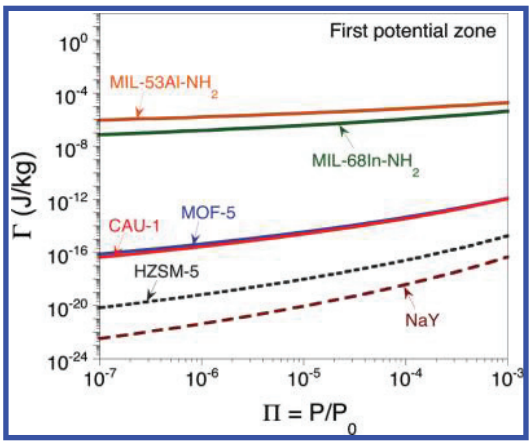

Figure 6. Evolution of parameter Γ, ascribed to the compression tension for a constant $\delta k_1/\delta V_c$, as a function of the relative pressure for the different MOF solids and zeolites tested in this study.

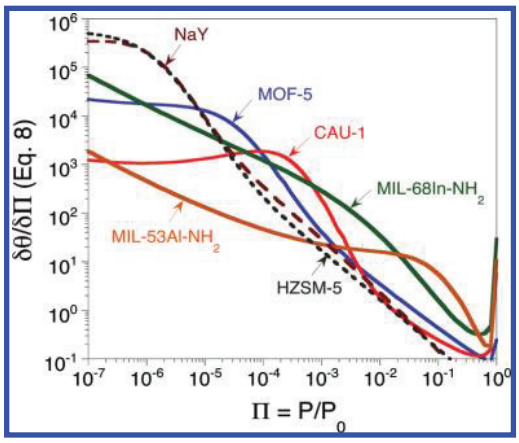

Figure 7. Evolution of the slope of the isotherms plotted in Figure 4 for the different MOFs and zeolites obtained by fitting of eq 10 as a function of the relative pressure.

upon adsorption. Taking into account that the derivative $\delta k_1/\delta V_c$ is hardly measurable, a parameter Γ can be defined from eq 15 as a measure of the compression stress of the framework

$$\Gamma(T,Z) \equiv \frac{\delta\Phi/\delta V_c|_{T,Z}}{\delta k_1/\delta V_c|_{T,Z}} = RT\frac{q_M G^\circ}{m_1}\frac{Z^{m_1}}{(1+k_1 Z^{m_1})} > 0 \quad (16)$$

Figure 6 plots the evolution of parameter Γ computed from eq 16 as a function of the relative pressure for low pressures, corresponding to the first potential zone of the thermodynamic isotherm (i.e., $\Pi < 10^{-3}$), for the collection of MOF solids and reference zeolites considered in this study. In all cases, the parameter Γ increases with the applied pressure, reflecting higher compressive tensions. It is noteworthy that, when comparing the trends observed for the different solids, much higher Γ values for MIL-type materials are obtained unlike the other MOF and zeolite solids (up to 17 orders magnitude difference!). Although the elastic coefficients of MOF materials are unknown, these allowing the translation of surface tensions into deformations following the standard elastic theory (Young equation in the case of linear deformation), we feel entitled to propose that sorbate-induced framework deformation, most probably linked to a phase transition, is at the basis of the observed heterogeneity of MIL-68(In)-NH_2 and MIL-53(Al)-NH_2 solids, involving abnormally low m_1 parameter values.

3.5. Nature of Henry's Region in MOFs at Low Pressures: Nonlinear Trends in Flexible Materials. It is generally accepted that, at low sorbate loadings, the adsorption isotherm for a given sorbate−sorbent system, regardless of its form, can be linearized to a Henry's-type linear isotherm with a characteristic slope or Henry's coefficient, H, reflecting the magnitude of the sorbate−sorbent interaction and confinement level of the sorbate

$$H = \lim_{q\to 0}\frac{\delta\theta}{\delta\Pi} \quad (17)$$

One of the characteristics of gas/vapor adsorption in zeolites is the presence of sharp adsorption trends at low pressures (usually $<10^{-4}$ for N_2 adsorption at 77.4 K, see Figure 2 and Table 2). As a consequence, Henry's region is usually found in an extremely reduced pressure interval, this interval being displaced to higher pressures for weaker adsorbents. This translates into a displacement of this region to the plateau zone in the representation of the thermodynamic isotherm.

Figure 7 plots the evolution of the slope of the adsorption curves, $\delta\theta/\delta\Pi$, against the relative pressure for the four MOF materials prepared in this study and reference zeolites NaY and ZSM-5. The experimental slopes can be successfully reproduced and resolved using the following expression derived from the thermodynamic isotherm (see ref 60 for further details)

$$\frac{\delta\theta}{\delta\Pi} = \frac{1}{\Pi\ln^2(\Pi)}\frac{\delta\theta}{\delta Z} = \frac{G^\circ\lambda_1\lambda_2}{\Pi\ln^2(\Pi)}\frac{(m_2\lambda_1+m_1\lambda_2)}{(\lambda_1+\lambda_2+\lambda_1\lambda_2)^2} \quad (18)$$

One interesting characteristic of Figure 7 is the absence of linear trends typical of Henry's region at low pressures in the case of MIL-53(Al)-NH_2 and MIL-68(In)-NH_2 materials. Contrary to what would be expected from our experience gathered on zeolite adsorption, eq 11 predicts a monotonous increase of the slope, practically linear, for relative pressures $<10^{-6}$. As a matter of fact, this pressure value can usually be considered as a threshold value for the beginning of Henry's (linear) region in zeolites.[60] Note also that the extrapolation of eq 18 to relative pressures $<10^{-9}$ for MIL-68(In)-NH_2 and MIL-53(Al)-NH_2 materials does not predict the presence of a "true" linear trend, the slope increasing monotonously while reducing the pressure. We attribute this observation to the structural deformation on these materials ascribed to high surface tensions, providing higher energy heterogeneity compared to "robust" MOF-5 and CAU-1 materials and zeolites NaY and HZSM-5. We have already demonstrated in a previous publication[60] that linear trends in Henry's region (constant slope) are only possible as long as $m_1 > 12$ for a high range of k_1 values, as is usually the case encountered in zeolites.

Interestingly, eq 18 admits lower and upper bounds for the existence of a linear Henry's region in gas adsorption as a function of the relative values of parameters m_1 and k_1 for a given sorbent but irrespective of parameters m_2 and k_2 and G°. Figure 8 plots the bounds predicted by eq 18, as well as the threshold pairs [m_1, k_1] for the MOF solids and zeolites considered here. As can be observed, MOF-5, CAU-1, and zeolites NaY and HZSM-5 appear in the linear zone, confirming the presence of a linear trend in Henry's region (constant slope) in Figure 7. In contrast, the MIL-type materials slightly overcome the upper bound, appearing as a consequence in a

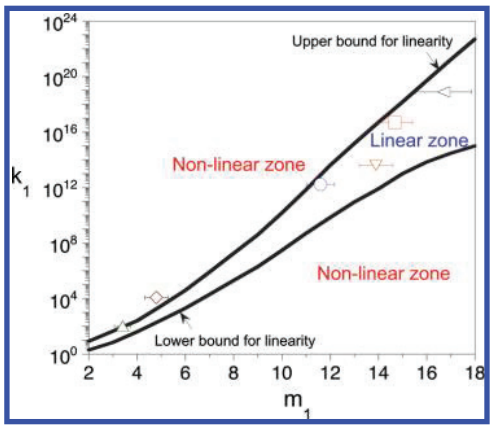

Figure 8. Evolution of parameter Γ, ascribed to the compression tension for a constant $\delta k_1/\delta V_c$, as a function of the relative pressure for the different MOF solids and zeolites tested in this study. Calculations: $G° = 10$, $m_2 = 2.0$, $k_2 = 3000$.

nonlinear region. This is mainly due to the abnormally low m_1 values for these materials ascribed to their high energy heterogeneity, being therefore at the origin of their unexpected lack of linear trend in Henry's adsorption domain.

4. Conclusions

In this study, we have shown that the DA isotherm fails to reproduce successfully N_2 adsorption data at 77.4 K in MOF materials for relative pressures <0.1. This inherent limitation can be overcome using the thermodynamic isotherm characterized by eq 2. Rigid MOF materials show comparable energy heterogeneity to that usually observed in zeolites, characterized by $m_1 > 10$. In the case of MIL-68(In)-NH_2 and MIL-53(Al)-NH_2 materials, showing flexible frameworks, sorbate-induced framework deformation appears to promote energy heterogeneity, the materials showing unexpectedly low m_1 values (<5). This fact appears to be at the origin of a lack of a "true" linear Henry's region at low pressures, as is usually found (and often postulated *a priori*) in zeolites and other "robust" microporous materials.

Glossary

$E°$	Characteristic energy of the DA isotherm ($J \cdot mol^{-1}$)
$G°$	Integral free energy of the sorbate at $P°$, eqs 1−5
H	Henry's constant, eq 17
k	Parameter in eqs 1−5
m	Exponent in eqs 1−5
$P°$	Saturation pressure (Pa)
P	Pressure (Pa)
q_M	Saturation loading ($mol \cdot kg^{-1}$)
R	Gas constant (8.314 $J \cdot mol^{-1} \cdot K^{-1}$)
T	Temperature (K)
V_c	Unit cell volume ($m^3 \cdot kg^{-1}$)
Z	$1/-\ln(\Pi)$

Greek Symbols

α	Exponent in the DA isotherm
β	Affinity coefficient in the DA isotherm
σ	Tension exerted by the sorbate to the solid ($J \cdot kg^{-1}$ solid)
Φ	Surface potential of the sorbate ($J \cdot kg^{-1}$ solid)
Γ	Parameter defined by eq 16 ($J \cdot kg^{-1}$ solid)
λ	kZ^m
Π	$P/P°$
Π_k	Π value corresponding to the disipation of $G°/2$
θ	Surface coverage
Ψ	Integral Gibbs free energy relative to saturation ($J \cdot kg^{-1}$)

Subscripts

1, 2	First and second zone in the thermodynamic isotherm

Acronyms

DA	Dubinin−Astakhov isotherm
DR	Dubinin−Radhuskevitch isotherm
TVFM	Theory of volume filling in micropores

References and Notes

(1) Yang, R. T. *Adsorbents: Fundamentals and Applications*; John Wiley & Sons: Hoboken, NJ, 2003.
(2) Jones, S. C.; Bauer, C. A. *J. Am. Chem. Soc.* **2009**, *131*, 12516.
(3) Hoskins, B. F.; Robson, R. J. *J. Am. Chem. Soc.* **1990**, *112*, 1546.
(4) Wang, Z.; Cohen, S. M. *J. Am. Chem. Soc.* **2007**, *129*, 12368.
(5) James, S. L. *Chem. Soc. Rev.* **2003**, *32*, 276.
(6) Kitagawa, S.; Kitaura, R.; Noro, S. *Angew. Chem., Int. Ed.* **2004**, *43*, 2334.
(7) Ockwig, N. W.; Delgado-Friedrichs, O.; O'Keeffe, M.; Yaghi, O. M. *Acc. Chem. Res.* **2005**, *38*, 176.
(8) Ferey, G.; Mellot-Draznieks, C.; Serre, C.; Millange, F. *Acc. Chem. Res.* **2005**, *38*, 217.
(9) Ferey, G.; Serre, C. *Chem. Soc. Rev.* **2009**, *38*, 1380.
(10) Düren, T.; Bae, Y.-S.; Snurr, R. Q. *Chem. Soc. Rev.* **2009**, *38*, 1237.
(11) Li, J.-R.; Kuppler, R.-J.; Zhou, H.-C. *Chem. Soc. Rev.* **2009**, *38*, 1477.
(12) Murray, L. J.; Dinc, M.; Long, J. R. *Chem. Soc. Rev.* **2009**, *38*, 1294.
(13) Farrusseng, D.; Aguado, S.; Pinel, C. *Angew. Chem., Int. Ed.* **2009**, *48*, 7502.
(14) Lee, J. Y.; Farha, O. K.; Roberts, J.; Scheidt, K. A.; Nguyen, S. T.; Hupp, J. T. *Chem. Soc. Rev.* **2009**, *38*, 1450.
(15) Ma, L.; Abney, C.; Lin, W. *Chem. Soc. Rev.* **2009**, *38*, 1248.
(16) Livage, C.; Egger, C.; Ferey, G. *Chem. Mater.* **2001**, *13*, 410.
(17) Livage, C.; Guillou, N.; Marrot, J.; Ferey, G. *Chem. Mater.* **2001**, *13*, 4387.
(18) Barthelet, K.; Marrot, J.; Riou, D.; Ferey, G. *Angew. Chem., Int. Ed.* **2002**, *41*, 281.
(19) Serre, C.; Millange, F.; Thouvenot, C.; Nogues, M.; Marsolier, G.; Loueur, D.; Ferey, G. *J. Am. Chem. Soc.* **2002**, *124*, 13519.
(20) Barthelet, K.; Adil, K.; Millange, F.; Serre, C.; Riou, D.; Ferey, G. *J. Mater. Chem.* **2003**, *13*, 2208.
(21) Riou-Cavellec, M.; Lesaint, C.; Nogues, M.; Greneche, J. M.; Ferey, G. *Inorg. Chem.* **2003**, *42*, 5669.
(22) Guillou, N.; Livage, C.; van Beek, W.; Nogues, M.; Ferey, G. *Angew. Chem., Int. Ed.* **2003**, *42*, 644.
(23) Guillou, N.; Livage, C.; Drillon, M.; Ferey, G. *Angew. Chem., Int. Ed.* **2003**, *42*, 5314.
(24) Devic, T.; Serre, C.; Auderbrand, N.; Marrot, J.; Ferey, G. *J. Am. Chem. Soc.* **2005**, *127*, 12788.
(25) Ferey, G.; Mellot-Draznieks, C.; Serre, C.; Millange, F.; Dutour, J.; Surble, S.; Margiolaki, I. *Science* **2005**, *307*, 2040.
(26) Serre, C.; Mellot-Draznieks, C.; Surble, S.; Audebrand, N.; Filinchuk, Y.; Ferey, G. *Science* **2007**, *315*, 1828.
(27) Rowsell, J. L. C.; Yaghi, O. M. *Microporous Mesoporous Mater.* **2004**, *73*, 3.
(28) Eddaoudi, M.; Kim, J.; Rosi, N.; Vodak, D.; Wachter, J.; O'Keeffe, M.; Yaghi, O. M. *Science* **2002**, *205*, 469.
(29) Millward, A. R.; Yaghi, O. M. *J. Am. Chem. Soc.* **2005**, *127*, 17998.
(30) Walton, K. S.; Millward, A. R.; Dubbeldam, D.; Frost, H.; Low, J. J.; Yaghi, O. M.; Snurr, R. Q. *J. Am. Chem. Soc.* **2008**, *130*, 406.
(31) Rowsell, J. L. C.; Yaghi, O. M. *J. Am. Chem. Soc.* **2006**, *128*, 1304.
(32) Wong-Foy, A. G.; Matzger, A. J.; Yaghi, O. M. *J. Am. Chem. Soc.* **2006**, *128*, 3494.
(33) Chui, S. S. Y.; Lo, S. M. F.; Charmant, J. P. H.; Orpen, A. G.; Williams, I. D. *Science* **1999**, *283*, 1148.
(34) Alaerts, L.; Kirschhock, C. E. A.; Maes, M.; van der Veen, M. A.; Finsy, V.; Depla, A.; Martens, J. A.; Baron, G. V.; Jacobs, P. A.; Denayer, J. E. M.; de Vos, D. E. *Angew. Chem., Int. Ed.* **2007**, *46*, 4293.
(35) Murray, L. J.; Dinca, M.; Long, J. R. *Chem. Soc. Rev.* **2009**, *38*, 1294.
(36) McKinlay, A. C.; Xiao, B.; Wragg, D. S.; Wheatley, P. S.; Megson, I. L.; Morris, R. E. *J. Am. Chem. Soc.* **2008**, *130*, 10440.

(37) Kitagawa, S.; Uemura, K. *Chem. Soc. Rev.* **2005**, *34*, 109.
(38) Bureekaew, S.; Shimomura, S.; Kitagawa, S. *Sci. Technol. Adv. Mater.* **2008**, *9*, 1.
(39) Horike, S.; Matsuda, R.; Tanaka, D.; Matsubara, S.; Mizuno, M.; Endo, K.; Kitagawa, S. *Angew. Chem., Int. Ed.* **2006**, *45*, 7226.
(40) Bourrelly, S.; Llewellyn, P. L.; Serre, C.; Millange, F.; Loiseau, T.; Ferey, G. *J. Am. Chem. Soc.* **2005**, *127*, 13519.
(41) Trung, T. K.; Trens, P.; Tanchoux, N.; Bourrelly, S.; Llewellyn, P. L.; Loera-Serna, S.; Serre, C.; Loiseau, T.; Fajula, F.; Ferey, G. *J. Am. Chem. Soc.* **2008**, *130*, 16926.
(42) Coudert, F.-X. Jeffroy, M. Fuchs, A. H. Boutin, A. Mellot-Draznieks, C. *J. Am. Chem. Soc.* **2008**, *130*, 14294.
(43) Serre, C.; Bourrelly, S.; Vimont, A.; Ramsahye, N. A.; Maurin, G.; Llewellyn, P. L.; Daturi, M.; Filinchuk, Y.; Leynaud, O.; Barnes, P.; Ferey, G. *Adv. Mater.* **2007**, *19*, 2246.
(44) Düren, T.; Sarkisov, L.; Yaghi, O. M.; Snurr, R. Q. *Langmuir* **2004**, *20*, 2683.
(45) Sagara, T.; Klassen, J.; Ganz, E. *J. Chem. Phys.* **2004**, *121*, 12543.
(46) Sarkisov, L.; Düren, T.; Snurr, R. Q. *Mol. Phys.* **2004**, *102*, 211.
(47) Mellot-Draznieks, C.; Serre, C.; Surble, S.; Audebrand, N.; Ferey, G. *J. Am. Chem. Soc.* **2005**, *127*, 16273.
(48) Garberoglio, G.; Skoulidas, A. I.; Johnson, J. K. *J. Phys. Chem. B* **2005**, *109*, 13094.
(49) Ramsahye, N. A.; Maurin, G.; Bourrelly, S.; Llewellyn, P. L.; Devic, T.; Serre, C.; Loiseau, T.; Ferey, G. *Adsorption* **2005**, *13*, 461.
(50) Yang, Q. Y.; Zhong, C. L. *J. Phys. Chem. B* **2006**, *110*, 17776.
(51) Yang, Q. Y.; Zhong, C. L. *ChemPhysChem* **2006**, *7*, 1417.
(52) Skoulidas, A. I.; Sholl, D. S. *J. Am. Chem. Soc.* **2007**, *129*, 8552.
(53) Salles, F.; Ghoufi, A.; Maurin, G.; Bell, R. G.; Mellot-Draznieks, C.; Ferey, G. *Angew. Chem., Int. Ed.* **2008**, *47*, 8487.
(54) Özgür Yazaydin, A.; Benin, A. I.; Faheem, A.; Jakubczak, P.; Low, J. J.; Willis, R. R.; Snurr, R. Q. *Chem. Mater.* **2009**, *21*, 1425.
(55) Brunauer, S.; Emmett, P. H.; Teller, E. *J. Am. Chem. Soc.* **1938**, *60*, 309.
(56) Dubinin, M. M. Astakhov, V. A. Radushkevich, L. V. *Physical Adsorption of Gases and Vapors in Micropores, Progress and Membrane Science*; Academic Press: New York, 1975; Vol. 9.
(57) Walton, K. S.; Snurr, R. Q. *J. Phys. Chem. B* **2005**, *109*, 15760.
(58) Llorens, J.; Pera-Titus, M. *J. Colloid Interface Sci.* **2009**, *331*, 302.
(59) Llorens, J.; Pera-Titus, M. *Colloids Surf., A* **2009**, *350*, 63.
(60) Pera-Titus, M.; Llorens, J. *Appl. Surf. Sci.* **2010**, *256*, 5305.
(61) Pera-Titus, M. *J. Colloid Interface Sci.* **2010**, *345*, 410.
(62) Nakai, K.; Sonoda, J.; Yoshida, M.; Hakuman, M.; Naono, H. *Adsorption* **2007**, *13*, 351.
(63) Mueller, U.; Schubert, M.; Teich, F.; Puetter, H.; Schierle-Arndt, K.; Pastre, J. *J. Mater. Chem.* **2006**, *16*, 626.
(64) Li, H.; Eddaoudi, M.; O'Keeffe, M.; Yaghi, O. M. *Nature* **1999**, *402*, 276.
(65) Ravon, U.; Savonnet, M.; Aguado, S.; Domine, M. E.; Janneau, E.; Farrusseng, D. *Microporous Mesoporous Mater.* **2010**, *129*, 319.
(66) Ahnfeldt, T.; Guillou, N.; Gunzelmann, D.; Margiolaki, I.; Loiseau, T.; Férey, G.; Senker, J.; Stock, N. *Angew. Chem., Int. Ed.* **2009**, *48*, 5163.
(67) Savonnet, M.; Bazer-Bachi, D.; Pinel, C.; Lecocq, V.; Bats, N.; Farrusseng, D. Patent Pending FR 09/05.101.
(68) Bauer, S.; Serre, C.; Devic, T.; Horcajada, P.; Marrot, J.; Férey, G.; Stock, N. *Inorg. Chem.* **2008**, *47*, 7568.
(69) Stoeckli, F. *Adsorpt. Sci. Technol.* **1993**, *10*, 3.
(70) Marsh, H.; Rand, B. *J. Colloid Interface Sci.* **1970**, *33*, 101.
(71) Sundaram, N. *Langmuir* **1993**, *9*, 1568A.
(72) Kapoor, A.; Ritter, J. A.; Yang, R. T. *Langmuir* **1989**, *5*, 1118.
(73) Mahle, J. J. *Carbon* **1997**, *35*, 432.
(74) Neimark, A. V.; Coudert, F.-X.; Boutin, A.; Fuchs, A. *J. Phys. Chem. Lett.* **2010**, *1*, 445.

JP104788P

DOI: 10.1002/anie.200((will be filled in by the editorial staff))

Tailoring Metal-Organic Framework Catalysts by Click Chemistry: Synergistic Effect by Tandem Functionalization

*Marie Savonnet, Aurélie Camarata, Jerome Canivet, Delphine Bazer-Bachi, Nicolas Bats, Vincent Lecocq, Catherine Pinel and David Farrusseng**

Metal-organic frameworks (MOFs) are porous crystalline materials composed of cationic metal systems that behave like nodes with polytopic organic ligands acting as spacers.[1] These materials are often viewed as a new class of zeolites due to their porous structure. MOFs of the most recent generation present molecular recognition properties[2] originating from their considerable dynamic flexibility[3], which is usually under the control of host-guest interactions. It is acknowledged that MOFs could ultimately mimic enzymes using a "locking" concept favoring high chemo-, regio- and enantioselectivity.[4] MOFs could indeed be viewed as potential "artificial enzymes" combining several properties in a concerted fashion at the nanometer scale. Fairly few MOFs bear more than one reactive function, however. The catalytic properties of these materials have, to date, essentially relied on the features of the inorganic nodes.[5] For example, inorganic clusters with unsaturated coordination (such as HKUST-1) or bridging hydroxyl groups (such as MIL-53) have been shown to perform Lewis [6] and Brønsted type catalysis [7] respectively.

One solution for synthesizing advanced MOFs suitable for specialized and sophisticated applications is the controlled addition of more complex functionalities into the porous network. Through this functionalization, if the physical environment of the pores and the cavities within the MOFs can be modified, the interactions with guest species can in turn be adapted, thereby fine-tuning the chemical reactivity.[8] However, the introduction of reactive chemical functions by self-assembly methods is not a trivial task and cannot be generalized to all MOFs.[9] Various synthetic strategies have been employed with the aim of achieving MOF post-functionalization, as detailed in extensive reviews by Cohen *et al*.[10] Post-synthetic modification (PSM) using covalent-type grafting methods has undergone outstanding progress during the last five years.[11] We have recently reported an original PSM method starting from amino derived MOFs.[12] The first step consists in converting the amino groups on the framework walls into their analogous azido (N_3). Without isolation nor purification, the desired triazolyl functionalized MOF materials are obtained by grafting the corresponding alkyne using "clik chemistry" (Figure 1). Using two different MOFs templates, the DMOF [Zn(2-amino-terephthalate)(dabco)] (dabco = 1,4-diazabicyclo[2.2.2]octane) and the IHM-2 [In(OH)(2-amino-terephthalate)], we showed that this novel PSM method presents key benefits for the engineering of MOF: i) the softness of the method allows no restriction on the choice of starting amino-MOFs and ii) the grafting yield can be controlled by adjusting the MOF:alkyne ratio.

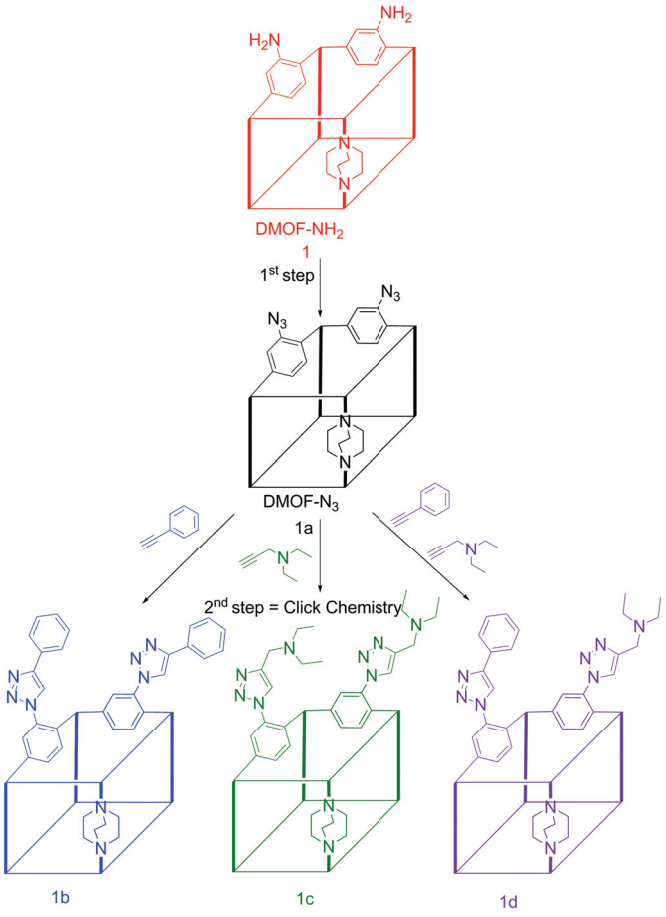

Figure 1. Synthesis of MOF catalysts by "click chemistry"

Despite intensive efforts to develop new efficient, selective and recyclable solid base catalysts such as Layered Double Hydroxides (LDH),[13] hydrotalcite, KF and amine supported compounds, the development of green processes involving basic catalysts remains a challenge.[14]

In this contribution, we demonstrate that PSM by "click chemistry" enables the engineering of MOFs for application in base catalysis. The controlled post-modification of the frameworks introducing basic and/or hydrophobic features allows a rational

[*] A. Camarata, Dr. J. Canivet, Dr. C. Pinel, Dr. D. Farrusseng
IRCELYON, University of Lyon 1
CNRS, 2 avenue Albert Einstein
F-69626, Villeurbanne Cedex
Fax: (+33) 4 72 44 53 99
E-mail: david.farrusseng@ircelyon.univ-lyon1.fr

M. Savonnet, Dr. D. Bazer-Bachi, Dr. N. Bats, Dr. V. Lecocq
IFP Energies Nouvelles
BP n°3, 69360, Solaize, France

[**] We thank IRCELYON and IFP Scientific Services.

Supporting information for this article is available on the WWW under http://www.angewandte.org or from the author.

design of catalytic MOFs for the transesterification reaction.[15] We show for the first time that outstanding synergistic catalytic effect can be obtained by an optimal formulation of our functionalized material.

The base-catalyzed model reaction considered here is the transesterification of ethyldecanoate in methanol (Scheme 1).

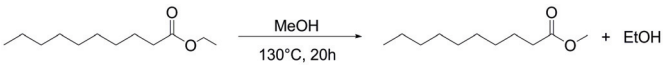

Scheme 1. Transesterification of ethyldecanoate in methanol

For this reaction to proceed efficiently, both substrates must be co-adsorbed into the MOF and MeOH should be activated by a base in order to favour the nucleophilic attack on the carbonyl group. The DMOF parent structure was selected as the starting platform since it contains neither Lewis nor Brønsted acid groups that could have a catalytic effect. Two different functional groups were selected for post-modification: a 1,2,3-triazolyl substituted with phenyl, corresponding to **b** compounds, or tertiary amine at the 4-position, corresponding to **c** compounds (Figure 1). They are obtained by reacting the DMOF-N_3 (**1a**) with phenylacetylene to give **1b** and with propargylamine to give **1c**. The former **1b** presents moderate basicity originating from the triazolyle group (pKa ≈ 1,2) as well as strong hydrophobicity, whereas the latter **1c** is a much stronger base (pKa ≈ 11 for alkylamines). A bifunctionalized MOF modified with **b** groups (phenyl) and then subsequently modified with **c** groups (tertiary amine) on the remaining azido sites was obtained and hereafter denoted **1d**. The degree of modification of the MOF catalysts is given in Table 1.

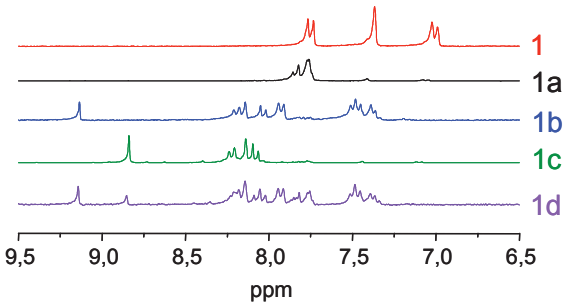

Figure 2. ^{1}H NMR of digested **1**, **1a**, **1b, 1c** and **1d** compounds

Clear proof of the azide formation and of the subsequent full (3+2) cycloaddition can be characterized by liquid ^{1}H NMR on a quantitative manner (figure 2). The spectrum of digested DMOF-N_3 (**1a**) reveals the formation of the azido corresponding compound through the appearance of new aromatic signals (7.73-7.83 ppm). This coincides with the complete disappearance of the aromatic signals of DMOF-NH_2 (**1**) at 7.15 ppm, 7.44 ppm and 7.8 ppm, thus indicating almost full conversion to the azido form. After the cycloaddition step, new aromatic shifts of the post-modified compounds **1b** and **1c** confirm that the corresponding triazole derivative is formed as the sole product. The post-digestion ^{1}H NMR spectrum of **1d** shows contributions of both **b** and **c** and also of the remaining azide in a 30:30:40 ratio (see Table 1).

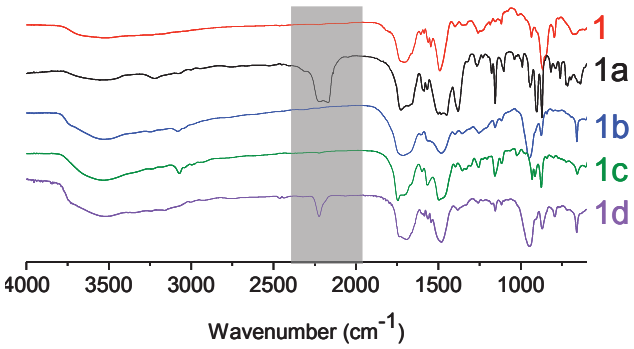

Figure 3. FT-IR of **1**, **1a**, **1b, 1c** and **1d** compounds

IR spectroscopy studies confirm these results (Figure 3). The appearance of the IR absorption band at 2123 cm^{-1} is characteristic of the N_3 asymmetric stretching vibration of DMOF-N_3 **1a**. In the cases of **1b**, **1c**, its disappearance after the cycloaddition step is proof of almost total conversion to the final compound. In the case of **1d** ,the less intense $-N_3$ signal is well in line with the partial conversion as quantified by ^{1}H NMR (see table 1). Despite solvent effects on DMOF structure and crystallinity,[12, 16] powder X-ray diffraction patterns (PXRD) indicates that long-range order is preserved for all samples (Figure 4).

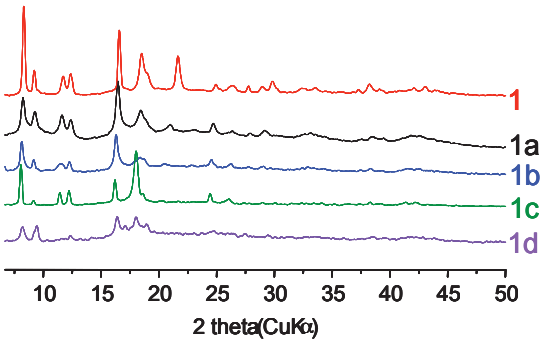

Figure 4. Powder XRD patterns of **1**, **1a**, **1b, 1c** and **1d** compounds

Following similar methodology, samples with variable degree of modification were prepared. They are obtained by adjusting the amount of alkyne reactants, phenylacetylene or diethyl-propargylamine, with respect to **1a**. There are denoted hereafter **1b-15**, **1b-40** and **1b-80** for degrees of modification with **b** groups (phenyl) of 15%, 40% and 80% respectively, and **1c-40**, **1c-85** for degrees of modification with **c** groups (tertiary amine) of 40% and 85% respectively. Synthesis details and characterization can be found in the supporting information.

These DMOF catalysts were involved in the transesterification of ethyldecanoate with methanol and all the catalytic results are summarized in the Table 1. It is worthy to note that the transesterification conversion obtained using the unmodified DMOF-NH_2 (**1**) as catalyst is not higher than that obtained without catalyst (c.a. 10%, entries 1 and 2).

Table 1. Transesterification conversion of functionalized MOFs and reference catalysts [a]

Entry	Catalyst	b (%)	c (%)	conversion (%)
1	**none**	-	-	10
2	**1**	-	-	10
3	**1b-40**	40	-	48
4	**1b-40** [b]	40	-	0
5	**1b-80**	80	-	82
6	**1c-40**	-	40	21
7	**1c-85**	-	85	28
8	**1d**	**30**	**30**	**84**
9	$Cu(ACN)_4PF_6$ [c]	-	-	32
10	$Cu(OAc)_2$ [c]	-	-	40
11	**linker b** [c]	100	-	30
12	**linker c** [c]	-	100	21

[a] Conditions: ethyldecanoate (2.5 mL) is allowed to react in methanol (10 mL) using 20 mg of DMOF catalyst (~0.03 mmol MOF, c.a 0.06 mmol $–NH_2$) at 130°C for 20h [b] 2-ethyl-1-butanol is used instead of methanol [c] Homologue catalysts used under homogenous conditions (scheme 2); 0.3 mmol of catalyst are used.

The figure 5 illustrates also how the degree of modification affects ethyldecanoate conversion in the case of the monofunctionalized materials. It appears that the activity of these DMOF materials increases linearly with the degree of modification. The syntheses and tests were performed twice for **1b-80** in order to verify experimental reproducibility; both times the ethyldecanoate conversion was approximately 80% (Table 1, entry 5).

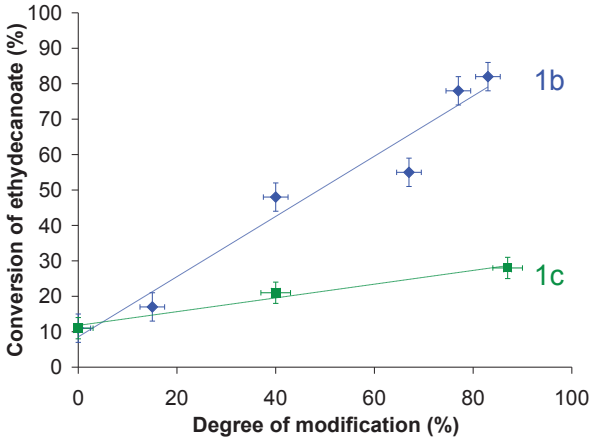

Figure 5. Effect of the degree of modification for **1b** (♦) and **1c** (■) on ethyldecanoate conversion at 130°C after 20 h

The DMOF grafted with **c** groups could have been expected to show better activity based on the higher basic strength of the trialkylamine compared to that of the phenyl substituent. Surprisingly, the introduction of hydrophobic functions via **b** exhibits a more beneficial effect on catalytic activity. Furthermore, the corresponding organic functionalized linker found in **1b** and **1c,** respectively **linker b** (dimethyl-2-(4-phenyl-1H-1,2,3-triazol-1-yl)-terephthalate) and **linker c** (dimethyl-2-(4-diethylaminomethyl-1H-1,2,3-triazol-1-yl)-terephthalate), were synthesized (Scheme 2).

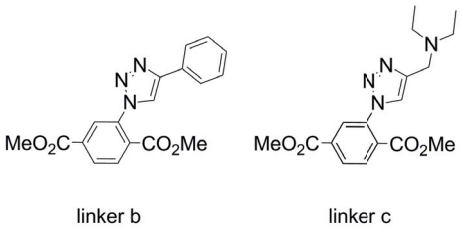

linker b linker c

Scheme 2. Molecular homologues of the catalysts **1b** and **1c**.

The **linker b** and the **linker c** were tested in the transesterification reaction under homogeneous conditions and show moderate activity compared to the corresponding grafted MOFs with conversions of 30% and 21% respectively (Table 1, entries 11 and 12) against 82% for **1b-80** (entry 5) and 28% for **1c-85** (entry 7). These results confirm the moderate activity of the triazolyl group itself.

In contrast, the tandem post-modified **1d** shows outstanding performances compared to the monofunctionalized DMOF samples. Although **1d** contains only 30% of **b** and 30% of **c**, 84% conversion was achieved (entry 8). Under similar reaction conditions, using **1b-40** and **1c-40** with similar degree of modification, the conversion only reached 48% and 21%, respectively (entries 3 and 6). This superior activity can be attributed to a synergistic effect resulting from the combination of both basic and hydrophobic groups at molecular level.

In order to assess our hypothesis of a synergistic basic-hydrophobic effect, liquid adsorption isotherms with an ethyldecanoate/isooctane mixture were investigated for **1** and for **1b-40**, containing 40% of 4-phenyl-1,2,3-triazolyl functions (Figure 6).

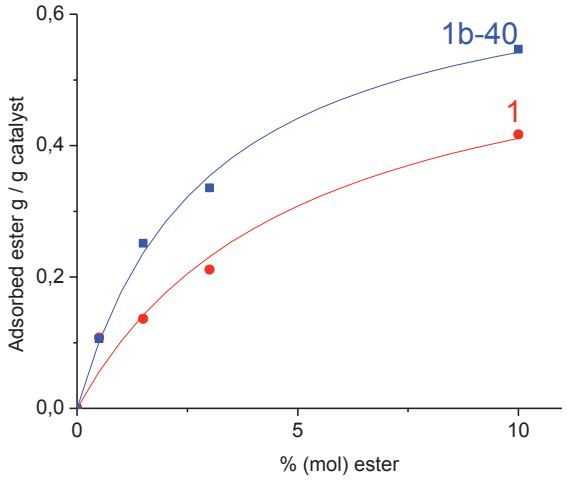

Figure 6. Liquid adsorption isotherms of ethyldecanoate in the ethyldecanoate/isooctane mixture for **1** (●) and **1b-40** (■)

These adsorption measurements confirm the stronger hydrophobicity of the latter material. Consequently, we suggest that the higher apparent activity of **1b** compared to **1c** should be due to a more appropriate co-adsorption ratio of both substrates inside the pores on the more hydrophobic MOF. Hence, **1d** with a tandem functionalization reaches an optimal basic/hydrophobic balance to perform the reaction.

Entry for the Table of Contents (Please choose one layout)

Metal-Organic Frameworks

Marie Savonnet, Emanuel Kockrick, Aurélie Camarata, Delphine Bazer-Bachi, Nicolas Bats, Vincent Lecocq, Catherine Pinel and David Farrusseng*

_____ Page – Page

Tailoring Metal-Organic Framework Catalysts by Click Chemistry: Synergistic Effect by Tandem Functionalization

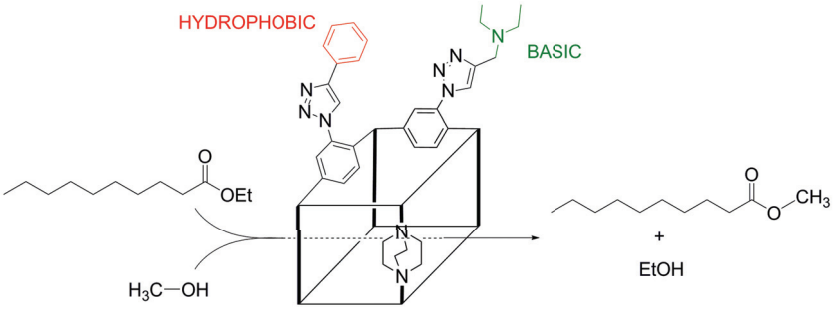

Click reaction into MOFs is an efficient tool to engineer its intrinsic properties and give new opportunities for catalyst design at molecular level. We successively introduce new basic catalytic centers and modify their environment by addition of hydrophobic groups. The resulting bifunctionalized MOF provides an optimized balance between basicity and hydrophobicity and shows outstanding performance for the transesterification reaction.